Examining the Contribution of Mitochondria During Human Neurogenesis Using Human Pluripotent Stem Cell-Derived Systems

By

Alejandra Inés Romero Morales

Dissertation

Submitted to the Faculty of the

Graduate School of Vanderbilt University

in partial fulfillment of the requirements

for the degree of

DOCTOR OF PHILOSOPHY

in

Cell and Developmental Biology

February 28th, 2022

Nashville, Tennessee

Approved:

Vivian Gama, Ph.D.

Ethan Lee, Ph.D.

Rebecca Ihrie, Ph.D.

Kevin Ess, M.D, Ph.D.

Jeffrey Rathmell, Ph.D.

Dedication

I dedicate this thesis to

Mis papás Marlene Morales Hernández y Juan Carlos Romero Araya,
mis hermanos Daniela y Esteban Romero Morales y Otti
que han sido mi pilar y mi más grande fuente de fuerza
e inspiración durante estos años.

And my dear husband Kenneth Taubenslag that has supported
and cheered me during all this craziness.

Los amo a todos.

Acknowledgments

Graduate school has been an interesting experience, I never thought that 5 years could change someone so much as it did. There are so many amazing people that helped me during my PhD journey that I may not have enough space to thank them all, but if you have been around during this time and you are reading this know that I hold a special place in my heart and thoughts for you.

I will start by thanking everyone that help me get into grad school, going as far as the Tecnológico de Costa Rica and the University of Costa Rica. I want to thank my advisor Miguel Rojas Chaves, PhD who encourage and advise me to apply to grad school. Also, Guy Lamoureux Lamontagne, PhD not only for making Organic chemistry fun but also for suggesting I apply to VISRA (Vanderbilt International Summer Research Academy) and then to the grad school. In VISRA I was hosted by Claudia Andl, PhD and not only I was able to do great research in her lab, but I met there one of the most important persons in my life: my now-husband Kenny Taubenslag.

I would like to also thank Dr. Kathy Gould, PhD for all her help and encouragement to join Vanderbilt for grad school. Dr. Gould was the director of VISRA and VISP (Vanderbilt International Scholar Program) when I joined. I really appreciate those catch-up conversations in the hall or during the walk home.

I have no words in English or Spanish to thank my mentor, Dr. Vivian Gama, enough. She has not only been a wonderful boss -helping me stay on track with my research goals, troubleshooting experiments, and celebrating the little victories- but the most amazing friend and role model. I can only aspire to model my career to Vivian's. I appreciate the couple of minutes turned to a couple of hours crash meetings in your office and your capacity to tell me to slow down and breathe when I needed to pull the breaks. I have been so honored to be part of the lab for all these years and witness how it has taken shape to be the incredibly supportive and productive science family that is now. I also must thank Dr. José Gómez and Andrés Gómez Gama that have also been wonderful and supportive. Gracias, gracias, gracias a todos por hacerme sentir tan bienvenida y querida. Los voy a extrañar muchísimo.

I couldn't have accomplished half of the thing that I did during grad school without the support system that is the Gama Lab, past and present members. When younger grad students ask me how they know that a lab is a good fit for them I usually advise them to look for a place where they feel like they can not only grow but flourish. The lab environment created by Dr. Megan Rasmussen and Dr. Natalya Ortolano was key for me deciding to join the lab. They made me feel so welcomed during my rotation

that joining just *felt right* (I know, very sciency). Both are stellar scientists and humans, and I feel beyond blessed to spend so many hours beside them. Dr. Piyush Joshi join a bit later, bringing a new layer of complexity to our nascent neuroscience knowledge. With Piyush, we also gained the extraordinary presence of Caroline Bodnya in the lab. Caroline stayed around as our lab manager and now is on her grad school journey, and I am CERTAIN will be so incredibly successful. She knows all the wonderful things that I think of her as a human and a scientist, and I'm so grateful to be able to count her as one of my close friends.

Another lab member that I am insanely grateful for is Gabriella Robertson. She is a super science rock star. I am a big fan of her and wish for all the good things to go her way. Soon-to-be Dr. Robertson is not only one of the kindest souls that I have met but a knowledgeable and determined scientist. During COVID, Gabriella became my work-wife and one of my grad school best friends. I promise to keep enabling and contributing to the house plant addiction until Steven bans all communications.

I feel so grateful that I had time to interact with the newer members of the lab Tierney Baum, Marina Hanna, and Melanie Gil. All of them terrific scientists with oh-so-bright futures. Thank you, Tierney, for the very needed therapy sessions/science discussions. Marina and Melanie, I can't think of more capable hands to continue the MCL-1 projects. Both of you have such amazing futures ahead of you, enjoy the journey, and never forget that I am a call/text away if you ever need me!

Besides grad students, the lab has always been full of wonderful managers and undergrads. I must give a special shout-out to AJ Rastogi, MSc. AJ not only turned the lab into an efficient machine during his time as lab manager, but when he told us that he was there to help with whatever we needed during his interview, he wasn't kidding! Thanks for being an amazing co-author for the LS project and helping me keep the ball rolling even when I was overwhelmed by it. Also in the hall of fame is our undergrad-turned-lab manager Stellan Riffle. Sarcastic, sassy, and funny, Stellan always has a good disposition. I'm sure whatever he decides to do in the future he would do it as the kind, capable, and carrying individual that he is.

I also must give a special thank you to the undergrads that I mentored: Ela Contreras-Panta, Hoor Temuri, Adriana Calderón-Acón, and Emma Follman. Thank you all for trusting me to be your mentor and thank you for all the hard work that you did. Thank you for always keeping me sharp on the basics and for pushing me to improve as a teacher. I am so proud of all that you have accomplished, and I am beyond grateful for your trust in me.

Research is a team effort, and I was able to work with multiple groups of amazing scientists during my PhD both in and out of Vanderbilt. I would like to thank Dr. Ethan Lippmann, Dr. Leon Bellan, Dr. Dmitry Markov, and Dr. Lisa McCawley for all their collaborative efforts on the organoid project. Also, a special thanks to Dr. José Gómez and his lab for allowing me to help with their kidney organoid modeling work. Moreover, a big thank you to Dr. Julie Siegenthaler and her grad student Hannah Jones for all the collaborative efforts and cool data that we have acquired. Also, I want to thank the Cores that help and made my research possible. Special thanks to Karen Thompson and Sherry Smith at the VUMC Translational Pathology Shared Resource Core for all their help thought the years. Dr. Bryan Millis, Dr. Nick Mignemi, and Kari Seedle at Vanderbilt Cell Imaging Shared Resource Core were also key for my growth as a scientist; thank you for teaching me and helping me discover the beauty of microscopy.

I would also like to thank the CDB department for being such a welcoming and collaborative environment. I really want to highlight Mark Wozniak and Susan Walker, the MVPs of the department. Also, I would like to thank the VPMM (Vanderbilt Program in Molecular Medicine) for the unique opportunity to merge my thesis work with clinical experience.

My work would not be possible without the guidance and contributions of my thesis committee: Dr. Ethan Lee, Dr. Kevin Ess, Dr. Rebecca Ihrie, and Dr. Jeffery Rathmell. Thank you for encouraging me to think critically and keep pushing the boundaries. I would also like to thank other faculty members, Dr. Kris Burkewitz, Dr. Irina Kaverina, Dr. Andrea Page-McCaw, Dr. Jonathan Irish, Dr. Mark Magnuson, and Dr. Chris Wright, for their helpful discussions and coordination of departmental seminars and courses. A special thank you is due to Dr. Chris Wright whose mentorship and generosity with his ideas and time always exceed my expectations. Thank you so much for the trust you have put in me and for allowing me to explore teaching and expand my knowledge in your classes.

Being a woman in science, an even more specifically an international woman in science, is not easy, and having great mentors to model your career after and to remind your dreams are achievable and sustainable is crucial. For this, I not only had Vivian but also Dr. Rebecca Ihrie and Dr. Marija Zanic. Thank you all for your time, kind words, and encouragement. Thank you for showing me that it can be done without losing your essence and passion.

I want to thank my pre-grad school and grad school friends for all their support during these years. To my high school, undergrad, dance, and med school friends; thank you for believing in me and celebrating even the smallest of wins. You all inspire me to be a better person and professional. Thanks

for keeping tabs on me and turning around your schedules to at least be able to grab a quick coffee whenever I'm back in Costa Rica. And to my grad-school friends, thank you for existing and being the amazing support system/therapy group that you are.

Anything I have done past, present, or future had been possible without my family. From my grandparents Inés Hernández Salazar, Otoniel Morales Alfaro, Ana Cecilia Araya Roses and Carlos Romero Monge and my grand-aunt Luz Marina Hernández Salazar; to my parents Juan Carlos Romero Araya and Marlene Morales Hernández; to my siblings Esteban and Daniela Romero Morales and Otti; to my aunts, uncles, and cousins. They have taught me integrity, responsibility, hard work, and resilience. I missed all of them every day that I have been away, but I also know that they miss me and that they are incredibly proud of me for following my dreams and for creating this path for myself. I want to thank my parents so much for all their effort not only in raising us strong and independent but to give us one of the greatest -yet intangible- gifts: our education. Thank you for encouraging me to come here and pursue my science career. Thanks for believing in me, keeping me company in hours-long video calls, and always being concerned if an experiment fails or cells got contaminated. I can only hope to retribute something for all the amazing things you have given me, and I can only hope I have made you proud. Gracias por siempre estar ahí, por todo el apoyo, las palabras de aliento y la paciencia. Ustedes son lo más grande que tengo y cada una de mis metas cumplidas es una señal más de lo mucho que me han dado y todo lo que me inspiran.

Lastly, I would like to thank my amazing and loving husband Kenny Taubenslag. Thank you, love, for being my therapist, cheerleader, and proofreader. Thank you for encouraging me, giving me advice, and being Reviewer 3 whenever I need it. Seeing your progress and completing your training has been inspiring. You are a committed, passionate, and kind physician. Thank you for your support, first from afar and now from my side. This journey hasn't been easy but having you by my side has made it more enjoyable.

.

Table of Contents

List of Figures

List of Supplemental Figures

List of Tables and Supplemental Tables

Abbreviations

2D: Two dimensional

3D: Three dimensional

ABS: Acrylonitrile butadiene styrene

ALK: Anaplastic lymphoma kinase

ApoER2: Apolipoprotein E receptor 2

ASCL1: Achaete-scute homolog 1

ATP: Adenosine triphosphate

BAX: BCL-2 associated X protein

BAK: Bcl-2 homologous antagonist killer

BMP: Bone morphogenetic protein

BRN2/POU3F2: Brain-Specific Homeobox 2/POU Domain Protein 2

ClC3: Cleave caspase 3

CNS: Central nervous system

CTIP2/BCL11B: COUP-TF-Interacting Protein 2/ B-Cell Lymphoma 11B

CUX1: Cut Like Homeobox 1

CUX2: Cut Like Homeobox 2

Dab1: Disabled 1

DLD: Dihydrolipoamide dehydrogenase

DNA/RNA: Deoxyribonucleic acid/ Ribonucleic acid

EB: Embryoid body

ECM: Extracellular matrix

EMT: Epithelial-mesenchymal transition

ESCs/hESCs: Embryonic stem cells/ Human embryonic stem cells

ETC: Electron transport chain

FOXG1: Forkhead box G1

FGF: Fibroblast growth factor

GFAP: Glial fibrillary acidic protein

INDEL: Insertion/deletion

iPSCs/hiPSCs: induced pluripotent stem cells/ Human induced pluripotent stem cells

LS: Leigh Syndrome

MAP2: Microtubule Associated Protein 2

mPAR3: Mammalian partition defective protein 3

MSI1: Musashi RNA binding protein 1

MYTL1: Myelin transcription factor 1 like

mtDNA: Mitochondrial DNA

MT-ATP6: Mitochondrially Encoded ATP Synthase Membrane Subunit 6

MT-ND3: Mitochondrially Encoded NADH:Ubiquinone Oxidoreductase Core Subunit 3

NEUROD1: Neuronal differentiation 1

NESTIN: Neuroepithelial stem cell protein

NGN2: Neurogenin-2

NSC/hNSC: Neural stem cells/ Human neural stem cells

NPC/hNPC: Neural progenitor cells/ Human neural progenitor cells

OCT4/POU5F1: Octamer-Binding Protein 4/ POU Domain Class 5, Transcription Factor 1

oRG: outer radial glia cells

OXPHOS: oxidative phosphorylation

PAX6: Paired Box 6

PBS: Phosphate-buffered saline

PDH: Pyruvate dehydrogenase

PDHc: Pyruvate dehydrogenase complex

PGC-1α: Peroxisomal proliferating activating receptor γ coactivator-1α

PSCs/hPSCs: Pluripotent stem cells (iPSCs & ESCs)/ Human pluripotent stem

PSA-NCAM: Polysialylated neuronal cell adhesion molecule

PTFE: Polytetrafluoroethylene

RA: Retinoic acid

RG: radial glia cells

ROS: Reactive oxygen species

RPM: Revolutions per minute

SATB2: Special AT-Rich Sequence-Binding Protein 2

SFEBq: Serum-free floating culture of embryoid body-like aggregates with quick aggregation

SIM: Structured illumination microscopy

SHH: Sonic Hedgehog

SMAD: Mothers against decapentaplegic

SNP: Single-nucleotide polymorphism

SOX1: Sex-determining region Y-box 1

SOX2: Sex-determining region Y-box 2

SOX5: Sex-determining region Y-box 5

SOX6: Sex-determining region Y-box 6

SOX9: Sex-determining region Y-box 9

SOX10: Sex-determining region Y-box 10

SpinΩ: Spin omega

Spin∞: Spinfinity

sVZ: subventricular zone

SURF1: Surfeit locus protein 1

TBR1: T-Box Brain Transcription Factor 1

TBR2: T-Box Brain Transcription Factor 2

TFAM: Mitochondrial transcription factor A

UV: Ultraviolet

Vldlr: Very low–density lipoprotein receptor

VZ: ventricular zone

WES: Whole exome sequencing

Chapter 1

INTRODUCTION:

PLURIPOTENT STEM CELL DERIVED MODELS FOR THE STUDY OF MITOCHONDRIAL FITNESS IN HUMAN NEUROGENESIS

Adapted from:

Romero-Morales, AI & Gama, V. Revealing the impact of mitochondrial fitness during early neural development using human brain organoids. Under review, Frontiers in Molecular Neuroscience.

I. Introduction

From the brain, and from the brain only, arise our pleasures, joys, laughter and jests, as well as our sorrows, pains, griefs and tears. Through it, in particular, we think, see, hear, and distinguish the ugly from the beautiful, the bad from the good, the pleasant from the unpleasant, in some cases using custom as a test, in others perceiving them from their utility.

-Hippocrates (c. 460 B.C. - c. 370 B.C.)

Studies on human brain function and development have been a topic of controversy and ethical concerns throughout scientific history (Bredenoord et al., 2017; Farahany et al., 2018; National Academies of Sciences, Engineering, 2021; Di Pietro et al., 2012). It is undeniable that access to human-derived material has contributed greatly to the advance of therapies and drugs and expanded our understanding of the processes that have been studied in other biological models. The comparison between different organisms is critical to assess the specie-specific differences that have arisen from evolution and the similarities that have been conserved and can be advantageous for the use of non-human models in translational science.

The human brain has unique characteristics that separate *Homo sapiens* from even our closest primate relatives. Cortical expansion, upper neuronal layer enlargement, increased neuronal diversity and function, complex connectivity and circuitry, are unique features of the human brain (Dehay and Kennedy, 2020; Forbes and Grafman, 2010; Fuster, 2002; Heide et al., 2020; Kaas, 2008; Molnár et al., 2019). The study of how these differences evolved has proven challenging as access to developing human tissue has been limited due to ethical considerations

(Farahany et al., 2018; Greely et al., 2016; Presidential Commission for the Study of Bioethical, 2015).

Although simple in comparison to the human central nervous system (CNS), non-human models have been shown to reproduce the developmental stages, cellular composition, cytoarchitecture, and activity seen in the human brain (Arlotta and Paşca, 2019). The advent of human cellular models, like pluripotent stem cell (PSCs)-derived systems, and the intersection with research in non-human models have propelled human brain development research and complemented each other to advance the existing knowledge.

As the brain consumes nearly 20% of the oxygen and calories from the body (Picard and McEwen, 2014; Raichle and Gusnard, 2002), energetic homeostasis is key for cellular maintenance and survival. Mitochondrial diseases, traditionally linked to disruption in oxidative phosphorylation (OXPHOS), are usually associated with neurological phenotypes such as developmental delay, atrophy, and epileptic encephalopathy (Ortiz-González, 2021; Povea-Cabello et al., 2021). Advances in genomic testing suggests that the causal mutations of mitochondrial diseases includes not only metabolic genes but proteins that affect the mitochondrial shape, motility, recycling and organelle interaction (Baum and Gama, 2021). Hence, mitochondrial adaptation and homeostasis its essential for the execution of the intrinsic developmental programs of neural differentiation and corticogenesis.

II. Human brain development: a finely orchestrated choreography of commitment, migration, and expansion.

The human CNS is composed of approximately 86 billion neurons, with a roughly equal number of glial cells (Herculano-Houzel et al., 2015). Ninety-nine percent of all neurons are located inside the cranium. The cerebral cortex is composed by ~20% of all neurons, although it represents ~50% of the CNS volume (Herculano-Houzel et al., 2015, 2016; Molnár and Pollen, 2014; Sousa et al., 2017)

The human brain has specie-specific characteristics that highlight the need for more representative modeling of development. For example, the developing brain has expanded

proliferative zones (*e.g.*, outer subventricular zone) with diverse subtypes of neural stem and progenitor cells (*e.g.*, outer radial glia (oRGCs)) that facilitate the expansion of the neocortex (Bystron et al., 2008; Molnár et al., 2019; Sousa et al., 2017). The timing and duration of neurogenesis is also a factor to consider when examining the differences between species. Extended human neurogenesis results in an increased number of progenitor cells that give rise to larger neocortical structures with increased number of upper-layer neurons (Hutsler et al., 2005; Smart et al., 2002; Taverna et al., 2014). In addition to the ventricular zone and the cortical plate (discussed in detail below), the human brain contains an additional layer, called the outer subventricular zone. The outer subventricular zone is characteristic for primate brains and it contains oRGCs or basal radial glia cells. In rodent brains, these cells are not present, or present in only very small numbers (Kalebic and Huttner, 2020; Wang et al., 2011a, 2011b). But, in primates, they act as a transit amplifying population during neurogenesis (Fietz et al., 2010; Hansen et al., 2010; Sauerland et al., 2018) contributing to the expansion of the cortex. Developmental studies in rodents segregate the birth of excitatory neurons and interneurons to the progenitors in the cortex and ganglionic eminence, respectively, yet lineage tracing of primary human neural progenitors show that individual cortical progenitors have the capacity to generate both excitatory and cortical interneurons (Delgado et al., 2022).

Human brain development is a prolonged and intricate process that starts around 2 weeks post conception and continues until early adulthood. The initial stages of this process rely primarily on the genetic control and the correct activation of neural programs, although, environmental factors can also affect the efficiency of the process.

a) Initial development: neural tube formation

The genesis of the nervous system initiates about 2 weeks post conception. At this stage, the developing embryo is organized as a three-layered spherical structure. Cells in ectoderm, one of the three germ layers, thicken to form the neural plate. The lateral edges of the neural plate will give rise to the neural folds that will folds on itself and join at the midline forming the neural tube. The closure of these tube occurs from the center to the cranial and caudal ends and defects at this point can cause developmental conditions such as anencephalia and spina bifida. The formation of the neural tube leads to the formation of the central nervous system by the cells

located in the inner part of the tube, while the outer cells will give rise to the peripheral nervous system (Bayer and Altman, 2007; O'Rahilly and Müller, 2005).

Once the neural tube closes, around 4 weeks post-conception, the cranial end of the neural tube will expand to become a three-vesicle structure: the prosencephalon, the mesencephalon, and the rhombencephalon. By week 5 post-conception, the prosencephalon will give rise to the telencephalon, which will correspond with the forebrain and includes the cerebral hemispheres; and the diencephalon that will develop into the thalamus and hypothalamus (O'Rahilly and Müller, 2008). The mesencephalon will give rise to the mature midbrain; and the rhombencephalon will generate the metencephalon which in time will derived the pons and the cerebellum, and the myelencephalon that will develop into the medulla (Bayer and Altman, 2007; O'Rahilly and Müller, 2005, 2010)

Morphogen signaling during this period is crucial for the establishment of the development axis (Figure 1-1). The notochord, a structure derived from the axial mesoderm immediately ventral to the ectoderm (Di Gregorio, 2020; Grow, 2018), and the somites, transient paired structures derived from mesenchymal paraxial mesoderm that flank the neural tube (Cook et al., 2017), define the dorso-ventral axis of the embryo by releasing different signaling molecules (Seal and Monsoro-Burq, 2020).

Fibroblast growth factors (FGF), in particular FGF8, are produced by the paraxial mesoderm, and it's downregulated before neural differentiation (Bertrand et al., 2000; Muñoz-Sanjuán and Brivanlou, 2002). This downregulation is necessary for the expression of early neural transcription factors such as *NEUROM*, *PAX3*, *HES4*, *TFAP2A* and *MSX1* in the neural tube (Bang et al., 1997; Diez del Corral et al., 2002; Garnett et al., 2012; Monsoro-Burq et al., 2005).

Retinoic acid (RA) signaling is produced by the paraxial mesoderm for the induction of neural differentiation and patterning by downregulating the FGF production (Colas and Schoenwolf, 2001; Diez del Corral and Storey, 2004; Franco et al., 1999). Sonic hedgehog (SHH) is produced by the notochord for the ventralization of neural cell types in a concentration dependent manner (Jessell and Dodd, 1990; Liem et al., 2000). WNT signaling is secreted by the paraxial mesoderm and the non-neural ectoderm. Its activation, especially from Wnt3a, is also

important for the induction of posterior patterning (Kiecker and Niehrs, 2001; McGrew et al., 1995). WNT signaling repression is critical for the generation of the anterior neural fate (Yamaguchi, 2001).

Bone morphogenetic proteins (BMPs) are produced by the non-neural ectoderm and the ventral mesoderm. High BMP signaling in the ventral ectoderm promotes the epidermal fate and represses the neural fate. BMP antagonists, such as Noggin, Chordin, Cerberus and Follistatin, are secreted by the Spemann-Mangold organizer (Muñoz-Sanjuán and Brivanlou, 2002; Spemann and Mangold, 1924, 2001), generating a low-to-high gradient of BMP signaling from the midline towards the lateral zones that allows for the neural specification of the dorsal ectoderm (Barth et al., 1999; Lee and Jessell, 1999; Lee et al., 1998; Liem et al., 2000; Nguyen et al., 2000; Ybot-Gonzalez et al., 2007).

b) NPC expansion and Radial Glia cell proliferation

Once the closure of the neural tube is complete, the cells lining the lumen of the tube will develop into the ventricles. This single cell layer of neuroepithelia is a pseudostratified epithelium composed by neuroepithelial progenitor cells (Götz and Huttner, 2005) (Figure 1-2A). These are highly polarized along the apical-basal axis (Chenn et al., 1998). Transmembrane proteins such as prominin-1 are found in the apical plasma membrane, while tight and adherens junctions are present at the apical end of the lateral plasma membrane (Aaku-Saraste et al., 1996; Chenn et al., 1998; Manabe et al., 2002; Zhadanov et al., 1999). Receptors for basal lamina components, such as integrins, are located in the basal plasma membrane that is in contact with the basal lamina (Wodarz and Huttner, 2003).

This epithelium appears as stratified due to the cell nuclei migrating up and down the apical–basal axis during the cell cycle in a process known as interkinetic nuclear migration (Bayer and Altman, 2007; Frade, 2002; His, 1889; Rodrigues et al., 2019; Sauer, 1935; Schaper, 1897). In this process the nuclei migrate to the apical side during mitosis and remains basally during the S phase. This movement exposes the nuclei to diffused morphogens, such as Notch receptor ligand Delta, and influence the fate of the daughter cells (Azizi et al., 2020; Del Bene et al., 2008; Chenn and McConnell, 1995; Chenn et al., 1998; Murciano et al., 2002; Spear and Erickson, 2012).

The neuroepithelial progenitor cells divide in either a symmetric or asymmetric manner (Götz and Huttner, 2005; Huttner and Brand, 1997). Symmetric cell division generate two daughter cells that remain mitotically active and can expand the population of progenitor cells (Kornack and Rakic, 1995; Mione et al., 1997). In contrast, in an asymmetric division at least one of the daughter cells exist the cell cycle and differentiates into a specialized cell (Fishell and Kriegstein, 2003; Qian et al., 1998; Reid et al., 1997; Wodarz and Huttner, 2003).

Rounds of cell division from the neuroepithelial cells form several layers surrounding the lumen (Figure 1-2A-B). The inner-most apical layer becomes populated with the progenitor cells and due to the proximity with the ventricles is known as the ventricular zone (VZ). As asymmetric division mark the beginning of neurogenesis, neuroepithelial cells have been shown to downregulate the expression of tight junction and certain apical plasma membrane proteins (Aaku-Saraste et al., 1996, 1997)

Neuroepithelial cells give rise to a progenitor cell type that is more cell fate-restricted, the radial glial cells (RGC) (Bentivoglio and Mazzarello, 1999; Koelliker, 1896; Magini, 1888). These cells can be observed in the developing embryo as early as week 6 post conception (Choi, 1981). RGCs are characterized by bipolar processes extending to reach the pial and ventricular surfaces, while their cell bodies remain in the VZ (Haubensak et al., 2004; Levitt and Rakic, 1980; Rakic, 1972, 1978). These processes help guide the radial migration of newborn neurons from the ventricular zone. Moreover, these cells share some astrocytic characteristics such as glycogen granules and the expression of the intermediate filament protein, glial fibrillary acidic protein (GFAP) (Choi, 1981; Levitt and Rakic, 1980) and VIMENTIN, as well as brain-lipid-binding protein (BLBP) (Hartfuss et al., 2001). RGCs also maintain the expression of the neuroepithelial marker NESTIN (Campbell and Götz, 2002; Chanas-Sacre et al., 2000; Pixley and de Vellis, 1984), apical-basal polarity with the presence of adherence junctions (Aaku-Saraste et al., 1996; Wodarz and Huttner, 2003), basal lamina contact (Halfter et al., 2002), and interkinetic nuclear migration. Regionalization of the brain is also an ongoing process at this stage. Dorsal RGCs express the neural progenitor marker Paired box protein 6 (PAX6) (Götz et al., 1998) which commit them into a cortical fate; while the ventral RGCs express the cellular retinol-binding protein (RBP-1) (Toresson et al., 1999) and will commit to form the basal ganglia.

Prior to the peak in neurogenesis, RGCs divide symmetrically to amplify the progenitor cell population. However, during the peak phase of neurogenesis, radial glial cells primarily divide asymmetrically to both self-renew and giving rise to outer radial glia (oRGCs), intermediate progenitors (IPCs), astrocytes or neurons (Alvarez-Buylla et al., 2001; Anthony et al., 2004; Kriegstein and Alvarez-Buylla, 2009; Malatesta et al., 2000, 2003; Miyata et al., 2001; Noctor et al., 2001). The cell fate specification during the asymmetrical neurogenesis has been associated with the subcellular distribution of the mammalian partition defective protein 3 (mPAR3) by differentially regulating Notch signaling activity in the two daughter cells (Bultje et al., 2009)

Outer radial glia and intermediate progenitors will establish the subventricular zone (SVZ) around week 9 post conception (Zecevic et al., 2005). oRGs retain the basal processes but lack the apical junctions (Miyata et al., 2001), and undergo a distinct migratory behavior or mitotic somal translocation before undergoing cell division (Fietz et al., 2010; Hansen et al., 2010; Wang et al., 2011b). These cells can also undergo proliferative and asymmetric cell divisions and require Notch signaling to induce neuronal differentiation (Hansen et al., 2010; Kowalczyk et al., 2009). IPCs are transient amplifying cells with limited proliferative divisions, which are predominantly symmetrical to produce two neurons (Haubensak et al., 2004; Kowalczyk et al., 2009; Noctor et al., 2001; Sessa et al., 2008, 2010; Wu et al., 2005). These cells have multipolar morphology and are not anchored to either the apical or basal cortical surface (Haubensak et al., 2004; Noctor et al., 2001). IPCs contribute to radial expansion and folding of the human brain (Baala et al., 2007; Englund, 2005; Miller et al., 2019) and have been associated to the generation of the upper cortical layers (Arnold et al., 2008; Lv et al., 2019; Martínez-Cerdeño et al., 2006).

The different types of progenitors can be identified not only by their morphology and presence of polarizing membrane proteins, but by the expression of certain fate markers (Figure 1-2C). Radial glia express PAX6, a homeodomain transcription factor, in contrast IPCs upregulate T-Box Brain Protein 2 (TBR2), a T-domain transcription factor, and downregulate PAX6 (Englund, 2005). oRGCs and SVZ progenitors also express the non-coding RNA subventricular-expressed transcript 1 (SVET1) (Tarabykin et al., 2001), as well as the transcription factor Cut Like Homeobox2 (CUX2) (Nieto et al., 2004; Zimmer et al., 2004). Moreover, oRGs preferentially

express genes related to extracellular matrix formation, migration, and stemness (Fan et al., 2020; Nowakowski et al., 2017; Pollen et al., 2015).

c) Corticogenesis: neural differentiation and migration

The generation of cortical neurons, or corticogenesis, can be distinguished by the enlargement of the SVZ that has an inner (ISVZ) and outer region (OSVZ), and it is separated by a thin fiber layer (Zecevic et al., 2005). Cells undergoing mitosis can be observed in all levels of the SVZ, in contrast with the VZ where mitotic cells are only found in the ventricular surface (Smart et al., 2002) (Figure 1-2A-B).

Early born neurons migrate away from the ventricular surface, segregating themselves from the progenitors and forming the preplate. The first wave of neurons is composed by specialized pioneering cells or Cajal-Retzius neurons. These neurons organize adjacent to the pial surface forming the marginal zone, that in the adult human brain correspond with Layer I (Marin-Padilla, 1978; Raedler and Raedler, 1978) and that act as the stop sign for neuronal migration (Tissir and Goffinet, 2003). These cells secrete REELIN, a large extracellular matrix glycoprotein. REELIN regulate processes of neuronal migration and positioning in the developing brain by controlling cell–cell interactions specifically by binding to the transmembrane receptors, the very low–density lipoprotein receptor (Vldlr), and the apolipoprotein E receptor 2 (ApoER2) present on migrating neurons (D'Arcangelo et al., 1995; Hiesberger et al., 1999). The binding of REELIN to the previously mentioned receptors induces the phosphorylation of Disabled 1 (Dab1), a cytosolic protein that activates tyrosine kinases (Kim et al., 2002; Trommsdorff et al., 1999) that in time modulates the phosphorylation of Tau affecting the assembly and stability of the neuronal cytoskeleton (Hiesberger et al., 1999; Rice and Curran, 2001). REELIN also interacts with α3β1 integrin, which regulates neuron–glia interactions by and promoting the detachment of the migratory neuron from the radial glia via Dab1 and is required to achieve proper laminar organization (Dulabon et al., 2000).

As new neurons are born and start migrating into the preplate, this area is divided into the marginal zone, which is pushed outwards, and the subplate (Molnár et al., 2019). The subplate is a voluminous yet transient compartment in the cerebral wall composed of post-

migratory and migratory neurons, glia and axons; as well as of abundant extracellular matrix (Hoerder-Suabedissen and Molnár, 2015; Kostovic and Rakic, 1990). This structure is key for the correct formation and subsequent function of the brain as it is involved in the formation of neural circuits (Kostovic and Rakic, 1990).

Between the marginal zone and the subplate, new born neurons migrate and organize forming the cortical plate around post-conception weeks 8-9 (Clancy et al., 2001). In this area, the nascent neurons stop migrating and differentiate into their final laminar identity in an inside-out fashion (Greig et al., 2013), with newer born neurons positioning closer to the marginal zone (Leone et al., 2008; Marín-Padilla, 2014; Molyneaux et al., 2007; Shibata et al., 2015). Hence, neurons of the deepest layers (VI and V) are generated at the earliest stages, followed by neurons of layers IV, III, and II. For the neuronal maturation process, final positioning of the neurons is required; and can last until early adulthood in humans (Huttenlocher, 1979; Petanjek et al., 2008, 2011).

Cortical neurons are generated primarily (~80%) by IPCs, while the other 10-20% can be traced back to RGCs (Kowalczyk et al., 2009; Vasistha et al., 2015) (Figure 1-2A). Moreover, cortical progenitors undergo fate restriction as they produce new neurons. Late cortical progenitors are not capable to generate earlier neuronal fates even when exposed to environments that mimic the early stages of corticogenesis (Desai and McConnell, 2000; Frantz and McConnell, 1996; Walsh and Cepko, 1993). This fate restriction has been associated with changes in the length of the cell cycle and the number of divisions before terminal differentiation (Calegari et al., 2005; Pilaz et al., 2009; Shen et al., 2006).

Fate acquisition has also been linked with the expression of subtype-specific transcription factors expressed in progenitors before neurogenesis; suggesting an early commitment to a particular cortical layer (Greig et al., 2013) (Figure 1-2C). The transition from the pioneering Cajal-Retzius cells into the generation of deep-layer neurons has been shown to be mediated by the repression of the transcription factor Forkhead Box G1 (FOXG1) in neural progenitors (Hanashima et al., 2004).

Deep-layer progenitors express the transcription factors FEZF2 (Fez family zinc finger 2), OTX1 (Orthodenticle Homeobox 1), and EMX2 (Empty Spiracles Homeobox 2) (Chen et al., 2005; Frantz et al., 1994; Inoue et al., 2004; Leingärtner et al., 2003; Lodato et al., 2014; McKenna et al., 2011) that have been associated with neurons present in layers VI and V. OTX1, for example, is expressed in ventricular zone precursors that will give rise to cortical layers VI and V, but it is downregulates in progenitor cells that are committed to upper layer neurogenesis (Frantz et al., 1994; Weimann et al., 1999).

The generation of layer VI neurons, around post-conception week 11-12 (Clancy et al., 2001), is mediated by the expression of the transcription factor T-Box Brain Protein 1 (TBR1) (Bedogni et al., 2010; Hevner et al., 2001). TBR1 downregulates the expression of FEZF2 (Han et al., 2011) and CTIP2 (COUP-TF-Interacting Protein 2) (McKenna et al., 2011) by binding to the *FEZF2* gene and inhibiting its transcription. FEZF2 acts upstream of CTIP2 to control the differentiation of layer V neurons (Arlotta et al., 2005; Chen et al., 2005) by reducing TBR1 expression (McKenna et al., 2011). TBR1 expression is also downregulated directly by FOXG1 and indirectly by the FOXG1 mediated upregulation of FEZF2 (Toma et al., 2014). Moreover, SOX5 (Sex Determining Region Y-Box 5) directly represses FEZF2 by binding to a required enhancer element for its expression (Kwan et al., 2008; Lai et al., 2008; Shim et al., 2012) and induces the activation and maintenance of TBR1 (Bedogni et al., 2010).

As deep layer progenitors express OTX1 before neurogenesis, upper layer progenitors express the noncoding RNA *SVET1*. The expression of this marker is exclusive of layer II-IV and its activation is dependent on the correct expression of PAX6 (Tarabykin et al., 2001). Expression of *SVET1* has been also identified in IPC-derived upper cortical layer neurons (Molyneaux et al., 2007)

Transition to the production of upper layer neurons is mediated by the interaction of *FEZF2*, *CTIP2*, *TBR1*, and *SATB2* (Special AT-Rich Sequence-Binding Protein 2). TBR1 is a downstream target of SATB2, and its repression is necessary for the differentiation of layer IV neurons (Srinivasan et al., 2012). Moreover, downregulation of FEZF2 by negative feedback (Toma et al., 2014) is necessary for the acquisition of SATB2 expression (Chen et al., 2008), and

in time, SATB2 binds to and represses the expression of *CTIP2* (Alcamo et al., 2008; Britanova et al., 2008).

Co-expression of Brain-Specific Homeobox/POU Domain Protein 1 (BRN1) and Brain-Specific Homeobox/POU Domain Protein 2 (BRN2/POU3F2) in most layer II-V cortical neurons is preceded by its expression in VZ progenitors and they are required for the control of radial migration in neurons residing in those cortical layers (Dominguez et al., 2013; McEvilly et al., 2002). Moreover, disruption in the expression of these transcription factors causes defective migration of neurons due to the inability of the neurons to express Dab1 (Sugitani et al., 2002)

Expression of the transcription factor CUX2 in progenitors has been associated with the generation of cortical neurons from layers II/III (Molyneaux et al., 2009; Nieto et al., 2004; Zimmer et al., 2004) at post-conception week 12 (Clancy et al., 2001). This predisposition to generate upper layer neurons is observed in the progenitor cells in the VZ that undergo proliferative cell division during the phase of deep-layer neuronal generation. These cells then switch to neurogenic differentiation to generate superficial-layer neurons (Franco et al., 2012). CUX1 and CUX2 are also part of the regulatory network modulated by FEZF2, where its inactivation allows for the progression to upper layer specification (Lodato et al., 2014).

d) Gliogenesis

During cortical neurogenesis, the promoters for astrocytic fate, such as GFAP, are heavily methylated and inaccessible to be activated by STAT3 (Signal Transducer And Activator Of Transcription 3) (Takizawa et al., 2001). Expression of Neurogin 1 (NGN1) competes with STAT3 for the EP300-SMAD activator complexes and suppress the JAK/STAT and BMP signaling pathway (Sun et al., 2001). At the end of neurogenesis, levels of NGN1 drop and the *GFAP* promoter is demethylated to induce astrocytic fate and promote the differentiation of radial glia cells into glial progenitors (Takizawa et al., 2001). This demethylation of the astrocyte-specific genes is mediate by the Notch signaling pathway activation of the nuclear factor IA(NFIA) (Deneen et al., 2006; Namihira et al., 2009). NFIA is also directly regulated by SOX9 (Sex Determining Region Y-

Box 9), with the SOX9/NFIA complex directly regulating genes implicated in astrocyte precursor migration and metabolism (Kang et al., 2012).

Astrocytes arise from radial glia in the ventricular zone and PAX6+/HOPX+ oRGs in the outer subventricular zone (Cameron and Rakic, 1991; Ge et al., 2012; Kriegstein and Alvarez-Buylla, 2009; Noctor et al., 2008; Rash et al., 2019; Zweifel et al., 2018) around post-conception week 12 (Empie et al., 2015). Local proliferation of differentiated astrocytes that undergo symmetric division generate mature astrocytes (García-Marqués and López-Mascaraque, 2013) that are able to form endfeet with blood vessels and are perform functions such as glutamate uptake (Ge et al., 2012).

Another class of glial cells, oligodendrocytes, originate from precursors in the proliferative dorsal and ventral zones of the developing brain (Richardson et al., 2006). These cells migrate to the developing white matter, divide, and terminally differentiate. The activation of the transcription factors OLIG1 (Oligodendrocyte Transcription Factor 1) and OLIG2 (Oligodendrocyte Transcription Factor 2) are indispensable for the oligodendroglial fate acquisition. OLIG1 directly binds to DLX1/2 (Distal-Less Homeobox 1/2) enhancers to repress neurogenic fate and induce the expression of OLIG2 (Petryniak et al., 2007; Silbereis et al., 2014). ASCL1 (Achaete-Scute Family BHLH Transcription Factor 1) is also downregulated in the transition from NPCs to oligodendrocyte progenitor cell, although its expression in these cells is biphasic as it needs to be upregulated again for oligodendrocyte terminal differentiation (Battiste et al., 2007; Dimou et al., 2008; Sugimori et al., 2008). Expression of several SOX (Sex Determining Region Y-Box) members is key for the specification and differentiation of oligodendrocytes. SOX5 and SOX6 are expressed in oligodendrocyte progenitor cells and influence migration patterns, while SOX10 induces terminal differentiation and myelin gene expression (Stolt et al., 2002, 2006)

SHH signaling, through the activation of OLIG2, is necessary for oligodendrocyte development (Agius et al., 2004); yet their maturation is SHH independent (Orentas et al., 1999; Soula et al., 2001). Expression of the EGF receptor has also been associated with the generation of OPCs (Huang et al., 2020). EGFR-expressing oRGs may act as intermediate progenitors for oligodendrogenesis and potentially amplify the OPC progenitor pool (Huang et al., 2020). BMP and WNT expression have been shown to oppose oligodendrocyte cell fate and directing the

progenitors into an astrocyte fate (Mekki-Dauriac et al., 2002; Samanta and Kessler, 2004; Shimizu et al., 2005).

III. hPSC derived models for the study of brain development

The study of human embryonic development *in vitro*, specifically organogenesis and cell fate specification, has been greatly improved by the isolation and maintenance of pluripotent stem cells (Evans and Kaufman, 1981; Thomson and Marshall, 1998; Thomson et al., 1995, 1998). The accessibility to somatic cells and the ability to reprogram them into induced pluripotent stem cells (Takahashi and Yamanaka, 2006; Takahashi et al., 2007) has increase the ability to model developmental diseases that are considered rare or difficult to phenocopy in model organisms (Saha and Jaenisch, 2009). This, coupled with the ability to generate differentiated cells such as neurons (Vierbuchen et al., 2010; Zhang et al., 2001), has allowed for the expansion of the repertoire of techniques to model and study human brain development in vitro (Figure 1-3).

a) 2-D derived neurons

The generation of neural cells was based on observations of the grafting effects of mouse teratocarcinoma lines in early embryos and *in vitro* (Jones-Villeneuve et al., 1983). Cell aggregation in addition to treatment with retinoic acid (RA) was observed to promote the differentiation of mouse stem cells into cells expressing neuronal genes and capable of generating action potentials (Bain et al., 1995). The use of morphogens for the maintenance and generation of neuroepithelial precursors was highlighted by the use of basic fibroblast growth factor (bFGF or FGF2) (Mujtaba et al., 1999; Okabe et al., 1996). Removal of this compound promoted the differentiation of functional neuronal cells that were able to be cultured long term (Okabe et al., 1996). Furthermore, these ESCs-derived neural precursors were shown to be able to graft to embryonic ventricles and migrate without positional cues into the host brain to contribute to the three lineages of the nervous system (Brüstle et al., 1997).

The first account of human neural precursor cells differentiation from hESC was generated by the Thomson and Ben-Hur laboratories in 2001. After aggregation in embryoid bodies, generated neural tube-like structures in the presence of FGF2 (Reubinoff et al., 2001;

Zhang et al., 2001). Removal of this morphogen promoted differentiation into the neural lineages *in vitro*, while transplantation into the neonatal mouse brain allowed for their incorporation to different brain regions and further maturation into neurons and astrocytes.

An improved protocol that did not rely on embryoid bodies was generated by the Studer lab in 2009. Rapid and highly efficient neural conversion under adherent culture conditions was obtained by the synergistic use of two SMAD signaling pathway inhibitors: Noggin and SB431542 (Chambers et al., 2009). Noggin is a bone morphogenic protein (BMP) inhibitor identified initially in *Xenopus laevis* with neural-inducing properties following a dorsal fate pattern (Gerrard et al., 2005; Lee et al., 2007; Smith and Harland, 1992; Valenzuela et al., 1995). The drug SB431542 is an antagonist that inhibits the Nodal/Activin/Transforming growth factor β (TGFβ) pathways by blocking phosphorylation of the ALK4, ALK5 and ALK7 receptors. Activin and Nodal are responsible of mesodermal and endodermal differentiation during gastrulation, the inhibition of these pathways allows for an ectodermal and neural fate induction both *in vivo* and *in vitro* (Schier, 2003; Smith et al., 2008).

NPC fate is determined by the expression of neuroectoderm markers such as Sex Determining Region Y-Box 1 (SOX1), PAX6 and Neuroepithelial stem cell protein (NESTIN). The intermediate filament NESTIN is expressed in both neuroepithelial cells and radial glial cells with different morphologies depending on the cell type and size (Götz and Barde, 2005). Expression of SOX1 can be observed upon neuroectoderm formation. Subsequent expression of PAX6 is noted as early as the first somite formation and the closing of the neural fold in the cranial region (E8.0 in mouse and stage 10 in human). PAX6 is also expressed in radial glial cells, the precursors for most neurons of the cerebral cortex (Callaerts et al., 1997; Englund, 2005; Thakurela et al., 2016). The switch between SOX1 and PAX6 during neural fate commitment is required for the correct differentiation into committed cell types. Continuous expression of SOX1 inhibits the expression of PAX6 and other radial glial cell markers. PAX6 expression induces cell migration and differentiation into neurons (Cartier et al., 2006; Heins et al., 2002; Suter et al., 2009).

Further differentiation to different neuronal cell types from different parts of the CNS have been achieved (Pankratz et al., 2007; Zeng et al., 2010). Previous studies using mice and other model organisms expanded the knowledge on morphogens and growth factors required

for neural development (Gaspard et al., 2008). NPCs with anterior patterning fate have been used to generate dopaminergic neurons after exposure to FGF8 for anterior-posterior axis induction and signal SHH as a ventralizing signal (Perrier et al., 2004). Spinal motoneurons can be generated by the presence of SHH and the retinoic acid to promote the posterior axis fate (Lee et al., 2007; Li et al., 2005). Functional cortical glutamatergic neurons and telencephalic GABAergic neurons can also be generated by the manipulation of the endogenous WNT signaling in the NPCs (Li et al., 2009). Cerebral cortex development can also be recapitulated by the sequential generation of pyramidal neurons that express the markers of the different cortical layers (Espuny-Camacho et al., 2013; Shi et al., 2012).

As an alternative to hPSC-derived neurons, direct differentiation from somatic cells into functional NPCs and neurons have been achieved, using either genetic or chemical manipulation of the embryonic pathways that promote transdifferentiation. The transcription factors BRN2, ASCL1, Myelin Transcription Factor 1-Like Protein (MYTL1), and Neurogenic differentiation 1 (NEUROD1); as well as the microRNAs miR-9* and miR-124, were initially used to generate different types of neurons from fibroblasts (Ambasudhan et al., 2011; Caiazzo et al., 2011; Pang et al., 2011; Pfisterer et al., 2011b, 2011a; Son et al., 2011; Yoo et al., 2011). Single transcription factors, such as Sex Determining Region Y-Box 2 (SOX2) (Ring et al., 2012) and NEUROGENIN-2 (*NGN2*) (Zhang et al., 2013) have been utilized to generate functional excitatory cortical neurons.

b) Neural rosettes

The earliest *in vitro* recapitulation of nervous system development are neural rosettes (NR). These structures correspond to the third week of gestation (Chandrasekaran et al., 2017) and recapitulate the initial stages of central nervous system development. NRs are composed of long, radially organized, columnar neuroepithelial cells surrounding a central cavity or lumen (Chandrasekaran et al., 2017; Elkabetz et al., 2008; Hříbková et al., 2018; Zhang et al., 2001). NRs present apical-basal polarity, with the localization of apical markers (e.g. ZO1, N-Cadherin, β-Catenin) and interkinetic nuclear migration. Additionally, cells in NRs are positive for neuroepithelial markers such as PAX6, SOX1, NESTIN, Mushahi-1 (MSI1) and polysialylated neuronal cell adhesion molecule (PSA-NCAM). These cells also show self-renewal capacity, engraftment capacity, and can differentiate into different region-specific neural and glial types in

response to developmental cues (Elkabetz et al., 2008; Grabiec et al., 2016; Knight et al., 2018; Koch et al., 2009; Li et al., 2005; Perrier et al., 2004; Zhang et al., 2001).

NR-neural stem cells (NR-NSCs) can be isolated, expanded, and regionally specified without losing the rosette properties. Maintenance of the multipotency capacity has been shown to depend on the Notch signaling pathway, as low plating densities or the pharmacological inhibition of the pathway, increases the neuronal differentiation and causes a reduction in the rosette formation efficiency. Activation of the SHH has also been shown to be a key pathway in the maintenance of multipotency of NR-NSCs. Inhibition of both pathways cause rapid loss of rosette organization and reduction in the differentiation capacity (Elkabetz et al., 2008).

Although the default fate pathway for NR cells is the anterior CNS pattern by the expression of FOXG1 (Koch et al., 2009; Tao and Lai, 1992), re-specification towards caudal fates can be accomplished: midbrain and hindbrain neurons can be obtained by FGF8/SHH treatments, and spinal motor neurons can be generated by incubation in RA/SHH (Elkabetz et al., 2008; Perrier et al., 2004). Furthermore, NRs with ZO1 expression and interkinetic nuclear migration can also be spontaneously generated from NPC monolayer differentiation via dual SMAD inhibition (Chambers et al., 2009).

Neural rosettes formation consists of five morphogenetic changes: intercalation of two or more cell rows, cellular constriction or shrinkage, polarization, elongation, and lumen formation. The formation of the lumen is mediated by apoptosis, abolition of the cell death via caspase inhibition disrupts lumen formation and retard neurogenesis. Moreover, Ca^{2+} regulation plays a critical role in the formation of the NR by regulating multiple cytoskeletal proteins during the first three morphogenesis events. Calcium dysregulation also affects the localization of the polarizing proteins ZO1, PARD3 and β-catenin, which in turn impairs lumen formation. Disruption of the cytoskeleton (specifically actin, myosin II and tubulin) promotes premature neurogenesis and astrogenesis (Hříbková et al., 2018).

FGF and BMP signaling are also necessary for the correct formation of the NRs. FGF2 and its receptor FGFR1 present an apical polarization in the lumen of the NR. FGF2 overexpression or inhibition disrupts the formation of the NRs and affects ZO1 expression and localization. The

malformation of the NRs can be mediated by the displacement of ZO1 from the apical membrane which in time disrupts the membrane anchorage of FGFR1, causing the disruption on FGF2 signaling gradient, reduced cell proliferation, cell cycle exit and the premature differentiation of the NPCs (Grabiec et al., 2016). BMP signaling has been associated to the complex cluster formation of the NR. Inhibition of the pathway causes disrupted rosette morphology and alters the expression of the NSC markers PAX6, SOX2 and SOX1 (Fedorova et al., 2019).

c) Brain organoids

The brain organoid field started with the groundbreaking observations of the Yoshiki Sasai group. These initial studies demonstrated the ability of mouse ESCs to directly differentiate into telencephalic precursors in a serum-free suspension culture (SFEB culture). Treatments with WNT and Nodal antagonist resulted in a high yield of PAX6+ cells that could be further differentiated into ventral or dorsal fate after WNT3a or SHH, respectively (Watanabe et al., 2005). Optimization of the SFEB culture media by the inclusion of a BMP inhibitor and the introduction of Y-27632, the selective Rho-associated kinase (ROCK) inhibitor, allowed to translate these findings to human derived systems (Watanabe et al., 2007).

The derivation of optimized mouse and human culture media allowed for the generation of three-dimensional aggregates that recapitulate embryonic corticogenesis and regional specification (Eiraku et al., 2008). Polarized cortical neurepithelia resembling neural rosettes positive for the expected markers were observed in the floating aggregates. Moreover, cortical specification was obtained, mimicking early corticogenesis with the segregation of discrete layers containing radial glia, neuronal progenitors, and early neurons (Eiraku et al., 2008; Kadoshima et al., 2013; Mariani et al., 2012). Additionally, gene expression profile in these aggregates correlate with the embryonic telencephalon, specifically to the transcriptional program active at 8-10 weeks after conception (Mariani et al., 2012).

Cerebral organoids can be generated via undirected or directed differentiation. The undirected differentiation technique was described by the Knoblich group in 2013 (Lancaster et al., 2013). Single cell hPSCs were aggregated in a serum free media and then embedded in an extracellular matrix (ECM). The presence of ECM supports the formation of neuroepithelial buds

that expand into cortical structures under constant agitation (Lancaster and Knoblich, 2014; Lancaster et al., 2013; Renner et al., 2017). The lack of external signaling to induce patterning allows for the formation of organoids with various brain region identities and non-neural derivatives (Camp et al., 2015; Quadrato et al., 2017). Although variable, undirected organoids allow for a high degree of diversity in the cultures that serve as a platform to explore the CNS diversity and the effects of diseases onto different cell types (Kanton et al., 2019; Lancaster et al., 2017; Pașca, 2018; Velasco et al., 2019).

Directed differentiation uses small molecules to induce regional specification (Kadoshima et al., 2013). The absence of ECM, as well as static conditions, allows for the formation of spherical cultures that can be further differentiated into dorsal and ventral aggregates (Birey et al., 2017; Paşca et al., 2015; Sloan et al., 2018), enriched with astrocytes (Sloan et al., 2017) or oligodendrocytes (Marton et al., 2019). Long term culture of these spheroids allows for the continuous maturation and differentiation of the structures allowing for the exploration of brain development in mid-fetal stages (Gordon et al., 2021; Paşca et al., 2015; Sloan et al., 2017; Yoon et al., 2019). Regional patterning can also be achieved using shaking conditions such as miniaturized bioreactors to generate forebrain, midbrain and hypothalamus organoids (Qian et al., 2016, 2018).

d) Challenges and limitations of iPSCs models

Although a remarkable system to study neural development, iPSC-derived models present a set of limitations: cellular variability, lack of maturation, and limited reproduction of the brain cellular complexity (Dolmetsch and Geschwind, 2011; McTague et al., 2021; Qian and TCW, 2021; Volpato and Webber, 2020; Yamanaka, 2020). These limitations must be considered when translating findings to human development.

The generation of NPCs relied on the differentiation of the hPSCs into neuroectodermal fate (Chambers et al., 2009; Dhara and Stice, 2008), which continues into a preferential acquisition of dorsal forebrain identity (Nat et al., 2007; Watanabe et al., 2005; Zhang et al., 2018). Supplementation of exogenous SHH is necessary for a ventral fate acquisition (Liu et al.,

2013; Maroof et al., 2013; Nicholas et al., 2013; Ribes and Briscoe, 2009; Tao and Zhang, 2016), as the default dorsal identity is partially due to NPC expression of WNT ligands (Li et al., 2009). Moreover, variability in the capacity of the cells to generate NPCs based on its embryonic or induced origin has been reported (Koyanagi-Aoi et al., 2013), but a more in depth proteomic and genomic characterization has not been done.

Similarities of iPSC-derived cortical neurons to primary cortical neurons have been established through single cell analysis but, layer-specific subtype characterization remains challenging (Handel et al., 2016). NPC cultures are heterogeneous, with mixed populations of neural stem and progenitor cells during the first stages of differentiation. At later stages, combinations of neuron and astrocyte populations can be obtained in an stochastic manner (Hoffman et al., 2017, 2019). This can affect not only the functionality of each subtype but their maturation stage (Brennand et al., 2015). A cleaner, more mature neuronal population can be obtained using direct differentiation methods (Meijer et al., 2019; Mertens et al., 2018; Rhee et al., 2019), yet transfection and selection stress can influence the quality of the cell types that are generated.

Generation of astrocytes and oligodendrocytes is also challenging. Glial cell types appear later in development and require changes in the developmental cues. Current protocols, especially for oligodendrocyte generation, require the use of multiple small molecules and morphogens as well as month-long maintenance to generate cell populations suitable for experimentation (Douvaras and Fossati, 2015; Douvaras et al., 2014; TCW et al., 2017).

Due to the lack of vascularization, brain organoids display limited growth (Lancaster et al., 2013). Brain organoids generate neurons positive for the six different cortical layers, but layer organization as well as axonal projection patterns lack the expansion seen in similar developmental stages. Moreover, certain structures that are clearly delimitated in the developing brain -such as the subplate and the cortical plate- are difficult to differentiate (Qian et al., 2019). Likewise, intrinsic generation of non-neural cell types such as microglia, vascular cells, and immune cells; requires co-culturing conditions.

Another limitation of the brain organoid system is the inability to recapitulate developmental gradients. Fusion of regional aggregates has been useful to study neural migratory patterns and complex interregional interactions (Bagley et al., 2017; Birey et al., 2017; Miura et al., 2020; Xiang et al., 2017, 2019), but this approach requires the individual generation of the brain regions. The main hurdle to overcome is the correct localization and concentration of morphogens. A pioneering study by the Studer laboratory generated a SHH ventralizing gradient by utilizing a two-step EB formation process (Cederquist et al., 2019). First, a doxycycline-inducible hPSC line capable of expression of the morphogen was used. Sequentially, additional hPSCs were seeded around the SHH signaling EB, creating an organizing center. This approach successfully produces telencephalic organoids with a dorsal-ventral axis. Organoid-on-chip approaches are also being explored. Morphogen-soaked beads positioned near developing cerebral organoids have shown the effects of WNT and BMP4 gradients (Ben-Reuven and Reiner, 2020). WNT inhibition and BMP4 induction generated changes in the transcriptional profile of the areas proximal and distal to the bead, in a concentration dependent manner. These results suggest that recapitulating developmental morphogen gradients may require a combined approach between engineering and developmental biology. The brain organoids system recapitulates some aspects of human CNS development and complementation with other model systems and approaches can expand their capability and potential.

IV. Mitochondrial homeostasis and neural development

Mitochondria are ubiquitous and essential organelles for cell survival. Known primarily for their capacity to generate energy via oxidative phosphorylation (OXPHOS) and their role in cell death, mitochondria also act as a signaling hub and coordination center for a myriad of cellular processes including metabolite synthesis and calcium buffering. Mitochondrial network remodeling, through fusion and fission, is necessary for discarding damaged or not functional mitochondria (mitophagy), to adapt to new energetic requirements, and to redistribute the organelle throughout the cytoplasm (motility) (Anesti and Scorrano, 2006; Barnhart, 2016; Chan, 2012; Cogliati et al., 2013; Giacomello et al., 2020; Schwarz, 2013).

a) Mitochondrial form and function

i) Bioenergetics

The energy producing machinery of the mitochondria is located in the crista, invaginations of the inner mitochondrial membrane that increase the surface area (Cogliati et al., 2016). The proteins responsible for OXPHOS comprise five different complexes that assemble further into supercomplexes (Acín-Pérez et al., 2008; Dudkina et al., 2005; Schägger and Pfeiffer, 2001). These complexes couple the oxidation of reducing molecules, such as NADH and $FADH_2$, to the translocation of protons across the inner membrane. This influx of protons generates a proton electrochemical gradient that is used by the ATP synthase to generate ATP from ADP.

All five complexes are localized along the cristae membrane with an overlapping distribution (Wilkens et al., 2013). The formation of supercomplexes optimizes the electro transport and proton shuttling through the inner membrane (Acín-Pérez et al., 2008; Letts and Sazanov, 2017). ATP synthase is localized on the edges of the cristae forming dimers, with the other complexes located along both sides (Davies et al., 2011). This configuration seems to be fundamental for the creation of the proton gradient that accumulates in the concave side of the cristae (Rieger et al., 2014; Strauss et al., 2008).

The correct formation and maturation of the cristae is considered a hallmark of cellular maturation and differentiation. Pluripotent stem cells have fragmented mitochondria with immature cristae (Rafalski et al., 2012) and while oxidative phosphorylation still occurs, they rely preferentially on glycolysis for energy production (Chung et al., 2010; Piccoli et al., 2005; Prigione et al., 2010; Zhang et al., 2011). The differentiation of stem cells into neural stem cells is coupled to metabolic shifts that are essential. Inability to transition from glycolysis to OXPHOS during neural induction causes cell death in ESCs and iPSCs (Zheng et al., 2016a).

Besides ATP production, the mitochondria is a signaling organelle central to the production of TCA cycle metabolites such as citrate and oxaloacetate that can then generate macromolecules such as lipids and nucleotides (Chakrabarty and Chandel, 2021; DeBerardinis and Chandel, 2020; Martínez-Reyes and Chandel, 2020). The mitochondria also mediates the release of signaling molecules from the mitochondria (e.g., acetyl-coA, cytochrome c, and free

calcium) that control cell fate and function (Martínez-Reyes and Chandel, 2020). These aspects of mitochondrial signaling beyond ATP production are certainly crucial during the cellular transitions that underlie human brain development.

ii) Mitochondrial dynamics

The active remodeling of the mitochondrial network is crucial for the homeostatic and metabolic adaptation of the cell. Mitochondria are highly dynamic organelles that undergo fission and fusion event according to the cellular and environmental necessities. These highly conserved processes are regulated by large dynamin-related GTPases (Chan, 2012; Chen and Chan, 2004; Hoppins et al., 2007; Praefcke and McMahon, 2004).

Mitochondrial fission or fragmentation is executed by the highly conserved protein Dynamin-related protein 1 (DRP1) (Labrousse et al., 1999; Otsuga et al., 1998; Smirnova et al., 1998). Activation of DRP1, by multiple post-translational modifications, is required for its function at the outer mitochondrial membrane (Chang and Blackstone, 2010; Chou et al., 2012; Han et al., 2008; Prieto et al., 2016; Taguchi et al., 2007). At this site, DRP1 binds to adaptors located at the outer mitochondrial membrane. Mitochondrial fission 1 (FIS1), mitochondrial fission factor (MFF), and mitochondrial dynamics protein 49/51 (MID49/MID51) have been shown to be involved in DRP1 mediated fission (Gandre-Babbe and Van Der Bliek, 2008; Griffin et al., 2005; James et al., 2003; Liu and Chan, 2015; Mozdy et al., 2000; Osellame et al., 2016; Otera et al., 2010; Palmer et al., 2013; Shen et al., 2014; Tieu et al., 2002). DRP1 self-assembles in rings around the mitochondrial membranes where undergoes conformational changes mediated by GTP hydrolysis and constricts the organelle until it divides (Ingerman et al., 2005; Mears et al., 2011).

Mitochondrial fusion occurs when the outer and inner mitochondrial membrane merge with the corresponding membranes on another mitochondrion. Both fusion events are coordinated and occur simultaneously, resulting in the mixing of the mitochondrial contents in the matrix, membranes and intermembrane space and the homogenization of the mitochondrial DNA (mtDNA) and the formation and assembly of the electron transport chain (ETC) (Chan, 2012). Although coordinated, the fusion of the membranes is directed by distinct mechanisms.

Mitofusin 1 (MFN1) and Mitofusin 2 (MFN2) are the proteins responsible for the outer membrane fusion, while optic atrophy 1 (OPA1) mediates inner membrane fusion (Alexander et al., 2000; Chen et al., 2003; Delettre et al., 2000; Rojo et al., 2002; Santel and Fuller, 2001). MFN1 and 2 can homo- or hetero-dimerize with mitofusins in the adjacent mitochondria. OPA1 have two proteolytically cleaved proteins: long OPA1 (OPA1-L) and short OPA1 (OPA1-S). OPA1-L is anchored in the inner mitochondria membrane and coordinated the fusion process by forming homodimers with the opposite target membrane. OPA1-S has been associated with the stabilization of the mitochondrial cristae, maintenance of the mtDNA content and energetic competence (Del Dotto et al., 2017; Mishra et al., 2014).

Neurodevelopmental studies have shown mitochondrial dynamics are essential in neurogenesis. Mouse models deficient in DRP1 show smaller brain size and reduced developmental apoptosis in the neural tube (Lewis et al., 2018; Wakabayashi et al., 2009); as well as high mortality of newborn deep layer neurons (Ishihara et al., 2009). Although rare, mutations in DRP1 have been identified in patients with severe neurodevelopmental delays (Baum and Gama, 2021). Mutations in the adaptor proteins MFF and MID49 have also been associated with developmental delay, myopathies, and neuropathies (Bartsakoulia et al., 2018; Baum and Gama, 2021; Koch et al., 2016; Shamseldin et al., 2012). Mutations in MFNs and OPA1 have also identified as the causal mechanism behind neurodegenerative diseases such as Charcot-Marie-Tooth syndrome, autosomal dominant optic atrophy, spastic paraplegia, syndromic Parkinson and dementia (Alavi et al., 2007; Carelli et al., 2015; Verny et al., 2008; Yu-Wai-Man et al., 2010; Züchner et al., 2004).

b) Mitochondrial remodeling throughout neural differentiation and maturation

Mitochondrial diseases, which are traditionally linked to disruption in OXPHOS, are usually associated with neurological phenotypes such as developmental delay, atrophy, and epileptic encephalopathy (Ortiz-González, 2021; Povea-Cabello et al., 2021). Due to advances in exome sequencing, the range of causal mutations for mitochondrial diseases has expanded to include not only metabolic genes but proteins that affect mitochondrial shape, cristae stability,

recycling, motility, and interactions with other organelles (Baum and Gama, 2021). Thus, the capacity of the mitochondria to adapt and maintain its homeostasis its key for the correct execution of the intrinsic developmental programs of neural and corticogenesis, while also being responsive to environmental and intercellular signals.

Remodeling of the mitochondrial network as hPSCs commit to a neuronal cell fate is necessary for their survival and function (Figure 1-4) (Chan, 2012; Iwata et al., 2020; Khacho and Slack, 2018; Khacho et al., 2016; Schwarz, 2013). Likewise, neural processes such as development, migration, maturation, and plasticity; demand high levels of energy (Klein Gunnewiek et al., 2020). Mitochondrial fragmentation is a hallmark of glycolytic cell types such as stem cells (Chen and Chan, 2017; Rastogi et al., 2019; Teslaa and Teitell, 2015; Zhang et al., 2018a), and the ability to transition to a more complex and elongated network that facilitates aerobic respiration is crucial for the survival of the newborn neurons (Chan, 2012; Schwarz, 2013; Zheng et al., 2016a).

Studies in mouse models have shown significant cristae structural changes at the end of neural tube closure, as cells progress into neural progenitor stage. This modification in the mitochondria morphology correlates with the transition from a highly glycolytic metabolism to an OXPHOS dependent one (Fame et al., 2019). This switch in the mitochondrial structure, and the subsequent energetic requirements, are dependent on the downregulation of MYC, which has been shown to be a key regulator of ribosomal biogenesis, protein synthesis, and cellular proliferation at this stage (Chau et al., 2018). In vitro differentiation of mouse cortical neurons causes changes in mitochondrial mass due to increase mitochondrial biogenesis mediated by upregulation of mitochondrial transcription factor A (TFAM) and peroxisomal proliferating activating receptor γ coactivator-1α (PGC-1α) (Agostini et al., 2016). Glycolysis-to-OXPHOS transition was also observed during neuronal differentiation.

Disruption of mitochondrial fission and fusion proteins has been shown to result in both neurodevelopmental and neurodegenerative disease, both age-associated and progressive (Khacho and Slack, 2018). Mitochondrial dysfunction and aberrant mitochondria morphology are hallmarks of impaired brain development in both animal and human derived models. (Fang et al., 2016; Ishihara et al., 2009; Spiegel et al., 2016; Wakabayashi et al., 2009; Waterham et al., 2007).

The regulation of mitochondrial dynamics and its physiological relevance in the context of tissue architecture is still an unexplored landscape (Liesa and Shirihai, 2013; Noguchi and Kasahara, 2017). Studies of the mitochondrial morphology in adult mouse brain have shown that different cellular stages of differentiation possess a distinct mitochondrial morphology. Adult hippocampal radial glia-like NSCs have mixed globular and tubular shape mitochondria, while IPCs have more thin and more elongated network and adult neurons featured a wider and highly elongated morphology (Beckervordersandforth et al., 2017). Neurons also have higher mitochondrial volume, which can be correlated with an increase in bioenergetics mediated by the ETC and OXPHOS activity (Bélanger et al., 2011).

In the developing mouse brain, Khacho et al. (2016) described the morphology of the mitochondria at different cortical compartments. Neural stem cells in the VZ, positive for the marker SOX2, presented an elongated mitochondrial network; while IPC, stained with the marker TBR2, in the SVZ have a fragmented morphology. Newly committed neurons expressing TUJ1 (βIII-tubulin), regained an elongated mitochondria structure in the cortical plate. Deletion of OPA1 and MFN1/2, GTPases that mediate mitochondrial membrane fusion, impaired neural stem cell self-renewal and promote early differentiation as a result of the sustained mitochondrial fragmentation. Promotion of highly fused mitochondria by manipulation of DRP-1, the main effector of mitochondrial fission, had the opposite effect by increasing the ability of neural stem cells to self-renew.

In a follow up study, Iwata et al. (2020) analyzed the changes of the mitochondrial network through the early stages of neurogenesis in 2D cultures of mouse and human neural cells. From their results, PAX6+ RGC displayed fused mitochondria and TBR2+ IPCs had an intermediate mitochondrial size. In their case, βIII-tubulin expressing neurons had a fragmented mitochondrion. Interestingly, they showed that the cell fate specification occurs during a restricted time window during the postmitotic period where daughter cells inheriting fragmented mitochondria differentiate and daughter cells inheriting a fused network will retain the capacity to self-renew.

Although we are beginning to elucidate the role of mitochondria morphology and homeostasis during neuronal specification, little is known in human models about the role that

these organelles play during gliogenesis. Astrocytes rely on glycolysis more than OXPHOS for their energy production, specially by the utilization of fatty-acids as source of fuel (Eraso-Pichot et al., 2018; Fecher et al., 2019; White et al., 2020). Moreover, developing astrocytes contain a highly interconnected functional network of mitochondria and upregulation of the mitochondrial network is crucial for coordinating post-natal astrocyte maturation and synaptogenesis (Zehnder et al., 2021).

Oligodendrocytes, on the other hand, rely on OXPHOS during the progenitor stage and switch to glycolysis when mature (Amaral et al., 2016; Fecher et al., 2019; Fünfschilling et al., 2012; Rao et al., 2017; Rinholm et al., 2011). Mitochondrial fragmentation is key in mature oligodendrocytes as myelin sheets contained smaller mitochondria if compared to the network surrounding the nucleus (Battefeld et al., 2019; Rinholm et al., 2016). Yet, the effects of the mitochondrial dynamics during their development and specification remains unknown.

Summary

The brain is one of the most complex and mysterious organs in the human body. Centuries of research have shown that it is generated by a finely orchestrated series of events that take place in the first weeks of life up to early adulthood. How does a cluster of cells acquire the fate necessary to generate millions of neurons, astrocytes, and oligodendrocytes? Our laboratory proposes that mitochondrial homeostasis provides guidance to the intrinsic developmental programs of neuro and corticogenesis, while also being responsive to environmental and intercellular signals. To address this hypothesis, I utilize 2D and 3D platforms to interrogate the capacity of cells to generate neuronal and glia progeny in a background of metabolic dysregulation. In Chapter 2, I discuss the generation of Spin∞, an optimization of published bioreactors. We addressed deficiencies perceived by the use of the original design and proposed changes that not only increased the lifespan of the bioreactor but also optimized the generation of cerebral organoids for our laboratory. The effects of dysregulation of the mitochondria are analyzed in Chapter 3. We generated and characterized three commercially available fibroblast cell lines from Leigh Syndrome (LS) patients. LS is a fatal neurometabolic disease that is characterized by defective energy production, with highly metabolic tissues such as the brain being deeply affected. We generated iPSCs from these fibroblasts and analyzed their capacity to generate neuronal lineages in 2D and 3D models. I discovered that the causing mutations affect the generation of upper cortical neurons in all phenotypes and that this dysregulation could be mediated by the deficient switch of the LS-derived neurons to transition from a glycolytic state to an aerobic respiration paradigm. Finally, Chapter 4 highlights the use of brain organoids as a model system to interrogate the required mitochondrial changes necessary for brain development and how this system can be used to assess the effects of mitochondrial health during corticogenesis.

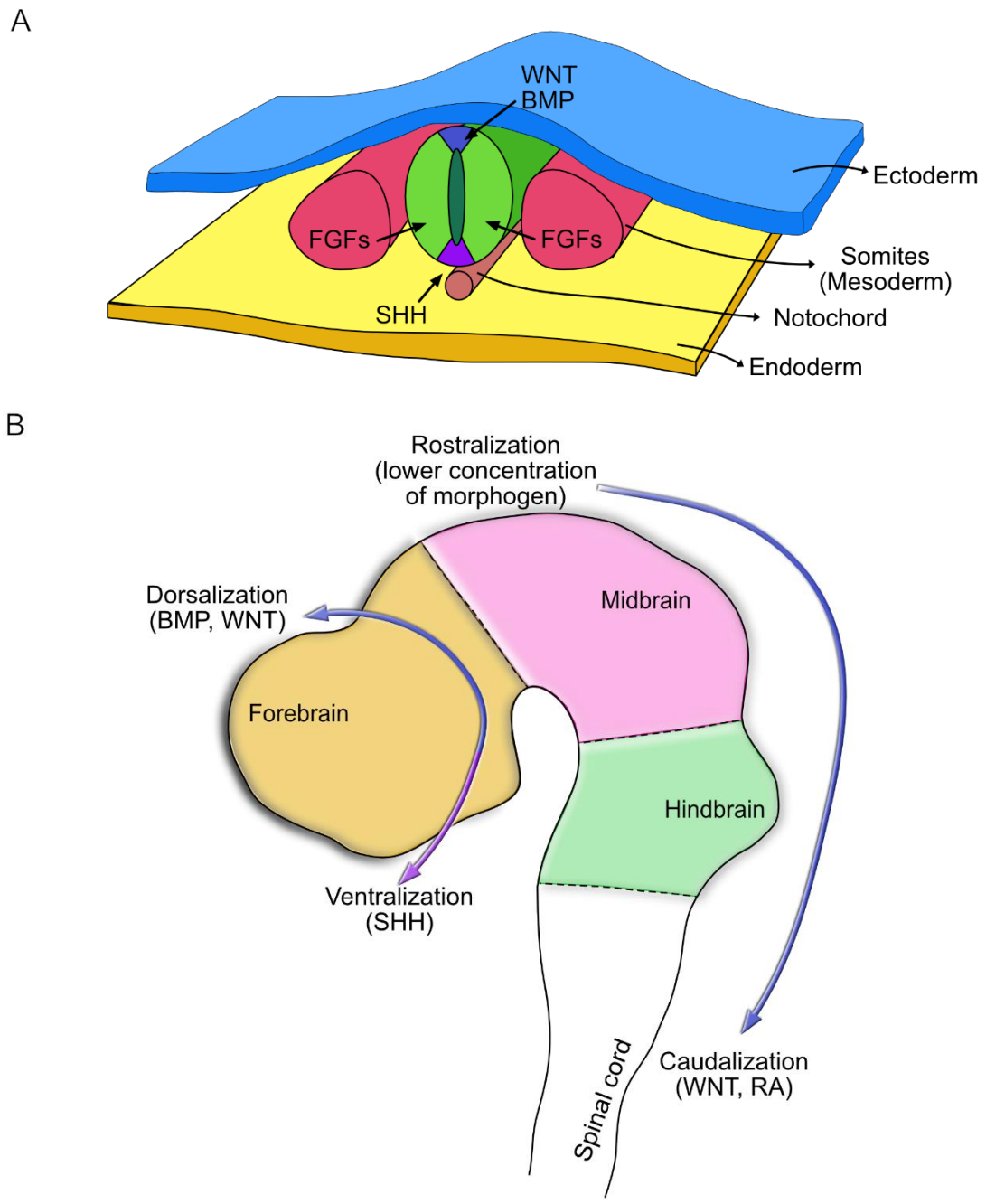

Figure 1-1. The schematic of the neural patterning principle.

A). Development of the neural tube and the signaling governing the Dorsal-ventral axis. B). Regional patterning of the developing CNS.

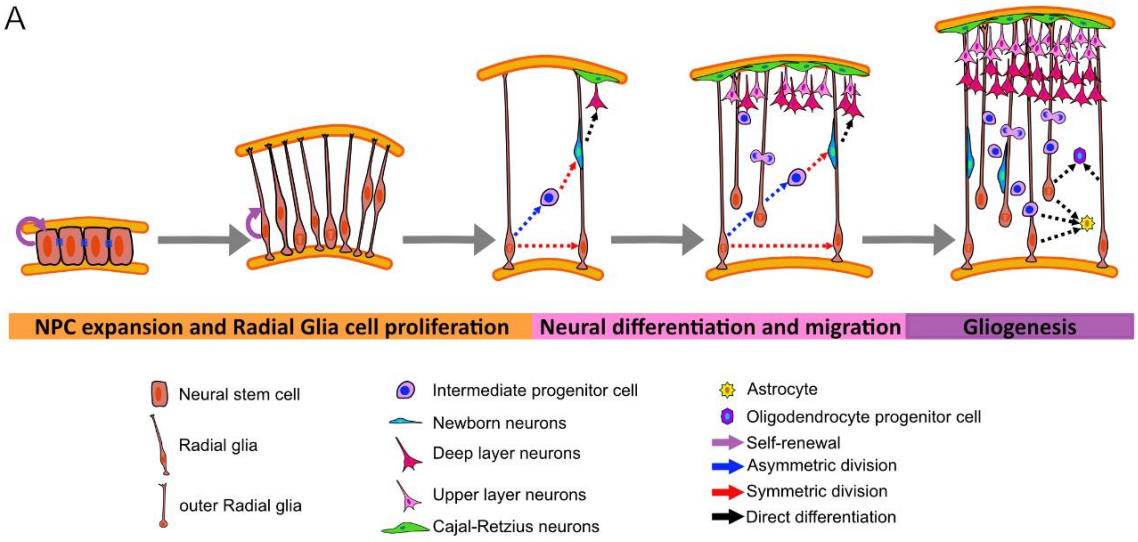
A
NPC expansion and Radial Glia cell proliferation
Neural differentiation and migration
Gliogenesis
Neural stem cell
Radial glia
outer Radial glia
Intermediate progenitor cell
Newborn neurons
Deep layer neurons
Upper layer neurons
Cajal-Retzius neurons
Astrocyte
Oligodendrocyte progenitor cell
Self-renewal
Asymmetric division
Symmetric division
Direct differentiation

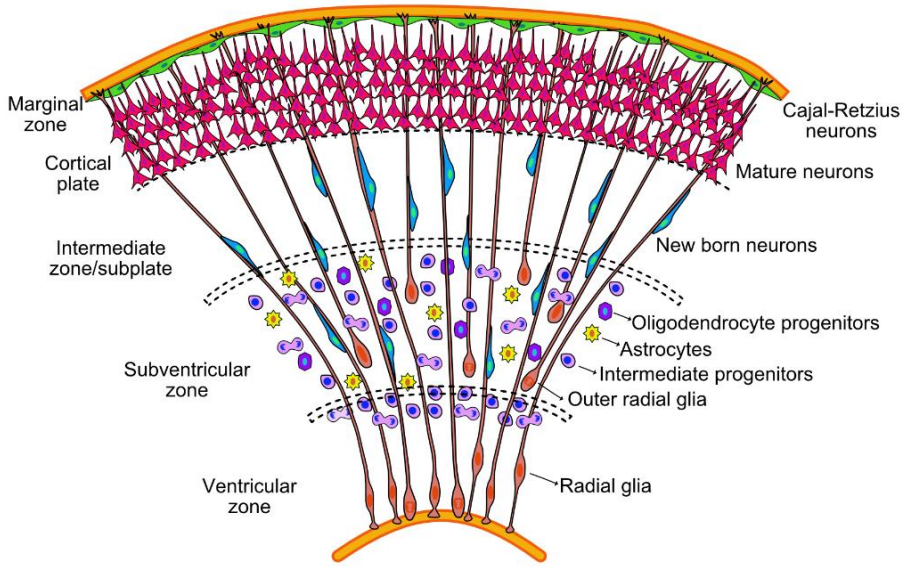
B
Marginal zone
Cortical plate
Intermediate zone/subplate
Subventricular zone
Ventricular zone
Cajal-Retzius neurons
Mature neurons
New born neurons
Oligodendrocyte progenitors
Astrocytes
Intermediate progenitors
Outer radial glia
Radial glia

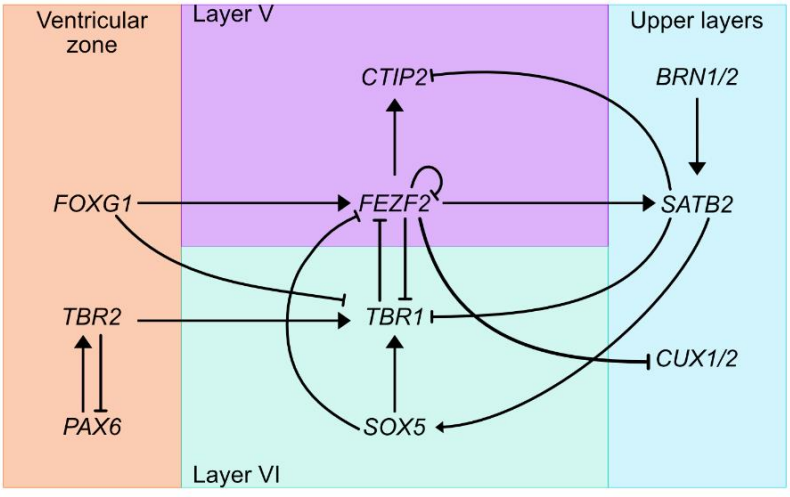
C
Ventricular zone
Layer V
Upper layers
Layer VI
CTIP2
BRN1/2
FOXG1
FEZF2
SATB2
TBR2
TBR1
CUX1/2
PAX6
SOX5

Figure 1-2. Human neocortical development.

A). Schematic illustration of neurogenesis in the human cortex. B). Cortical expansion in humans allows for the formation of different areas where progenitor lineages migrate, proliferate, and differentiate. C). Transcriptional regulators and genes governing cell fate acquisition and specification during neurogenesis.

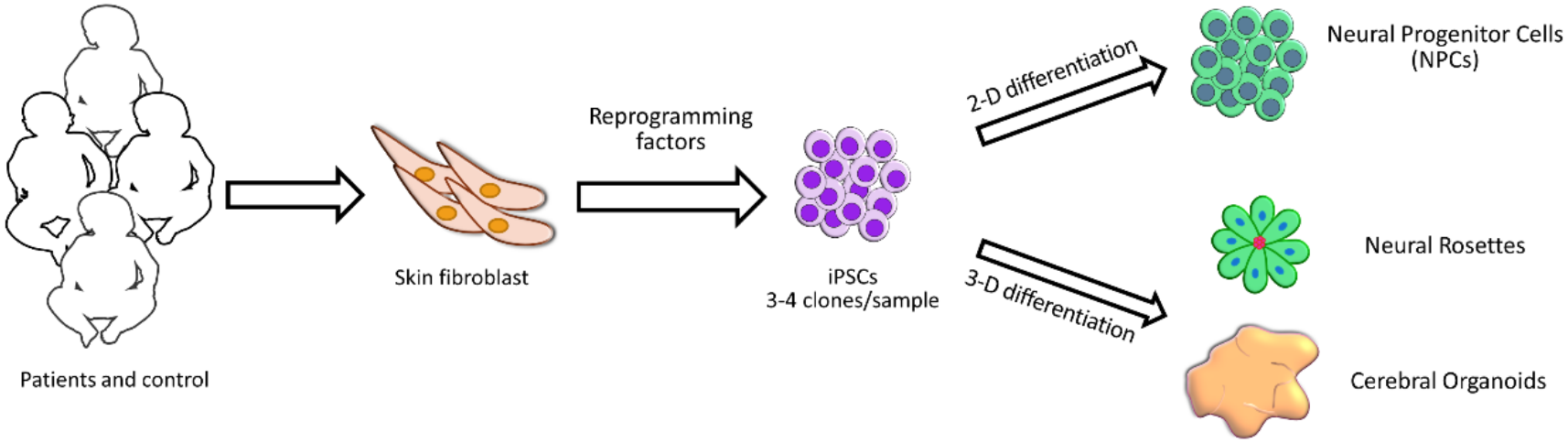

Figure 1-3. Neural development research approach utilizing induced pluripotent stem cells (iPSCs).

Skin fibroblast can be derived from patients and controls by a minimally invasive biopsy. These fibroblasts can be reprogrammed using the Yamanaka factors into induced pluripotent stem cells. iPSCs can be the utilized to generate neural cells under 2-dimensional and 3-dimensional paradigms. This allows for the study of neural development under health and disease conditions.

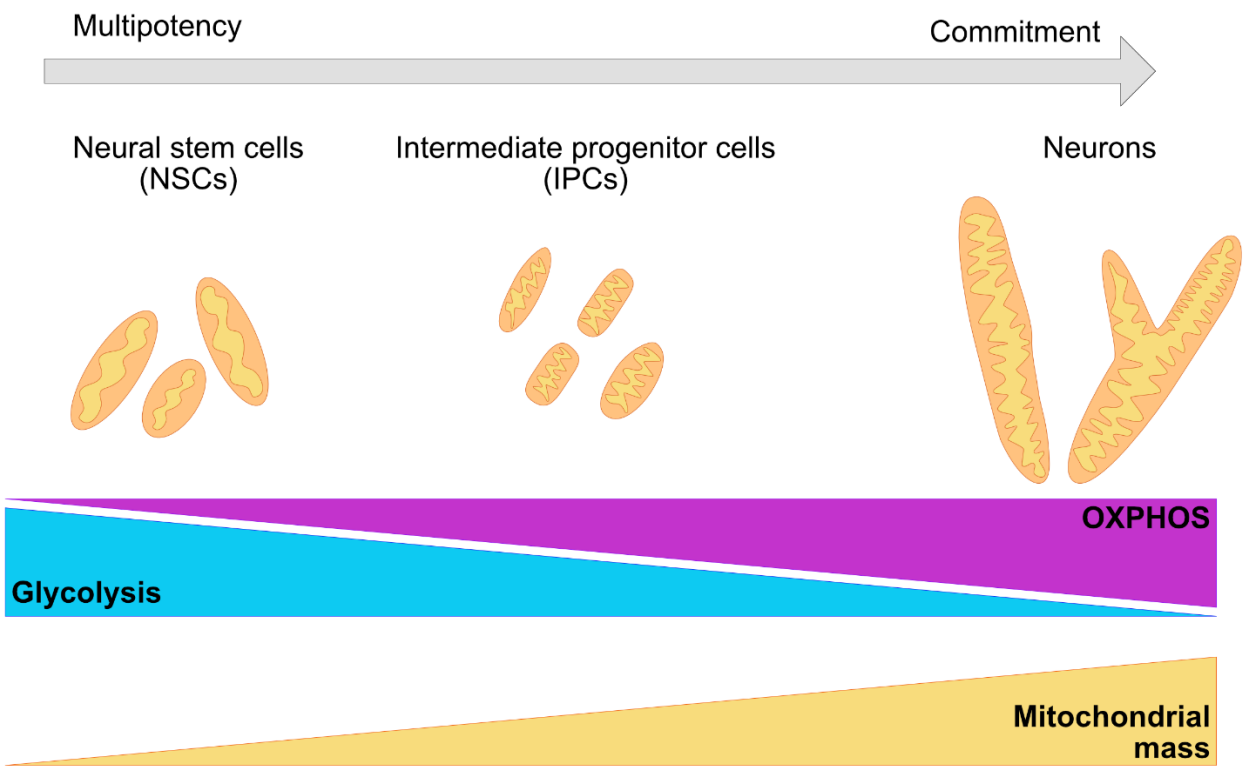

Figure 1-4. Changes in the morphology of the mitochondrial network are required for the commitment of neuronal fate.

During neurogenesis, the mitochondrial network undergoes crucial remodeling to adapt to the bioenergetic necessities of the cell, as well as the requirements of the environment. NSC have been shown to present a mildly elongated mitochondrial network with a mix of globular and tubular mitochondrion. IPCs cells are characterized for fragmented, thin, and elongated networks. Committed neurons have a wider and elongated mitochondrial network. A metabolic switch from glycolysis to OXPHOS is necessary for the acquisition of the neuronal fate and it is associated with remodeling of the mitochondrial cristae, as well as with the increase of the number of mitochondria and mitochondrial mass.

Chapter 2

IMPROVING CURRENT MODELS OF BRAIN DEVELOPMENT

Adapted with permission from:

Romero-Morales, AI.[#], O'Grady, B. [#], Balotin, K., Bellan, L., Lippmann, ES., Gama, V. Spinꝏ: An update on a miniaturized spinning bioreactor design for the generation of human forebrain organoids. #Equal contribution. HardwareX. 2019, 9(e00084). PMID: 32864515

Romero-Morales, AI.[#], O'Grady, B. [#], Balotin, K., Bellan, L., Lippmann, ES. & Gama, V. Spinꝏ: An update on a miniaturized spinning bioreactor design for the generation of human forebrain organoids. #Equal contribution. VU19193P1; MBF Ref. 093386-9276-US01; Appl. No. 62/868,332

Abstract

Three-dimensional (3D) brain organoids derived from human pluripotent stem cells (hPSCs), including human embryonic stem cells (hESCs) and induced pluripotent stem cells (iPSCs), have become a powerful system to study early development events and to model human disease. Cerebral organoids are generally produced in static culture or in a culture vessel with active mixing, and the two most widely used systems for mixing are a large spinning flask and a miniaturized multi-well spinning bioreactor (also known as Spin Omega (SpinΩ)). The SpinΩ provides a system that is amenable to drug testing, has increased throughput and reproducibility, and utilizes less culture media. However, technical limitations of this system include poor stability of select components and an elevated risk of contamination due to the inability to sterilize the device preassembled. Here, we report a new design of the miniaturized bioreactor system, which we term Spinfinity (Spinꝏ) that overcomes these concerns to permit long-term experiments. This updated device is amenable to months-long (over 200 days) experiments without concern of unexpected malfunctions.

Introduction

Brain organoids are three-dimensional (3D) structures formed from neural stem cells (NSCs) derived from human pluripotent stem cells (hPSCs) that can effectively model human brain development up to 12-14 weeks post-conception (Camp et al., 2015; Lancaster et al., 2013;

Quadrato et al., 2017; Subramanian et al., 2017), a time period which includes critical patterning events in the cerebral cortex and other brain regions (Paşca et al., 2015; Pașca et al., 2019). On a cellular level, brain organoids show a high level of similarity to the in vivo developing human brain in the early stages of development, including progenitor zones (ventricular zone and subventricular zone consisting of PAX6+/SOX2+ NSCs) that form around central lumens (Lancaster et al., 2013; Subramanian et al., 2017). These 3D organoid cultures therefore provide a robust system amenable to extended cultivation and manipulation, which makes them a useful tool to model development and disease in the context of the complex brain microenvironment (Kadoshima et al., 2013; Kelava and Lancaster, 2016; Lancaster and Knoblich, 2014).

Recently, two protocols have been published on enhancing cortical plate formation within hPSC-derived cerebral organoids: one using large spinner flasks and microfilaments as a solid support (Lancaster et al., 2013, 2017) and another that uses a miniature spinning bioreactor termed Spin Omega (SpinΩ) (Qian et al., 2016, 2018), which consists of 3D printed gears and paddles driven by a single electric motor. The SpinΩ provide an accessible and versatile format for culturing brain-region-specific organoids due to its reduced incubator footprint, decreased media consumption, and increased throughput, but several technical caveats limit its use in long-term experiments, most prominently the choice of components used to fabricate the device and the design of the device with respect to limiting the chances of contamination and mechanical failure. Here, we redesigned the SpinΩ to overcome these problems, leading to the creation of a device that we have termed Spinfinity (Spin∞).

To develop this improved device, we first considered the choice of motor that drives the spinning bioreactor. Motor life span inside an incubator can be a major hurdle when using a bioreactor system because motors that are not designed to withstand harsh environments (high humidity, 5% carbon dioxide, and elevated heat) can easily corrode and break, leading to unexpected failures in the middle of long-term experiments. We therefore selected a motor with the ability to operate at increased temperatures (max 70°C) and humidity (90% humidity). Additionally, parylene vapor deposition was applied to the motor to provide an additional moisture barrier to further the lifetime of the motor and increase durability (Tan and Craighead,

2010). Next, we considered the basic design of the bioreactor. Due to the humidity issue raised above, we used stainless steel screws, standoffs, nuts, and washers in order to reduce the oxidation of the metal and prolong the life of the bioreactor. These parts also have the advantage of being autoclavable as separate components or with the assembled bioreactor, and the updated design now allows the majority of the equipment (including the 3D printed parts) to be assembled and autoclaved to reduce external handling and improve sterility. The addition of an upper acrylic lid on the bioreactor (where the motor is anchored) further enhances stability and consistency of the device. The SpinΩ motor was anchored in two points on the upper lid, which frequently caused the motor to shift and oscillate, thereby putting unnecessary additional stress on the motor leading to eventual failure. Because the updated Spin∞ was designed using a separate acrylic sheet, hex standoffs, and a larger, more durable motor, all components are kept in perpendicular alignment to the well plate, thus preventing shifting and oscillation. Additionally, because the Spin∞ is designed with hex standoffs and an autoclavable 3D printed base, the lid is securely placed on the 12-well plate, which prevents spills and possible contamination points. By comparison, the original SpinΩ design freely rests on the top of the plate, making this design prone to spillage and contamination. Overall, these changes yield a miniaturized spinning bioreactor that is exceptionally easy to maintain and performs consistently. This updated device is amenable to months-long experiments without concern of unexpected malfunctions.

Hardware description

The Spin∞ is built primarily from 3D printed ULTEM 1010 resin to permit autoclaving. Alternate 3D printing filaments, such as acrylonitrile butadiene styrene (ABS), can be used but require more extensive sterilization steps such as sequential washes in 10% bleach, 70% ethanol, distilled water washes and UV irradiation. The bottom 3D printed frame contains an inset to hold a 12-well plate, as well as inserts for the metal standoffs. The top 3D printed frame houses PTFE collars, gears, and paddles, which are manually assembled. All the gears except one are used solely for turning, while the remaining gear connects directly to a DC 12V 100RPM gear motor (Greartisan) attached to an acrylic plate. The acrylic plate rests on the metal standoffs and is screwed into place to ensure mechanical stability. All components can be optionally coated with parylene to prevent corrosion of the metal housing on the motor and to add an additional

hydrophobic barrier to prevent absorption of media into the 3D printed parts. The motor connects to a L298n bridge and a Raspberry Pi 3A+ that controls the motor speed through a touchscreen interface.

- Increased motor life span under high temperature and humidity conditions.
- Can be autoclaved after assembly, thus removing the need for disassembly for cleaning and sterilization.
- Sturdy, fully enclosed assembly to prevent leaks and spills while ensuring consistent operation.
- Integrated touch screen for changing motor speed.

Results and Discussion

Brain organoids were generated using the STEMdiff™ Cerebral Organoid Kit (Stem Cell Technologies) with some modifications (Figure 2-1A and 2-1B) (Lancaster and Knoblich, 2014; Lancaster et al., 2013; Qian et al., 2016; Sutcliffe and Lancaster, 2017). As the generation of homogeneous embryoid bodies (EBs) is critical for achieving homogenous organoids, we utilize a 24-well plate AggreWell™ 800 (Stem Cell Technologies, catalog 34815) (Marton et al., 2019; Yoon et al., 2019) to increase the reproducibility and the yield of EBs (Figure 2-2A and 2-2B). After 4 days of culture in the AggreWells, we transfer the organoids to a 10 cm ultra-low attachment plate to allow further growth of the EBs before the Matrigel embedding process (Figure 2-1B). The diameter of the EBs increased over time; by the embedding day (day 7) the average diameter was 387 µm (±57) and by the bioreactor transfer day (day 10) the average diameter was 661 µm (±112) (Figure 2-2B). High resolution images show the formation of organized neural rosettes within the EBs at day 8 (Lancaster et al., 2013; Qian et al., 2016). Alpha-tubulin (α-tubulin filaments) can be seen organized radially from the lumen (Figure 2-2C) (Elkabetz et al., 2008; Gerrard et al., 2005; Hříbková et al., 2018; Zhang et al., 2001). These polarized neuroepithelium-like structures resemble neural tube formation and are the precursors to the formation of the brain lobules (Lancaster et al., 2017).

Characterization of the organoids was performed at day 60 and day 150. Organoids were fixed in 4% PFA for 15 min at 4°C, followed three 5 min washes in PBS and 30% sucrose dehydration overnight at 4°C. Embedding for sectioning was performed as reported previously (Lancaster et al., 2013). Cryosections (15 µm thick) were stained using neural progenitor cell (NPC), mature pan-neuronal, and cortical layer markers. As previously reported for day 60 organoids (Qian et al., 2016), the cells that stain positive for neural progenitor markers are localized in the periphery to the ventricle-like structures (Figure 2-3A). Multi-layer stratified structures can be readily seen and are comprised of NPC+ cells marked by SOX1, SOX2, and PAX6 marking the progenitor zone (Figure 2-3A-C). PAX6 expression confirmed the forebrain identity in the regions of interest (Lancaster et al., 2013). NESTIN positive cells mark radial glia, key structures for the expansion of the mammalian cortex by differentiating into neurons and intermediate progenitor cells (Figure 19A and 19B) (Kriegstein and Alvarez-Buylla, 2009).

Pre-plate formation was confirmed by the presence of TBR1+ cells (Figure 2-3B and 2-3C). This marker also identifies cells localized to the early-born layer VI of the cortex (Hevner et al., 2001). TBR1+ neurons are vital for guiding the subsequent neuronal migrations (Hevner et al., 2001). Radial organization can be seen by MAP2, a neuronal marker for dendritic outgrowth and branching (Figure 2-3C) (Shafit-Zagardo and Kalcheva, 1998). Cajal-Retzius cells, a cell population crucial to the generation of the cortical plate architecture, is present by REELIN+ neurons located along the organoid surface (Figure 2-4A). These early born cells localize to the marginal zone of the cortex (layer I) and contribute to the formation of the inside-out layering of the neurons in the neocortex (Frotscher, 1998).

At day 60, early born neurons from layer V were positive for CTIP2 (also known as BCL11B) (Figure 2-4A and 2-4B). Furthermore, late-born neurons from the superficial layers (layer IV) can be seen as SATB2+ cells (Figure 2-4C). Interestingly, these markers show a clear separation from the neural progenitor zone, indicating a spatial separation of the different neuronal lineages, as well as the recapitulation of the cortical architecture observed in other brain organoid protocols.

Neurons expressing layer II/III markers CUX1 and BRN2 are present by day 150 (Figure 2-5A and 2-5B). Presence of these late born neurons (Kadoshima et al., 2013; Lancaster et al., 2013;

Paşca et al., 2015; Qian et al., 2016) underlie the capacity of the organoid system to recapitulate the cytoarchitecture of the developing cortex.

Finally, we analyzed the expression of the apoptosis marker cleaved Caspase 3 (ClC3). At day 60 and day 150, the presence of apoptosis is evident, but the integrity of the cortical structures is maintained (Figure 2-6A and 2-6B). Apoptosis is a key process during brain formation, controlling cellularity in the developing brain (Kuan et al., 2000; Nonomura et al., 2013). Work in human (Anlar et al., 2003), mouse (Nonomura et al., 2013), and rat (White and Barone, 2001) brain samples shows high incidence of cell death during the development of the neocortex. As the overall architecture of the organoids was maintained, the observed cell death may be the result of the normal elimination of cells that takes place in the developing brain.

Here we have shown that organoids cultured Spin∞ have the growth capacity and laminar organization previously reported in the literature (Lancaster and Knoblich, 2014; Lancaster et al., 2013; Qian et al., 2016; Sutcliffe and Lancaster, 2017). Brain organoids grow above 3 mm in diameter and have distinct and organized segregation between all cortical layers. Human NPC markers, as well as deep cortical and pan-neuronal markers can be identified in a structured manner and in the expected stages. Evaluation of the apoptotic marker ClC3 shows cell death in the core of the organoid as expected with no major compromise of the organoid integrity.

Our system demonstrated the following capabilities:

- While the data shown here only include brain organoids grown up to day 150, we have successfully culture them over 200 days without the need to change motors, which demonstrates the increased motor life span of Spin∞ under high temperature and humidity conditions.
- No contamination was detected even after long-term culture, which we suggest is due in part to the ability to autoclave most of the Spin∞ components after assembly.

Figures

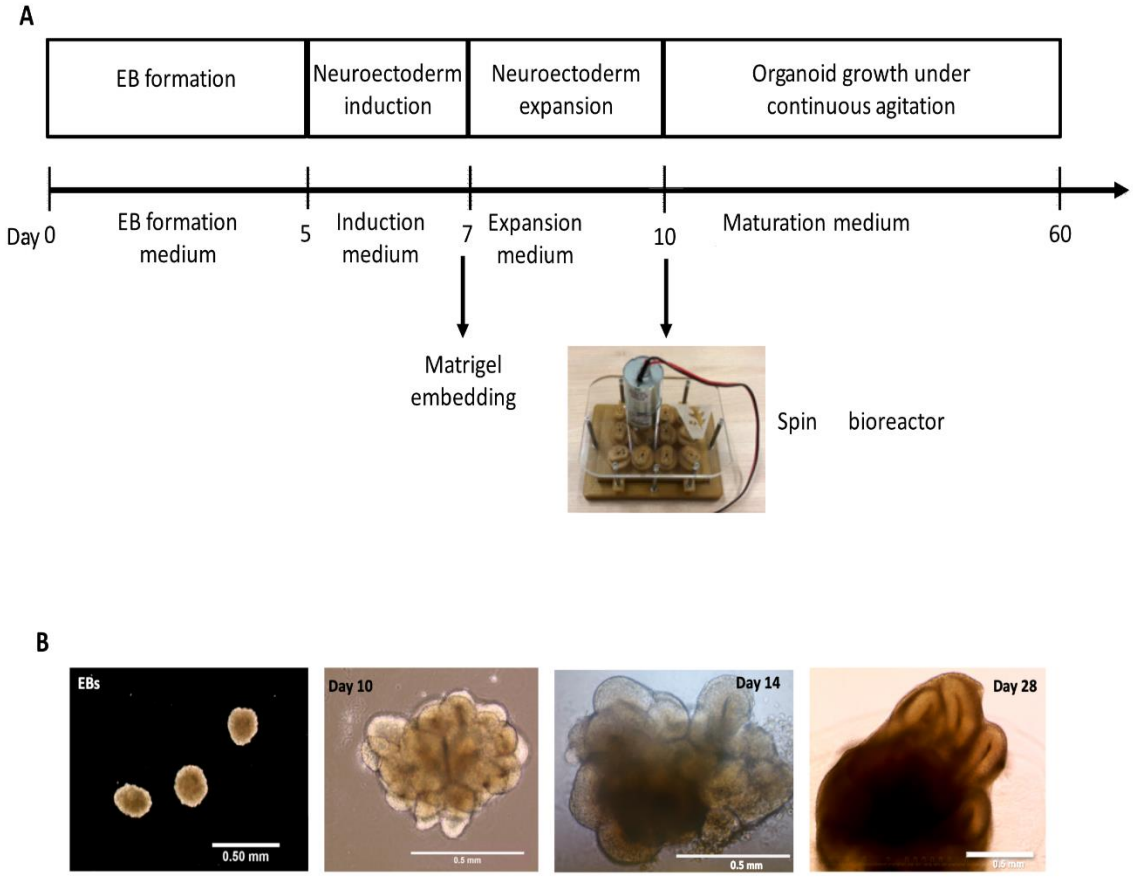

Figure 2-1. Protocol for the generation of brain organoids using Spin∞.

A) Schematic of the major stages in the culture protocol. B) Macroscopic images of the organoid growth and development. Scale bars: 0.5mm.

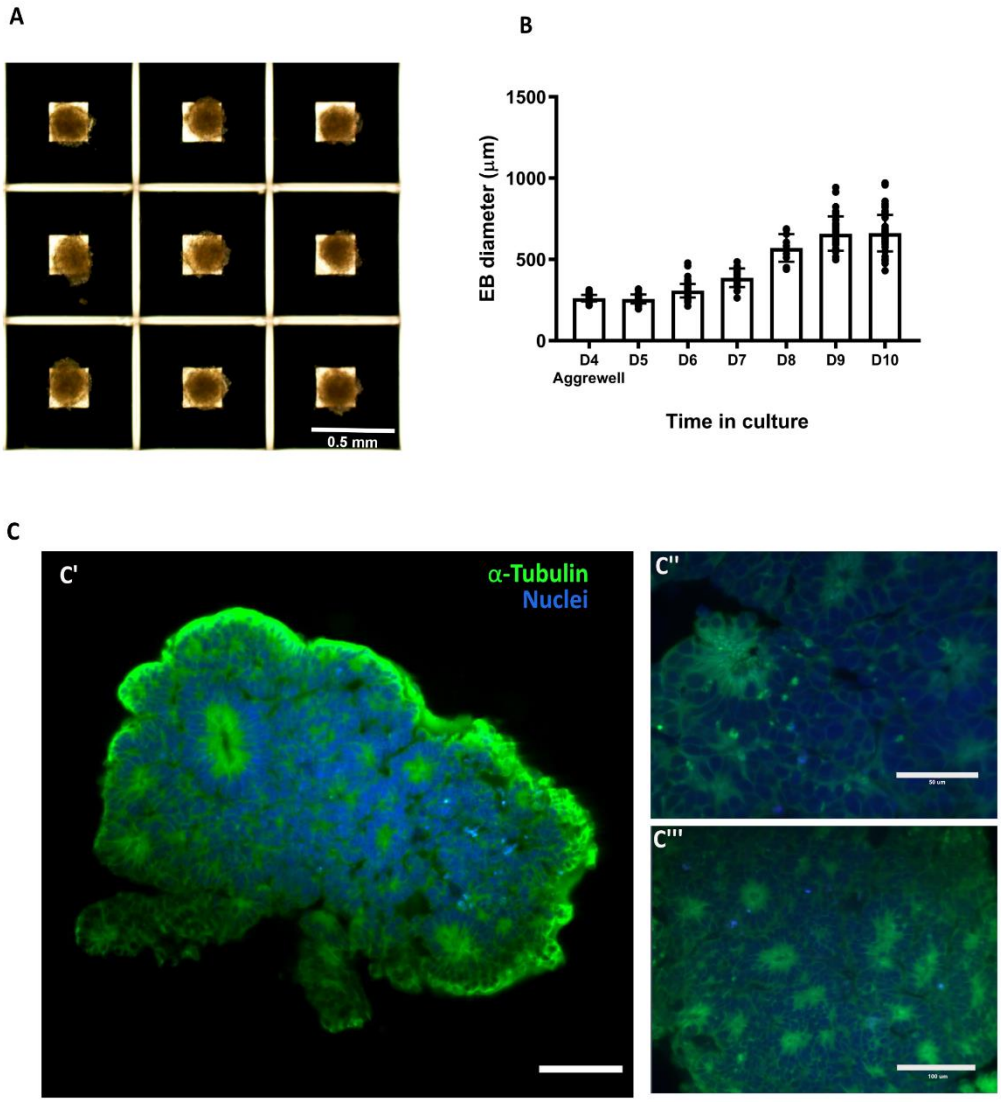

Figure 2-2. Embryoid body generation and size over time.

A) Four days old Embryoid bodies generated using microwells. B) Relative growth of the embryoid bodies over time. C) Light sheet microscope images of day 7 embryoid body showing the formation of organized neural rosettes. C'' and C'' show close up to the rosettes Data are mean ± s.d. Scale bars: (A) 0.5mm, (C') 100 µm, (C'') 50µm, (C''') 100µm.

Day 60 organoids

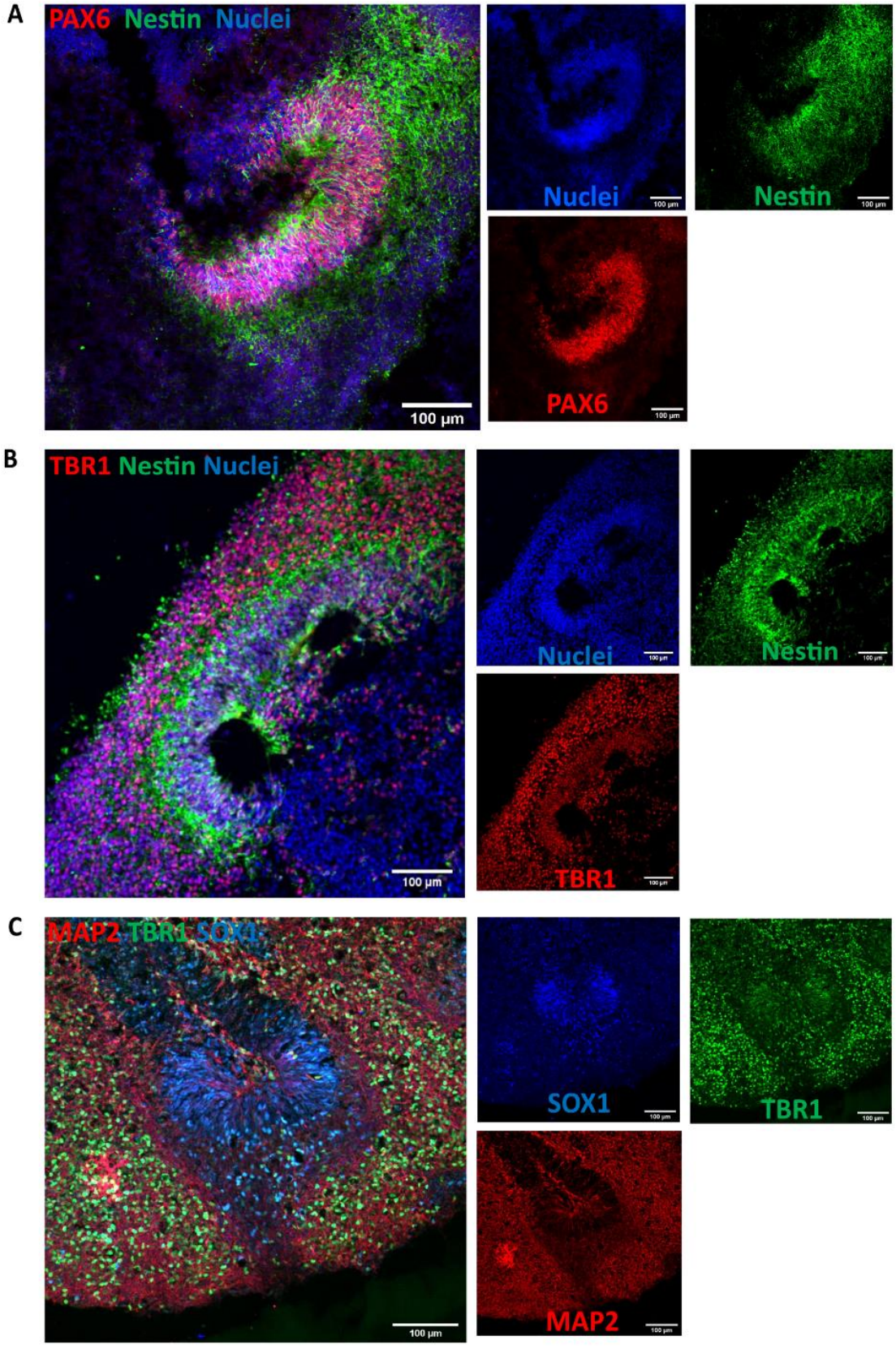

Figure 2-3. Staining for neural progenitor cells and cortical neurons.

A) Day 60 organoids showing the presence of neural progenitor markers PAX6 and NESTIN. B) Cortical plate marker TBR1 shows the organization of the pre-plate. C) MAP2 positive cells indicate the presence of committed neurons at this stage. Scale bars: (A-C) 100μm.

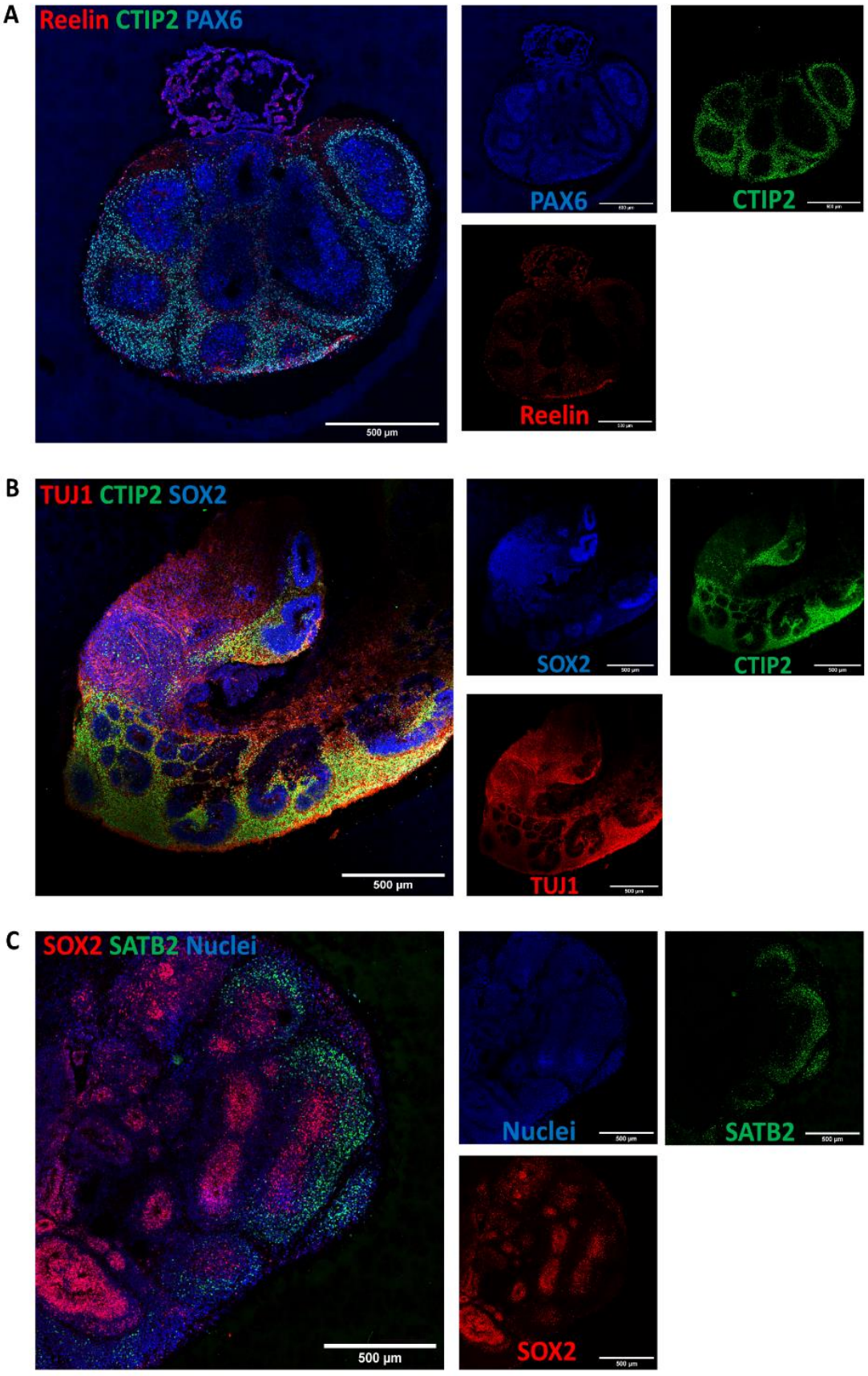
A
Reelin CTIP2 PAX6
500 µm
PAX6
CTIP2
Reelin
B
TUJ1 CTIP2 SOX2
500 µm
SOX2
CTIP2
TUJ1
C
SOX2 SATB2 Nuclei
500 µm
Nuclei
SATB2
SOX2

Figure 2-4. Characterization of cortical layers presents after 60 days in culture.
A) Cajal-Retzius neurons stained for reelin show the presence of marginal zone. B) Staining for deep-layer neurons (CTIP2) and neuronal markers (TUJ1). C) Upper-layer marker SATB2 indicates the presence of neurons belonging to the cortical layer IV. Stitched images at 20X, scale bars: 500µm.

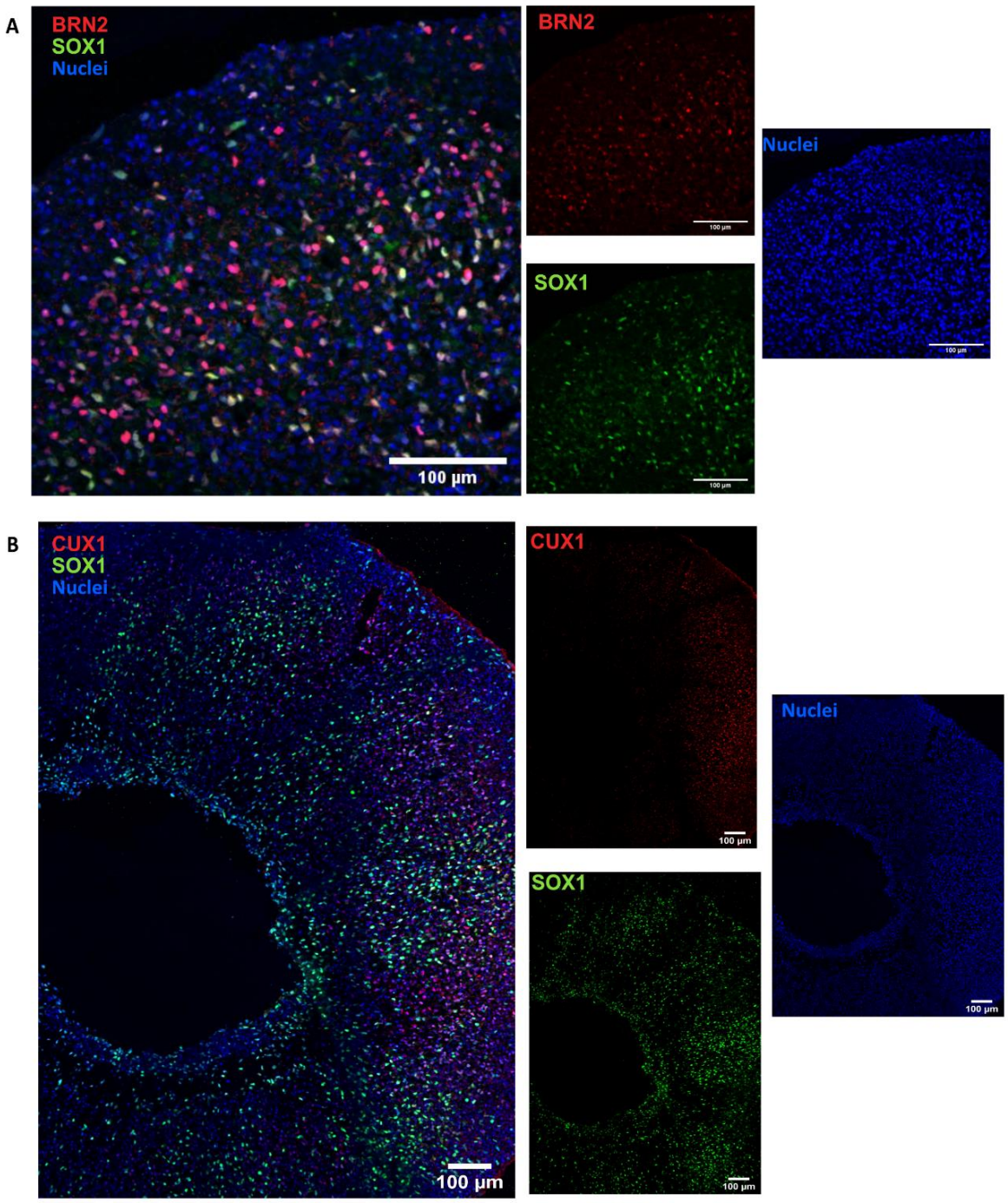

Figure 2-5. Long-term culture of brain organoids allows upper layer specification.
Sample images of immunostaining for superficial layer neuron markers (A) BRN2 and (B) CUX1 in cerebral organoids at day 150. Scale bars: 100 µm.

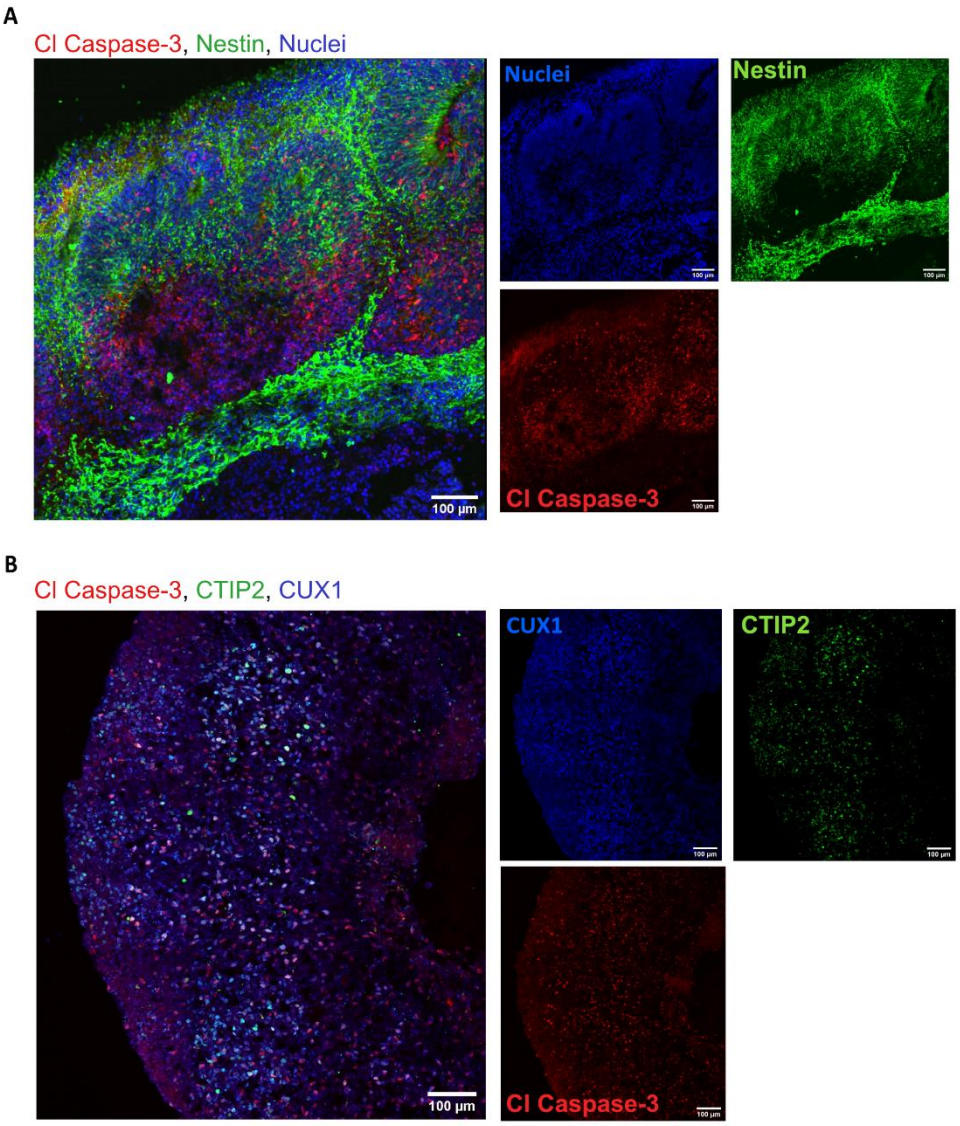

Figure 2-6. Immunostaining for apoptosis marker Caspase 3.

A) Cells positive for cleavage caspase 3 at day 60 B) and day 150 show no structural compromise of the cortical architecture. Scale bars: 100µm. (B) stitched image.

Supplemental Figures

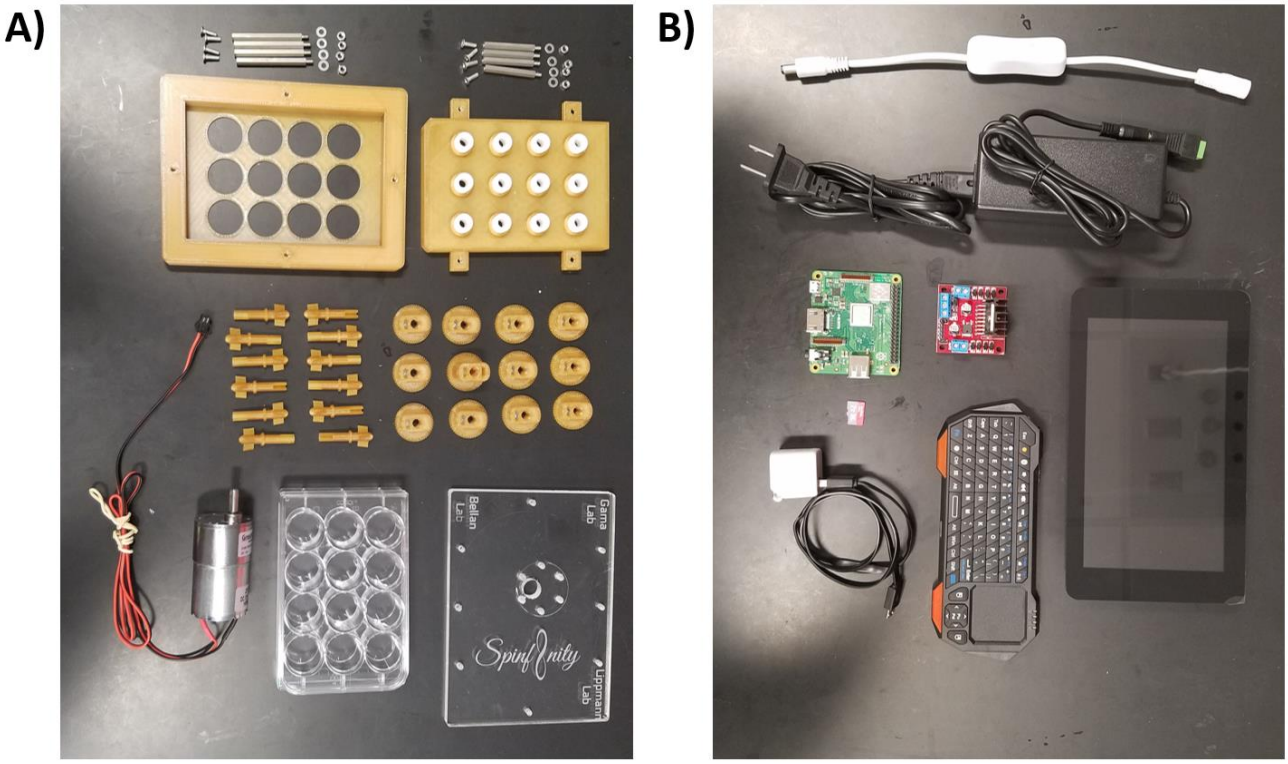

Supplemental Figure 2-1. All individual components used to build the Spin∞.

A) Hardware and 3D printed components. B) Electronic components.

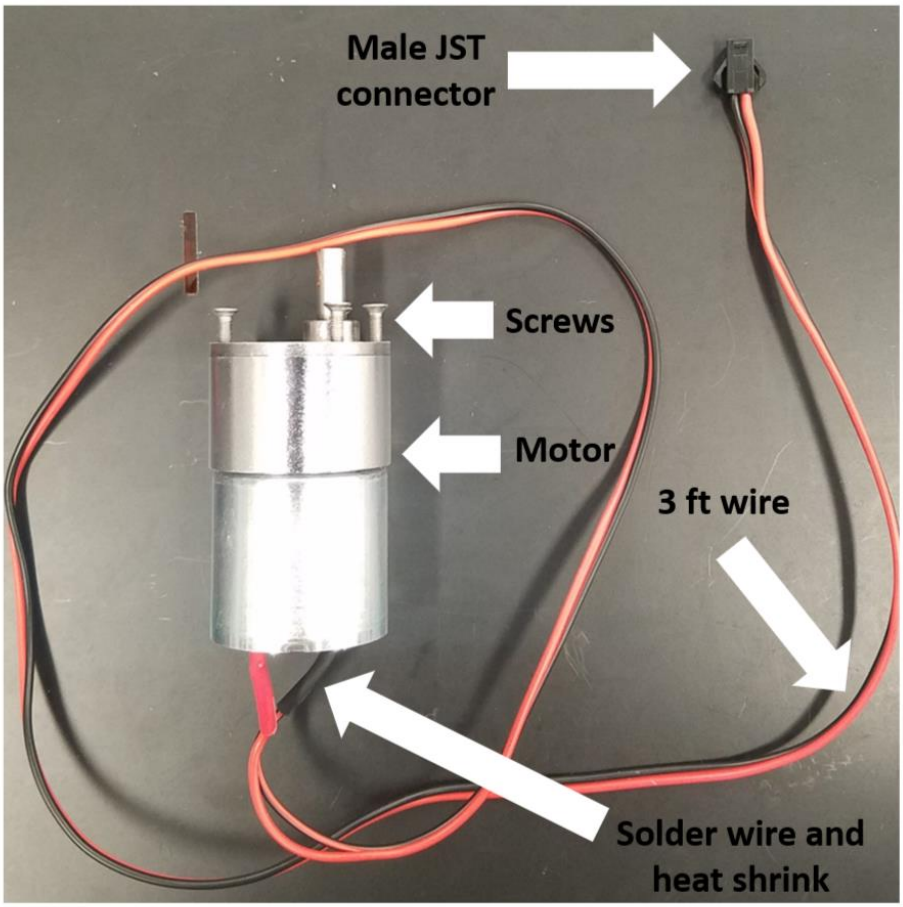

Supplemental Figure 2-2. Motor preparation.

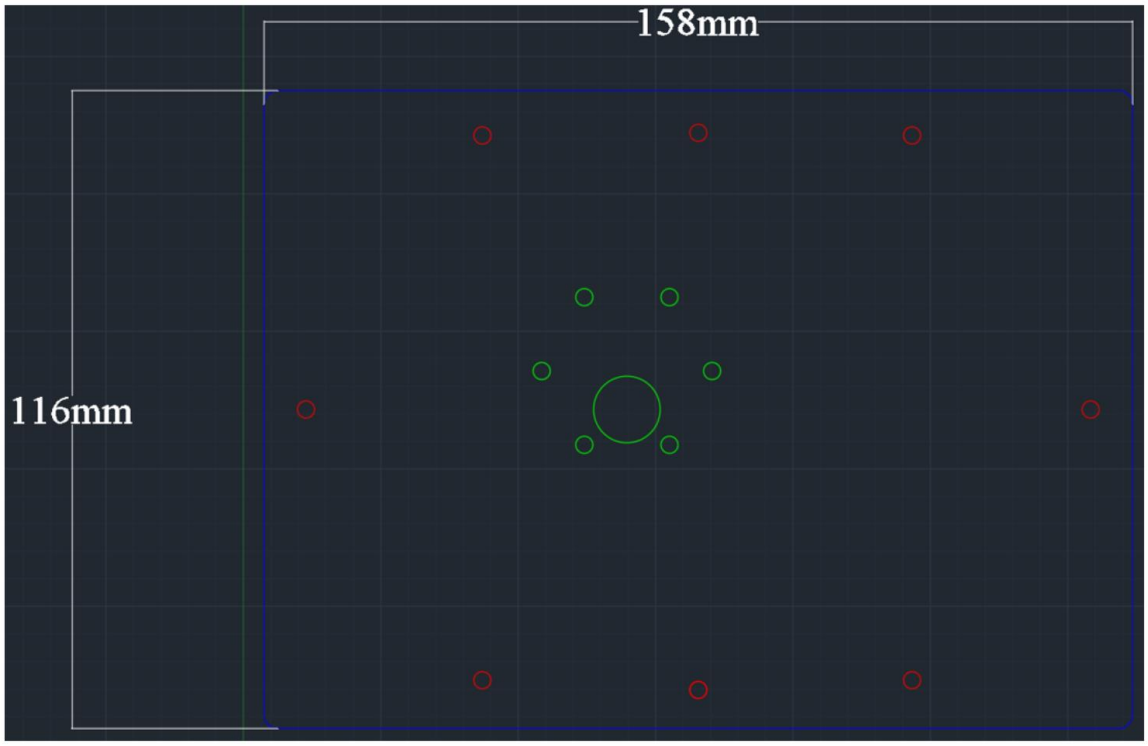

Supplemental Figure 2-3. Acrylic plate dimensions for laser cutting.

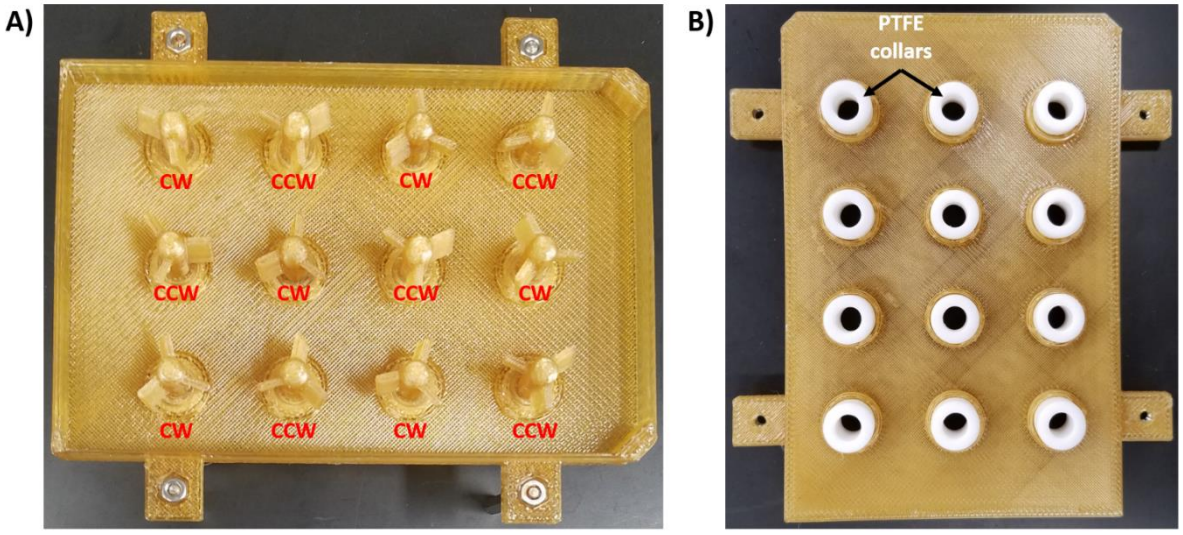

Supplemental Figure 2-4. Insertion of paddles into the 12-Well Plate Lid.

A) Positioning of the CW Paddles and CCW Paddles are noted. B) Positioning of the PTFE collars are shown on the opposite side of the lid.

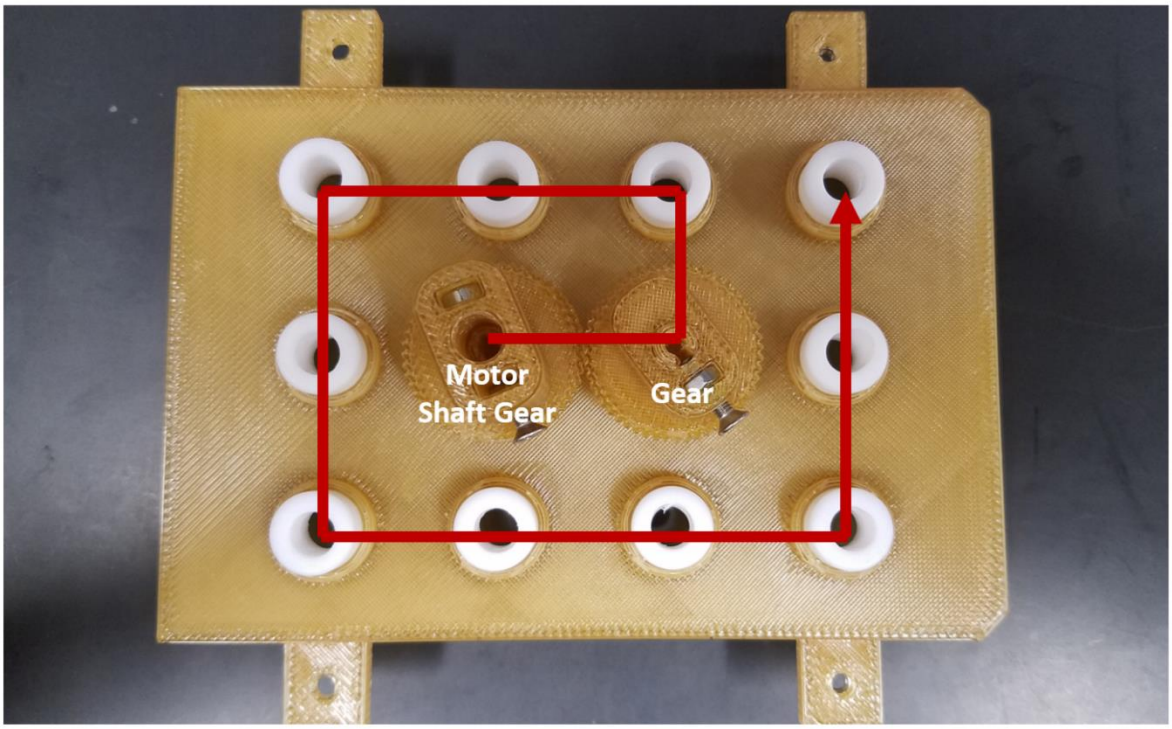

Supplemental Figure 2-5. Assembly pattern of the Gears to ensure proper operation.

Make sure each gear is properly threaded before moving on to the next one. The position of the Motor Shaft Gear is noted.

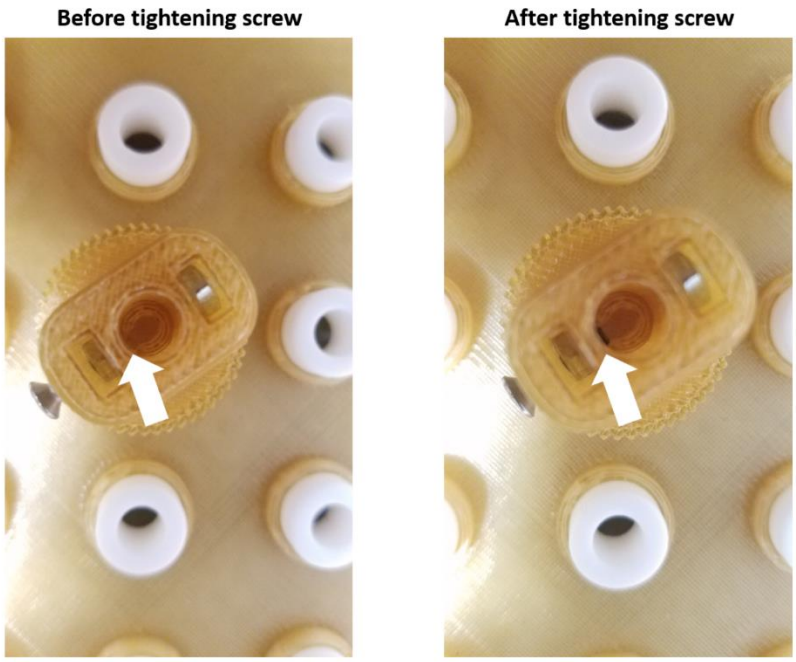

Supplemental Figure 2-6. Proper positioning of screws in the Gears.

Screws should not be overtightened.

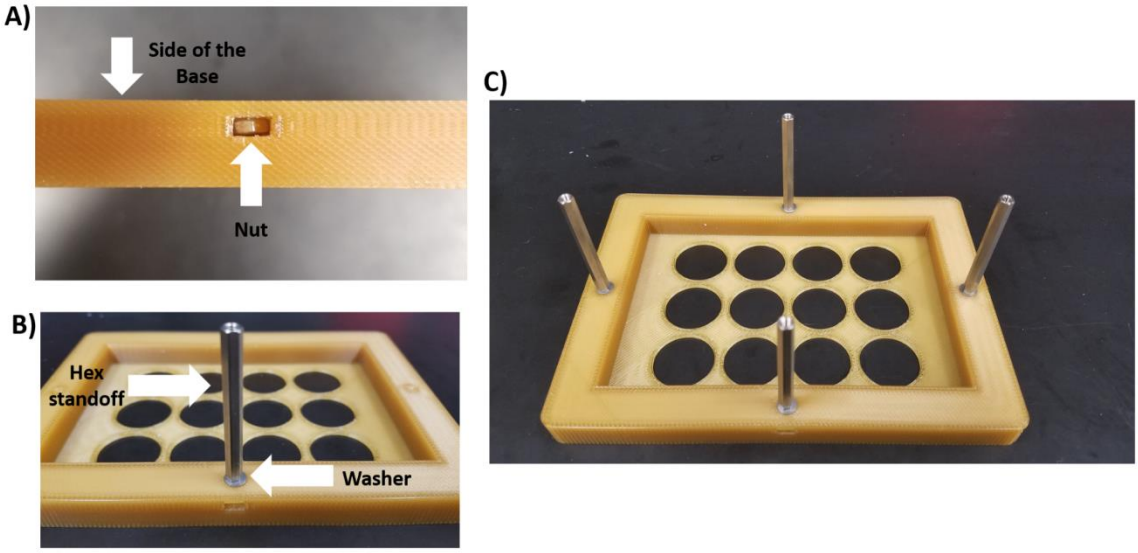

Supplemental Figure 2-7. Attachment of the 45 mm hex standoffs to the Base.

A) Each nut is placed into the side of the Base. B) A washer is added to the 45 mm hex standoff, which is then screwed into the nut. C) Image showing all hex standoffs attached to the Base.

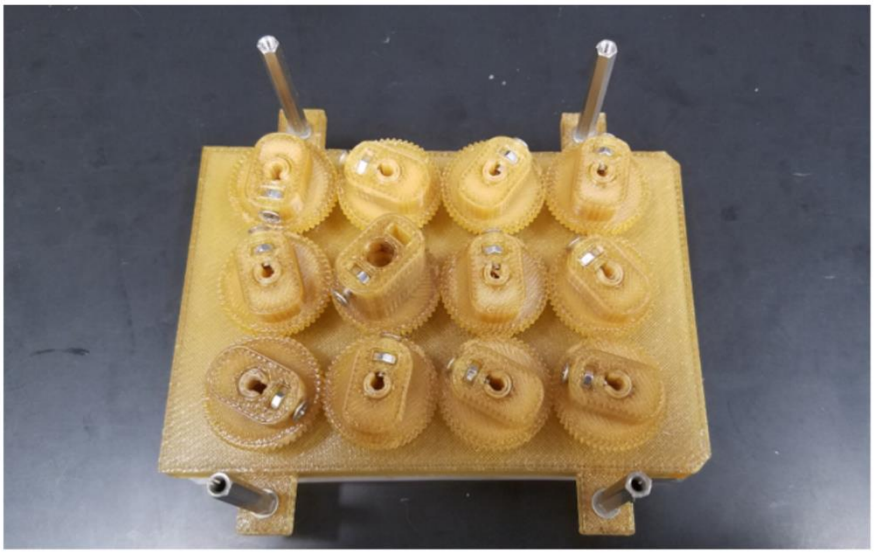

Supplemental Figure 2-8. Attachment of the 35 mm hex standoffs to the 12-Well Plate Lid.

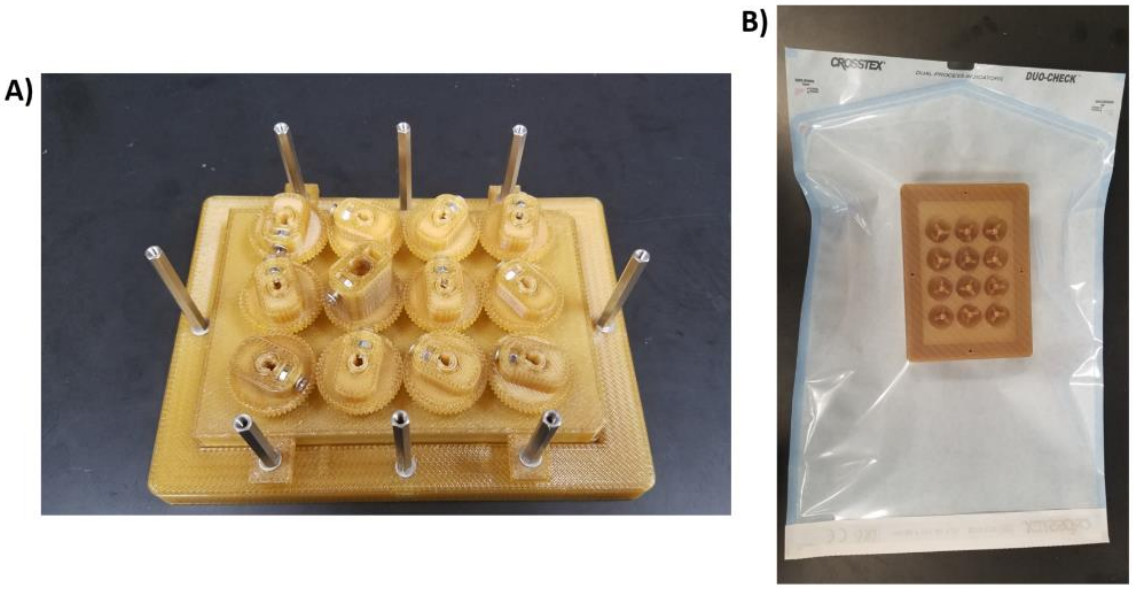

Supplemental Figure 2-9. Preparation of the bioreactor for autoclaving.

A) The Base with the hex standoffs, the 12-Well Plate Lid with the Paddles and Gears, and the stainless-steel screws can all be autoclaved. B) The piece should be placed upside down in an autoclavable bag (the Base should face the clear side of the bag).

Supplemental Figure 2-10. Attachment of the motor to the acrylic plate.

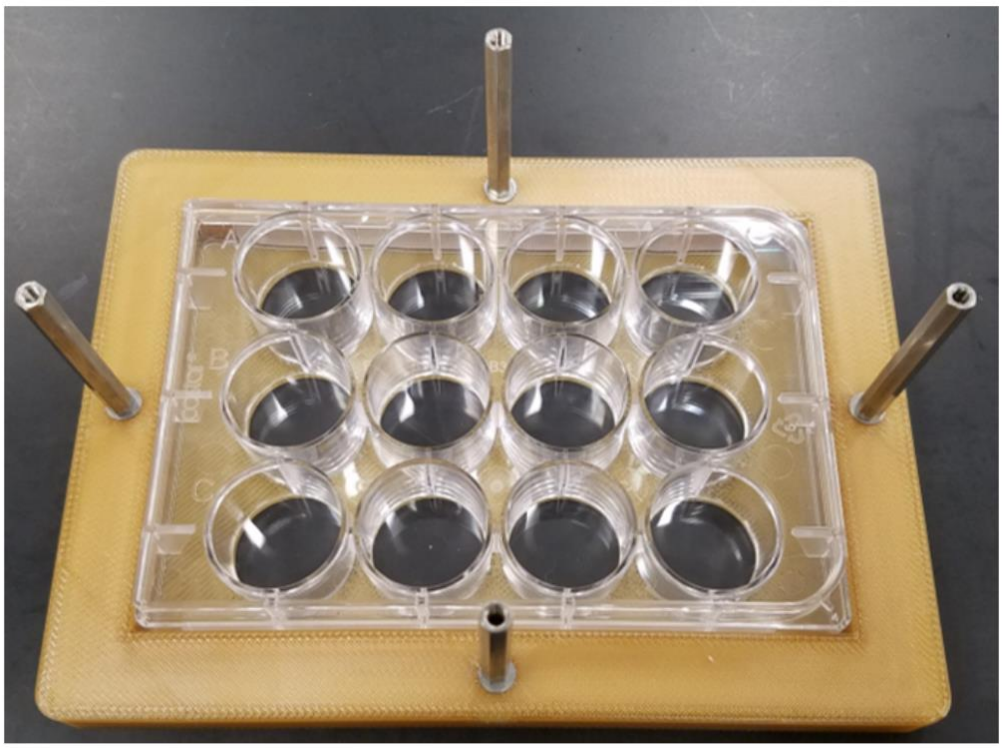

Supplemental Figure 2-11. Placement of a 12-well plate into the Base.

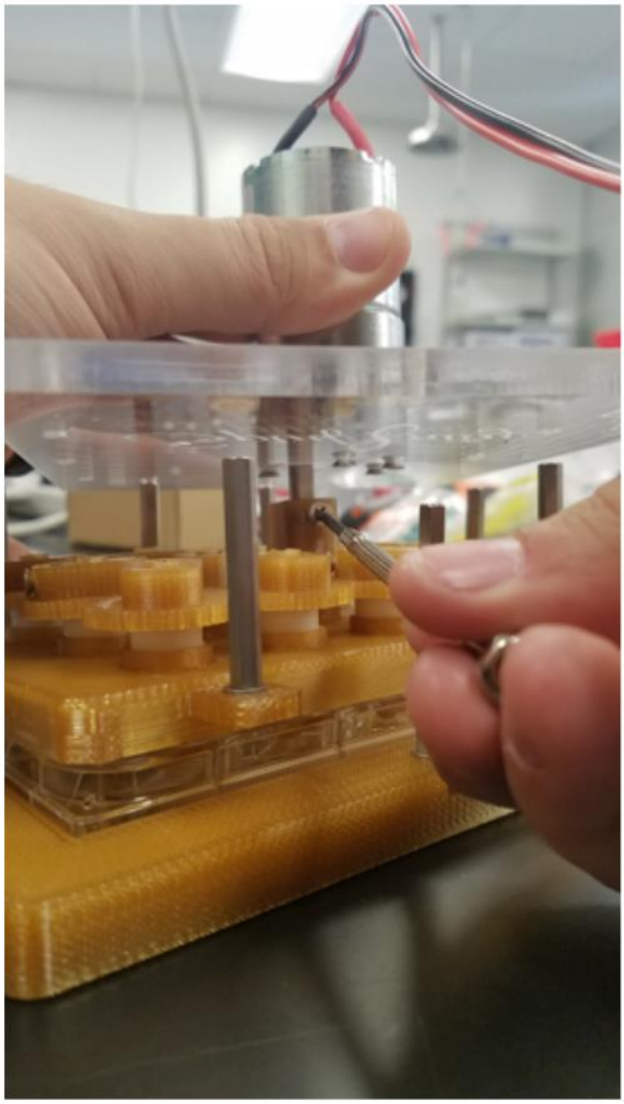

Supplemental Figure 2-12. Attachment of the beveled side of the motor shaft into the Motor Shaft Gear.

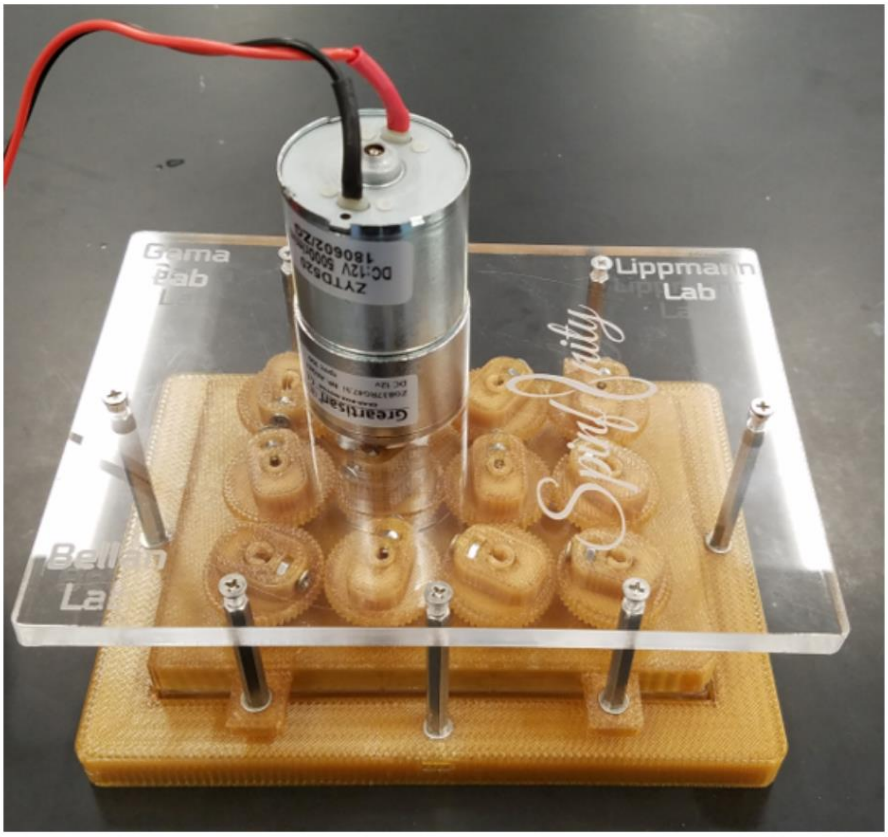

Supplemental Figure 2-13. Fully assembled bioreactor.

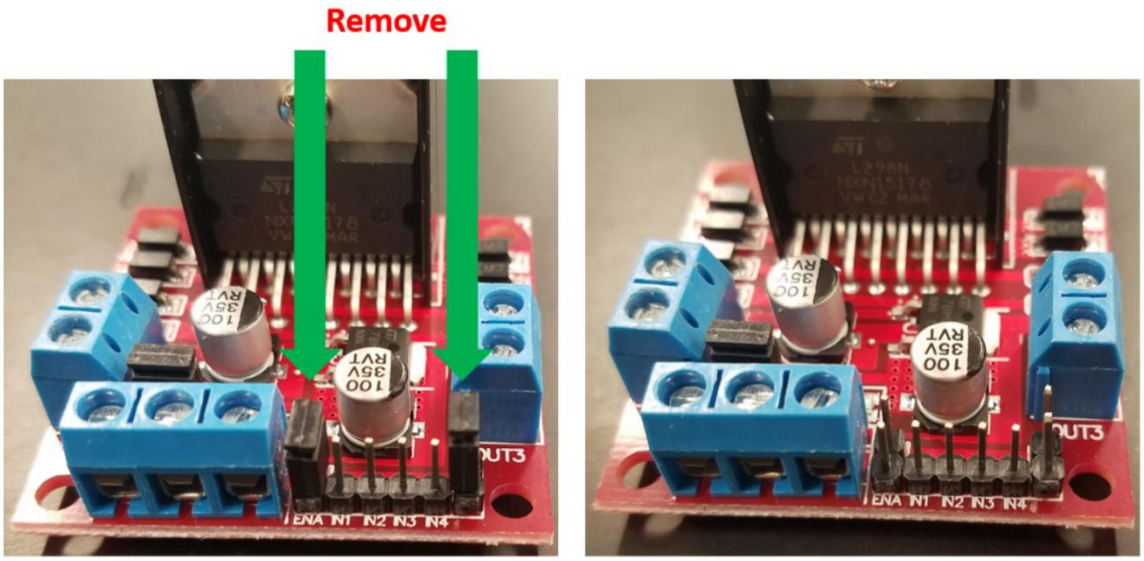

Supplemental Figure 2-14. Removal of the jumpers from the L298n bridge.

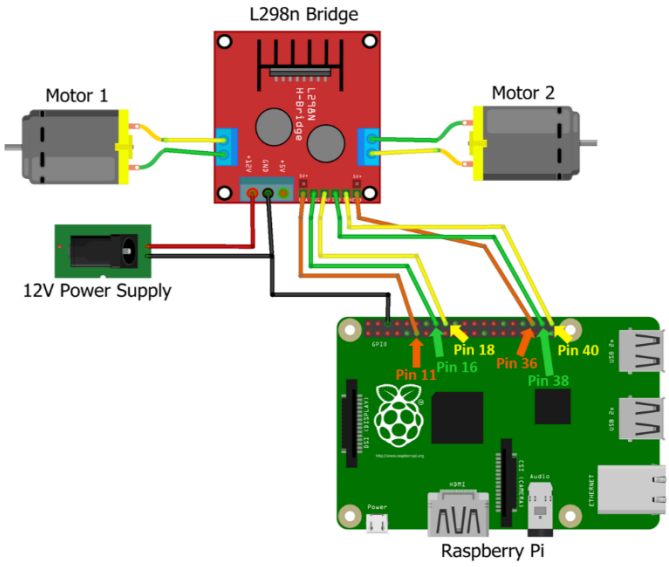

Motor 1		Motor 2	
L298n Bridge Pins	Raspberry Pi Pins	L298n Bridge Pins	Raspberry Pi Pins
ENA pin	11	ENA pin	36
IN1	16	IN1	38
IN2	18	IN2	40
Motor 3		Motor 4	
L298n Bridge Pins	Raspberry Pi Pins	L298n Bridge Pins	Raspberry Pi Pins
ENA pin	29	ENA pin	32
IN1	31	IN1	35
IN2	33	IN2	37

Motor 5	
L298n Bridge Pins	Raspberry Pi Pins
ENA pin	22
IN1	24
IN2	26

Supplemental Figure 2-15. Example for how to connect an L298n bridge to two motors and a Raspberry Pi.

The accompanying table provides pin locations for connecting the Raspberry Pi to up to five motors.

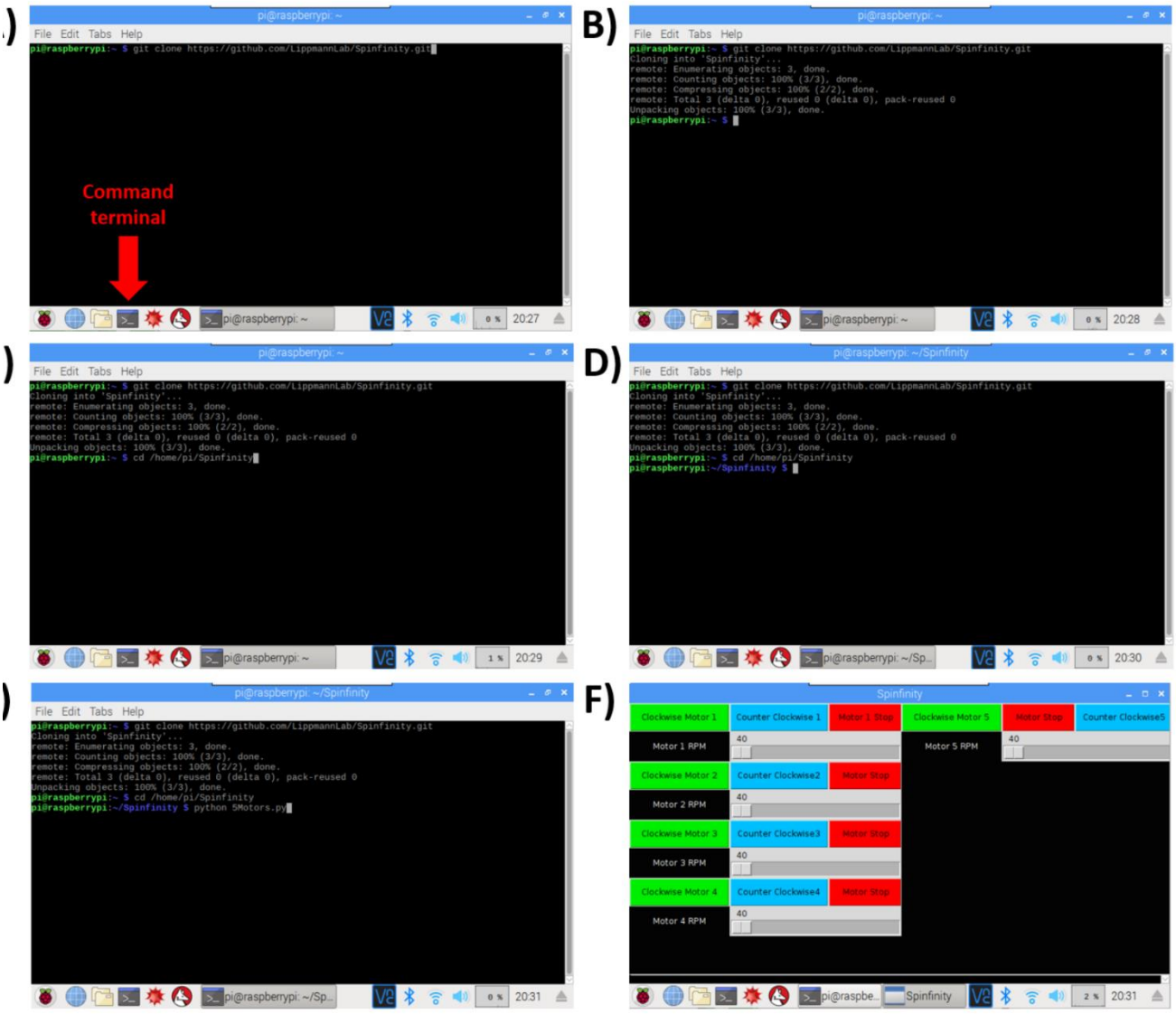

Supplemental Figure 2-16. Software installation setup.

A-B) The Command Terminal is opened, and by entering the text shown in the figure, the repository will be cloned from Github into a folder on the Raspberry Pi. C-D) Opening of the repository. E-F) Opening of the software, which leads to the user interface with touchscreen control.

Chapter 3

METABOLIC DISEASES AND THEIR EFFECT ON NEURAL IDENTITY AND BRAIN DEVELOPMENT

Adapted from:

Romero-Morales, AI, Robertson, GL., Rastogi, A., Rasmussen, ML., Temuri, H., McElroy, GS., Chakrabarty, RP., Hsu, L., Almonacid, P.M, Millis, B., Chandel, NS., Cartailler, JP. & Gama, V. Human iPSC-derived cerebral organoids model features of Leigh Syndrome and reveal abnormal corticogenesis. Under review, Development.

Abstract

Leigh syndrome (LS) is a rare, inherited neurometabolic disorder that presents with bilateral brain lesions caused by defects in the mitochondrial respiratory chain and associated nuclear-encoded proteins. We generated human induced pluripotent stem cells (iPSCs) from three LS patient-derived fibroblast lines. Using whole-exome and mitochondrial sequencing, we identified unreported mutations in pyruvate dehydrogenase (GM0372, PDH; GM13411, MT-ATP6/PDH) and dihydrolipoyl dehydrogenase (GM01503, DLD). These LS patient-derived iPSC lines were viable and capable of differentiating into progenitor populations, but we identified several abnormalities in three-dimensional differentiation models of brain development. LS patient-derived cerebral organoids showed defects in neural epithelial bud generation, and cortical architecture at 100 days. The double mutant MT-ATP6/PDH line produced organoid neural precursor cells with abnormal mitochondrial morphology, characterized by fragmentation and disorganization, and showed an increased generation of astrocytes. These studies aim to provide a comprehensive phenotypic characterization of available patient-derived cell lines that can be used to study Leigh syndrome.

Introduction

Leigh syndrome (LS), or sub-acute necrotizing encephalomyelopathy, is an inherited neurometabolic disorder that affects the central nervous system (CNS) (Baertling et al., 2014; Gerards et al., 2016; Leigh, 1951; Sorbi and Blass, 1982). LS is a rare, progressive, early-onset

disease with a prevalence of 1 in 40,000 live births (Lake et al., 2016). The pathologic features of LS are focal, bilateral lesions in one or more areas of the CNS, including the brainstem, thalamus, basal ganglia, cerebellum, cortex, and spinal cord (Alves et al., 2020; Sofou et al., 2018). The most common underlying cause is defective oxidative phosphorylation (OXPHOS), due to mutations in genes encoding complexes of the mitochondrial respiratory chain (Baertling et al., 2014; Lake et al., 2015, 2016).

The availability of animal models (Ferrari et al., 2017; Jain et al., 2016, 2019) and brain tissue from biopsies has provided critical insight into this disease. However, our understanding of the etiology and pathology of complex neurological diseases like LS would benefit from human-derived platforms such as induced pluripotent stem cell-derived models (Quadrato et al., 2016). The ability to reprogram somatic cells into induced pluripotent stem cells (iPSCs), followed by differentiation into specific lineages has become a useful tool for complex disease modeling (Kelava and Lancaster, 2016; Di Lullo and Kriegstein, 2017; Pașca, 2018; Quadrato et al., 2016). In the context of LS, iPSCs have been successfully generated from patients with mutations in mitochondrially encoded ATP Synthase Membrane Subunit 6 (MT-ATP6) (Galera-Monge et al., 2016; Grace et al., 2019; Lorenz et al., 2017; Ma et al., 2015), mitochondrially encoded NADH:Ubiquinone Oxidoreductase Core Subunit 3 (MT-ND3) subunit (Hattori et al., 2016), and the nuclear-encoded gene Surfeit locus protein 1 (SURF1) (Inak et al., 2021). These iPSC-model systems have been proposed for drug discovery (Inak et al., 2017; Lorenz et al., 2017) as well as testing platforms for potential metabolic rescue treatments (Ma et al., 2015).

Many studies have used LS patient fibroblasts commercially available at the Coriell Institute (Galera-Monge et al., 2016; Hinman et al., 1989; Huh et al., 1990; Iyer et al., 2012; Johnson et al., 2019; Ma et al., 2015; Sorbi and Blass, 1982; Vo et al., 2007; Zheng et al., 2016a). Here we report our findings on the genomic and phenotypic characterization of iPSCs generated from these LS patient-derived fibroblast lines. Whole exome and mitochondrial sequencing revealed previously unidentified mutations in these patient-derived cell lines. Three-dimensional differentiation of LS patient-derived iPSCs into neural rosettes and cerebral organoids resulted in severe abnormalities. LS patient-derived cerebral organoids grown for 100 days showed defects in the generation of neural epithelial buds and impaired corticogenesis. These results indicate

that aberrant corticogenesis may drive LS pathogenesis and demonstrate the utility of iPSC-derived systems to recapitulate CNS phenotypes and test potential strategies to restore neurogenesis in LS.

Results

Genomic characterization of Leigh syndrome fibroblasts.

Due to the limited genomic information available for the three cell lines (Supplemental Table 3-1), we performed whole-exome sequencing (WES) and mitochondrial sequencing of the fibroblasts before reprogramming (Figure 3-1 A-D and Supplemental Figure 3-1; data repository with the raw and analyzed WES and mitochondrial results can be found at https://www.ncbi.nlm.nih.gov/sra/PRJNA626388 & https://vandydata.github.io/Romero-Morales-Gama-Leigh-Syndrome-WES/). Comparison between the high impact, moderate impact, and all variants for identified insertion/deletions (INDELs) and single-nucleotide polymorphisms (SNPs) showed significant overlap between the three cell lines (Supplemental Figure 3-1A & B In-depth analysis of the top 15 high-impact SNPs (Supplemental Figure 3-1C) also confirmed an overlap between genotypes, with only three genes with confirmed SNPs related to neurological diseases (FRG2C for bipolar disorder and CDC27 and KIR2DL4 for white matter microstructure measurements) (Buniello et al., 2019).

Targeted analysis of the genes associated with Leigh syndrome (Lake et al., 2016) revealed a loss of function INDEL frameshift in pyruvate dehydrogenase complex (PDHc) E1 alpha 1 subunit or pyruvate dehydrogenase (PDHA1, c.79delC, p.Arg27fs) in the lines GM03672 and GM13411 (Figure 3-1E). A SNP in the PDHc E3 subunit or dihydrolipoyl dehydrogenase (DLD, c.100A>G, p.Thr34Ala) was identified in GM01503 (Figure 3-1E). In addition to being part of PDHc, DLD is also a component of the α-ketoglutarate and branched-chain α-ketoacid dehydrogenase complexes (Craigen, 1996). Despite the lack of genomic data, dysfunction of the PDH complex was previously suggested as the main driver of the disease in these patients (Hinman et al., 1989; Huh et al., 1990; Sorbi and Blass, 1982) (Supplemental Table 3-1). To our knowledge, mutations in the nuclear genome of GM13411 have not been reported to date.

Mitochondrial sequencing identified several SNPs in all the cell lines (Figure 3-1D). A loss of function SNP in the MT-ATP6 gene was identified in the GM13411 line. This mutation was reported in the original clinical case (Pastores et al., 1994). The authors described the T to G mutation at position 8993 that results in the substitution of a highly conserved leucine residue for an arginine (L156R). MT-ATP6 is part of the F0 domain of ATP synthase, which functions as a proton channel (Figure 3-1E). The L156R substitution prevents the induction of c-ring rotation of ATP synthase (Kühlbrandt and Davies, 2016), resulting in decreased ATP synthesis (Uittenbogaard et al., 2018). Heteroplasmy analysis of fibroblasts showed a 92% frequency of this mutation in the cell population, consistent with previous reports (Galera-Monge et al., 2016; Iyer et al., 2012; Pastores et al., 1994).

Characterization of iPSCs derived from commercially available Leigh syndrome fibroblasts.

Reprogramming of fibroblasts was performed as previously described (Takahashi et al., 2007) (Supplemental Figure 3-2A). Pluripotency was evaluated using the microarray-based analysis PluriTest (Müller et al., 2011). All three LS cell lines showed a high pluripotency score and a low novelty score (Supplemental Figure 3-2B,C), congruent with the transcriptional profile of pluripotent stem cells. Moreover, all the reprogrammed cells expressed the pluripotency markers NANOG and POU5F1 (OCT4) (Supplemental Figure 3-2D). The MT-ATP6/PDH cell line showed increased levels of NANOG ($p<0.0001$) compared to control.

To assess the ability of the LS and control cell lines to differentiate into the three germ layers, we performed trilineage differentiation as previously described (Kuang et al., 2019; Roberts et al., 2019) and measured expression of several genes using real time quantitative PCR (RT-qPCR). Commitment to ectodermal fate was evaluated by expression of the genes GATA3 and PAX6, endoderm fate was evaluated by the expression of the genes CDX2 and SOX17, and mesodermal fate was evaluated by the expression of the genes TBXT and NCAM (Supplemental Figure 3-2E). Although all the mutant cell lines can generate cells positive for the three germ layer markers without statistical differences, we observed an inherent variability in the differentiation efficiency among clones that may be due to differences in the genetic backgrounds

(heteroplasmy or potential X-linked gene silencing) (Juchniewicz et al., 2021; Lissens et al., 2000; Migeon, 2020).

Two-dimensional neural differentiation is not significantly altered by Leigh syndrome-associated mutations.

To determine if the LS mutations impact the commitment and development of the neural lineage, neural precursor cells (NPCs) (a mixed population of neural stem and progenitor cells) were generated by a dual SMAD inhibition protocol (Chambers et al., 2009) (Supplemental Figure 3-3A). NPCs expressed expected neural markers: PAX6, NESTIN, and SOX2 (Figure 3-2A and Supplemental Figure 3-3B). A slight increase was observed in PAX6+ nuclei in the PDH mutant ($p=0.494$, Figure 3-2B), but no other differences were identified (Figure 3-2B and Supplemental Figure 3-3B). The multipotent capacity of NPCs to generate neurons, astrocytes, and oligodendrocytes was evaluated using immunostaining and RT-qPCR (Figure 3-2A-C). We identified an increase in the mean fluorescence intensity of the astrocyte marker S100β in the DLD mutant line ($p=0.0185$), suggesting a propensity of these cells to commit to the astrocyte lineage.

Neural cell death is a hallmark of LS; thus, we performed a cell viability assay to investigate the sensitivity of the LS patient-derived NPCs to different apoptotic stimuli (Supplemental Figure 3-3C). Treatment with DNA damaging agents, etoposide and neocarzinostatin, and the microtubule depolymerizing agent nocodazole did not show increased sensitivity to cell death. Treatment with CCCP, a mitochondrial uncoupler, did not show increased susceptibility of the NPCs to mitochondrial damage. Thus, LS causing mutations do not affect the sensitivity of the NPCs to apoptotic stimuli.

To investigate the metabolic effects of LS causing mutations at the iPSC and NPC states, we performed metabolic analyses using the Seahorse Mito Stress Test. This assay provides a readout of bioenergetic function by assessing several parameters including oxygen consumption rate (OCR) and extra cellular acidification rate (ECAR). Previous studies show that iPSCs mainly rely on glycolysis to generate ATP and intermediates that contribute to pluripotency and self-renewal

(Chandel et al., 2016; Folmes et al., 2011; Hamanaka and Chandel, 2010; Kondoh et al., 2007). The low levels of OXPHOS have been attributed at least in part to an immature and fragmented mitochondrial network (Cho et al., 2006; Chung et al., 2010; Folmes et al., 2011; Prigione et al., 2010; Zhang et al., 2011). While LS patient-derived iPSCs do not show significant differences in OCR (Supplemental Figure 3-4A), ECAR (proxy of glycolysis) was reduced in the MT-ATP6/PDH mutants compared to control (Supplemental Figure 3-4B). Analysis of other bioenergetic parameters in these cells also showed dysregulation in the non-mitochondrial oxygen consumption rate ($p=0.0284$, Supplemental Figure 3-4C), which has been associated with highly proliferative cells (Herst and Berridge, 2007; Krisher and Prather, 2012; Manes and Lai, 1995; Muller et al., 2019; Starkov, 2008).

Differentiated cells have more complex mitochondrial networks and utilize OXPHOS as the main source of ATP (Mandal et al., 2011; Suhr et al., 2010; Wu et al., 2016; Yanes et al., 2010). The metabolic switch from glycolysis to OXPHOS is a hallmark of NPC differentiation (Agathocleous et al., 2012; Zheng et al., 2016b). While all lines showed similar levels of glycolysis, only PDH and DLD NPCs showed similar levels of OXPHOS compared to control (Supplemental Figure 3-4D-E). OCR values in MT-ATP6/PDH mutant cells were significantly lower after FCCP treatment (Supplemental Figure 3-4D), which translate into a reduced spare respiratory capacity (Supplemental Figure 3-4F, $p=0.0354$), reflecting lower metabolic fitness and a deficiency in engaging the metabolic switch during differentiation. Non-mitochondrial oxygen consumption was also lower in MT-ATP6/PDH NPCs ($p=0.0317$).

LS mutations cause morphological alterations in three-dimensional models of neurodevelopment.

Previous studies using cells from LS patients carrying homozygous SURF1 (c.769G>A and c.530T>G) and MT-ATP6 (m.9185T>C) mutations showed an abnormal generation of neural lineages (Lorenz et al., 2017) and impaired neurogenesis in cerebral organoids (Inak et al., 2021). Therefore, we investigated the effects of the PDH, DLD, and MT-ATP6/PDH mutations on

neurogenesis using three-dimensional models of neural development (Lancaster and Knoblich, 2014; Romero-Morales et al., 2019).

To examine the effects of LS-associated mutations in the early stages of CNS development, we generated neural rosettes (NR) using embryoid bodies (EBs) grown in the presence of SMAD inhibitor media (Figure 3-3A) (Elkabetz et al., 2008; Zhang et al., 2001). These structures have previously been shown to recapitulate the early neural tube formation stage of development (Elkabetz et al., 2008; Wilson and Stice, 2006). NRs were stained with the tight junction marker ZO-1 (Elkabetz et al., 2008; Hříbková et al., 2018) and the centrosomal marker CDK5RAP2 (Figure 3-3B). Quantification of the number of NRs per field of view showed fewer of these structures in the DLD mutant (Figure 3-3C, $p<0.001$). Lumen area quantification revealed that PDH and MT-ATP6/PDH mutants have larger lumen areas, while the DLD mutant line showed a smaller area relative to controls (Figure 3-3D PDH: $p<0.0001$, DLD: $p=0.0236$ and MT-ATP6/PDH: $p<0.0001$). The NRs obtained from all cell lines followed the expected morphological changes described previously (Hříbková et al., 2018). The polymerization of α-tubulin and generation of the ZO-1 ring at the apical region of the rosettes are conserved in the LS mutants. Increased NR lumen size has previously been associated with activation of the TGFβ pathway (Medelnik et al., 2018), Notch and sonic hedgehog (SHH) pathway, and inhibition of WNT (Elkabetz et al., 2008). Large rosette formation is thought to be a consequence of coalescence or fusion of smaller rosettes (Fedorova et al., 2019) or apical domain opening and expansion rather than a process dependent on cell proliferation (Medelnik et al., 2018).

Leigh syndrome-associated mutations disrupt corticogenesis in cerebral organoids.

Cortical abnormalities in LS have been associated with developmental delay and disease progression. Imaging studies have shown an incidence of cortical lesions over 20% of the patients, with this finding being highly associated with mtDNA etiology (Alves et al., 2020). To investigate the effects of these mutations during corticogenesis, we generated cerebral organoids from LS patient-derived iPSCs (Supplemental Figure 3-5A).

Differences between the cell lines became apparent as early as the neuroepithelial bud expansion phase. After Matrigel embedding, the MT-ATP6/PDH mutant cell line showed poor budding with large areas of non-neuroepithelial cells (Supplemental Figure 3-5B). Defective organoid formation in this cell line was significantly higher than control and the other two LS cell lines (Supplemental Figure 3-5C). A previous report showed that when iPSCs generated from fibroblasts harboring the same T8993G mitochondrial mutation were differentiated into EBs, there was rapid regression and death after 7 days in suspension, while the monolayer culture did not show obvious deficits in cell growth (Grace et al., 2019). Given that the neuroectoderm expansion phase happens during days 7-10, the degeneration of the MT-ATP6/PDH organoids after embedding is consistent with these reports. Higher metabolic requirements are associated with NPC proliferation and migration in three-dimensional scaffolds and development (Fang et al., 2020; Homem et al., 2015). As the PDH mutant line did not show this particular phenotype at this stage, the presence of the mitochondrial mutation in the MT-ATP6/PDH line may be responsible for the reduction in organoid formation efficiency.

To assess the effect of the LS mutations during the first stages of neural development, we collected mRNA of day 30 organoids and evaluated the expression of NPC and cortical markers by RT-qPCR (Supplemental Figure 3-6A). SOX2, an NPC marker, expression was reduced in all three LS mutants (PDH: $p=0.0156$, DLD $p=0.0303$, MT-ATP6/DPH: $p<0.0001$). The expression of NPC markers NESTIN and PAX6 were increased in PDH mutant organoids ($p=0.0156$ and $p=0.0134$, respectively). MT-ATP6/PDH organoids showed a reduction in the expression of PAX6 ($p=0.0231$) and an increase in the expression of the intermediate progenitor cell (IPC) marker TBR2 ($p=0.0224$). The cortical plate marker CTIP2 was found to be reduced in both DLD ($p=0.0080$) and MT-ATP6/PDH ($p<0.0001$); and the neuronal marker βIII-TUBULIN (TUBB3) was reduced in MT-ATP6/PDH ($p=0.0302$). No significant differences were noted in expression of the glycoprotein REELIN or the cortical plate marker TBR1 among the different genotypes.

The reduction in expression of NPC markers SOX2 and PAX6 in MT-ATP6/PDH mutant organoids with a concomitant increase in TBR2 may suggest a premature commitment to IPCs (Englund, 2005; Hutton and Pevny, 2011; Sansom et al., 2009). This premature differentiation

into IPCs and reduced expression of committed neuronal markers, such as CTIP2 and TUBB3, may suggest an inability to acquire a neuronal fate in this genotype.

Brain organoids were sectioned and stained for ventricular zone (VZ), subventricular zone (sVZ), and cortical plate (CP) markers (Supplemental Figure 3-6B-E). Day 30 organoids were obtained from at least 3 independent batches of differentiation and representative images were obtained from at least 4 individual organoids per batch. Quantification of immunofluorescence images revealed no significant differences in the number of NPCs positive for SOX2, PAX6, and NESTIN or the IPC marker TBR2 (Supplemental Figure 3-6F). In agreement with the defective neuroepithelial expansion, the overall architecture in MT-ATP6/PDH organoids was compromised. Few ventricle-like structures were present, and the foci of PAX6+ cells were not organized in the expected radial pattern. Migration of early-born neurons in vivo depends on pioneer Cajal-Retzius neurons that are positive for the glycoprotein REELIN (Lancaster et al., 2017). Cells positive for this marker were identified in superficial regions of all organoids. Early born neurons positive for CTIP2+ and TBR1+ were observed in all genotypes. The neuronal marker Microtubule-associated protein 2 (MAP2) was also present in all samples at similar levels to control (Supplemental Figure 3-6E, F). Expression of the outer radial glia (oRG) marker Homeodomain-only protein (HOPX) was significantly reduced in the PDH ($p<0.0001$) and MT-ATP6/PDH mutants ($p=0.0417$). Metabolic stress has been correlated with reduced specification in organoids, especially in oRG and newborn neurons (Bhaduri et al., 2020). Hence, lower levels of HOPX positive cells in the cell lines harboring a PDH mutation may be associated with defects in cellular fate specification at this timepoint.

To assess cortical layer fate specification during development, we grew cerebral organoids until day 100 and probed for upper cortical layer markers (Florio and Huttner, 2014; Lui et al., 2011; Saito et al., 2011). RT-qPCR analysis of the gene expression at this time point showed no significant differences in expression of NPC markers SOX2, and PAX6; oRG marker HOPX, and IPC marker TBR2. Major dysregulation was observed in the neuronal markers (Figure 3-4A). Cortical layer makers CTIP2 ($p<0.0001$ in all cases), TBR1 ($p=0.0002$ for PDH and DLD, $p<0.0001$ for MT-ATP6/PDH), SATB2 ($p<0.0001$ in all cases), and BRN2 ($p=0.0005$ for PDH, $p=0.0001$ for DLD and $p=0.0002$ for MT-ATP6/PDH) were significantly reduced at this timepoint. Pan-neuronal marker

TUBB3 (p=0.0013 for PDH, p=0.0002 for DLD, and p=0.0003 for MT-ATP6/PDH) was also lower for all three mutants, suggesting a reduced capacity of commitment to a neuronal fate. Interestingly, the neuronal marker CUX1 did not show significant differences in expression among cell lines. While CUX1 is predominantly expressed in pyramidal neurons of the upper layers II-IV of the developing cortex (Leone et al., 2008; Nieto et al., 2004), its expression has been reported in the SVZ (Nieto et al., 2004) and cortical plate (Saito et al., 2011). It has also been reported as being co-expressed with PAX6+ and TBR2+ cells (Cipriani et al., 2015). Due to the reduced expression of the cortical and neuronal markers, the maintained expression of CUX1 could reflect its conserved expression in NPC and IPC populations rather than in committed upper-layer neurons.

Quantification of the immunofluorescence images (Figure 3-4B-F) showed that the late-born superficial layer marker SATB2 (layer IV) was reduced in PDH (p=0.0305) and DLD (p=0.0013) organoids (Figure 3-4B, F). Cortical layer III marker BRN2 was reduced in the DLD mutant (p=0.0455, Figure 3-4C, F). CTIP2+ cells were also reduced in DLD and MT-ATP6/PDH organoids (p<0.0001 in both cases. Figure 3-4B, C, F). On day 100, MT-ATP6/PDH organoids had a significant increase in PAX6+ cells (p<0.0001, Figure 3-4B, C, F) suggesting an aberrant persistence of NPCs and lack of commitment to neuronal cell fate.

As astrogliosis is a hallmark for LS (Lake et al., 2015), we looked at the expression of astrocyte markers at the mRNA and protein level. q-RT PCR analysis of the neuronal marker TUBB3 reveals a marked downregulation in all three lines (PDH p=0.0013, DLD p=0.0002, and MT-ATP6/PDH p=0.0003) that may be associated with the reduction in the number of cortical neurons. Astrocyte marker SOX9 (Sun et al., 2017) did not show major differences in expression. Analysis of other astrocyte markers such as Glial Fibrillary Acidic Protein (GFAP), S100 calcium-binding protein-β (S100B), Aldehyde Dehydrogenase Family 1 Member L1 (ALDH1L1), and VIMENTIN showed an increased, yet not significant, upregulation in some genotypes (Figure 3-5A). In the case of DLD, all the above-mentioned markers were increased compared to the control. The double mutant MT-ATP6/PDH had increased expression of VIMENTIN and ALDH1L1, while PDH showed an increment in S100B and VIMENTIN. At a protein level, DLD and PDH cerebral organoids showed increased staining of astrocyte markers GFAP and S100B, respectively, at day 100 (Figure 3-4C,

Figure 3-5B, D). S100B was also increased in the double mutant, but the results were not statistically significant. Staining for ALDH1L1 did not show major differences between the genotypes (Figure 3-5C, D). Immunofluorescence staining of the organoids for β3-TUBULIN showed a statistical difference between control and DLD ($p=0.0174$), but not in the other two mutants. The decrease in diversity of neuronal cell types and increase in the presence of S100β+ cells in the double mutants may suggest a switch to astrocyte fate during cortical development. Interestingly, the DLD organoids had higher GFAP staining ($p=0.0141$) that may suggest an increase in the reactivity of the astrocyte population. Upregulation of the astrocyte markers GFAP, S100β, and VIMENTIN have been associated with astrocyte reactivity and in response to injury (Clarke et al., 2018; Escartin et al., 2021; Liddelow and Barres, 2017; Liddelow et al., 2017; Qi et al., 2017; Zamanian et al., 2012). Although the gene expression of these pan-reactive markers was not significant, it may suggest activation of the glial population in response to the metabolic dysregulation in LS organoids.

Metabolic dysregulation in Leigh syndrome-derived cerebral organoids

To explore changes in metabolites, we performed metabolomic profiling of Day 40 organoids. Metabolomic analysis showed 43 different metabolites that were significantly dysregulated in the LS organoids (Supplemental Table 3-2 and Supplemental Figure 3-7). Out of these metabolites, 8 were dysregulated in PDH, 16 in DLD, and 32 in MT-ATP6/PDH (Figure 3-7A and Supplemental Figure 3-7).

The metabolites proline, 6-phosphogluconic acid, and hydroxyphenyllactic acid were dysregulated in all three LS mutants. High levels of proline have been associated with negative effects in brain function by interference in glutamatergic neurotransmission (Gogos et al., 1999; Vorstman et al., 2009). On the other hand, 6-phosphogluconic acid was reduced in all three LS cell lines. High concentrations of this metabolite have been associated with an active pentose phosphate pathway in early brain development in rats (Hakim et al., 1980) and its supplementation increased the diameter of neurospheres derived from the embryonic Ts1Cje mouse model of Down syndrome (Seth et al., 2020). Hydroxyphenyllactic acid was elevated in DLD and PDH mutant organoids but downregulated in MT-ATP6/PDH. High levels of this

metabolite have been reported in association with high lactate and pyruvate in pediatric lactic acidosis in patients with PDHc deficiency (Kumps et al., 2002; Stern, 1994).

Pyruvate was also increased in the MT-ATP6/PDH mutant organoids, correlating with the lactic acidosis expected in the organoids based on the patient phenotypes and the presence of the PDH mutation that hinders flux from pyruvate into the TCA cycle through acetyl-CoA. Moreover, the glycolysis/gluconeogenesis intermediate phosphoenolpyruvate was also elevated in these mutants. Increased levels of phosphoenolpyruvate in rat brains after ischemic injury are thought to have a protective role in cerebral ischemia in vivo (Geng et al., 2021) and in oxygen/glucose deprivation in vitro (Jiang et al., 2019).

Besides the previously mentioned metabolites, MT-ATP6/PDH mutant organoids presented increased levels of choline, cytidine, and leucine. Choline is a crucial metabolite for normal CNS development. Neural tube defects have been associated with a lack of choline during early pregnancy (Zeisel, 2006). It has also been shown to increase cell proliferation and decrease apoptosis in fetal rat hippocampal progenitor cells (Albright et al., 1999b, 1999a; Zeisel and Niculescu, 2006). Choline is also crucial for the production of the neurotransmitter acetylcholine, the sphingolipid sphingomyelin, and myelin (Oshida et al., 2003). Concomitantly, cytidine is used with choline for the generation of cytidine-5-diphosphocholine, a crucial intermediate in the biosynthesis of the cell membrane phospholipids phosphatidylcholine and phosphatidylethanolamine (Cansev, 2006; Rema et al., 2008). Increased abundance of the branched-chain amino acid leucine has been associated with the metabolic illness maple syrup urine disease and can be extremely neurotoxic (Bridi et al., 2005; García-Cazorla et al., 2014). This amino acid is considered ketogenic as its end products can enter the TCA cycle for energy generation or act as precursors for lipogenesis and ketone body production (Manoli and Venditti, 2016).

Pathway analysis of the dysregulated metabolites (Supplemental Tables 3-3 to 3-5) show overlap in pyrimidine metabolism, taurine and hypotaurine metabolism, pentose phosphate pathway, arginine and proline metabolism, and aminoacyl-tRNA biosynthesis. Pyrimidine nucleotides are essential precursors for nucleic acid synthesis and are involved in polysaccharide and phospholipid biosynthesis, detoxification processes, and protein and lipid glycosylation

(Fumagalli et al., 2017). Taurine and hypotaurine are osmotic regulators in the brain, as well as agonists to GABAergic and glycinergic neurons (Albrecht and Schousboe, 2005). Its presence in the developing brain is necessary for the correct development of axons and the formation of synaptic connections (Sturman, 1993). Dysregulation of the aminoacyl-tRNA biosynthesis pathways is well documented as causal etiology for several neurodevelopmental disorders such as leukoencephalopathies, microcephaly, and Leigh syndrome (Francklyn and Mullen, 2019; Ognjenović and Simonović, 2018).

We also performed metabolite set enrichment analysis (Figure 3-7B-C). Besides the previously mentioned pathways, the Warburg effect or aerobic glycolysis was also shared among the LS mutants. Although this effect is considered one of the hallmarks of cancer, it has also been associated with several homeostatic processes, including cell turnover and proliferation, and brain development (Bubici and Papa, 2019). Energy generation through aerobic glycolysis as a compensatory mechanism to overcome the metabolic deficiency in LS could suggest a survival adaptation of the cerebral organoids. Moreover, the shutoff of aerobic glycolysis is critical to neuronal differentiation in human NPCs. Inability to transition to neuronal OXPHOS causes apoptosis due to excessive conversion of pyruvate to lactate, and potentially a cell fate shift into GFAP-positive glial cells (Zheng et al., 2016b). Considering our observations that there is a marked deficit in MT-ATP6/PDH mutants to commit and generate neuronal subtypes and an increased signal in astroglial markers, these mutations may be impairing the ability to transition from aerobic glycolysis to OXPHOS as previously described with SURF mutations (Inak et al., 2021). The preferential switch to a glial fate may be promoted by astrocytes having low expression levels or lower activity levels of the PDHα subunit (Bélanger et al., 2011; Halim et al., 2010; Itoh et al., 2003; Laughton et al., 2007).

Discussion

Leigh syndrome is a rare inherited neurometabolic disease with more than 75 causal genes identified in both nuclear and mitochondrial DNA. It has an early onset, affecting most patients within their first year of life, although cases during teenage years and adulthood have been

reported (Finsterer, 2008; Lake et al., 2016). As it is a highly heterogeneous disease, establishment of animal and in vitro models have been challenging and limited to only select mutations. Here we report the characterization and the subsequent generation of brain organoids from three commercially available Leigh syndrome fibroblast cell lines and age-matched control.

Three-dimensional differentiation generates higher numbers of NPCs and more mature neurons than two-dimensional differentiation (Chandrasekaran et al., 2017; Di Lullo and Kriegstein, 2017; Muratore et al., 2014; Paşca et al., 2015) in part due to an improved spatial cellular environment that influences cell fate specification. We observed that all the LS cerebral organoids failed to thrive at different time points. Although organoid development initially appeared normal in cell lines with nuclear-encoded LS mutations, at later time points the developmental program was compromised, presumably due to failure to generate upper-layer neurons.

Although the number of cells positive for the upper neural markers seems to be reduced, the organoid still maintains a cellular density similar to control. It would be interesting to reveal the fate and identity of these cells (Quadrato et al., 2017). Further analysis of these organoids at later times of maturation using single cell RNA sequencing (Kanton et al., 2019; Velasco et al., 2019) or mass cytometry (Brockman et al., 2021; Leelatian et al., 2017) would be useful to identify the effects of the LS associated mutations in cortical cell fate specification.

Clinical data from LS patients include marked gliosis as part of the characteristic findings (Baertling et al., 2014, 2016; Lake et al., 2015; Schubert and Vilarinho, 2020). While this gliosis phenotype is potentially associated with a reactive process secondary to neuronal damage, an intriguing alternate possibility is that NPCs may have an increased propensity to differentiate down the astrocyte lineage due to LS-causative mutations and mitochondrial-associated dysregulations. Previous studies have shown that reactive astrocytes acquire molecular hallmarks of radial glial cells. It was also shown through genetic fate mapping that mature astroglial cells can dedifferentiate and resume proliferation (Robel et al., 2009, 2011). Thus, the increase in the glial-specific marker S100β in PDH organoids and DLD multipotency cultures, as well as in GFAP staining in DLD organoids and the upregulation, albeit not significant, in mRNA

expression of the astrocyte markers could either reflect that chronic metabolic stress induced by Leigh syndrome mutations activates a brain injury response, or that the inhibition of mitochondrial metabolism in NPCs could cause defects in lineage selection (Escartin et al., 2021). Due to the differential expression and activation levels of the PDH complex in astrocytes (Bélanger et al., 2011; Halim et al., 2010), a predisposition of these cell lines to commit to an astroglial fate cannot be ruled out. Culturing these organoids for longer than 100 days is required to analyze the gliosis phenotype in more detail. Analysis of A1 specific reactivity markers may clarify whether the upregulation of GFAP, S100B, ALDH1L1, and VIMENTIN is associated with a neuroinflammation response to neuronal damage (Escartin et al., 2021; Liddelow et al., 2017).

The formation of lesions in LS has been described as the result of OXPHOS dysfunction and subsequent ATP depletion. Neuronal dysfunction is suspected to trigger chronic gliosis (Baertling et al., 2016). In patients, the gliosis phenotype can be accompanied by vascular hypertrophy and the production of excess ROS, which increases neuronal damage (Lake et al., 2015). However, due to the lack of vascularization in the organoid model, replicating the vascular abnormalities associated with LS is not feasible.

In a previous study (Hattori et al., 2016), the metabolic signature analysis of iPSCs derived from a mitochondrial encoded LS mutation (m.10191T>C) showed differences in the abundance of pyruvate and lactate, among others. In our study, metabolomic analysis from organoids shows that the observed changes in the metabolites are in line with the clinical observations of LS patients. Changes in blood and cerebral spinal fluid concentration of lactate and pyruvate are common diagnostic tools for LS (Hattori et al., 2016) and other mitochondrial diseases (Barshop, 2004; Buzkova et al., 2018; Esterhuizen et al., 2017; Rahman and Rahman, 2018). While changes in the NADH/NAD+ ratio, de novo nucleotide synthesis, and in other metabolites from the ETC complex III and TCA cycle, were also identified, these were modest considering the genetic alterations in the mutant cell lines should directly affect these pathways. This could point to metabolic compensatory mechanisms that could be engaged during development. Moreover, the disruption in the metabolic network observed in LS cerebral organoids correlates with the severity and mortality of the disease in the probands. Although aerobic glycolysis was identified as a significantly affected pathway in all the mutants, the effects of the MT-ATP6/PDH mutation

reflected the importance of competent glycolysis to OXPHOS transition in early brain development.

The metabolic dysregulation of the affected tissues in LS may have a direct effect on mitochondrial morphology and function. Mitochondrial fragmentation is a hallmark of glycolytic cell types such as stem cells and cancer cells (Chen and Chan, 2017; Rastogi et al., 2019). Moreover, neurogenesis defects have been observed in the context of mitochondrial morphology dysregulation and are considered to be upstream regulators of self-renewal and cell fate decisions in stem cells (Iwata et al., 2020; Khacho et al., 2016). Also, the capacity of cells to undergo a metabolic switch during neurodevelopment is crucial for their survival and correct fate determination (Zheng et al., 2016b). The double mutant MT-ATP6/PDH showed a reduced energetic capacity in both iPSC and NPC stages that does not appear to affect their ability to differentiate into the three neural lineages nor increase their sensitivity to apoptotic stimuli. The MT-ATP6/PDH NPCs did not show major alterations of the mitochondrial network in two-dimensional cultures.

Energetic requirements have been shown to directly impact the capacity of NPCs to survive, migrate and differentiate (Zanotelli et al., 2018, 2019). The effects of LS causing mutations on mitochondrial network integrity and overall development of the neural lineage became more apparent in the 3D systems. Tissue architecture, mechanical cues, cell-to-cell communication, nutrient accessibility, oxygen tension, and morphogen gradients characteristic of 3D systems aid to recapitulate the microenvironment in the developing CNS in a manner that is not supported by 2D neural differentiations (Pampaloni et al., 2007; Tibbitt and Anseth, 2012).

To our knowledge, this is the first time that mitochondrial morphology in the cortex has been analyzed in a human model system of LS brain development and highlights the critical function of mitochondrial network plasticity for the proper specification of cell fate and survival. However, limitations in mitochondrial segmentation and resolution when using conventional confocal microscopy need to be addressed. Large, interconnected areas of mitochondrial network can be mistaken with aggregated mitochondria especially in high cellular density areas due to limitations in the spatial resolution and thresholding of the images. However, increased accessibility to super resolution microscopy, 2D and 3D structured illumination microscopy, high content imaging,

improved artificial intelligence and machine learning approaches may resolve these challenges (Chaudhry et al., 2020; Jakobs, 2006; Leonard et al., 2015).

Taken together, our study sheds new light on the morphological and functional LS alterations impacting early events of neurogenesis. We identified new genetic alterations in LS samples by using whole-exome sequencing and mitochondrial DNA sequencing. We described the effects of LS mutations on early development, underscoring the critical function of metabolism in human neurogenesis. Our work also provides a comprehensive phenotypic characterization of available patient samples to encourage their utilization as model systems for uncovering the mechanisms underlying neuronal cell death in the context of LS and as human platforms for drug discovery.

Figures

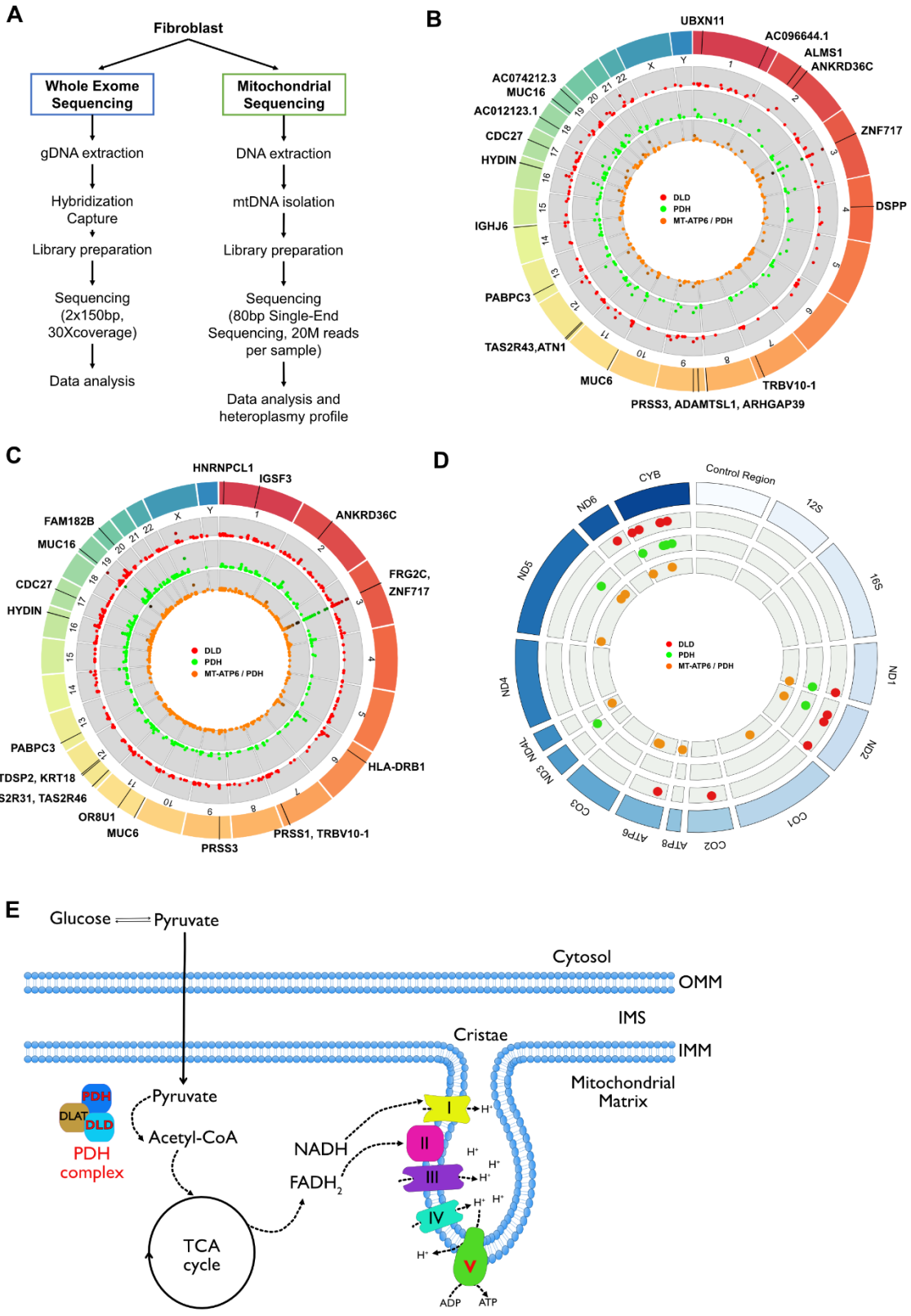
A
Fibroblast
Whole Exome Sequencing
Mitochondrial Sequencing
gDNA extraction
Hybridization Capture
Library preparation
Sequencing (2x150bp, 30Xcoverage)
Data analysis
DNA extraction
mtDNA isolation
Library preparation
Sequencing (80bp Single-End Sequencing, 20M reads per sample)
Data analysis and heteroplasmy profile
B
UBXN11
AC096644.1
ALMS1
ANKRD36C
ZNF717
DSPP
TRBV10-1
PRSS3, ADAMTSL1, ARHGAP39
MUC6
TAS2R43,ATN1
PABPC3
IGHJ6
HYDIN
CDC27
AC012123.1
MUC16
AC074212.3
DLD
PDH
MT-ATP6 / PDH
C
HNRNPCL1
IGSF3
ANKRD36C
FRG2C, ZNF717
HLA-DRB1
PRSS1, TRBV10-1
PRSS3
MUC6
OR8U1
TAS2R31, TAS2R46
CTDSP2, KRT18
PABPC3
HYDIN
CDC27
MUC16
FAM182B
DLD
PDH
MT-ATP6 / PDH
D
CYB
Control Region
12S
16S
ND1
ND2
CO1
CO2
ATP8
ATP6
CO3
ND3
ND4L
ND4
ND5
ND6
DLD
PDH
MT-ATP6 / PDH
E
Glucose
Pyruvate
Cytosol
OMM
IMS
Cristae
IMM
Mitochondrial Matrix
PDH
DLAT
DLD
PDH complex
Pyruvate
Acetyl-CoA
TCA cycle
NADH
FADH2
I
II
III
IV
V
H+
ADP
ATP

Figure 3-1. Whole exome sequencing identifies novel mutations in Leigh syndrome-derived fibroblasts.

A. Schematic of the WES and mitochondrial sequencing workflow. B-C. Representation of WES data, highlighting the top 20 genes containing high impact indels (B) and top 20 genes containing high impact SNPs (C, increased likelihood of disrupting protein function). D. Mitochondrial sequencing identifies novel mutations in LS fibroblasts. Representation of mitochondrial sequencing data, highlighting mitochondrial genes containing mutations (transitions, deletions, or transversions). Red dots: DLD line. Green dots: PDH line. Orange dots: MT-ATP6/PDH line. E. Representation of the affected proteins in the LS cell lines. PDH and DLD are part of the pyruvate dehydrogenase complex (PDHc). MT-ATP6 is a subunit of the ATP synthase, represented here as the electro transport chain complex V. PDH: Pyruvate dehydrogenase. DLD: Dihydrolipoyl dehydrogenase. MT-ATP6/PDH: Mitochondrially Encoded ATP Synthase Membrane Subunit 6/ Pyruvate dehydrogenase.

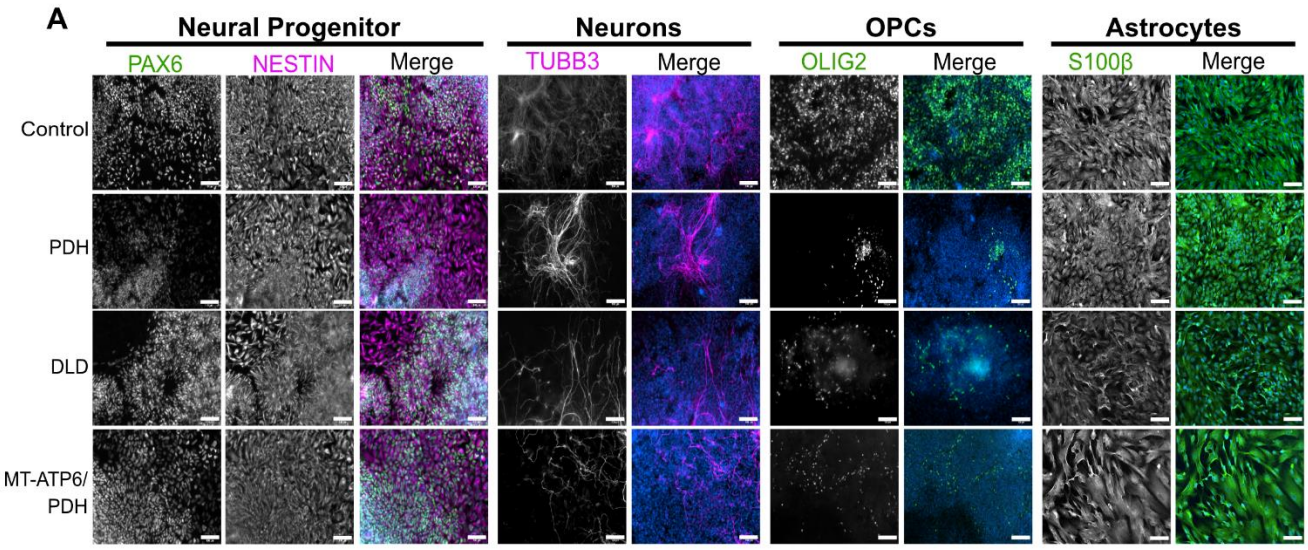
A
Neural Progenitor
Neurons
OPCs
Astrocytes
PAX6
NESTIN
Merge
TUBB3
Merge
OLIG2
Merge
S100β
Merge
Control
PDH
DLD
MT-ATP6/
PDH

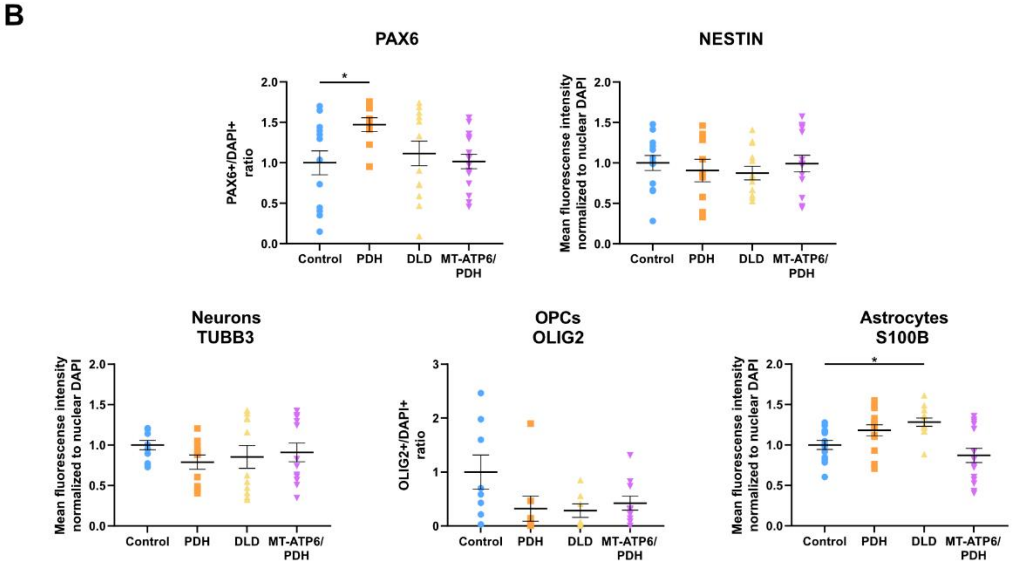
B
PAX6
PAX6+/DAPI+ ratio
NESTIN
Mean fluorescense intensity normalized to nuclear DAPI
Neurons
TUBB3
OPCs
OLIG2
OLIG2+/DAPI+ ratio
Astrocytes
S100B
Control
PDH
DLD
MT-ATP6/
PDH

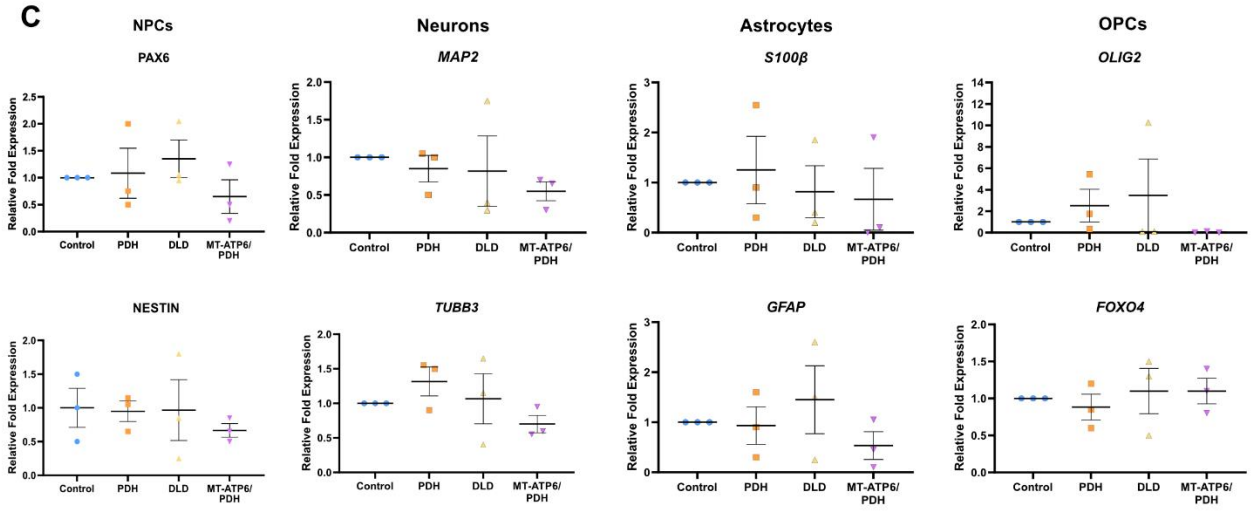
C
NPCs
PAX6
Neurons
MAP2
Astrocytes
S100β
OPCs
OLIG2
NESTIN
TUBB3
GFAP
FOXO4
Relative Fold Expression
Control
PDH
DLD
MT-ATP6/
PDH

Figure 3-2. Leigh syndrome-derived NPCs are multipotent.

A. Representative images of the expression of neural multipotency markers. NPCs stained by PAX6 and NESTIN, neurons marked with βIII-TUBULIN (TUBB3), oligodendrocyte progenitor cells (OPCs) were stained with Olig2, and astrocytes are marked with S100β. Merged panels show the color image of the grayscale lineage marker and the nuclear staining DAPI in blue. Scale bar: 100µm. B. Immunofluorescence quantification. A slight increase in the number of PAX6+ cells was observed in PDH ($p=0.494$). Three independent differentiations were performed. Positive nuclei number for nuclear markers, and mean fluorescence intensity for cytoplasmatic markers were normalized to the nuclear DAPI intensity/number and the intensity values of control. C. RT-qPCR Analysis of the NPC markers PAX6 and NESTIN, as well as the multipotency markers MAP2 and TUBB3 for neuronal lineage, S100B and GFAP for astrocytic lineage, and OLIG2 and FOXO4 for OPCs. Fold change normalized to GPI and GAPDH as house-keeping genes.

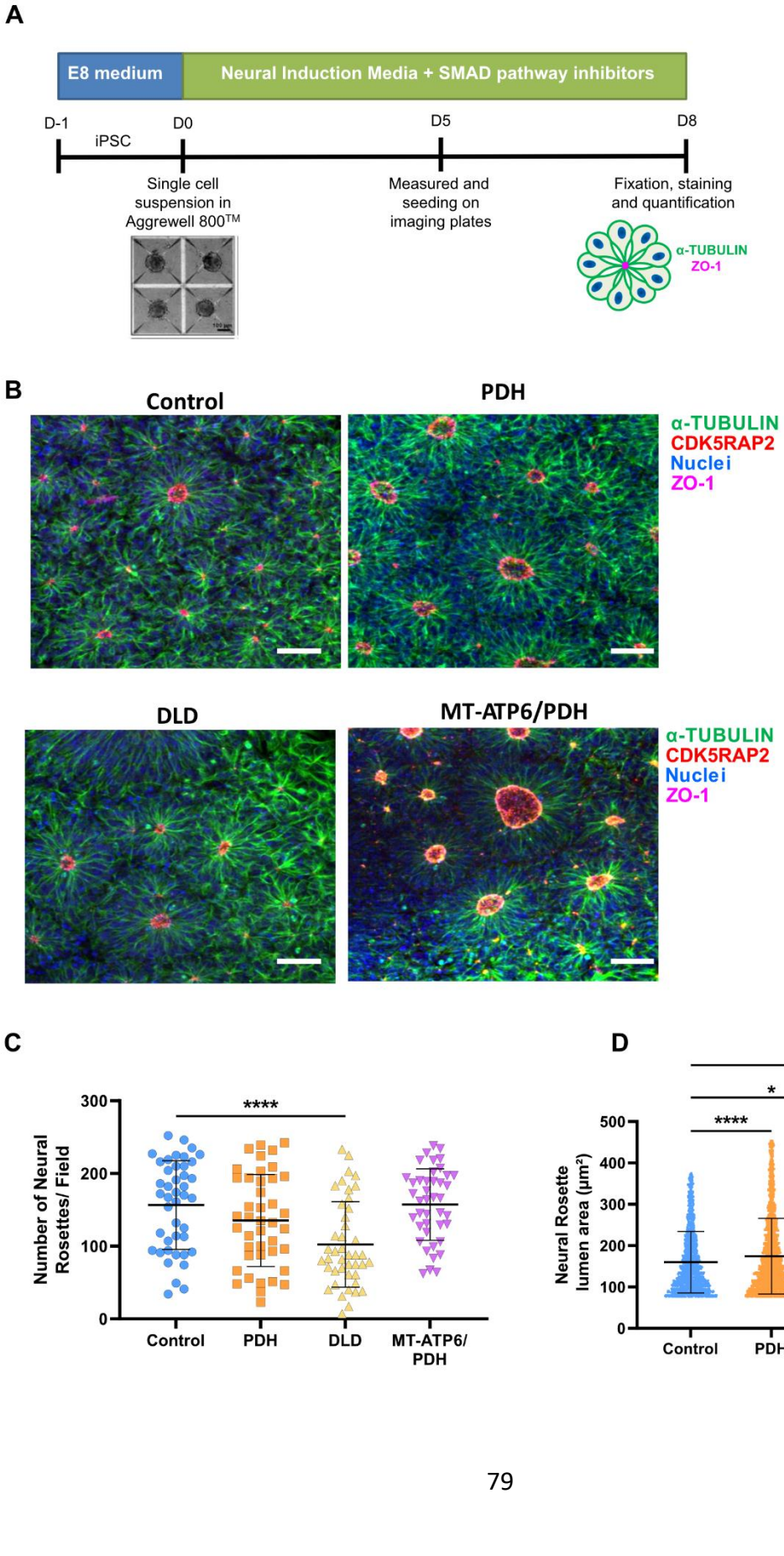
A
E8 medium
Neural Induction Media + SMAD pathway inhibitors
D-1
iPSC
D0
D5
D8
Single cell suspension in Aggrewell 800™
Measured and seeding on imaging plates
Fixation, staining and quantification
α-TUBULIN
ZO-1
B
Control
PDH
α-TUBULIN
CDK5RAP2
Nuclei
ZO-1
DLD
MT-ATP6/PDH
α-TUBULIN
CDK5RAP2
Nuclei
ZO-1
C
Number of Neural Rosettes/ Field
****
300
200
100
0
Control
PDH
DLD
MT-ATP6/ PDH
D
Neural Rosette lumen area (µm²)
****
*
****
500
400
300
200
100
0
Control
PDH
DLD
MT-ATP6/ PDH

Figure 3-3. Three-dimensional differentiation reveals abnormalities during induction of neural rosettes in LS cell lines.

A. Schematic of neural rosette generation protocol. B-D. Representative confocal images of neural rosettes (B) show decreased numbers of neural rosettes per field in the DLD mutant line (C). Quantification of the lumen area (µm2) indicates increased lumen area in the PDH and MT-ATP6/PDH mutant cell lines and a decreased lumen area in the DLD mutant line (D). Scale bar: 50µm. $*p<0.05$; $**p<0.01$; $***p<0.001$; $****p<0.0001$. Quantification was performed with images acquired using a 10X objective. Representative figures were acquired at 20X magnification to better appreciate the differences in morphology.

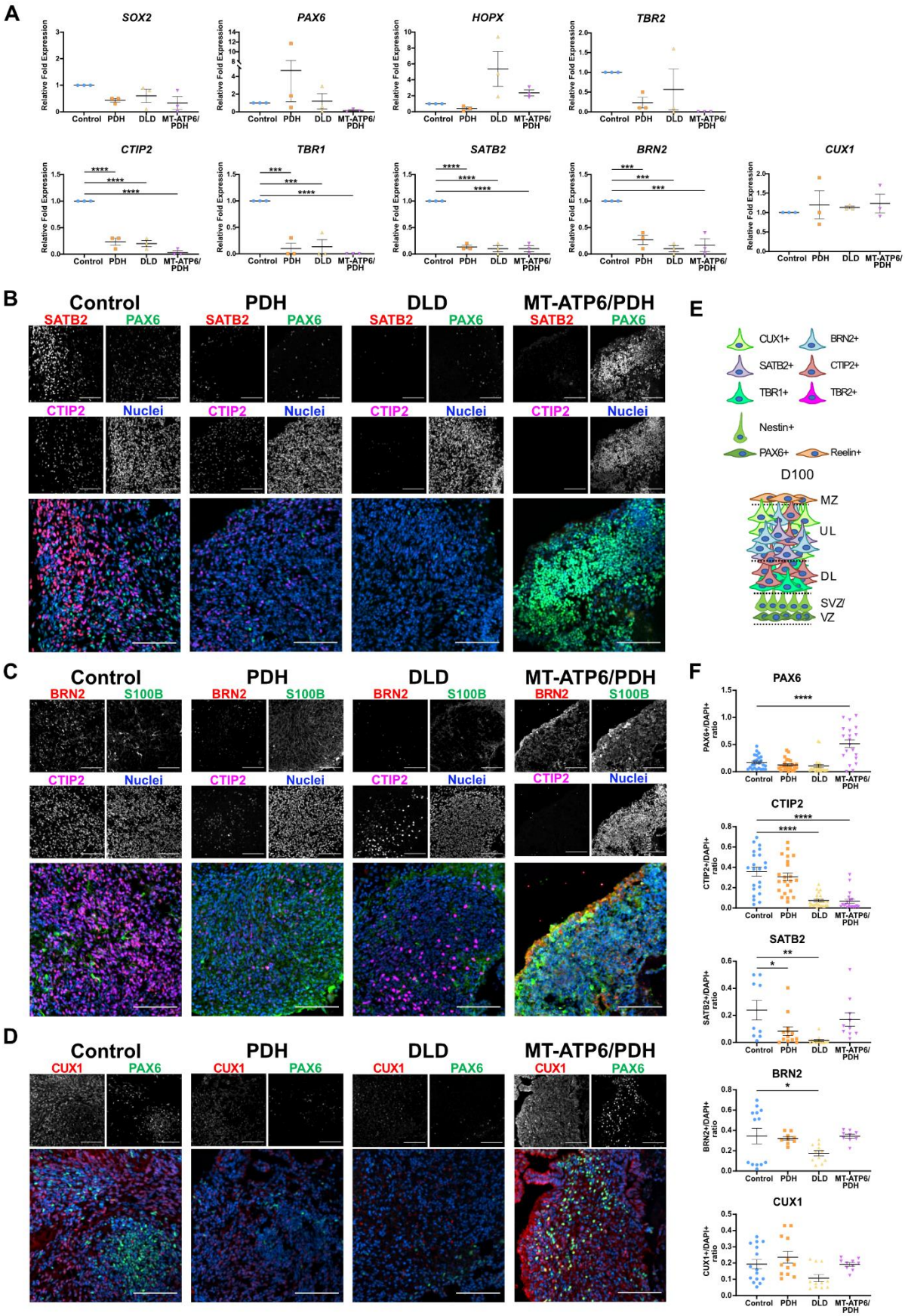
A
SOX2
PAX6
HOPX
TBR2
CTIP2
TBR1
SATB2
BRN2
CUX1
Relative Fold Expression
Control
PDH
DLD
MT-ATP6/PDH
B
Control
PDH
DLD
MT-ATP6/PDH
SATB2
PAX6
CTIP2
Nuclei
C
BRN2
S100B
D
CUX1
E
CUX1+
BRN2+
SATB2+
CTIP2+
TBR1+
TBR2+
Nestin+
PAX6+
Reelin+
D100
MZ
UL
DL
SVZ/
VZ
F
PAX6
PAX6+/DAPI+ ratio
CTIP2
CTIP2+/DAPI+ ratio
SATB2
SATB2+/DAPI+ ratio
BRN2
BRN2+/DAPI+ ratio
CUX1
CUX1+/DAPI+ ratio

Figure 3-4. LS-derived brain organoids show defects in cortical layer formation at day 100.

A. RT-qPCR quantification. NPCs populations were evaluated by the expression of SOX2 and PAX6. IPCs were identified with the marker TBR2 and oRG was evaluated by the expression of HOPX. Markers CTIP2, TBR1, SATB2, BRN2, and CUX1 were assessed for cortical development. B-D. Representative confocal images. LS patient-derived brain organoids present reduced expression of the upper layer markers SATB2 (B) and BRN2 (C) and deep layer marker CTIP2 (B,C). Expression of the astrocyte marker S100β was also observed in the cell lines (C). LS patient-derived brain organoids express the upper layer marker CUX1 and NPC marker PAX6 (D). Images were generated from at least three different organoids per genotype from independent organoid batches. Scale bar for B-D: 100µm. E. Schematic representation of the expected organization of the brain organoids at day 100. F. Quantification of immunofluorescence staining. Upper layer marker SATB2 was significantly reduced in PDH mutant ($p=0.0305$). DLD mutant presented reduced expression of the cortical layer markers CTIP2 ($p<0.0001$), SATB2 ($p=0.0013$), and BRN2 ($p=0.0455$). The double mutant MT-ATP6/PDH shows a significant increase in the PAX6+ population ($p<0.0001$), as well as reduced expression of the cortical plate marker CTIP2 ($p<0.0001$). Data are shown as mean ±SEM. Comparisons were performed as ordinary one-way ANOVA with a Dunnett's multiple comparisons test post-hoc. SVZ: subventricular zone, VZ: ventricular zone, DL: deep layers UL: upper layers, MZ: marginal zone. $*p<0.05$; $**p<0.01$; $***p<0.001$; $****p<0.0001$.

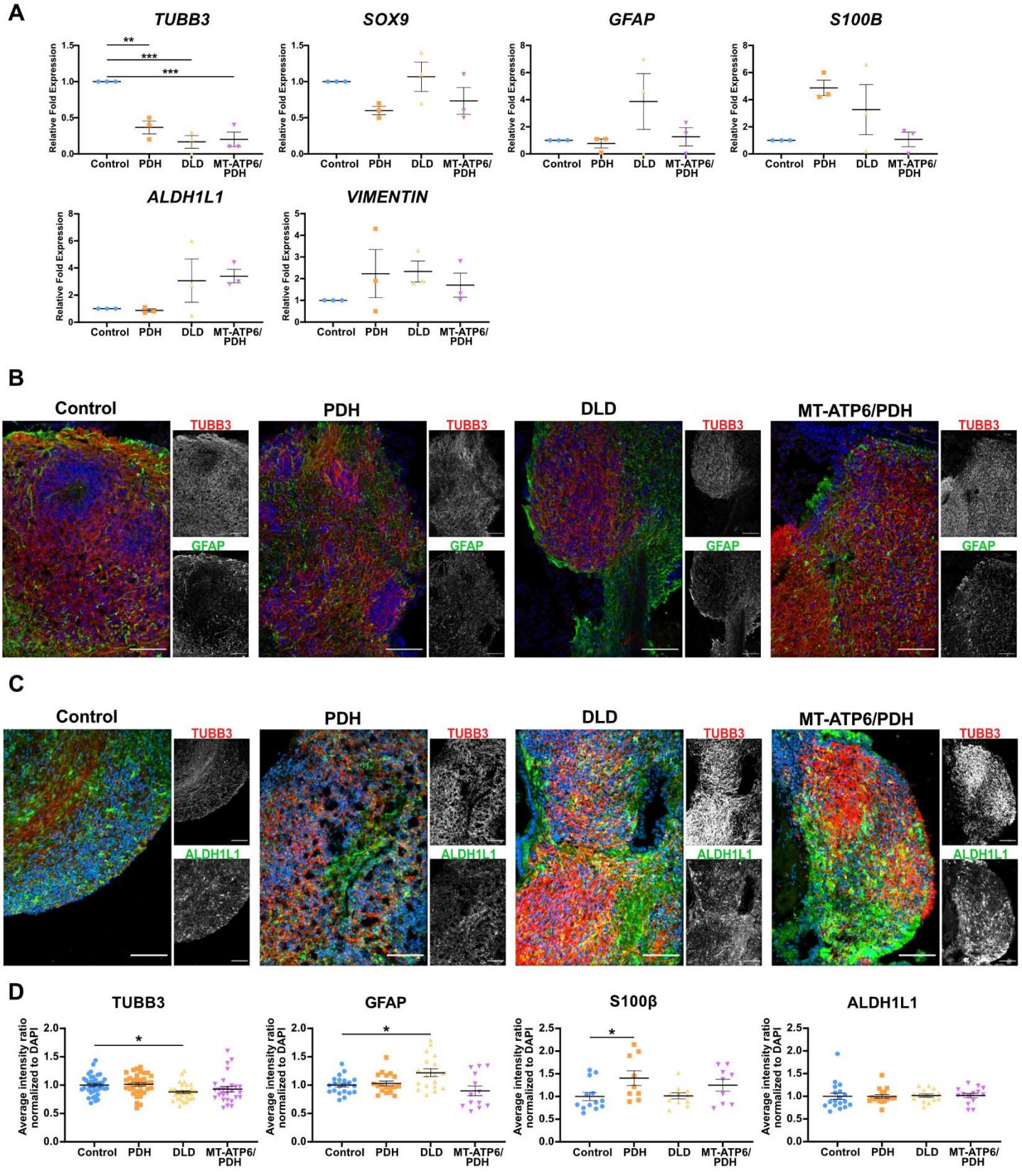
A
TUBB3
SOX9
GFAP
S100B
ALDH1L1
VIMENTIN
Relative Fold Expression
Control
PDH
DLD
MT-ATP6/PDH
B
Control
PDH
DLD
MT-ATP6/PDH
TUBB3
GFAP
C
ALDH1L1
D
Average intensity ratio normalized to DAPI
S100β

Figure 3-5. LS-derived brain organoids show dysregulation of neuronal and glial markers at day 100.

A. RT-qPCR analysis of neuronal and astrocytic genes. Neuronal marker TUBB3 and astrocytic markers SOX9, GFAP, S100B, VIMENTIN, and ALDH1L1 were evaluated. A significant decrease in the expression of the neuronal marker TUBB3 was observed. Fold change normalized to GPI and GAPDH as housekeeping genes. B-C. Immunofluorescence images of astrocytic markers GFAP (B) and ALDH1L1 (C), and neuronal marker βIII TUBULIN (TUBB3). Nuclei in the merged image correspond to the blue channel. Scale bar: 100µm. D. Immunofluorescence quantification of the neuronal and astrocytic staining. DLD mutant presented decrease staining in the neuronal marker TUBB3 ($p=0.0174$) and an increase in the astrocytic marker GFAP ($p=0.0141$). PDH mutant shows a significant increase in the S100β+ population ($p=0.0354$). Scale bar: 100µm. Data are shown as mean ±SEM. Comparisons were performed as ordinary one-way ANOVA with a Dunnett's multiple comparisons test post-hoc. $*p<0.05$; $**p<0.01$; $***p<0.001$; $****p<0.0001$.

A

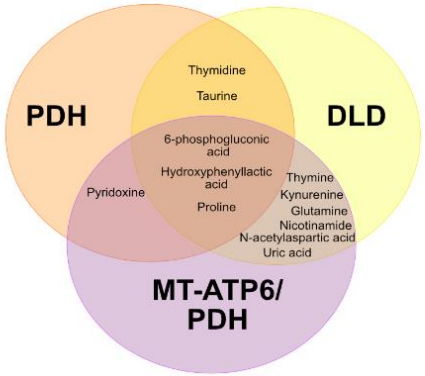

PDH	MT-ATP6/PDH		DLD
Deoxyuridine	NADP	Tyrosine	Sorbitol/Galactitol/L-iditol/Manitol
CDP-choline	Phenylalanine	Galactosamine/glucosamine	D-galactonic acid
	Leucine/isoleucine	Pyruvic acid	Guanosine
	Acetylcholine	N-acetylglucosamine 1/6-phosphate	Fructose-1-phosphate
	Lysine	DOPET	Deoxyinosine
	Cystine	Cysteine-S-sulfate	
	Alanine	Choline	
	Phosphoenolpyruvate	L-cysteic acid	
	Cytidine	3- / 7-methylguanine	
	Valine	D-sedoheptulose-7-phosphate	
	Pyrroline hydroxycarboxylic acid	Methionine	
	Histidine	DOPEG	

B PDH

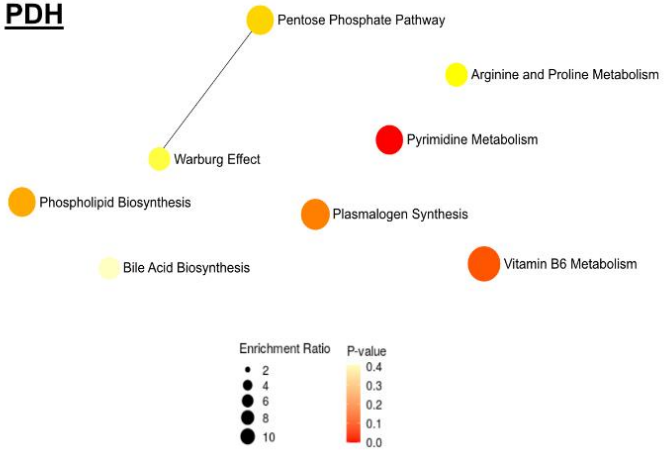

C DLD

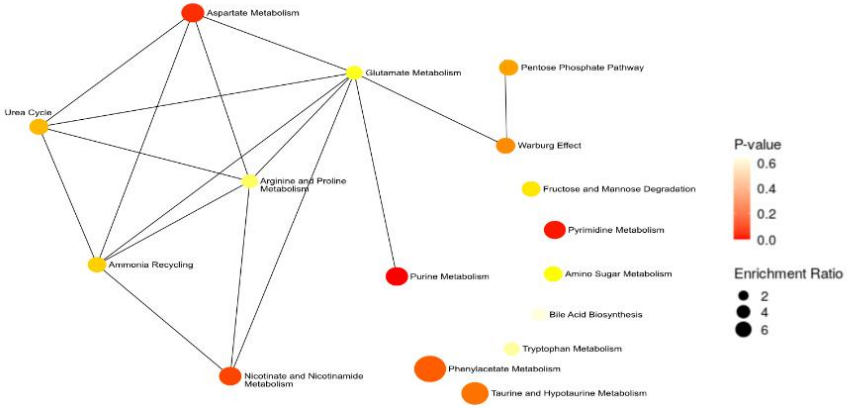

D MT-ATP6

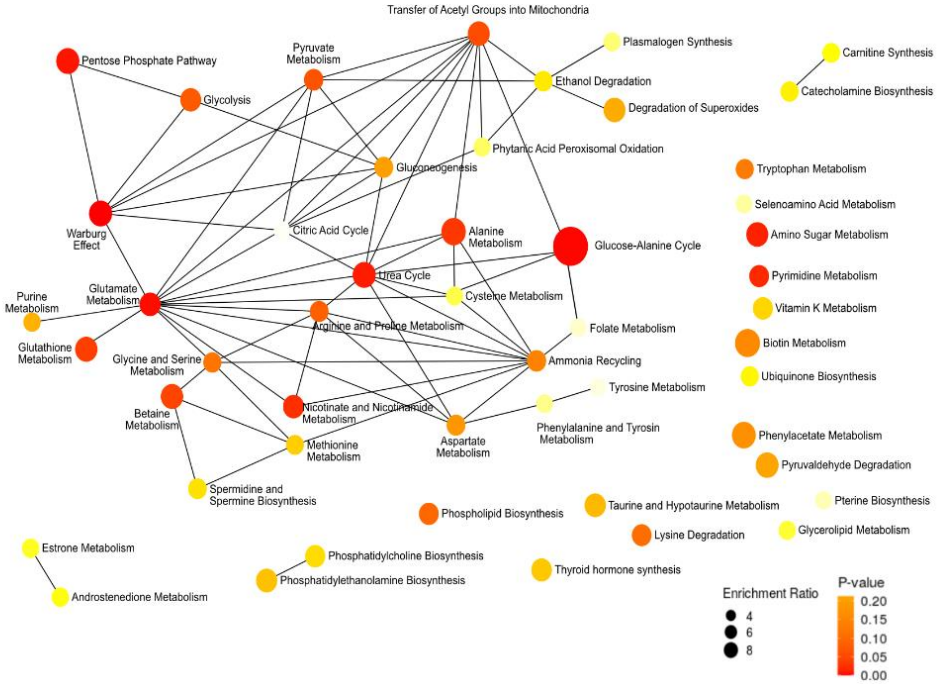

Figure 3-6. Day 40 LS-derived brain organoids show changes in their metabolic profiles.

A. 43 metabolites were statistically dysregulated ($p<0.05$ and FDR of 0.01) segregated by affected cell line. A total of three batches of 40-day organoids per line (4 independent organoids per line per batch) were analyzed as described in methods. B. Metabolite Set Enrichment Analysis for dysregulated metabolites enriched in the PDH mutant. C. Metabolite Set Enrichment Analysis for dysregulated metabolites enriched in the DLD mutant. D. Metabolite Set Enrichment Analysis for dysregulated metabolites enriched in the MT-ATP6/PDH mutant. Diameter of the node is determined by the level of enrichment, while the color of the node represents the p-value of the interaction.

Supplemental Figures

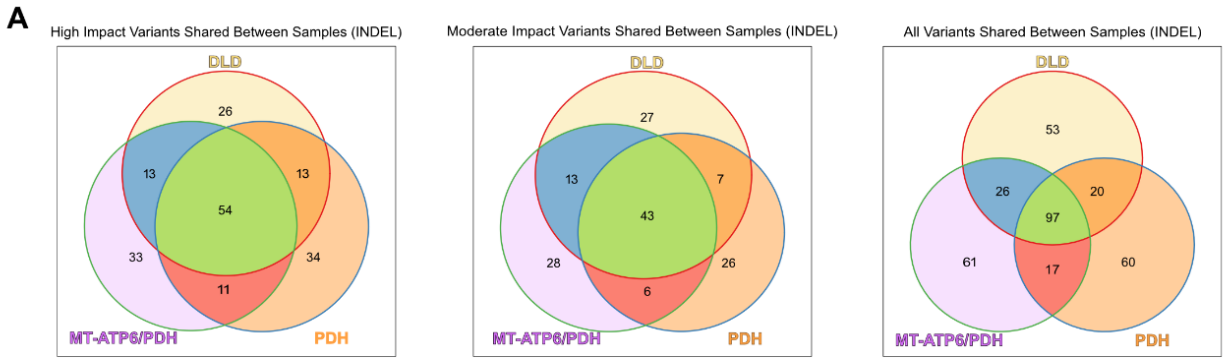

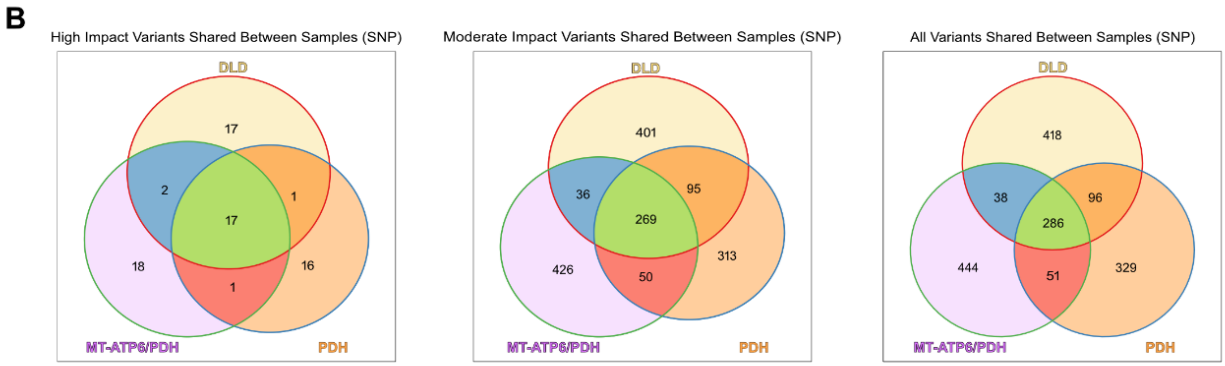

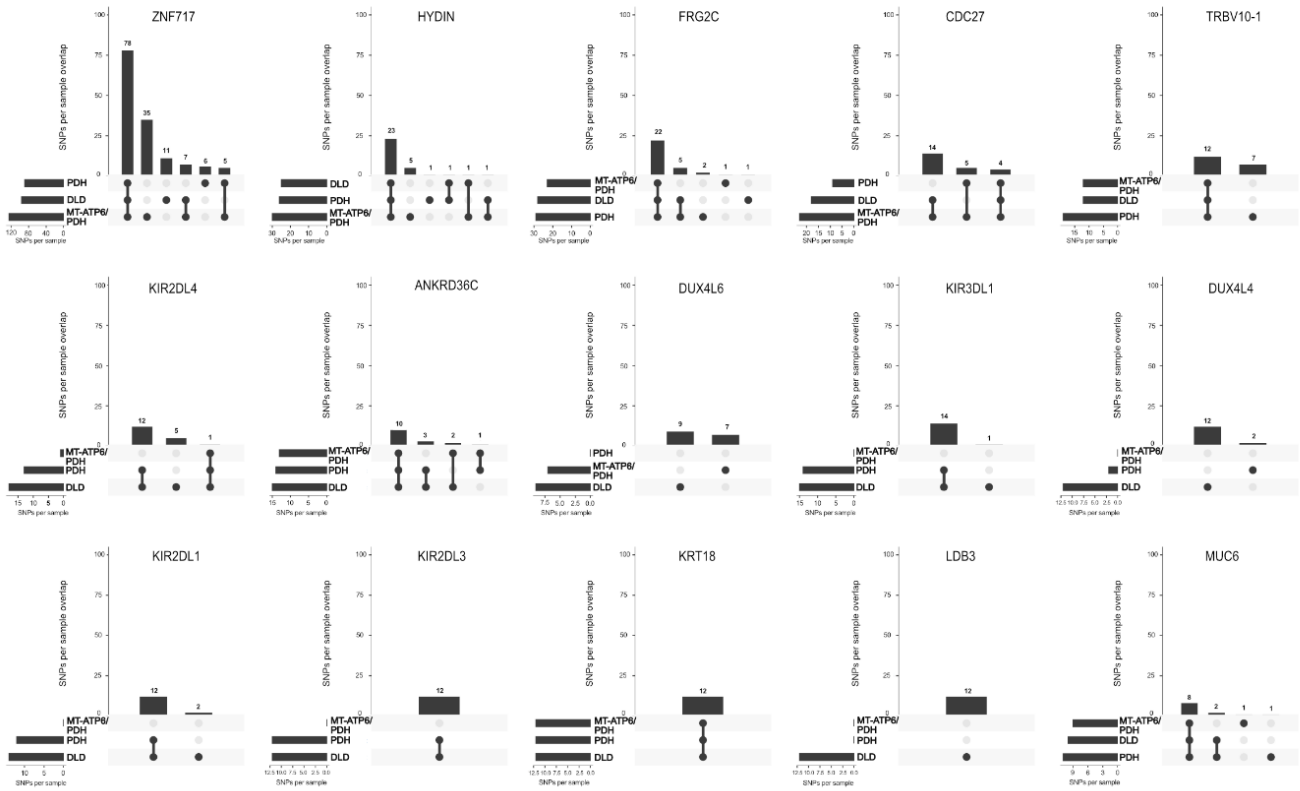

Supplemental Figure 3-1. Whole exome analysis of the Leigh syndrome patient derived cells reveals the presence of INDELS and SNPs.

A-B. Venn diagram of the distribution of high, moderate and all impact annotations across samples for INDELs (A) and SNPs (B). Pie charts of the annotation distributions within samples. C. Top 15 genes with high impact SNP variants identified in the WES analysis. Number of overlapping SNPs per sample are denoted in as vertical bars, while the number of SNPs present in each phenotype are noted in the horizontal bars. ZNF717: Zinc finger protein 717, HYDIN: HYDIN axonemal central pair apparatus protein, FRG2C: FSHD region gene 2 family member C, CDC27: Cell division cycle 27, TRBV10-1: T cell receptor beta variable 10-1, KIR2DL4: Killer cell immunoglobulin like receptor, two Ig domains and long cytoplasmic tail 4, ANKRD36C: Ankyrin repeat domain 36C, DUX4L6: Double homeobox 4 like 6, KIR3DL1: Killer cell immunoglobulin like receptor, three Ig domains and long cytoplasmic tail 1, DUX4L4: Double homeobox 4 like 4 , KIR2DL1: Killer cell immunoglobulin like receptor, two Ig domains and long cytoplasmic tail 1, KIR2DL3: Killer cell immunoglobulin like receptor, two Ig domains and long cytoplasmic tail 3, KRT18: Keratin 18, LDB3: LIM domain binding 3, MUC6: Mucin 6.

A

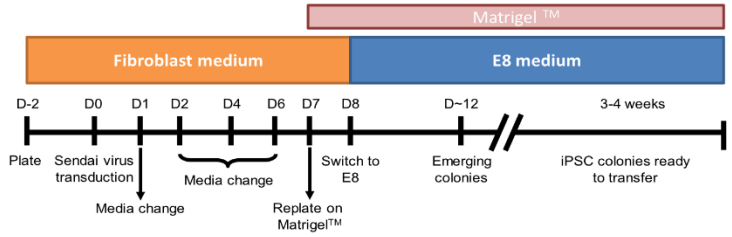

B

Sample	Pluritest Result	Pluricor	NovelCor
Control	Pass	38.62112	1.61562
PDH	Pass	37.78063	1.547368
DLD	Pass	36.43402	1.626429
MT-ATP6/ PDH	Pass	36.21865	1.509551
Non iPSC control	Fail	-48.9629	2.790166

C

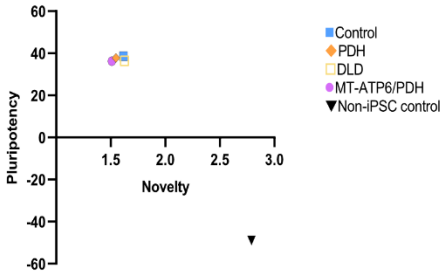

D

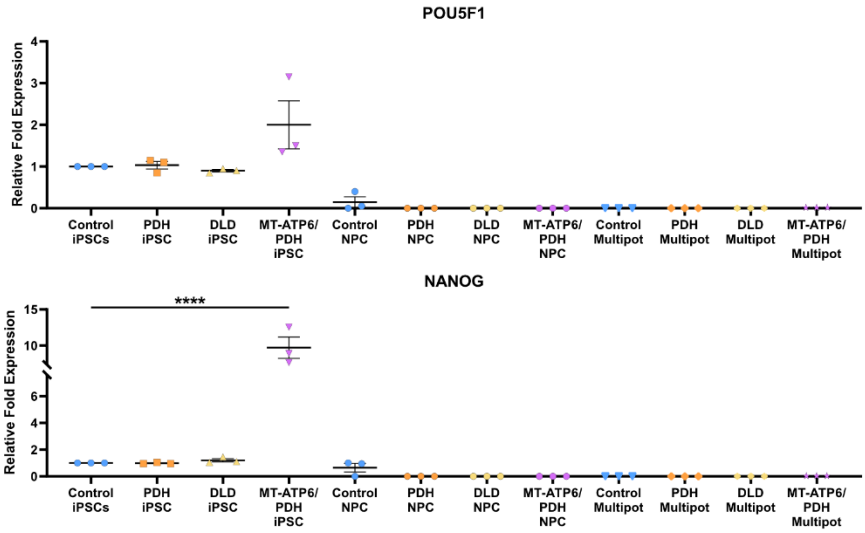

E

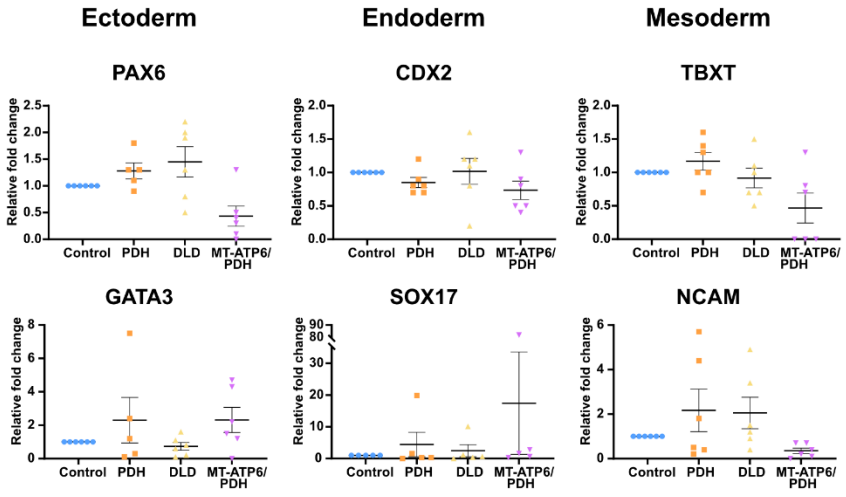

Supplemental Figure 3-1. Characterization of Leigh syndrome patient-derived iPSCs.

A. Schematic representation of the fibroblast reprogramming protocol. B-C. Pluripotency characterization of the LS iPSCs. Samples were analyzed against samples in a reference data set (The International Stem Cell Initiative, 2018) (B). The distribution of the samples compared with a non-iPSC control shows clustering of the samples in the high pluripotency and low novelty quadrant (C). D. qPCR for the pluripotency genes POU5F1 and NANOG ($p<0.001$). E. Induced pluripotent stem cells derived from Leigh syndrome patient fibroblasts are capable of differentiation into specific lineages. RT-qPCR analysis for the ectodermal genes GATA3 and PAX6, ectodermal genes CDX2 and SOX17 the mesodermal genes TBXT and NCAM. Fold change normalized to GPI and GAPDH as house-keeping genes. iPSC: induced pluripotent stem cells, NPC: neural progenitor cells, Multipot: neural multipotency differentiation. Graphs represent mean ± SEM from at least three independent experiments. $*p<0.05$; $**p<0.01$; $***p<0.001$; $****p<0.0001$.

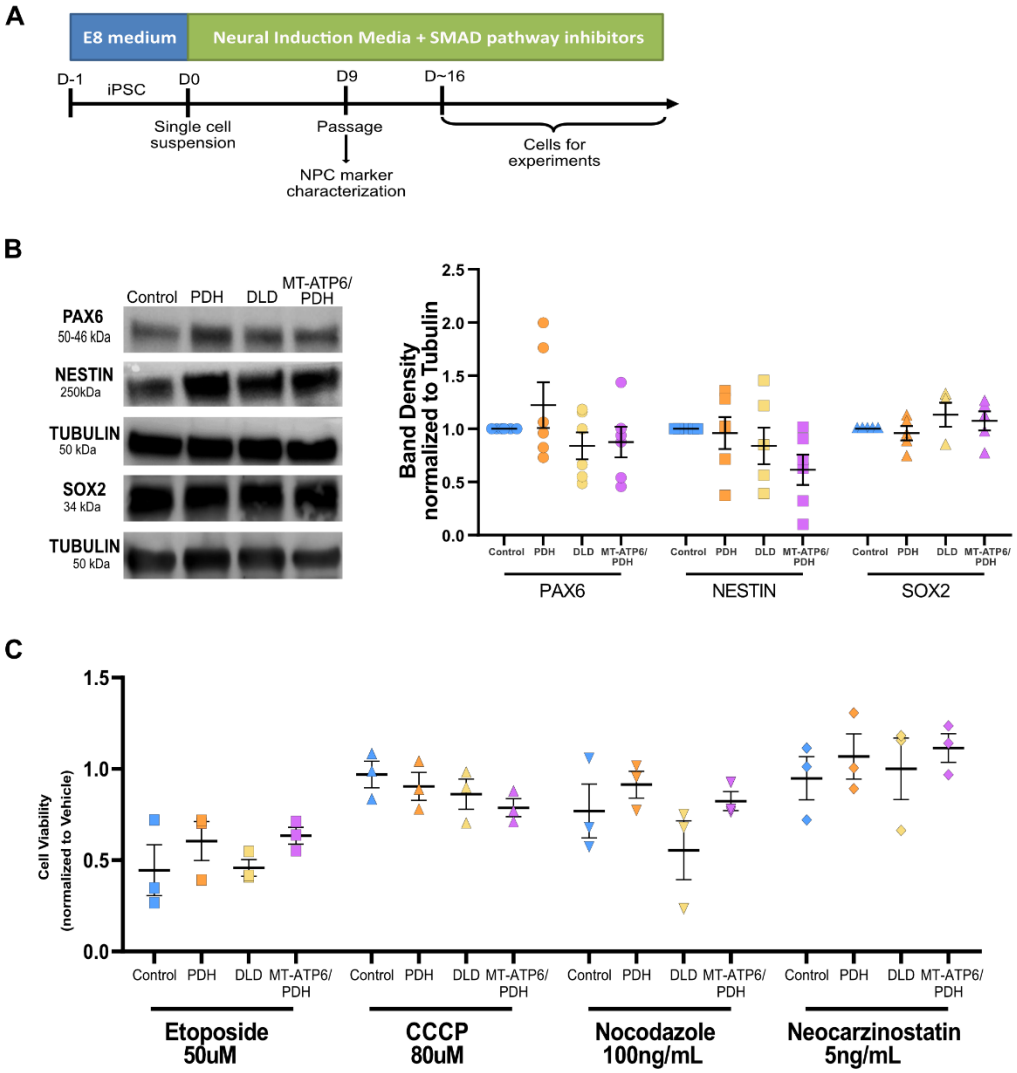

Supplemental Figure 3-2. Leigh syndrome patient-derived NPCs are multipotent and do not present increased sensitivity to pharmacological stressors.

A. Schematic of two-dimensional neural differentiation. B. Immunoblot of protein expression of neural markers PAX6, NESTIN, and SOX2 (Left). Quantification of protein expression of neural markers PAX6, NESTIN and SOX2. Band density normalized to TUBULIN as a loading control (Right). C. Leigh syndrome NPCs do not show enhanced sensitivity towards different stressors. LS NPCs have similar cell viability when exposed to the DNA damaging agents etoposide and neocarzinostatin, the mitochondrial toxicant CCCP, and the microtubule destabilizer nocodazole.

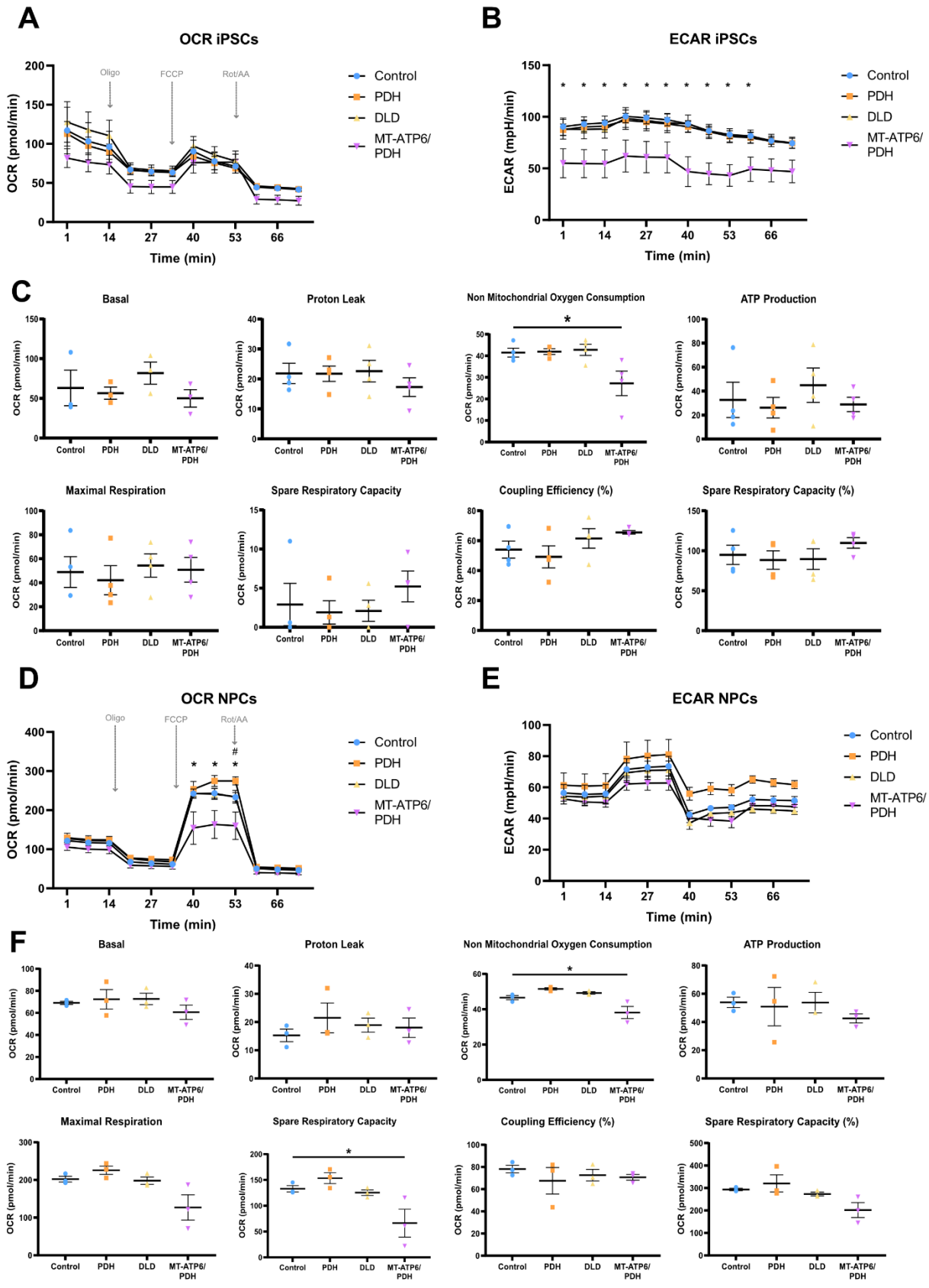
A
OCR iPSCs
Oligo
FCCP
Rot/AA
OCR (pmol/min)
Time (min)
Control
PDH
DLD
MT-ATP6/ PDH
B
ECAR iPSCs
ECAR (mpH/min)
Time (min)
C
Basal
Proton Leak
Non Mitochondrial Oxygen Consumption
ATP Production
Maximal Respiration
Spare Respiratory Capacity
Coupling Efficiency (%)
Spare Respiratory Capacity (%)
D
OCR NPCs
E
ECAR NPCs
F

Supplemental Figure 3-3. Bioenergetic profile of LS patient-derived iPSCs and NPCs.

A. Analysis of oxygen consumption rate (OCR) in control and LS patient derived iPSCs. B. Extra cellular acidification rate (ECAR) for control and LS patient derived iPSCs. MT-ATP6/PDH iPSCs show reduced glycolytic capacity. C. Bioenergetic parameters for LS and control iPSCs. MT-ATP6/PDH derived iPSCs presented with reduced non-mitochondrial oxygen consumption compared to control ($p=0.0284$). D. Analysis of oxygen consumption in control and LS patient derived NPCs. MT-ATP6/PDH derived NPCs are deficient in OXPHOS energy generation compared to control. E. Extra cellular acidification rate (ECAR) for control and LS patient derived NPCs. F. Bioenergetic parameters for LS and control NPCs. MT-ATP6/PDH NPCs have reduced non-mitochondrial oxygen consumption ($p=0.0354$) and spare respiratory capacity when compared to control ($p=0.0317$). Graphs represent mean ± SEM from at least three independent experiments. $*p<0.05$; $**p<0.01$; $***p<0.001$; $****p<0.0001$.

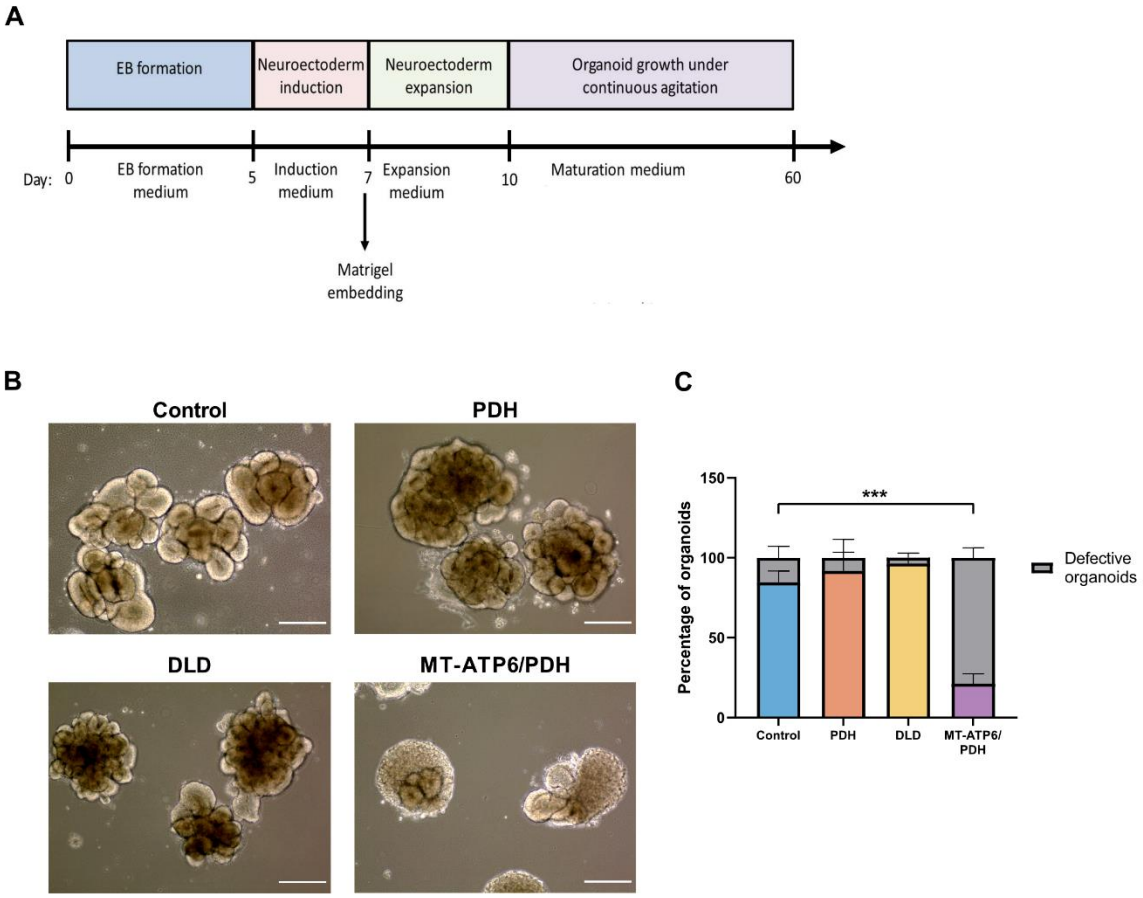

Supplemental Figure 3-4. MT-ATP6/PDH brain organoids display defective differentiation at day 10.

A. Schematic of the brain organoid generation protocol. B. Brightfield images (4X) of day 10 brain organoids. MT-ATP6/PDH shows disorganized cellular growth that do not resemble neuroepithelial buds. Scale bar: 300µm. C. Quantification of the defective organoids at day 10 by cell line. ∗p<0.05; ∗∗p<0.01; ∗∗∗p<0.001; ∗∗∗∗p<0.0001.

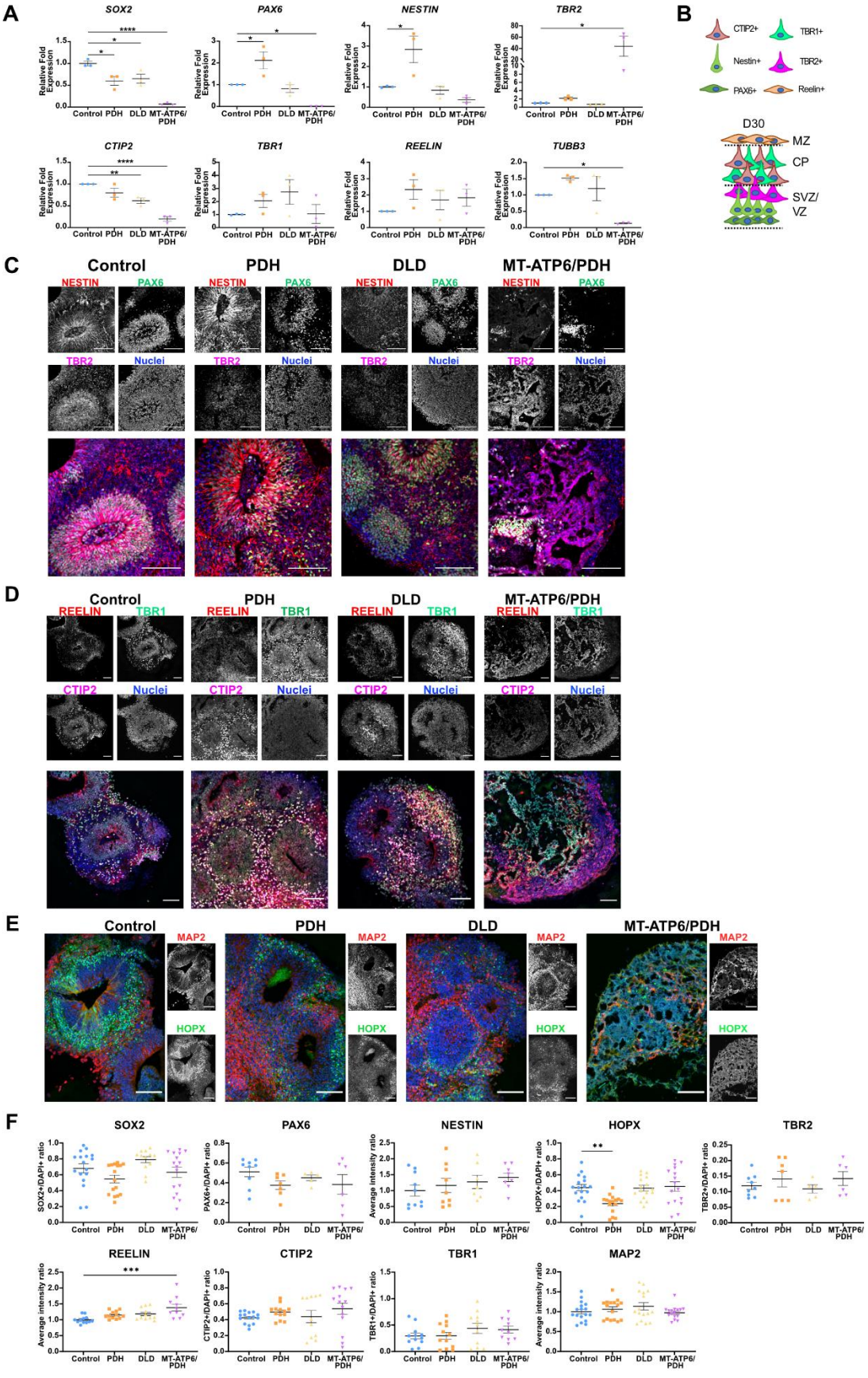
A
SOX2
PAX6
NESTIN
TBR2
CTIP2
TBR1
REELIN
TUBB3
Relative Fold Expression
Control PDH DLD MT-ATP6/PDH
B
CTIP2+
TBR1+
Nestin+
TBR2+
PAX6+
Reelin+
D30
MZ
CP
SVZ/VZ
C
Control
PDH
DLD
MT-ATP6/PDH
NESTIN
PAX6
TBR2
Nuclei
D
REELIN
TBR1
CTIP2
E
MAP2
HOPX
F
SOX2+/DAPI+ ratio
PAX6+/DAPI+ ratio
Average intensity ratio
HOPX+/DAPI+ ratio
TBR2+/DAPI+ ratio
TBR1+/DAPI+ ratio

Supplemental Figure 3-5. Leigh syndrome-derived brain organoids show defects in SVZ/VZ and CP formation.

A. qPCR quantification of the day 30 organoids. Neural progenitor cell populations were evaluated by the expression of SOX2, PAX6 and NESTIN. Intermediate progenitor cells were identified with the marker TBR2. Marginal zone marker REELIN, cortical plate markers TBR1 and CTIP2, and neuronal marker TUBB3 were also evaluated. Fold change normalized to GPI and GAPDH as house-keeping genes. B. Schematic representation of the expected organization of the brain organoids on day 30. C-E. Representative immunostaining confocal images of day 30 brain organoids. MT-ATP6/PDH mutant presents severe disorganization of the SVZ/VZ markers PAX6 and TBR2, as well as the neural progenitor marker NESTIN (C). Cajal-Retzius neurons positive for REELIN were observed in the surface of the organoids (D). Cortical plate markers CTIP2 and TBR1 (D), as well as outer radial glia marker HOPX and the neuronal marker MAP2 (E). For E, nuclei in merge image correspond to the blue channel. Scale bar: 100µm. Images were generated from at least three different organoids per genotype from 3 independent organoid batches. F. Quantification of day immunofluorescence staining for day 30 brain organoids. Outer radial glia marker HOPX was reduced in PDH organoids ($p=0.0032$) and MZ marker Reelin was increased ($p=0.0002$) in MT-ATP6/PDH mutant organoids. SVZ: subventricular zone, VZ: ventricular zone, CP: cortical plate, MZ: marginal zone. $*p<0.05$; $**p<0.01$; $***p<0.001$; $****p<0.0001$.

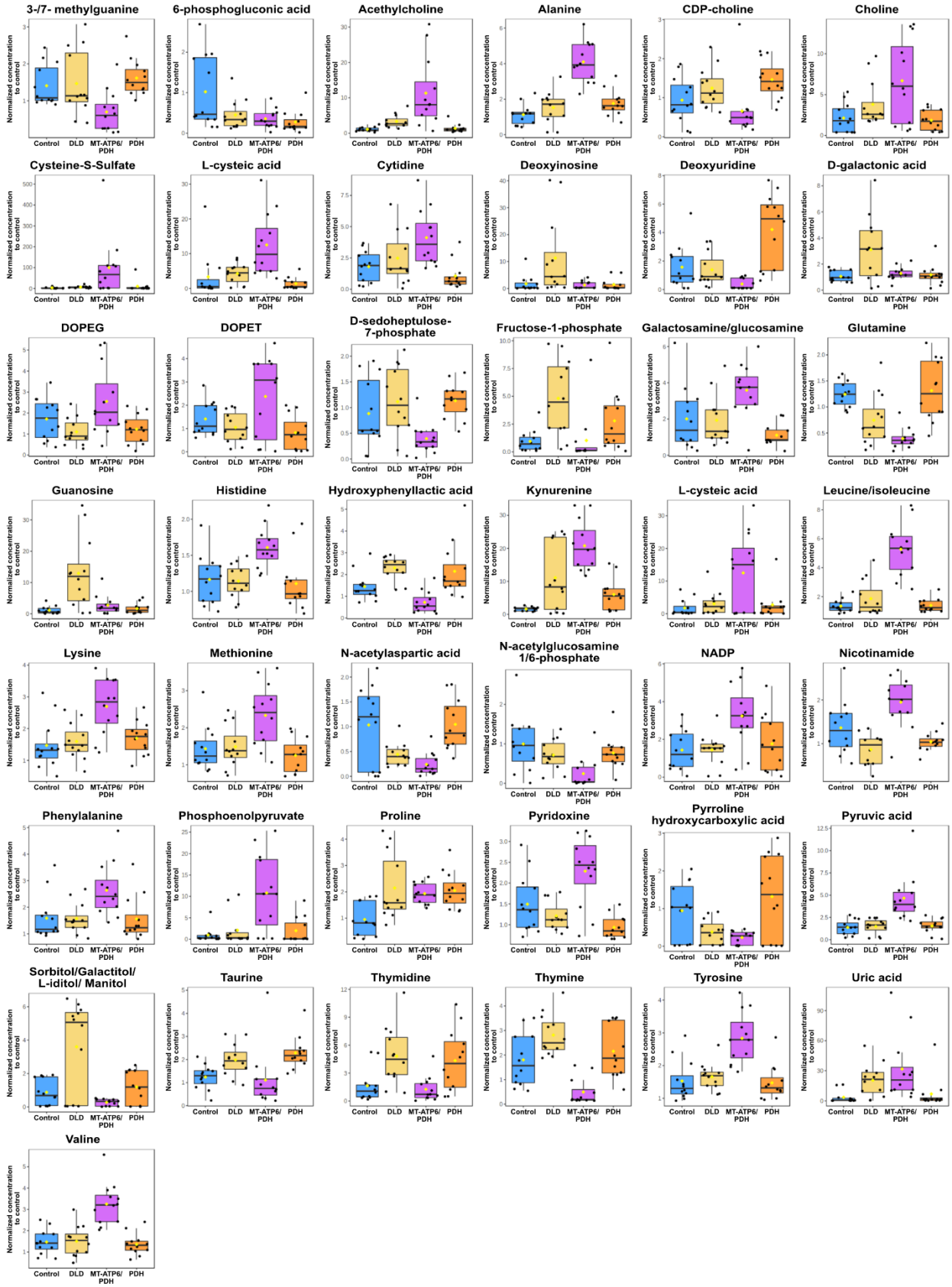
3-/7- methylguanine
6-phosphogluconic acid
Acethylcholine
Alanine
CDP-choline
Choline
Cysteine-S-Sulfate
L-cysteic acid
Cytidine
Deoxyinosine
Deoxyuridine
D-galactonic acid
DOPEG
DOPET
D-sedoheptulose-7-phosphate
Fructose-1-phosphate
Galactosamine/glucosamine
Glutamine
Guanosine
Histidine
Hydroxyphenyllactic acid
Kynurenine
L-cysteic acid
Leucine/isoleucine
Lysine
Methionine
N-acetylaspartic acid
N-acetylglucosamine 1/6-phosphate
NADP
Nicotinamide
Phenylalanine
Phosphoenolpyruvate
Proline
Pyridoxine
Pyrroline hydroxycarboxylic acid
Pyruvic acid
Sorbitol/Galactitol/ L-iditol/ Mannitol
Taurine
Thymidine
Thymine
Tyrosine
Uric acid
Valine
Normalized concentration to control
Control
DLD
MT-ATP6/ PDH
PDH

Supplemental Figure 3-6. Day 40 LS derived brain organoids show changes in their metabolic profiles.

Individual graph bars for the 43 metabolites identified as statistically dysregulated ($p<0.05$ and FDR of 0.01) in LS Organoids when compared to control. Statistical values can be found in Supplemental Table 3-2. A total of three batches of 40-day organoids per line (4 independent organoids per line per batch) were analyzed as described in methods.

Supplemental Tables

Cell line	Phenotype	Mutation	References
GM03672	1 y/o female, Caucasian. Developmental regression; microcephalic; elevated blood lactic acid and pyruvate; only affected family member	PDH (E1) LOF Pyruvate dehydrogenase (79delC, Arg27fs)	Hinman et al. 1989; Huh et al. 1990; Johnson et al. 2019
GM01503	3y/o female, Caucasian. Lactic acidosis, psychomotor delay; sister also affected. Subnormal activation of pyruvate dehydrogenase complex in disrupted fibroblasts	DLD (E3) Dihydrolipoamide dehydrogenase (A100G, Thr34Ala)	Cooper et al, 1969; Murphy JV, 1973; Sorbi& Blass, 1982; Hinman et al. 1989; Huh et al. 1990; Vo et al. 2007; Johnson et al. 2019
GM13411	8 month old male, Chinese. Lactic acidosis; developmental delay. Hypertrophic cardiomyopathy. Symmetric neural necrosis. Fibroblast: 90% heteroplasmy	MT-ATP6 (T8993G, Leu156Arg) PDH (E1) LOF Pyruvate dehydrogenase (79delC, Arg27fs)	Pastores et al. 1994; Iyer et al.2012; Ma et al. 2014; Galera-Monge et al. 2016; Zheng et al. 2016; Johnson et al. 2019

Supplemental Table 3-1. Summary characteristics of the Leigh syndrome patient derived fibroblast cell lines including the patient phenotype at diagnosis, the mutations identified, and published literature using the cell line.

Metabolite	f.value	p.value	-LOG10(p)	FDR	Fisher's LSD
leucine / leucineiso	32.463	3.17E-11	10.499	7.00E-09	MT-ATP6/PDH - Control; MT-ATP6/PDH - DLD; MT-ATP6/PDH - PDH
alanine	28.604	2.04E-10	9.6912	2.25E-08	MT-ATP6/PDH - Control; MT-ATP6/PDH - DLD; MT-ATP6/PDH - PDH
valine	18.839	5.25E-08	7.2801	3.87E-06	MT-ATP6/PDH - Control; MT-ATP6/PDH - DLD; MT-ATP6/PDH - PDH
kynurenine	17.496	1.27E-07	6.896	7.02E-06	DLD - Control; MT-ATP6/PDH - Control; MT-ATP6/PDH - DLD; MT-ATP6/PDH - PDH
thymine	13.799	1.77E-06	5.7523	7.82E-05	DLD - Control; Control - MT-ATP6/PDH; DLD - MT-ATP6/PDH; PDH - MT-ATP6/PDH
tyrosine	13.55	2.14E-06	5.6703	7.87E-05	MT-ATP6/PDH - Control; MT-ATP6/PDH - DLD; MT-ATP6/PDH - PDH
glutamine	13.161	2.88E-06	5.5408	9.09E-05	Control - DLD; Control - MT-ATP6/PDH; DLD - MT-ATP6/PDH; PDH - DLD; PDH - MT-ATP6/PDH
pyruvic acid	12.95	3.39E-06	5.4697	9.37E-05	MT-ATP6/PDH - Control; MT-ATP6/PDH - DLD; MT-ATP6/PDH - PDH
nicotinamide	12.723	4.05E-06	5.3925	9.95E-05	Control - DLD; MT-ATP6/PDH - Control; MT-ATP6/PDH - DLD; MT-ATP6/PDH - PDH
deoxyuridine	12.392	5.26E-06	5.2794	0.00011615	PDH - Control; PDH - DLD; PDH - MT-ATP6/PDH
pyridoxine	11.7	9.16E-06	5.0381	0.00018405	MT-ATP6/PDH - Control; Control - PDH; MT-ATP6/PDH - DLD; MT-ATP6/PDH - PDH
sorbitol / galactitol / L-iditol / manitol	11.289	1.28E-05	4.8919	0.00023619	DLD - Control; DLD - MT-ATP6/PDH; DLD - PDH

acetylcholine	10.88	1.80E-05	4.7444	0.00030625	MT-ATP6/PDH - Control; MT-ATP6/PDH - DLD; MT-ATP6/PDH - PDH
guanosine	10.42	2.66E-05	4.5755	0.00041955	DLD - Control; DLD - MT-ATP6/PDH; DLD - PDH
hydroxyphenyllactic acid	10.302	2.94E-05	4.5318	0.00043306	DLD - Control; Control - MT-ATP6/PDH; PDH - Control; DLD - MT-ATP6/PDH; PDH - MT-ATP6/PDH
phosphoenolpyruvate	9.3744	6.59E-05	4.1812	0.00091016	MT-ATP6/PDH - Control; MT-ATP6/PDH - DLD; MT-ATP6/PDH - PDH
cystine	8.3901	0.00016027	3.7951	0.0020835	MT-ATP6/PDH - Control; MT-ATP6/PDH - DLD; MT-ATP6/PDH - PDH
N-acetylaspartic acid	8.239	0.00018425	3.7346	0.0022622	Control - DLD; Control - MT-ATP6/PDH; PDH - DLD; PDH - MT-ATP6/PDH
lysine	7.7264	0.00029759	3.5264	0.0034614	MT-ATP6/PDH - Control; MT-ATP6/PDH - DLD; MT-ATP6/PDH - PDH
methionine	6.9562	0.00062316	3.2054	0.0067872	MT-ATP6/PDH - Control; MT-ATP6/PDH - DLD; MT-ATP6/PDH - PDH
galactosamine / glucosamine	6.921	0.00064493	3.1905	0.0067872	MT-ATP6/PDH - Control; MT-ATP6/PDH - DLD; MT-ATP6/PDH - PDH
cytidine	6.8316	0.00070382	3.1525	0.0070702	MT-ATP6/PDH - Control; MT-ATP6/PDH - DLD; MT-ATP6/PDH - PDH
histidine	6.6085	0.00087664	3.0572	0.0084224	MT-ATP6/PDH - Control; MT-ATP6/PDH - DLD; MT-ATP6/PDH - PDH
L-cysteic acid	6.5655	0.00091465	3.0387	0.0084224	MT-ATP6/PDH - Control; MT-ATP6/PDH - DLD; MT-ATP6/PDH - PDH

pyrroline hydroxycarboxylic acid	6.3042	0.0011864	2.9258	0.010293	Control - MT-ATP6/PDH; PDH - DLD; PDH - MT-ATP6/PDH
D-galactonic acid	6.2562	0.0012448	2.9049	0.010293	DLD - Control; DLD - MT-ATP6/PDH; DLD - PDH
thymidine	6.2461	0.0012575	2.9005	0.010293	DLD - Control; PDH - Control; DLD - MT-ATP6/PDH; PDH - MT-ATP6/PDH
choline	6.1696	0.0013579	2.8671	0.010718	MT-ATP6/PDH - Control; MT-ATP6/PDH - DLD; MT-ATP6/PDH - PDH
F1P	6.0835	0.001481	2.8295	0.011286	DLD - Control; DLD - MT-ATP6/PDH
proline	5.6016	0.0024208	2.616	0.017833	DLD - Control; MT-ATP6/PDH - Control; PDH - Control
taurine	5.3747	0.0030613	2.5141	0.021824	DLD - Control; PDH - Control; DLD - MT-ATP6/PDH; PDH - MT-ATP6/PDH
6-phosphogluconic acid	5.202	0.0036652	2.4359	0.025313	Control - DLD; Control - MT-ATP6/PDH; Control - PDH
NADP	5.1267	0.0039663	2.4016	0.026562	MT-ATP6/PDH - Control; MT-ATP6/PDH - DLD; MT-ATP6/PDH - PDH
uric acid	4.9978	0.0045425	2.3427	0.027934	DLD - Control; MT-ATP6/PDH - Control; MT-ATP6/PDH - PDH
phenylalanine	4.9917	0.0045714	2.3399	0.027934	MT-ATP6/PDH - Control; MT-ATP6/PDH - DLD; MT-ATP6/PDH - PDH
deoxyinosine	4.981	0.0046237	2.335	0.027934	DLD - Control; DLD - MT-ATP6/PDH; DLD - PDH
D-sedoheptulose-7-phosphate	4.9702	0.0046767	2.3301	0.027934	Control - MT-ATP6/PDH; DLD - MT-ATP6/PDH; PDH - MT-ATP6/PDH
DOPET	4.9279	0.0048903	2.3107	0.028441	MT-ATP6/PDH - Control; MT-ATP6/PDH - DLD; MT-ATP6/PDH - PDH

cysteine-S-sulfate	4.8891	0.0050957	2.2928	0.028876	MT-ATP6/PDH - Control; MT-ATP6/PDH - DLD; MT-ATP6/PDH - PDH
3- / 7-methylguanine	4.8504	0.0053089	2.275	0.029331	Control - MT-ATP6/PDH; DLD - MT-ATP6/PDH; PDH - MT-ATP6/PDH
N-acetylglucosamine 1/6-phosphate	4.8231	0.0054652	2.2624	0.029459	Control - MT-ATP6/PDH; DLD - MT-ATP6/PDH; PDH - MT-ATP6/PDH
DOPEG	4.4575	0.0080819	2.0925	0.042526	MT-ATP6/PDH - DLD; MT-ATP6/PDH - PDH
CDP-choline	4.3847	0.0087424	2.0584	0.044932	PDH - Control; DLD - MT-ATP6/PDH; PDH - MT-ATP6/PDH

Supplemental Table 3-2. Dysregulated metabolites in day 40 LS derived cerebral organoids.

LC-MS measured metabolite peak areas were normalized to the total ion count (TIC) by sample and fold change was determined by dividing each LS TIC normalized peak area by the control TIC normalized peak area for each metabolite. One way ANOVA was utilized to identified metabolites that were significantly dysregulated ($p<0.05$). Post-hoc comparison column using Fisher's least significant difference method (Fisher's LSD) shows the comparisons between different levels that are significant given the p value threshold. Results shown are averages for 3 independent runs with 4 individual organoids per phenotype per run. FDR: False Discovery Rate.

Metabolite	Total	Expected	Hits	Raw p	-LOG10(p)	Holm adjust	FDR	Impact
Pyrimidine metabolism	39	0.20129	2	0.0157	1.8041	1	1	0.1172
Taurine and hypotaurine metabolism	8	0.04129	1	0.0406	1.391	1	1	0.4286
Vitamin B6 metabolism	9	0.046452	1	0.0456	1.3408	1	1	0.0784
Pentose phosphate pathway	22	0.11355	1	0.1083	0.96538	1	1	0.1196
Glycerophospholipid metabolism	36	0.18581	1	0.1717	0.76513	1	1	0.0193
Arginine and proline metabolism	38	0.19613	1	0.1805	0.74359	1	1	0.0778
Primary bile acid biosynthesis	46	0.23742	1	0.2146	0.66836	1	1	0.0076
Aminoacyl-tRNA biosynthesis	48	0.24774	1	0.2229	0.65181	1	1	0

Supplemental Table 3-3. Summary of the metabolic pathways analysis for metabolites enriched in day 40 PDH brain organoids.

Statistical p values from enrichment analysis are adjusted for multiple hypothesis testing. Total: total number of compounds in the pathway. Hits: matched number from the uploaded data. Raw p: original p value calculated from the enrichment analysis. Holm p: p value adjusted by Holm-Bonferroni method. FDR p: adjusted p value using False Discovery Rate. Impact: pathway impact value calculated from pathway topology analysis.

Metabolite	Total	Expected	Hits	Raw p	-LOG10(p)	Holm adjust	FDR	Impact
Purine metabolism	65	0.62903	4	0.00271	2.5662	0.22805	0.228	0.0059
Pyrimidine metabolism	39	0.37742	3	0.00544	2.2645	0.45142	0.228	0.0971
Alanine, aspartate and glutamate metabolism	28	0.27097	2	0.02858	1.5439	1	0.8	0.2003
D-Glutamine and D-glutamate metabolism	6	0.058065	1	0.05677	1.2459	1	0.916	0
Nitrogen metabolism	6	0.058065	1	0.05677	1.2459	1	0.916	0
Taurine and hypotaurine metabolism	8	0.077419	1	0.07501	1.1249	1	0.916	0.4286
Aminoacyl-tRNA biosynthesis	48	0.46452	2	0.07632	1.1174	1	0.916	0
Arginine biosynthesis	14	0.13548	1	0.12779	0.89352	1	1	0
Nicotinate and nicotinamide metabolism	15	0.14516	1	0.1363	0.86549	1	1	0.1943
Fructose and mannose metabolism	20	0.19355	1	0.17774	0.75021	1	1	0.0304
Pentose phosphate pathway	22	0.2129	1	0.19379	0.71267	1	1	0.1196
Glyoxylate and dicarboxylate metabolism	32	0.30968	1	0.26974	0.56905	1	1	0
Arginine and proline metabolism	38	0.36774	1	0.31205	0.50578	1	1	0.0778
Tryptophan metabolism	41	0.39677	1	0.33233	0.47842	1	1	0.0942
Primary bile acid biosynthesis	46	0.44516	1	0.36491	0.43782	1	1	0.0076

Supplemental Table 3-4. Summary of the metabolic pathways analysis for metabolites enriched in day 40 DLD brain organoids.

Statistical p values from enrichment analysis are adjusted for multiple hypothesis testing. Total: total number of compounds in the pathway. Hits: matched number from the uploaded data. Raw p: original p value calculated from the enrichment analysis. Holm p: p value adjusted by Holm-Bonferroni method. FDR p: adjusted p value using False Discovery Rate. Impact: pathway impact value calculated from pathway topology analysis.

Metabolite	Total	Expected	Hits	Raw p	-LOG10(p)	Holm adjust	FDR	Impact
Aminoacyl-tRNA biosynthesis	48	0.71226	6	4.35E-05	4.3617	0.0036523	0.0036523	0
Alanine, aspartate and glutamate metabolism	28	0.41548	4	0.00059684	3.2241	0.049538	0.025067	0.20032
Cysteine and methionine metabolism	33	0.48968	3	0.011653	1.9336	0.95556	0.32629	0.10446
Arginine and proline metabolism	38	0.56387	3	0.017166	1.7653	1	0.33051	0.13058
Nicotinate and nicotinamide metabolism	15	0.22258	2	0.019673	1.7061	1	0.33051	0.1943
Citrate cycle (TCA cycle)	20	0.29677	2	0.034034	1.4681	1	0.47648	0.04634
Pyruvate metabolism	22	0.32645	2	0.040643	1.391	1	0.48771	0.20684
Glycolysis / Gluconeogenesis	26	0.38581	2	0.055171	1.2583	1	0.54228	0.20594
Phenylalanine, tyrosine and tryptophan biosynthesis	4	0.059355	1	0.058102	1.2358	1	0.54228	0.5
Glyoxylate and dicarboxylate metabolism	32	0.47484	2	0.079815	1.0979	1	0.55522	0
Glycine, serine and threonine metabolism	33	0.48968	2	0.084213	1.0746	1	0.55522	0
D-Glutamine and D-glutamate metabolism	6	0.089032	1	0.085928	1.0659	1	0.55522	0
Nitrogen metabolism	6	0.089032	1	0.085928	1.0659	1	0.55522	0
Glycerophospholipid metabolism	36	0.53419	2	0.097841	1.0095	1	0.5848	0.02582
Pyrimidine metabolism	39	0.57871	2	0.11206	0.95053	1	0.5848	0.03727
Taurine and hypotaurine metabolism	8	0.11871	1	0.11297	0.94705	1	0.5848	0
Ubiquinone and other terpenoid-quinone biosynthesis	9	0.13355	1	0.1262	0.89895	1	0.5848	0
Tyrosine metabolism	42	0.62323	2	0.12681	0.89685	1	0.5848	0.13972

Phenylalanine metabolism	10	0.14839	1	0.13924	0.85624	1	0.5848	0
Biotin metabolism	10	0.14839	1	0.13924	0.85624	1	0.5848	0
Arginine biosynthesis	14	0.20774	1	0.18957	0.72223	1	0.75827	0
Purine metabolism	65	0.96452	2	0.25062	0.60098	1	0.9489	0
Selenocompound metabolism	20	0.29677	1	0.25982	0.58533	1	0.9489	0
Pentose phosphate pathway	22	0.32645	1	0.28191	0.54989	1	0.98669	0.11955
Lysine degradation	25	0.37097	1	0.31387	0.50324	1	1	0
Glutathione metabolism	28	0.41548	1	0.34447	0.46285	1	1	0.0018
Tryptophan metabolism	41	0.60839	1	0.46262	0.33477	1	1	0.09417

Supplemental Table 3-5. Summary of the metabolic pathways analysis for metabolites enriched in day 40 MT-ATP6/PDH brain organoids.

Statistical p values from enrichment analysis are adjusted for multiple hypothesis testing. Total: total number of compounds in the pathway. Hits: matched number from the uploaded data. Raw p: original p value calculated from the enrichment analysis. Holm p: p value adjusted by Holm-Bonferroni method. FDR p: adjusted p value using False Discovery Rate. Impact: pathway impact value calculated from pathway topology analysis.

Chapter 4

FINAL DISCUSSION, CONCLUSIONS, AND FUTURE DIRECTIONS

INVESTIGATING MITOCHONDRIAL DYNAMICS DURING HUMAN NEUROGENESIS AND DISEASE USING BRAIN ORGANOIDS

Adapted with permission from:

Romero-Morales, AI, Robertson, GL., Rastogi, A., Rasmussen, ML., Temuri, H., McElroy, GS., Chakrabarty, RP., Hsu, L., Almonacid, P.M, Millis, B., Chandel, NS., Cartailler, JP. & Gama, V. Human iPSC-derived cerebral organoids model features of Leigh Syndrome and reveal abnormal corticogenesis. Under review, Development.

Joshi P., Bodnya C., Rasmussen ML., Romero-Morales AI., Bright A. & Gama, V. Modeling the function of BAX and BAK in early human brain development using iPSC-derived systems. Cell Death & Disease. 2020, 11(9):808. PMID: 32978370.

Robertson, GL., Romero-Morales, AI., Lippmann, ES., Gama, V. Uncovering cell biology in the third dimension. MBoC Special Issue in Stem Cells. 2020, 31(5):319-323. PMID: 32105584.

Romero-Morales, AI & Gama, V. Revealing the impact of mitochondrial fitness during early neural development using human brain organoids. Under review, Frontiers in Molecular Neuroscience.

Introduction

Mitochondrial function is central to the homeostasis of highly metabolic tissues. The brain is responsible of consuming nearly 20% of the oxygen and calories from the body, while representing about 2% of its total weight (Picard and McEwen, 2014; Raichle and Gusnard, 2002). Although mitochondrial dysfunction cause by mutations in mitochondrial or metabolic genes results in severe multisystemic disease, the brain is more vulnerable to these defects in mitochondrial function. Thus, mitochondrial health sustains the functional and structural plasticity of the central nervous system.

The exact mechanisms underlying the regulation of mitochondrial dynamics during human neural development have remained widely unexplored, as most studies have been done in yeast, cultured mammalian cells, and mice (Liesa and Shirihai, 2013; Noguchi and Kasahara, 2017). As mentioned previously the known differences between human and mouse brains (Arbour et al., 2008; Khacho and Slack, 2018; Khacho et al., 2016; Pressler and Auvin, 2013) make studies in human models imperative. Whether mitochondrial function in bioenergetics, calcium handling,

reactive oxygen species production, and other signaling events, differ among human neural populations and what is the contribution of mitochondrial fitness during the neuronal specification, migration, synaptic transmission, and cognition, could be revealed using human models (Ioannou et al., 2019).

Remodeling of the mitochondrial network as cells commit to a neuronal cell fate is crucial for survival and function (Chan, 2012; Iwata et al., 2020; Khacho and Slack, 2018; Khacho et al., 2016; Schwarz, 2013). Landmark studies demonstrate that modulation of mitochondrial dynamics during a post mitotic period can change the number of NPCs or neurons that are being produced in both mouse brains and hESC derived neurons (Hara et al., 2014; Iwata et al., 2020). In murine models, the mitochondrial network transitions from elongated structures in neural stem cells to fragmented mitochondria in intermediate progenitor cells and back to elongated structures in mature neurons (Iwata et al., 2020; Khacho and Slack, 2018). It is currently not clear whether these dynamic changes in mitochondrial shape are maintained in the human brain and their involvement in maintaining the metabolic profile of the neurons at different stages of differentiation and maturation.

Revealing the molecular underpinnings of mitochondrial form and function during the early stages of neurogenesis is fundamental to developing therapies that may control human disease. Coupling human brain organoids to super resolution microscopy, optogenetic approaches, gene editing and other technical approaches could uncover the role of mitochondria in the regulation of neurogenesis, synaptic transmission, brain function, and cognition. In the next sections, we provide an overview of recent advances in understanding the intricate relationship between mitochondrial function and brain development that have result from using human iPSC brain models.

Leigh syndrome-associated mutations disrupt the mitochondrial network in the ventricular zone of cerebral organoids.

Inborn errors of metabolism are rare genetic disorders resulting from defects in metabolic pathways (Agana et al., 2018; Das et al., 2010). Mitochondrial diseases are the most common group of inherited metabolic disorders and are among the most common forms of inherited

neurological disorders (Gorman et al., 2016). These illnesses involve multiple organ systems and have limited therapeutic options (Grier et al., 2018; Parikh et al., 2017; Schaefer et al., 2019).

Leigh syndrome (LS) is one of these rare inherited neurometabolic diseases. Mutations in more than 75 genes associated with ATP production have been identified as causal, both in nuclear and mitochondrial DNA. It affects mostly infants within their first year of life and has a poor prognosis and a low survival expectancy (Finsterer, 2008; Lake et al., 2016). It is characterized by abnormal motor findings, epileptic seizures, increased lactate in the blood and cerebrospinal fluid, failure to thrive, and focal, bilaterally symmetrical necrotic lesions in the brain (Sofou et al., 2014, 2018). As it is a highly heterogeneous disease, the establishment of animal and in vitro models has been challenging and limited to only select mutations.

Animal models have been used to test therapeutic approaches, with mixed results. Gene editing using adeno-associated virus in Ndufs4-/- mice has shown partial rescue of the phenotype (Di Meo et al., 2017). Supplementation of nicotinamide riboside to Sco2-/- mice showed improvement of the respiratory chain defect and increased exercise tolerance due to improved mitochondrial biogenesis (Cerutti et al., 2014). Hypoxia and low oxygen availability in the brain have also been shown to increase the life span and improve neurological findings in Ndufs4-/- mice (Ferrari et al., 2017; Jain et al., 2016, 2019).

Reprogramming of patient fibroblast harboring nuclear and mitochondrial mutations (Galera-Monge et al., 2016; Grace et al., 2019; Inak et al., 2021; Meshrkey et al., 2021; Romero-Morales et al., 2020; Zurita-Díaz et al., 2016) has been used to generate specialized cells for the study of the impact of LS-associated mutations in highly metabolic tissues. Human iPSC models have been proposed as platforms to test new therapeutic approaches such as somatic nuclear transfer (Ma et al., 2015). Direct reprogramming of fibroblasts into neurons has been used to overcome the effects of heteroplasmy during reprogramming and as an alternative for targeted high-throughput drug screening and advancing precision medicine (Villalón-García et al., 2020; Villanueva-Paz et al., 2019).

These approaches have proven useful to investigate the effects of LS causing mutations in early neural development (Inak et al., 2021; Romero-Morales et al., 2020). Inak and collaborators

generated iPSCs with mutations in the complex IV assembly gene Surfeit locus protein 1 (SURF1) and CRISPR/Cas9 corrected lines (Inak et al., 2021). As early as neural progenitor cells, deficiencies in the ability to switch to an OXPHOS energetic program and failure to differentiate into neurons were observed in both monolayer and brain organoid cultures. Aberrant cytoarchitecture was also observed in the LS mutant organoids. Importantly, rescue with SURF1 gene augmentation was able to rescue the observed phenotype, as well as pharmacological induction of PGC1A via bezafibrate, an antilipemic agent that lowers cholesterol and triglycerides (Behar et al., 2000).

In our LS derived model (described in Chapter 3), mitochondrial morphology was also evaluated in the VZ NPCs of the cerebral organoids. Cells positive for SOX2 demonstrated elongated mitochondrial networks that extend radially from the ventricle-like lumen (Figure 4-1A). These results are significant because it is the first evidence demonstrating that mitochondrial networks are remodeled in the developing human brain as reported in the developing mouse cortex (Iwata et al., 2020; Khacho et al., 2016). PDH mutant organoid NPCs have an increased mitochondrial axis length compared to control ($p=0.0078$, Figure 4-1B). As mentioned earlier, the stereotypical arrangement of the VZ was compromised in most MT-ATP6/PDH organoids. In the few areas where ventricle-like structures were identified with a conserved SOX2+ VZ, the mitochondrial network appeared more aggregated. This morphology was also observed in the clusters of SOX2+ cells that were scattered throughout the organoid. Quantification of the mitochondrial network for this mutant (Figure 4-1B) showed increased mitochondrial volume, diameter, surface area, and axis length ($p<0.0001$, in all cases), which suggests a mitochondrial aggregation phenotype in the VZ. Moreover, the difference in mitochondrial length may also correlate with the increased expression of TBR2 observed by RT-qPCR (Iwata et al., 2020).

As NPCs generated by a dual SMAD monolayer method did not show major differences among the different genotypes, we looked at their mitochondria morphology to evaluate if the differences observed in the organoids were recapitulated in this paradigm. Characterization and quantification of various parameters of the mitochondrial network using structured illumination microscopy (SIM) revealed that while control human NPCs showed elongation of the mitochondrial network, the DLD mutant displays an increase in mitochondrial number and

decreased sphericity. Both DLD and PDH mutants have a significant increase in the number of branches in the network. (Figure 4-1C, D), which may reflect an increase in fusion events (Sukhorukov et al., 2012; Westrate et al., 2014). These changes suggest that the mitochondrial network in DLD and PDH lines may be more fragmented than control, which could be linked to the underlying changes in metabolic capacity (Rafelski, 2013) and developmental defects (Westrate et al., 2014).

The metabolic dysregulation of the affected tissues in LS may have a direct effect on mitochondrial morphology and function. Mitochondrial fragmentation is a hallmark of glycolytic cell types such as stem cells and cancer cells (Chen and Chan, 2017; Rastogi et al., 2019). Moreover, neurogenesis defects have been observed in the context of mitochondrial morphology dysregulation and are considered to be upstream regulators of self-renewal and cell fate decisions in stem cells (Iwata et al., 2020; Khacho et al., 2016). In addition, energetic requirements have been shown to directly impact the capacity of progenitor cells to migrate and thrive in 3D environments (Zanotelli et al., 2018, 2019). Hence, mitochondrial morphology disruption observed in the double mutant MT-ATP6/PDH organoids is congruent with the metabolic and developmental profiles of these mutant organoids.

To our knowledge, this is the first time that mitochondrial morphology in the cortex has been analyzed in a human model system of LS brain development and highlights the critical function of mitochondrial network plasticity for the proper specification of cell fate and survival. Studies in murine brains demonstrated a period of plasticity in postmitotic cells where mitochondrial morphology determines the fate of the daughter cells (Iwata et al., 2020). Our results also highlight the direct link of mitochondrial morphology with early events in human brain development.

As mentioned in Chapter 3, LS is characterized for symmetric necrotic lesions that appear in different parts of the brain; as well as swelling or shrinking of neuronal cell bodies, demyelination, and gliosis (Lake et al., 2015). The reasons for these lesions are not well understood and it has been proposed that the cell death of neurons in these areas is due to the severe metabolic imbalance (Shtilbans et al., 2000), oxidative stress (Quintana et al., 2010) and/or excitotoxicity (Cavanagh, 1994; Visch et al., 2006). The use of iPSCs derived from LS patients for both 2D and

3D neuronal differentiation can open an avenue of investigation to determine the cause or causes for the neuronal death. Not only the possibility to generate mixed neuronal population exist, but when using 3D models, the interactions between the different cell types during the pathological process can be investigated. Specifically for the organoids system, there is the capacity to produce individual regions of the brain and investigate the effects of the LS causing mutations in the neuronal subpopulation. Moreover, assembloids (Miura et al., 2020; Pașca, 2018; Sloan et al., 2018) can be generated to investigate the interactions between these regions; specifically the metabolically demanding interneuronal migration that occurs from the ventral forebrain to the dorsal forebrain. Errors in myelination and formation of the axonal bundles can also be an avenue of interest as oligodendrocyte loss has also been observed in LS (Anzil et al., 1981; Marton et al., 2019; Pliss et al., 2004). Also, long term maintenance (>100 days) of brain organoids can be used to understand the role of astrocytes in the pathophysiology of LS.

Other potential use of the LS-derived iPSC derived systems is its use as a testing platform for drugs and therapies. Work in mice has shown that chronic hypoxia can prevent and even reverse some of the neurological findings in LS (Jain et al., 2019), but these has not been tested in human models yet. The use brain organoids may be an appropriate tool to test whether the reduction of oxygen tension can rescue the LS phenotype and to test for other therapeutic approaches that could alleviate the disease onset and progression.

Mitochondria morphology changes through neural differentiation and maturation.

Due to the highly dynamic nature of mitochondria, analysis of its morphology has been challenging in *in vivo* and 3-D settings. Most of the existing classification have resorted to manual and morphological classification (*e.g*. fused vs fragmented) of the mitochondrial networks, utilizing qualitative or semi-quantitative approaches (Faitg et al., 2021; Fogo et al., 2021; Noguchi and Kasahara, 2017; Prieto et al., 2016; Rafelski, 2013). Advances in imaging techniques coupled with computational approaches have improved the capacity to unbiasedly and consistently assess the morphology of these organelles (Leonard et al., 2015; Zahedi et al., 2018). Recently, machine learning algorithms (Kan, 2017) together with genetic perturbations of key

mitochondrial players, have been proposed as a potential alternative to not only evaluate the phenotypical aspects of the mitochondria but to assess the physiological relevance of those changes (Fogo et al., 2021).

As shown in this chapter (Figure 4-1), we have been able to image the mitochondrial network of brain organoids. Although we have characterized the SVZ/VZ in control and disease organoids, a comprehensive study of the mitochondrial network of different cell types may be required. In accordance with previous findings in the mouse brain and *in vitro* neurons (Iwata et al., 2020; Khacho et al., 2016), neural progenitor cells that are positive for the transcription factors PAX6 and SOX2 present an elongated mitochondria (Figure 4-2A & B). In contrast, committed neurons positive for the cytoskeletal marker βIII-tubulin have a fragmented network (Figure 4-1C).

Although the characterization we have performed at the moment is semi-quantitative, recent tools have been developed that can be coupled to refine the analysis of the mitochondrial morphologies in different cell types. For example, with the use of iLastik (Berg et al., 2019), a machine learning algorithm, we will be able to unbiasedly quantify the length of the mitochondrial networks in different areas of the brain organoids and at different points of organoid maturation. This analysis will allow us to compare the changes observed in mouse brains and 2-D hESCs-derived neurons to a 3-D model of development and shed light into the differences and similarities of the different research models.

This new method of mitochondrial scoring and quantification can be extended to other neural organoid protocols. For example, dorsal and ventral spheroids (Birey et al., 2017) or thalamic organoids (Xiang et al., 2019) can be used to explore the effects of mitochondrial and mitochondrial associated mutations in the migration of axons. This would be of particular interest in disease models where can be axonal migration can be affected or where proper formation of axonal tract play a crucial role in the pathophysiology of the disease (Giandomenico et al., 2019; Kitahara et al., 2020). By coupling the use of brain organoids with high resolution microscopy, it would be possible to address the morphological changes necessary for the cell fate specification and neurogenesis. Long term recording using systems such as light sheet microscopes (Cella Zanacchi et al., 2011; Fadero et al., 2018; Huisken et al., 2004; Power and Huisken, 2017) could allow the study of how the mitochondrial network adapt during the early stages of neural

induction. These tools, coupled with targeted genetic disruption of the mitochondrial dynamic and energetic machinery, could shed light into the molecular mechanisms governing acquisition of cell identity.

Also, these techniques can be used for the characterization of the mitochondrial morphology and the network regulation in other tissues during development and disease. Organoids that mimic highly metabolic tissues such as cardiac muscle, kidney and liver could be used to understand the effects of the mitochondrial dynamics under homeostatic and allostatic conditions.

Moreover, the ability of studying mitochondrial fitness during early development could allow for the understanding of other neurodevelopmental disease caused by environmental factors and maternal health. The organoid system could be used to determine the effects of metabolic stress and nutrient imbalance in the developing brain as maternal metabolic diseases has been shown to correlate with increased risk of neurodevelopmental and psychiatric diseases in both human and animal studies (Edlow, 2021; Shook et al., 2020). Also, the capacity to recapitulate the formation of the neural tube as neural rosettes or as neuruloids -self-organizing structures containing neural progenitors, neural crest, sensory placode and epidermis- (Haremaki et al., 2019) could allow for the exploration of the molecular and cellular mechanisms behind complex CNS birth abnormalities.

Apoptosis inhibition affects the mitochondria morphology and neural cell specification in day 30 brain organoids.

Mitochondria are at the crossroads of cell death and metabolism (Rastogi et al., 2019). The BCL-2 family of proteins regulates cell death at the mitochondria (Green, 2000; Vander Heiden et al., 1997; Hsu et al., 1997; Inohara et al., 1998; Jürgensmeier et al., 1998; Ke et al., 2018; Kluck et al., 1997, 1999; Knudson et al., 1995; Wei et al., 2000) and has been implicated in maintaining mitochondrial homeostasis in the absence of a cell death signal (Joshi et al., 2020; Li et al., 2008, 2013; Rasmussen et al., 2018, 2020; Salisbury-Ruf et al., 2018).

Programmed cell death (apoptosis) is an integral part of brain development and maturation (Kuan et al., 2000). Immature human brains have nearly 50% more neurons than adults, as many neurons die by apoptosis during normal brain morphogenesis and neuronal histogenesis. Apoptosis is assumed to prevent overgrowth of the neuroepithelium by controlling neural cell numbers in the developing brain (Akhtar et al., 2004; Kuan et al., 2000; Nonomura et al., 2013; Yamaguchi and Miura, 2015). Reduced cell death in mice bearing mutations in pro-apoptotic molecules (e.g. caspase 3, caspase 9) result in severe brain malformations including indented neuroepithelium, compressed brain ventricles, and neural tube closure defects (Nonomura et al., 2013). Additionally, in early brain development, massive cell death is restricted to specific areas, suggesting that local apoptosis might affect the gross organization of the developing organ (Akhtar et al., 2004; Kuan et al., 2000).

Our laboratory generated a double CRISPR knock-out cell line deficient in the apoptosis effectors BAK and BAX (Joshi et al., 2020). We investigated the effects of these two proteins as they have been implicated in the maintenance of the mitochondrial morphology (Arnoult et al., 2005; Delivani and Martin, 2006; Delivani et al., 2006; Frank et al., 2001; Tanaka and Youle, 2008; Youle and Karbowski, 2005). BAX/BAK deficient cells have been shown to have defect in their mitochondrial shape (Karbowski et al., 2006). Moreover, BAX has been observed to colocalize with the primary executioner of mitochondrial fission Dynamin related protein-1 (DRP-1) during early stages of apoptosis (Karbowski et al., 2002).

Previous studies showed that BAX/BAK deficient cells have some defects in mitochondrial morphology (Karbowski et al., 2006). BAX also is known to colocalize with the primary executioner of mitochondrial fission Dynamin related protein-1 (DRP-1) during early stages of apoptosis (Karbowski et al., 2002). Thus, BAX/BAK are also potential regulators of mitochondrial homeostasis during development. In Joshi et al. (2020), I generated day 30 brain organoids from the BAX/BAK double knockout (DKO) cell line to investigate the effect of apoptosis inhibition in human brain development and mitochondrial morphology. The brain organoids generated from the control lines showed the expected markers and architecture for this timepoint. hNPCS stained with PAX6, SOX2 and NESTIN formed the VZ/SVZ around the lumen-like structure. oRGs that were TBR2 positive decorated the edge of the VZ/SVZ, and cortical plate cells positive for

TBR1 and CTIP2 were observed. The DKOs, in the other hand, showed a profound loss of cortical organizations and a reduction in the cells positive for the aforementioned markers (Joshi et al., 2020).

Analysis of the areas of the organoids that were positive for the NPC marker SOX2, showed aggregation of the mitochondrial network (Figure 4-3) in the DKOs. Control organoids showed a conserved organization of the VZ/SVZ and the expected elongated network for SOX2+ NPCs. This loss of neural markers in conjunction with the disruption of the mitochondrial network in the DKO may suggest that BAX and BAK are key players in the regulation of the mitochondrial morphology, and their absence generate a downstream effect in the specification of the cell fate.

BAX/BAK KO iPSCs allow for the possibility to use this genetic background for the study of deleterious mutations than otherwise would cause cell death. It could also serve as a platform for the study of developmental apoptosis, and the signaling mechanisms that dying cells are involved. Collaborators have shown using this cell line that apoptosis is a key regulator for the epithelial-mesenchymal transition (EMT) necessary for the acquisition of cardiac lineage (Fort et al., 2021). Fort *et al*, showed that nucleotides released by dying cells as chemo-attractants for apoptotic cell clearance also function as essential paracrine signals in mesoderm specification vial WNT pathway. EMT is also crucial for the migration of the neural crest cells from the neural tube to the surrounding tissue for the formation of peripheral neurons, melanocytes, craniofacial bones and muscle, among other structures (Hay, 2005). As WNT pathway has also been implicated in the control of neural crest delamination, it would be interesting to investigate if a similar signaling mechanism mediates this process.

Particularly in the brain, developmental cell death is crucial for the during development and maturation of the neuronal connections. In the specific case of neuronal pruning, studies suggest that dysregulation of the mitochondrial membrane potential and the production of reactive oxygen species are signals for axonal retraction and degradation (Baranov et al., 2019; Lieberman et al., 2019). Yet, it is not known how the mitochondrial dynamics affect these events. Moreover, as apoptotic cells are key for the colonization of the brain by microglia (Arnò et al., 2014; Casano et al., 2016), co-culturing experiments between BAX/BAK KO organoids with microglia can help elucidate the mechanism of microglia migration and proliferation in the developing brain.

Contribution of mitochondria dysregulation to the abnormal corticogenesis caused by hypoxic injury.

Extreme prematurity and complications prior to or during birth can contribute to hypoxic episodes and subsequent brain injury in neonates (Lima et al., 2018). As survival increases, so does the life-long neurological disabilities associated with central nervous system (CNS) injury. Mitochondrial energy production is impaired when the tissue oxygen tension is reduced (Lages et al., 2015; Santore et al., 2002). After reoxygenation, mitochondrial respiration transiently resumes but it is later suppressed (Goda and Kanai, 2012; Weidemann and Johnson, 2008; Xie and Wolin, 1996). Mitochondrial hyperpolarization results in the increased production of reactive oxygen species (ROS) leading to accumulation of mutations (Grivennikova et al., 2010), decreased metabolic output, and increased susceptibility to cell death (Kudin et al., 2004).

Studies using rat brains showed that the mitochondrial morphology in neurons shifts from elongated to more granular/fragmented appearance after the hypoxic insult (Hallin et al., 2006; Puka-Sundvall et al., 2000). Mitochondrial migration towards the nucleus, as well as accumulation in the perinuclear region, has also been described and associated with the onset of cell death (Hallin et al., 2006; Northington et al., 2001).

Pathological mitochondrial fragmentation has been reported in in vivo and in vitro models. Loss of the mitochondrial membrane potential leads to the cleavage OPA1 - responsible for inner mitochondrial membrane fusion. Oxygen deprivation increases the amount of a short non-functional form of OPA1, resulting in rapid induction of fission and ultimately cell death (Baburamani et al., 2015; Ehses et al., 2009; Head et al., 2009; Kumar et al., 2016; Sanderson et al., 2015). Interestingly, downregulation of DRP1 can prevent the permeabilization of the mitochondrial membrane and the progression to cell death (Grohm et al., 2012) by potentially preventing cristae remodeling (Ramonet et al., 2013). However, it is not known if these morphological changes, their regulation, and their effects on mitochondrial function are involved during neonatal hypoxia. Prolonged depression in mitochondrial metabolism (Brekke et al.,

2017), as well as rapid induction of mitochondrial fragmentation (Demarest et al., 2016), validate the emerging evidence of the mitochondria as central regulators of the hypoxic injury cascade.

Results from animal models have shown that grey and white matter are the most vulnerable areas of the brain to neonatal hypoxia ischemic injury. The cerebral cortex is predominantly affected (Volpe, 2012) and the localization and extent of the insult have been shown to correlate with specific neurodevelopmental symptoms later in life (Gonzalez and Miller, 2006; Steinman et al., 2009). Considering that the spatiotemporal regulation of neuronal proliferation, migration and differentiation varies among mammals, a human derived model is needed to understand species specific variation.

The cerebral cortex is highly sensitive to hypoxic insult. Cell death in this region presents a laminar distribution, especially involving layers III and V (Volpe, 2012). Work in early stages of brain organoid formation have shown that hypoxic stress causes growth arrest, massive cell death (Daviaud et al., 2019) and reduced expression of the cortical markers TBR1, CTIP2, SATB2, and the astrocyte marker GFAP (Boisvert et al., 2019). In a model of encephalopathy of prematurity, human cortical spheroids resembling the cerebral cortex at midgestation were exposed to 48h of low oxygen tension (<1%) (Pașca et al., 2019). Hypoxia induced a reduction in TBR2+ intermediate progenitor cells and an increase in CTIP2+ cells, suggesting premature neural differentiation (Pașca et al., 2019).

As the mitochondrial network undergoes remodeling in the different cellular niches of the developing brain (Khacho and Slack, 2018; Khacho et al., 2016, 2019), it would be interesting to analyze if the that hypoxic insult affects each neural population differently due to dysregulation of mitochondrial dynamics. Hypoxic insult may affect the mitochondrial network plasticity due to dysregulation of the mitochondrial dynamic's machinery. Rates of fission may increase as OPA-1 undergoes cleavage into short non-functional form (Ehses et al., 2009). The high sensitivity to hypoxia of intermediate progenitor cells may be due to changes in mitochondrial dynamics and morphology. By taking advantage of the abovementioned BAX/BAK iPSC line, it would be possible to characterize the contribution of mitochondrial dynamics to the deleterious effects observed in intermediate progenitor cells. As the intermediate progenitor cells have been proposed to undergo cell death during hypoxic injury, characterization in this context has been challenging.

This model could also be used to examine other determinants of mitochondrial homeostasis including mitochondrial biogenesis and mitophagy.

Moreover, this hypoxic paradigm can be used to analyze confounding effect of oxygen deprivation and mitochondrial disfunction. Mitochondrial disorders can intensify the effects of hypoxia by exacerbating potential deleterious reactions (Volpe, 2012) or diminishing prosurvival mechanisms (Ten and Starkov, 2012). In Chapter 3, I described the generation of iPSCs from fibroblasts of patients with mitochondrial (MT-ATP6) and mitochondrial associated (PDH and DLD) mutations. This cell lines could be used to determine how mitochondrial impairment affects the response to hypoxia, as failure of the metabolic machinery has been shown to contribute to brain injury in mouse models (Niatsetskaya et al., 2012). Paradoxically, hypoxia has been shown to reverse some of the effects of mitochondrial disorders such as Leigh syndrome (Jain et al., 2019).

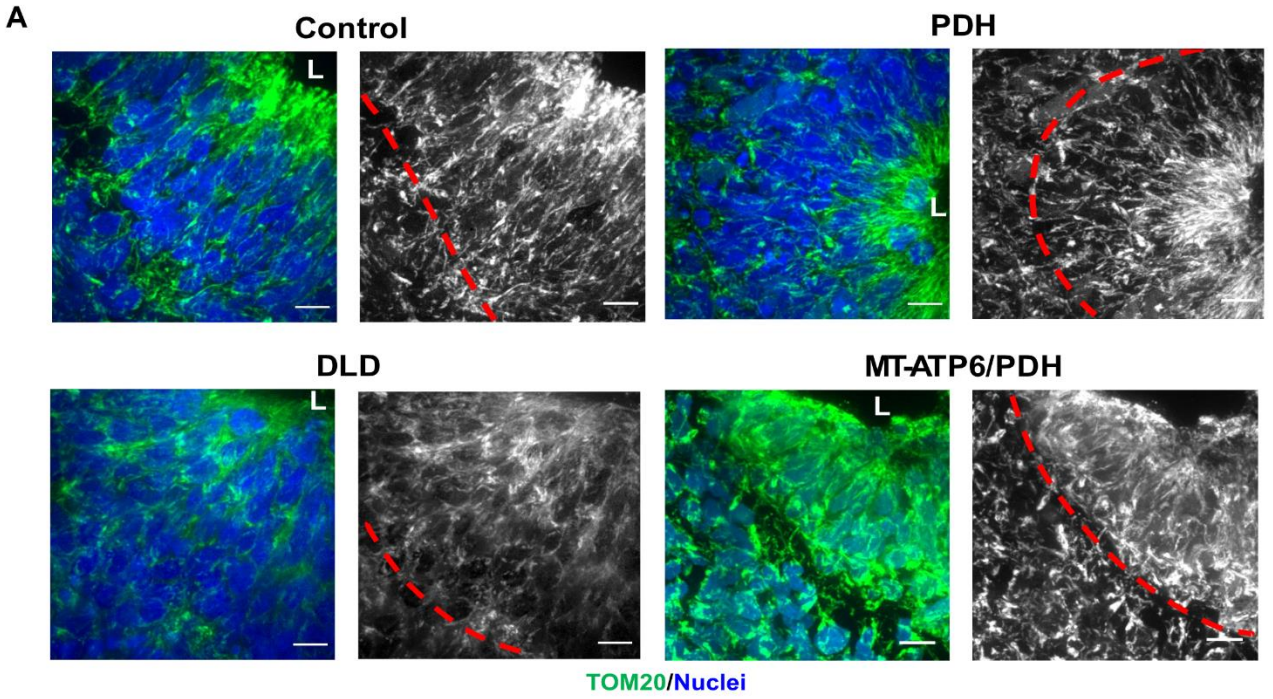
A
Control
PDH
DLD
MT-ATP6/PDH
L
TOM20/Nuclei

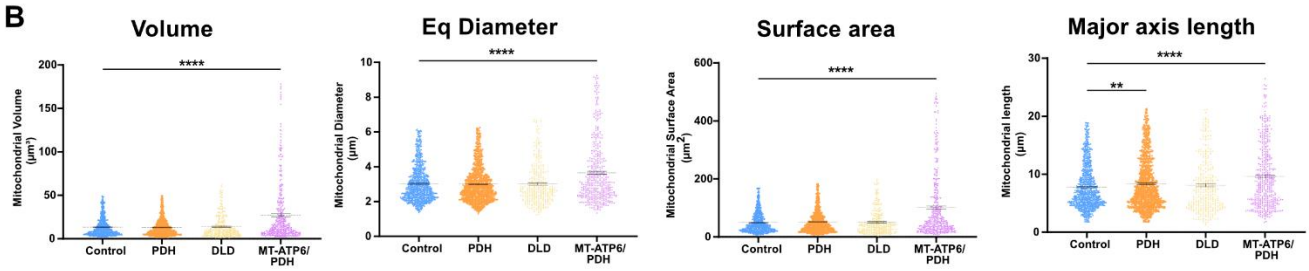
B
Volume
Eq Diameter
Surface area
Major axis length
Mitochondrial Volume (µm³)
Mitochondrial Diameter (µm)
Mitochondrial Surface Area (µm²)
Mitochondrial length (µm)
Control
PDH
DLD
MT-ATP6/PDH

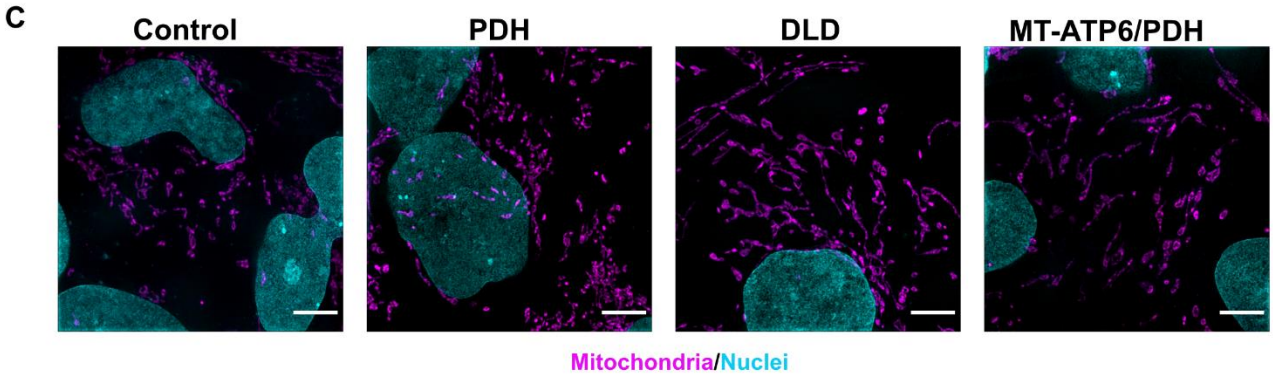
C
Control
PDH
DLD
MT-ATP6/PDH
Mitochondria/Nuclei

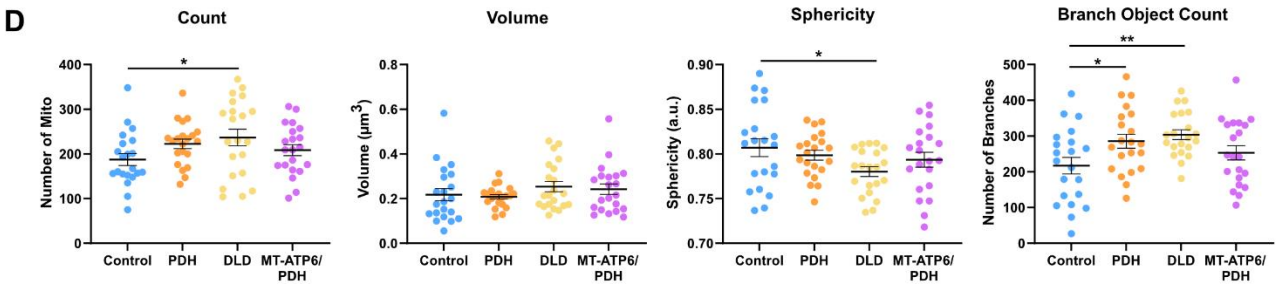
D
Count
Volume
Sphericity
Branch Object Count
Number of Mito
Volume (µm³)
Sphericity (a.u.)
Number of Branches
Control
PDH
DLD
MT-ATP6/PDH

Figure 4-1. Leigh syndrome-derived organoids show defects in mitochondrial morphology in the SVZ compartment.

A. Representative confocal images of day 30 brain organoids showing mitochondrial morphology (TOM20). The red line divides the Sox2+ NPCs surrounding the lumen (L) from newly committed neurons. MT-ATP6/PDH mutant organoids show disorganization and fragmentation of the mitochondrial network. Scale bar: 10µm. B. Quantification of average mitochondrial volume, diameter, surface area, and major axis length are shown. Graphs represent mean ± SEM from at least three independent SVZs per phenotype from 3 independent organoid batches. Quantification was performed by 3D reconstruction of the mitochondrial network of interest. C. Representative super-resolution images of mitochondrial morphology in LS and control NPCs. Scale bar: 5µm. D. Quantification of average mitochondrial number, volume, mitochondrial sphericity, and mitochondrial branching are shown. Graphs represent mean ± SEM from at least three independent experiments (n>20 cells per genotype). $*p<0.05$; $**p<0.01$; $***p<0.001$; $****p<0.0001$.

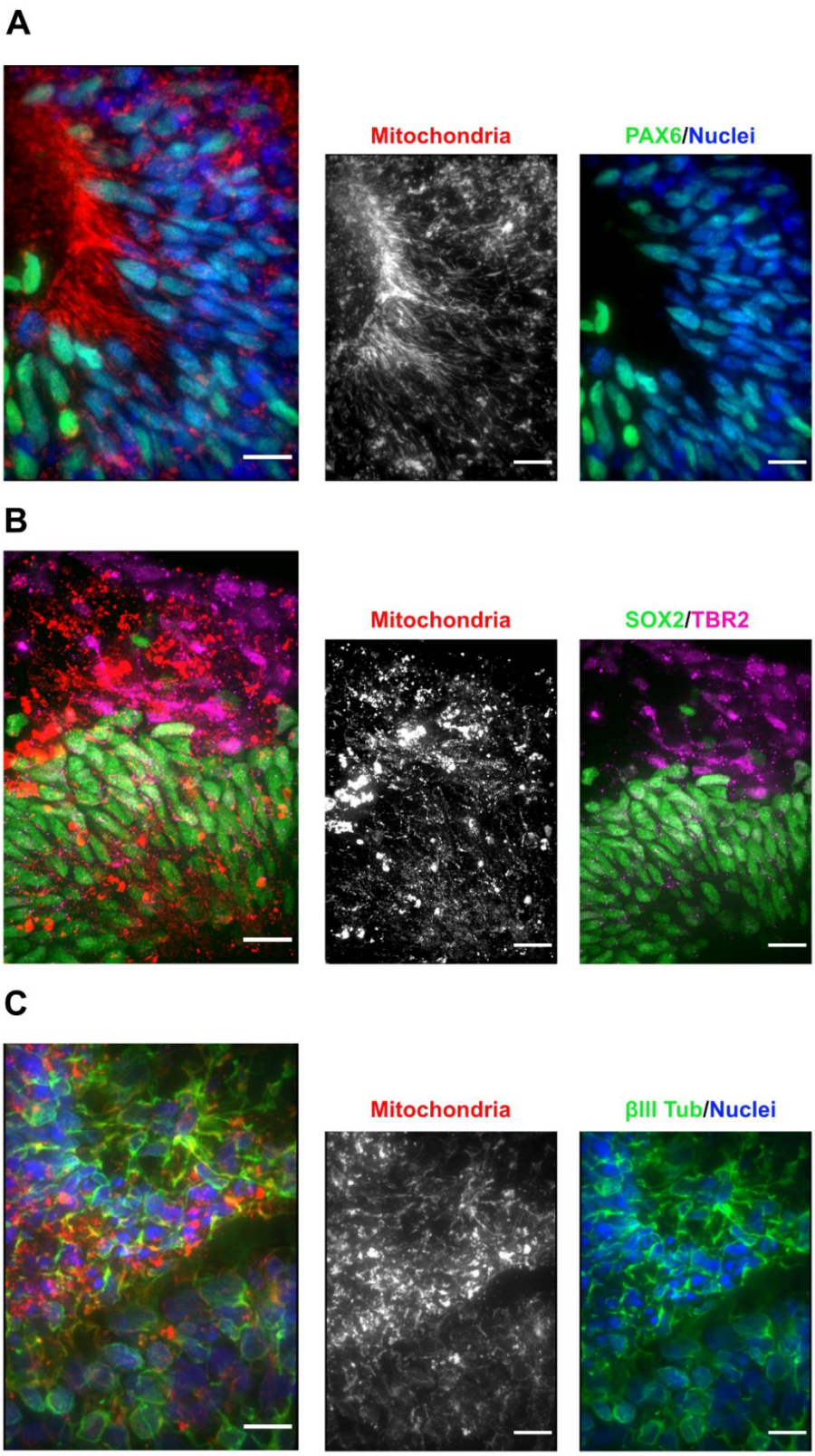
A
Mitochondria
PAX6/Nuclei
B
Mitochondria
SOX2/TBR2
C
Mitochondria
βIII Tub/Nuclei

Figure 4-2. Mitochondrial morphology changes in day 30 human derived brain organoids.

A. PAX6+ NPCs in the SVZ/ZV of brain organoids have an elongated mitochondrial network surrounding the lumen-like structure. B. Similarly, mitochondria in SOX2+ NPCs appear longer than the those in TBR2+ IPCs. C. Fragmented mitochondria can be observed in areas positive for the neuronal marker βIII-TUBULIN.

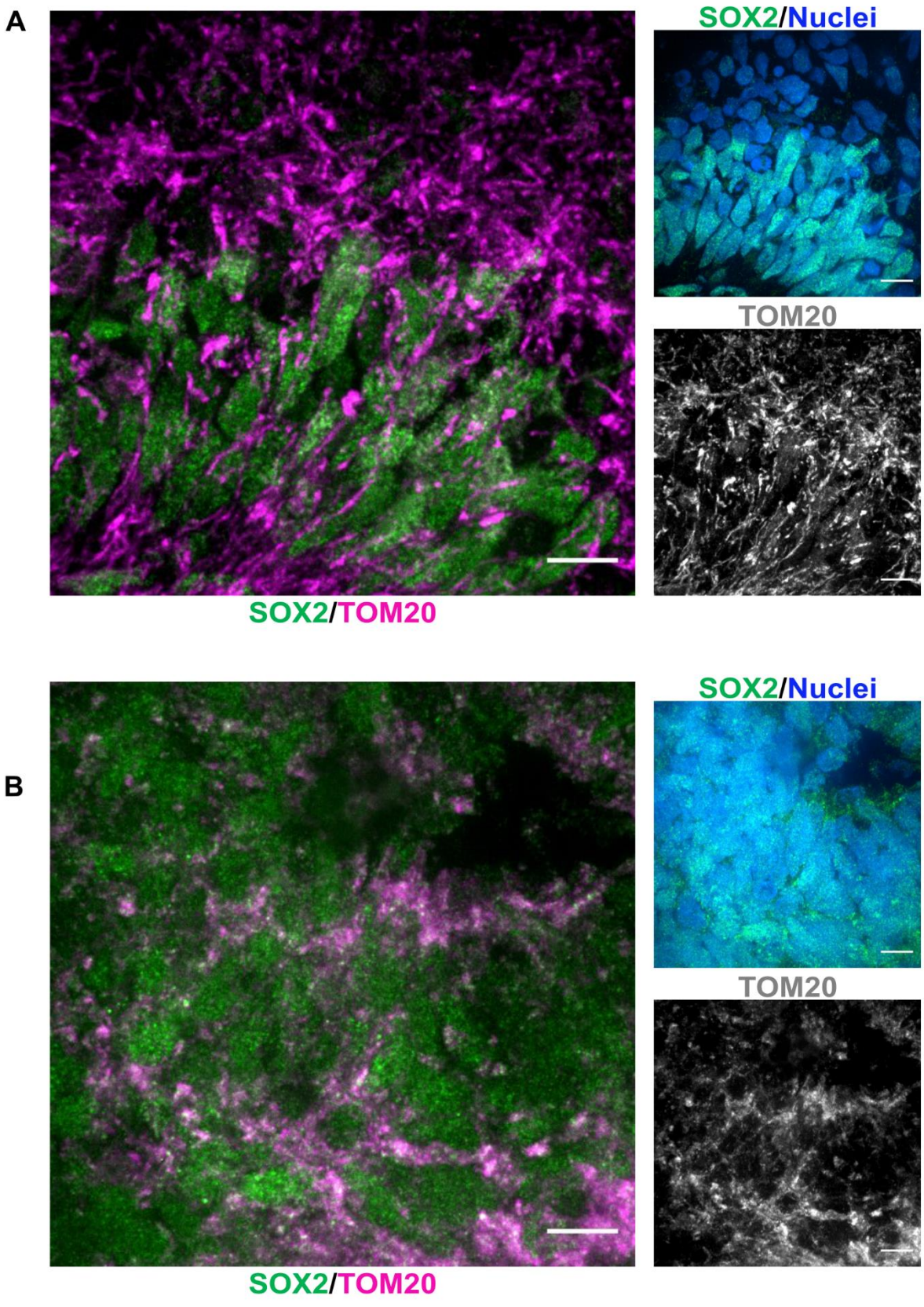
A
SOX2/Nuclei
TOM20
SOX2/TOM20
B
SOX2/Nuclei
TOM20
SOX2/TOM20

Figure 4-3. Day 30 DKO cerebral organoids have abnormal mitochondrial morphology.

A. Day 30 control cerebral organoids shows the expected elongated mitochondrial network (TOM20) in SOX2+ cells. B. Day 30 DKO cerebral organoid have an aggregated mitochondrial morphology. Scale bar=10µm.

Appendix

MATERIALS AND METHODS FOR CHAPTER 2

Human pluripotent stem cell culture

We have successfully used feeder-dependent hiPSCs reprogrammed from newborn human foreskin fibroblasts (ATCC, cat. no. CRL-2522), as well as human embryonic stem cells (H9 from WiCell). Human iPSC lines AICS-0012 (WTC-mEGFP-TUBA1B-cl105) used in the current study were obtained from the Allen Institute (Coriell Institute for Medical Research, New Jersey). This cell line has a N-term insertion of mEGFP in frame generated by CRISPR-Cas9 technology. Induced pluripotent stem cells were grown in feeder-free conditions in plates coated with Matrigel (Corning) and maintained in E8 media at 37°C with 5% CO2. Culture medium was changed daily. Cells were checked daily for differentiation and were passaged every 3-4 days using Gentle dissociation solution (Stem Cell Technologies). All experiments were performed under the supervision of the Vanderbilt Institutional Human Pluripotent Cell Research Oversight (VIHPCRO) Committee (Record ID#56).

Derivation of the brain organoids

Brain organoids were generated using the STEMdiff™ Cerebral Organoid Kit (Stem Cell Technologies) using the manufacturer protocol with some modifications (Lancaster and Knoblich, 2014; Lancaster et al., 2013; Qian et al., 2016; Sutcliffe and Lancaster, 2017). On Day 0, iPSCs were detached with Gentle Cell Dissociation Reagent for 8 minutes at 37°C. Cells were resuspended in 1mL of EB Seeding Medium and centrifuged at 300g for 5 minutes. The cell pellet was resuspended in 2mL of EB Seeding Medium. Homogeneous and reproducible EBs were generated by using 24-well plate AggreWell™ 800 (Stem Cell Technologies, catalog 34815). In each well, 2.7x106 cells were plated (approx. 9000 cells/microwell) following the manufacturers protocol. EBs were incubated at 37°C with 5% CO2, with minimal disruption during the first 48 hours. Media changes, 50-75% of the total volume, were performed every 2 days. On Day 4, EBs were harvest according to the manufacturer protocol and transferred to a 10 cm tissue culture dish (Eppendorf, catalog 0030702018). On Day 5, Induction Medium was added to each well and

incubated for 48 h at 37°C. On Day 7, high quality EBs (smooth and optically translucent edges) were embedded in Matrigel (Corning). EBs were transferred to a 15mL conical tube and resuspended in Expansion Medium. Using a P100 pipette, 67uL containing ~20-30 EBs in medium were transferred to a microcentrifuge tube. Next, 100uL of thawed Matrigel was added to the microcentrifuge tube (3:2 ratio) and mix with the medium and EBs by pipetting up and down multiple times. Using a cut tip, the Matrigel-EB mixture was pipetted and spread onto the center of an ultra-low attachment six-well plate. Matrigel coat should fully envelop the EBs in 3D (thickness of >1mm). EBs should be evenly distributed to avoid contacting each other or the wall of the well. Incubate the Matrigel at 37°C for 30 min to solidify. Gently add 3mL of Expansion Medium and incubate at 37°C for 3 days.

On Day 10, the Matrigel coat was broken by vigorously pipetting up and down. Organoids were transferred to a 15mL conical tube. Healthy organoids will precipitate faster than Matrigel clumps and organoid debris. By gently mixing, debris can be removed with supernatant after the healthy organoids precipitate to the bottom of the tube. Organoids were then resuspended in Maturation media and distribute into an ultra-low attachment 12-well plate (6-10 organoids per well). Maturation media was added to a final volume of 3mL/well. Subsequently, the plate was inserted into the bottom frame of the Spin and the lid was positioned in place. The whole system was ten moved to a 37°C incubator and the shaking speed was set at 90rpm. Full Maturation Medium change was performed every 3–4 days. Reconstitution of extracellular matrix was performed on Day 40. Matrigel was thawed on ice and dissolved in Maturation Media in a 1:50 dilution. Transmitted-light images were acquired using an EVOS® XL Core Imaging System. The software used for processing was ImageJ.

Tissue preparation and Immunohistochemistry

Cerebral organoids were fixed in 4% Paraformaldehyde in Phosphate Buffered Saline (PBS) for 15-20 min at 4°C. Organoids were washed 3 times with PBS and then incubated in 30% sucrose solution overnight at 4°C. Organoids were embedded in 7.5% gelatin/10% sucrose solution

(Sigma, catalog G1890-100G and S7903-250G) and sectioned with a cryostat (Leica CM1950) at 15um thickness.

For immunostaining, freezing medium was washed with PBS before permeabilization with 0.2% Triton-X in PBS for 1 hr. Tissues were blocked with blocking medium consisting of 10% donkey serum in PBS with 0.1% Tween-20 (PBST) for 30 min. Primary antibodies diluted in blocking solution were applied to the sections overnight at 4ºC. After washing 3 times with PBST, secondary antibodies were diluted in blocking solution were applied to the sections for 1 hr at room temperature. Finally, sections were washed 3 times with PBST and stained with Hoechst. Confocal images were acquired using an Andor DU-897 EMCCD camera mounted on a Nikon Spinning Disk Microscope. The software used for image acquisition and reconstruction was NIS-Elements Viewer (Nikon).

MATERIALS AND METHODS FOR CHAPTER 3

Experimental Model and Subject Details

The Coriell cell line IDs were as follows: GM01503, GM03672, GM1341. Information about the Leigh syndrome cell lines used in this study can be found in Supplementary Table1. Control skin fibroblast cell line AG16409 was also obtained from Coriell Institute, Philadelphia, PA, and analyzed for contamination. The donor was a 12-year-old apparently healthy Caucasian male. Cells were negative for Mycoplasma.

Fibroblasts were maintained in Dulbecco's Modified Eagle Medium: Nutrient Mixture F-12 DMEM/F-12 (Gibco cat # 11330032) supplemented with 10% Fetal bovine serum (Sigma cat# F2442) in 100mm cell culture plates (Eppendorf, cat # 0030702115) in a 37°C 5% CO2 incubator.

Whole Exome sequencing

Fibroblast cell pellets from each cell line (>1 million cells) were shipped on dry ice for whole-genome exome sequencing to Genewiz, Plainfield, NJ. The Illumina HiSeq-X was used to perform 150nt paired-end sequencing.

Mitochondrial sequencing

Fibroblast cell pellets from each patient (>1 million cells) were shipped on dry ice for mitochondrial sequencing to Girihlet Inc. Oakland, CA. The sequencing configuration used was 80bp single-end sequencing, 20 million reads per sample.

hiPSC Generation and Characterization

Human fibroblasts were purchased from healthy control and patients (Coriell Institute, Philadelphia, PA, USA). Induced pluripotent stem cells were derived from human fibroblasts using Sendai virus-based reprogramming kit (CytoTune-iPS Sendai Reprogramming Kit; cat #. A13780-01; Thermo Fisher), according to manufacturer’s instructions. After 3-4 weeks, 2-3 colonies per

sample were transferred to fresh 6-well plates and were expanded and gardened for 3 passages before freezing. All iPSC cell lines were maintained in E8 medium in plates coated with Matrigel (Corning, cat # 354277) at 37°C with 5% CO_2. Culture medium was changed daily. Cells were checked daily for differentiation and were passaged every 3-4 days using Gentle cell dissociation solution (STEMCELL Technologies, cat # 07174). All experiments were performed under the supervision of the Vanderbilt Institutional Human Pluripotent Cell Research Oversight (VIHPCRO) Committee. Cells were checked for contamination periodically.

Analysis of Pluripotency

The pluripotency of each iPSC clone was determined using a microarray-based tool known as PluriTest (Thermo Fisher; cat# A38154) as an alternative to the teratoma assay. Samples were outsourced to Thermo Fisher for PluriTest and further analysis. Low passage iPSC cell pellets (>1 million cells) were frozen and shipped on dry ice. Additionally, the expression of pluripotency genes *POU5F1* and *NANOG* was assessed by qPCR.

Analysis of Chromosomal abnormalities

The presence of any chromosomal abnormalities in the newly generated iPSCs was determined using a microarray-based tool known as KaryoStat (Thermo Fisher; cat# A38153) as an alternative to chromosomal G-banding. Samples were outsourced to Thermo Fisher for KaryoStat and further analysis. Low passage iPSC cell pellets (>1 million cells) were frozen and shipped on dry ice to Thermo Fisher.

Trilineage differentiation

The STEMdiff Trilineage differentiation kit (STEMCELL Technologies, cat# 05230) was used to functionally validate the ability of newly established iPSCs to differentiate into three germ layers, as per the manufacturer's instructions. Single-cell suspensions of $2x10^6$ cells/well, $5x10^5$ cells/well, $2x10^6$ cells/well were seeded for ectoderm, mesoderm, and endoderm, respectively,

in their corresponding medium at day 0 in 6 well plates. The cultures were maintained for 7 days, 5 days, and 5 days for ectoderm, mesoderm, and endoderm, respectively. The differentiation was assessed by qPCR.

NPC differentiation and multipotency characterization

For monolayer differentiation of the iPSCs into NPCs, cells were dissociated into single cells using Gentle Cell Dissociation Reagent (STEMCELL Technologies, cat # 07174) for 8 minutes at 37°C. Live cell counts were performed using Trypan blue (0.4%) staining (Invitrogen, cat # T10282) using a Countess™ Automated Cell Counter. Cells were then seeded in a Matrigel-coated 6-well plate (Eppendorf, cat # 0030720113) to 2.5x106 cells/well in STEMdiff™ SMADi Neural Induction medium (STEMCELL Technologies, cat # 08581) (Chambers et al., 2009) supplemented with ROCK inhibitor. Daily media changes were performed and passaging of the cells was done every 7-9 days. Cells for NPC marker analysis were collected at the end of the first 9 days of differentiation.

For multipotency analysis, culture media was changed to NeuroCult™ media and maintained for 4 weeks. Samples were then fixed and stained for neuron and oligodendrocyte markers. Astrocyte differentiation was performed by seeding on a Matrigel-coated plate 1.5x106 cells/cm2 (TCW et al., 2017). The following day, the media was changed to Astrocyte medium (ScienCell, cat # 1801) and maintained for 20 days. Full media changes were done every 2 days. Samples were then fixed and stained for an astrocyte marker. Images were acquired with a Nikon Instruments Ti2 inverted fluorescence widefield microscope equipped with a Plan Apo Lambda 20X 0.75 NA objective, DS-Qi2 camera (Nikon Instruments), and X-Cite 120LED light source (Excelitas). The differentiation was also assessed by qPCR.

Neural rosette differentiation

To generate neural rosettes, we dissociated the cells into a single-cell suspension and seeded $3.0x10^6$ cells/well of an Aggrewell™ 800 in dual SMAD inhibitor media. EBs were incubated at 37°C with 5% CO2, with minimal disruption during the first 48 hours. Media changes, 50-75% of the total volume, were performed every 2 days. On Day 5, EBs were harvested according to the manufacturer protocol and transferred to a 35mm imaging plate (Cellvis, cat # D35-14-1.5-N)

coated with Matrigel. Daily media changes were performed up to day 9 when cells were fixed with 100% ice-cold Methanol (Fisher Scientific, cat # A454-4). Images were acquired on a Nikon Instruments Ti2 inverted fluorescence microscope, equipped with a Yokogawa X1 spinning disk head, Andor DU-897 EMCCD, Plan Apo Lambda 0.75 NA 20X objective for representative figures, and Plan Fluor 0.45 NA 10X objective for neural rosette quantification, piezo Z-stage, as well as 405-,488-,561-, and 647 -nm lasers. Acquisition and analysis were performed using NIS-Elements. Neural rosette quantification was accomplished by scripting a segmentation-based image analysis routine to detect, enumerate, and measure rosette lumen area based on the ZO-1 signal. Briefly, max intensity projections of each field were generated, followed by GPU-based denoising of the resulting image. Intensity-based thresholding was then applied based on criteria established for ZO-1 signal segmentation using control images. Restrictions on resultant binaries were implemented to throw out binaries intersecting image borders, morphometries deviating severely from rosette associated geometries, as well as for those not meeting minimum size requirements. This routine could be run in batch across many image stacks to increase the sample size and robust nature of the data. Measured data was exported to Excel for further analysis.

Cerebral Organoids

Cerebral organoids were generated as described in (Romero-Morales et al., 2019) with some modifications. Briefly, organoids were generated using the STEMdiff™ Cerebral Organoid Kit (STEMCELL Technologies; Cat# 08571, 08570). iPSCs were dissociated into single cells using Gentle Cell Dissociation Reagent (STEMCELL Technologies, cat # 07174) for 8 minutes at 37°C. Homogeneous and reproducible EBs were generated by using a 24-well plate AggreWell™ 800 (STEMCELL Technologies, cat # 34815). On Day 7, high-quality EBs were embedded in Matrigel (Corning, cat # 354277). On Day 10, the Matrigel coat was broken by vigorously pipetting up and down and the healthy organoids were transferred to a 60mm low attachment culture plate (Eppendorf, cat # 003070119). The plates were then moved to a 37°C incubator and to a Celltron benchtop shaker for CO2 incubators (Infors USA, cat # I69222) set at 85rpm. Full media changes were performed every 3–4 days. Transmitted-light images were acquired using an EVOS® XL Core Imaging System. The software used for processing was ImageJ.

For qPCR, all organoids were pooled together for RNA extraction. Day 40 cerebral organoids were utilized for metabolomics, 4 organoids per genotype were run and analyzed individually.

Organoid tissue preparation and Immunohistochemistry

Tissue preparation was performed as described in (Romero-Morales et al., 2019). Briefly, organoids were fixed in 4% Paraformaldehyde in Phosphate Buffered Saline (PBS), washed 3 times with PBS, and then incubated in 30% sucrose solution overnight at 4°C. Organoids were embedded in 7.5% gelatin/10% sucrose solution (Sigma, catalog G1890-100G and S7903-250G) and sectioned with a cryostat (Leica CM1950) at 15um thickness. For immunostaining, slides were washed with PBS before permeabilization with 0.2% Triton-X in PBS for 1 hr. Tissues were blocked with blocking medium consisting of 10% donkey serum in PBS with 0.1% Tween-20 (PBST) for 30 min. Incubation with primary and secondary antibodies was done using standard methods. Confocal images of the organoids were acquired using the aforementioned spinning disk microscope with Plan Fluor 10X 0.45 NA and Plan Apo Lambda 0.75 NA 20X objectives (macrostructures) and Apo TIRF 1.49 NA 100X objective (mitochondria imaging). NIS-Elements software was used for image acquisition and rendering.

Bioenergetics assay (Seahorse assay)

The Seahorse Cell Mito Stress Test (Agilent, Santa Clara, CA) was conducted to assess mitochondrial function as described previously (Joshi et al., 2020). hiPSCs were replated in E8 media and hNPCs were replated in in STEMdiff™ SMADi Neural Induction medium at $8.0x10^4$ cells/well on Seahorse XF96 cell culture microplates (Agilent) 48h before the assay. A minimum of 6 technical replicates per cell line was used per assay. One day before the assay, Seahorse XFe96 extracellular flux assay cartridge (Agilent) was hydrated with 200 µl/well of water in a non-CO2 incubator overnight.

On the day of the assay, Seahorse XF Calibrant was added to Seahorse XFe96 extracellular flux assay cartridge for one hour before loading the drug treatments. Seahorse medium (Agilent) with

1mM pyruvate, 2 mM glutamine, and 10mM glucose warmed to 37°C was added to the cells 1h before the assay and the plate was incubated in a non-CO2 incubator. Appropriate concentrations of oligomycin (1.5 μM), FCCP (1.5 μM), and Rot/AA (0.5 μM) were added to Seahorse XFe96 extracellular flux assay cartridge and cartridge was loaded into XF Extracellular Flux Analyzer. After calibration step, cell plate was loaded into the XF Extracellular Flux Analyzer to assess mitochondrial function. Resulting data was analyzed using GraphPad PRISM.

Mitochondrial imaging and quantification

Mitochondrial imaging was performed by fixing the NPCs at 90% confluency and staining with anti-mitochondria (Abcam, cat #ab92824, 1:200 dilution). Structured Illumination Microscopy (SIM) was accomplished in 3D-SIM mode on a Nikon Instruments N-SIM, equipped with an Apo TIRF 100x SR 1.49NA objective, DU-897 EMCCD camera (Andor), 405nm and 561nm lasers. Images presented herein are maximum intensity projections after image stacks were first acquired (5 phase shifts and 3 rotations of diffraction grating, 120nm/axial step via piezo) and subsequent stack reconstruction in NIS-Elements software (Nikon Instruments, Inc.). Other than linear intensity scaling, no further image processing was performed post-reconstruction.

For the mitochondrial imaging in brain organoids, confocal images of the organoids were acquired using the aforementioned spinning disk microscope with Apo TIRF 1.49 NA 100X objective. NIS-Elements software was used for image acquisition and rendering.

NIS-Elements General Analysis (GA3) was utilized for the post-processing and quantification. For monolayer NPC differentiation, mitochondrial quantification was performed as described in (Rasmussen et al., 2020). Briefly, quantification was performed by segmenting mitochondria in 3D and performed skeletonization of the resulting 3D mask. For the Organoid mitochondrial quantification an area segmentation was performed to analyze the mitochondrial in the overlapping SOX2+ area. Several parameters such as skeleton major axis and sphericity were exported into Excel. Post processing was performed using GraphPad Prism 9, including ROUT (Robust regression and Outlier removal) method for the day 30 organoids, with a False Discovery Rate of 1%. The workflows used for each condition can be found below:

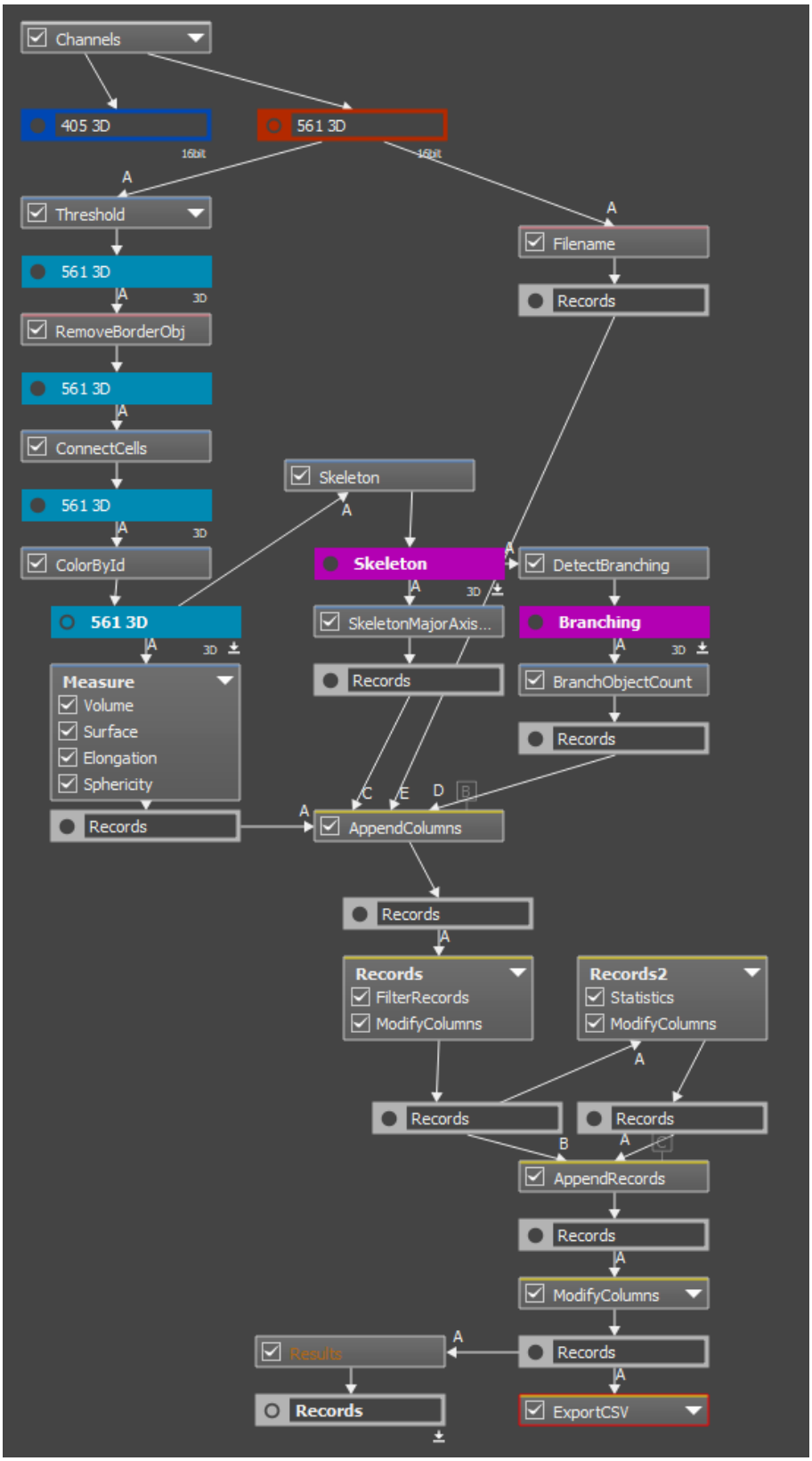

Monolayer NPC mitochondrial quantification workflow.

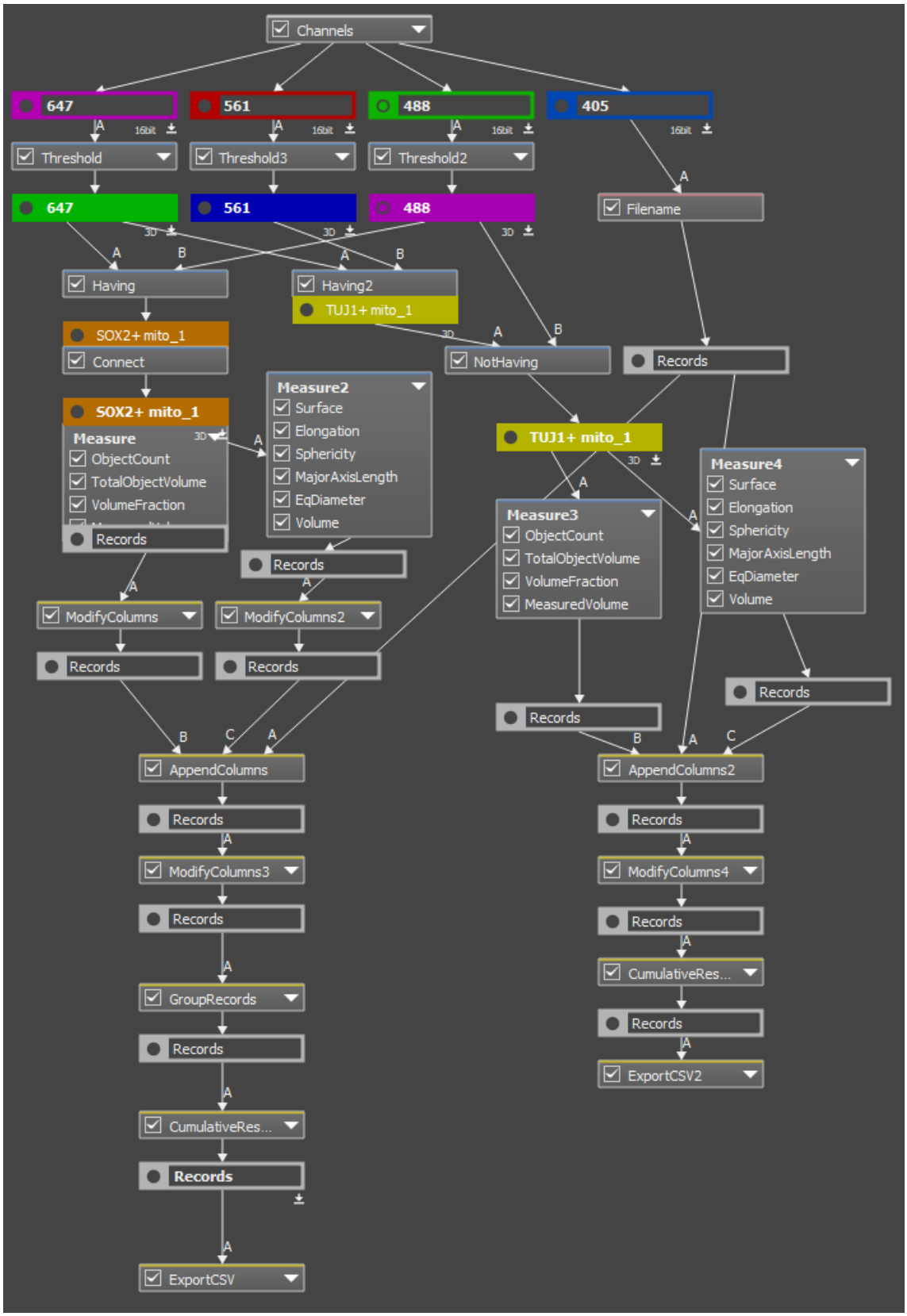

Organoid NPC mitochondrial quantification workflow

RNA Extraction and Synthesis of cDNA

Cells cultured in 6 well plate, were collected after a wash with PBS, using 600µl Trizol reagent. The samples were spun down at 12,000 g after the addition of 130µl of chloroform and incubated at room temperature for 3 minutes. The aqueous phase of the sample was collected 200µl at a time until reaching the edge of phase separation. RNA precipitation was done by incubating with 300µl of isopropanol for 25 minutes, followed by centrifugation at 12,000 g for 10 min at 4°C. The RNA pellet was washed with ethanol, semi-dried, and resuspended in 30µl of DEPC water. After quantification and adjusting the volume of all the samples to 1µg/µl, the samples were treated with DNAse (New England Biolabs, cat # M0303). 10µl of this volume was used to generate cDNA using the manufacturer's protocol (Thermofisher, cat#4368814).

For RNA isolation from brain organoids, the same protocol mentioned above was followed with the volumes adjusted for 1mL of Trizol.

Quantitative RT PCR (RT-qPCR)

1ug of cDNA sample was used to run RT-qPCR for the primers mentioned in the table. QuantStudio 3 Real-Time PCR machine, SYBR green master mix (Thermo Fisher, cat#4364346), and manufacturer instructions were used to set up the assay.

Immunocytochemistry

Cells were fixed with 4% paraformaldehyde (Electron Microscopy Sciences, cat # 15710-S) in PBS for 20 min at 4ºC. Blocking and permeabilization were done in 5% donkey serum (Jackson ImmunoResearch Inc, cat # 017-000-121) + 0.3% Triton X-100 (Sigma Aldrich, cat # T9284) in TBS for 1 hr at room temperature. After this, cells were treated with primary and secondary antibodies using standard methods. Cells were mounted in Vectashield (Vector Laboratories, cat # H-1000) prior to imaging.

Western Blotting

Cultured cells were lysed in 1% Triton buffer containing PMSF (ThermoFisher Scientific, cat # 36978), PhosSTOP (Roche, cat # 4906837001), and protease inhibitor cocktail (Roche, cat # 4693132001). Protein concentrations were determined using the bicinchoninic acid (BCA) method (Thermo Scientific, cat # 23227). Gel samples were prepared by mixing 30µg of protein with LDS sample buffer (Life Technologies, cat # NP0007) and 2-Mercaptoethanol (BioRad, cat # 1610710) and boiled at 95°C for 5 minutes. Samples were run on 4-20% Mini-PROTEAN TGX precast gels (BioRad, cat # 4561096) and transferred onto polyvinylidene difluoride (PVDF) membrane (BioRad, cat # 1620177) overnight at 4°C. Membranes were blocked in 5% milk in TBST prior to primary antibody incubation. Antibodies used for Western blotting are described in the Key Resource table.

Cell titer blue assay

After the 24-h exposure to individual treatments of 50µM etoposide, 80µM CCCP, 100ng/mL nocodazole, and 5ng/mL neocarzinostatin, 20 µl of Cell Titer Blue reagent from Cell Titer Blue assay (Promega, cat # G8081) was added to each well of 96 well plate. Background fluorescence was calculated by adding 10% Triton in PBS to some wells. The fluorescence generated by the reduction of resazurin to resorufin by live cells was measured using a Beckman coulter DTX 880 multimode plate reader (Beckman Coulter, Brea, California) (570/600 nm).

Metabolomics analysis

Day 40 brain organoids, at least 4 individual organoids per genotype, were collected rinsed with ice-cold sterile 0.9% NaCl and flash-freeze in liquid nitrogen. For metabolite extraction, cells were resuspended in 225uL of cold 80% HPLC grade methanol/20% HPLC grade water per $1x10^6$ cells. After resuspension, cells were flash-frozen in liquid nitrogen and thawed rapidly in a 37°C water bath 3 times. Next debris was removed by centrifugation at max speed in a tabletop microcentrifuge at 4°C for 15 min. Metabolite-containing supernatant was transferred to a new tube, dried, and resuspended in 50% acetonitrile while the pellet was used for protein quantification. Samples were analyzed by Ultra-High-Performance Liquid Chromatography and

High-Resolution Mass Spectrometry and Tandem Mass Spectrometry (UHPLC-MS/MS). Specifically, the system consisted of a Thermo Q-Exactive in line with an electrospray source and an Ultimate3000 (Thermo) series HPLC consisting of a binary pump, degasser, and auto-sampler outfitted with an Xbridge Amide column (Waters; dimensions of 4.6mm × 100mm and a 3.5µm particle size). Mobile phase A contained 95% (vol/vol) water, 5% (vol/vol) acetonitrile, 10mM ammonium hydroxide, 10mM ammonium acetate, pH = 9.0; and mobile phase B was 100% Acetonitrile. The gradient was as follows: 0 min, 15% A; 2.5 min, 30% A; 7 min, 43% A; 16 min, 62% A; 16.1-18 min, 75% A; 18-25 min, 15% A with a flow rate of 400µL/min. The capillary of the ESI source was set to 275°C, with sheath gas at 45 arbitrary units, auxiliary gas at 5 arbitrary units, and the spray voltage at 4.0kV. In positive/negative polarity switching mode, an m/z scan range from 70 to 850 was chosen, and MS1 data was collected at a resolution of 70,000. The automatic gain control (AGC) target was set at $1x10^6$ and the maximum injection time was 200 ms. The top 5 precursor ions were subsequently fragmented, in a data-dependent manner, using the higher energy collisional dissociation (HCD) cell set to 30% normalized collision energy in MS2 at a resolution power of 17,500. Data acquisition and analysis were carried out by Xcalibur 4.1 software and Tracefinder 4.1 software, respectively (both from Thermo Fisher Scientific). The peak area for each detected metabolite was normalized by the total ion current which was determined by the integration of all of the recorded peaks within the acquisition window.

Normalized data was uploaded to MetaboAnalyst (https://www.metaboanalyst.ca/home.xhtml) for analysis. Samples were normalized to control, and a one-way ANOVA was performed to compare between the groups. Fisher's least significant difference method (Fisher's LSD) was performed as a post-HOC comparison. Enrichment and pathway analysis was also performed using this platform.

Bioinformatic Analysis

Bioinformatic analysis began with Variant Call Format (VCF) files provided by GENEWIZ (see *Whole Exome sequencing* section above), both for SNP and indels. SnpSift version 4.3t (Cingolani et al., 2012) was used to process and filter these files for downstream analysis. Details extracted

included gene symbol, Entrez gene ID and name, UniProt ID, Ensembl ID, chromosome and position, reference variant, alternative variant, quality of the call, allele name, type of SNP, impact of the SNP, and the genotype of each sample. From these filtered outputs, we generated SNP/indel reports that allowed us to look at sample-specific SNPs and indels, as well as perform aggregate-level functions for grouping and statistical analysis.

To generate the SNP/indel circular chromosome plots, the top 20 genes that had variants in all three samples were plotted, ranked by frequency of variants per gene. The outside track is used to visualize the chromosomes and marked gene locations. For each sample, we used a single track to show the variant frequency as a circular scatter plot, with the height of the scatter points representative of the variant quality metric, which is a Phred-scaled probability that a REF/ALT polymorphism exists at the variant site. Similarly, for SNPs in the mitochondrial chromosome, we used the same approach for visualization.

Quantification and Statistical Analysis

No statistical methods were used to pre-determine sample sizes. All experiments were performed with a minimum of 3 biological replicates unless specified. Statistical significance was determined by unpaired Student's t-test or by one- or two-way ANOVA as appropriate for each experiment. GraphPad Prism v8.1.2 was used for all statistical analysis and data visualization.

Error bars in all bar graphs represent the standard error of the mean or standard deviation as described for each Figure, while scattered dot plots were represented with boxes (with median and SD) and whiskers (minimum and maximum values).

For neural rosette experiments, ROI were randomly selected using the nuclear (DAPI) staining channel. Images were processed with NIS Elements software with our Neural rosette lumen identification Macro. Outliers were removed from the neural rosette area analysis as post-processing quality control for the NIS Element macro using GraphPad Prism v8.1.2. ROUT (Robust regression and Outlier removal) method was used with a False Discovery Rate of 1%.

For cerebral organoid experiments, 4 independent batches were generated. At time points day 30 and day 100, at least 5 organoids per cell line were collected. Immunofluorescence images of at least 3 independent organoids were acquired per condition slide. Image processing was done by NIS Elements and Fiji software.

Organoid efficiency evaluation was performed on day 10 using 4X transmitted-light images acquired using an EVOS® XL microscope. Two observers were blinded to the cell line identifier and counted the number of normal and defective (no epithelial buds or more than 75% of the area is not developed) organoids. Criteria for normal and defective organoids was based on (Lancaster and Knoblich, 2014).

For the organoid quantification, images were processed with NIS Elements using the General Analysis 3 tool. 3D thresholding macros were generated for each set of slides and quantified by either bright spot count (nuclear staining) or mean intensity of the ROI. To avoid false positive counts, only bright spot count where there was overlapping with DAPI was count. GA3 analysis workflow can be found below:

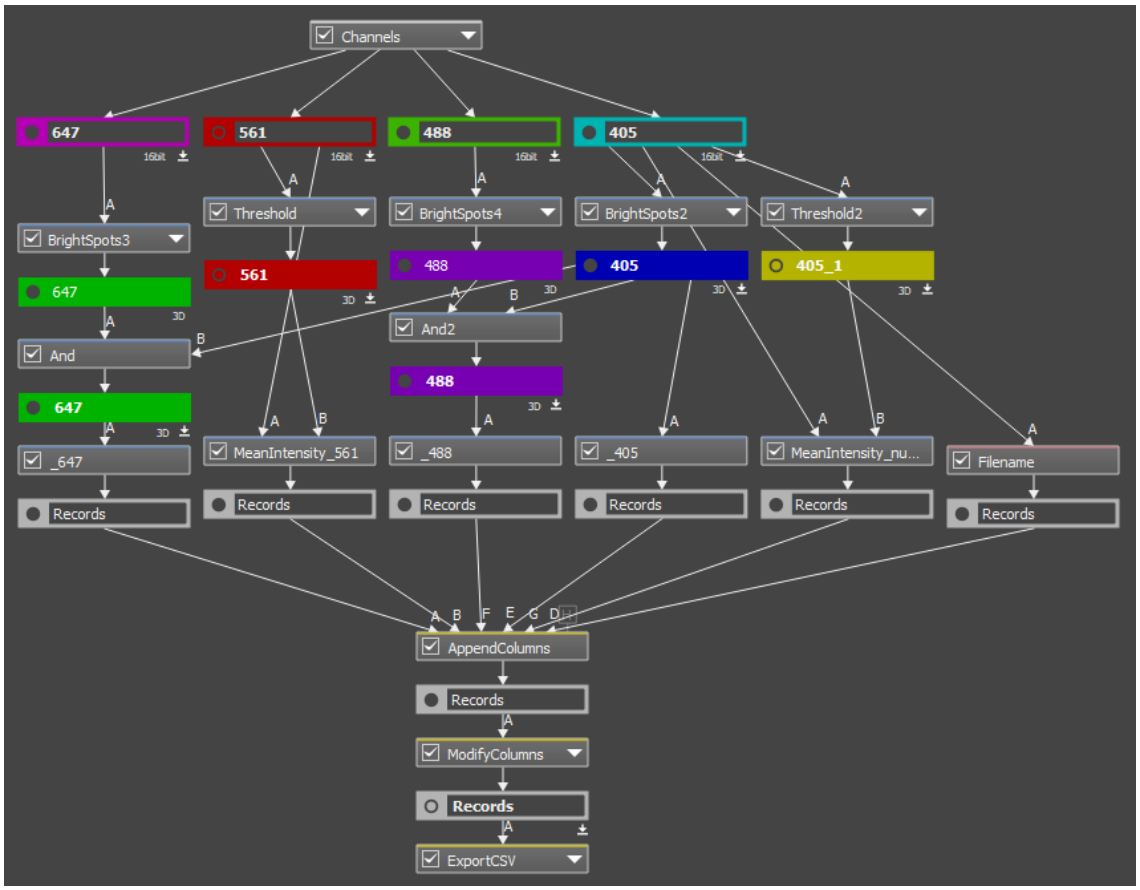

Organoid quantification workflow for GA3, NIS Elements.

Software and Data Availability

All raw data in FastQ format for whole-exome sequencing and mitochondrial sequencing have been deposited to the Short Read Archive as BioProject PRJNA626388, available at https://www.ncbi.nlm.nih.gov/sra/PRJNA626388. All source code and documents are available via https://vandydata.github.io/Romero-Morales-Gama-Leigh-Syndrome-WES/.

TABLES

Table 1. Design files for the Spinꝏ (Chapter 2)

Design file name	File type	Open source license	Location of the file
Base	STL	CC-BY-SA 4.0	https://osf.io/tavck/?view_only=e89148170d1046bebec51977b3177180
12-Well Plate Lid	STL	CC-BY-SA 4.0	https://osf.io/adqye/?view_only=e89148170d1046bebec51977b3177180
CCW Paddle	STL	CC-BY-SA 4.0	https://osf.io/qfxsy/?view_only=e89148170d1046bebec51977b3177180
CW Paddle	STL	CC-BY-SA 4.0	https://osf.io/8pshg/?view_only=e89148170d1046bebec51977b3177180
Gear	STL	CC-BY-SA 4.0	https://osf.io/abgmr/?view_only=e89148170d1046bebec51977b3177180
Motor Shaft Gear	STL	CC-BY-SA 4.0	https://osf.io/9dnbq/?view_only=e89148170d1046bebec51977b3177180
Parylene Template for Gears (*Optional)*	STL	CC-BY-SA 4.0	https://osf.io/wruvb/?view_only=e89148170d1046bebec51977b3177180
Parylene Template for Paddles (*Optional)*	STL	CC-BY-SA 4.0	https://osf.io/u89v3/?view_only=e89148170d1046bebec51977b3177180
X4 L298n Bridge Holder (*Optional)*	STL	CC-BY-SA 4.0	https://osf.io/9nyr2/?view_only=e89148170d1046bebec51977b3177180
5Motors	PY	CC-BY-SA 4.0	https://osf.io/trca4/?view_only=e89148170d1046bebec51977b3177180
Spinfinity Assembly	AVI	CC-BY-SA 4.0	https://osf.io/kb3g9/?view_only=e89148170d1046bebec51977b3177180

Table 2. Hardware components for the Spinoo (Chapter 2)

Quantity	Part Name	Supplier	Part Number	Cost
1	Acrylic Sheet 12” X 12” X ¼”	McMaster-Carr	8560K354	$17.34
4/Bioreactor	18-8 Stainless Steel 45 mm Hex	McMaster-Carr	93655A226	$4.25
4/Bioreactor	18-8 Stainless Steel 35 mm Hex	McMaster-Carr	93655A224	$4.11
8/Bioreactor	18-8 Stainless Steel Washer M3	McMaster-Carr	93475A210	$1.62 (Pack of 100)
8/Bioreactor	18-8 Stainless Steel Hex Nut M3 0.5mm Thread	McMaster-Carr	91828A211	$5.55 (Pack of 100)
14/Bioreactor	18-8 Stainless Steel Philips Flat Head Screw M3	McMaster-Carr	92010A120	$4.65 (Pack of 100)
12/Bioreactor	PTFE Collars	McMaster-Carr	2685t11	$6.16
1/Bioreactor	12-Well Cell Culture Plate	Corning	3737	$431.00 (Case of 100)
1/Bioreactor	Autoclavable Bags	Fisher Scientific	01-812-58	$182.00 (Pack of 100)
1/Bioreactor	Motor 100RPM, 12V, Eccentric Shaft	Amazon	B0721T1PXQ	$15.49
1 Set	Screwdriver Set	McMaster-Carr	52985A22	$30.62
1 Set	Solder	McMaster-Carr	7667A51	$38.77
1 Set	Heat Shrink Tubing	McMaster-Carr	6334K414	$12.71

Table 3. 3D print components for the Spinoo (Chapter 2)

Part Name	Quantity	Supplier
12-Well Plate Lid	1	Xometry (ULTEM 1010)
Base	1	Xometry (ULTEM 1010)
Motor Shaft Gear	1	Stratasys (ULTEM 1010)
Gear	11	Stratasys (ULTEM 1010)
CW Paddle	6	Stratasys (ULTEM 1010)
CCW Paddle	6	Stratasys (ULTEM 1010)
Parylene Template for Gears	1	Stratasys (ABS)
Parylene Template for Paddles	1	Stratasys (ABS)
L298n Bridge Holder	1	Stratasys (ABS)

Table 4. Electronic components for the Spinoo (Chapter 2)

Quantity	Part Name	Supplier	Part Number	Unit Cost
1/Bioreactor	Raspberry Pi 3 A+	Sparkfun	DEV-15139	$29.95
1/Bioreactor	Raspberry Pi 3 A+ Power supply	Sparkfun	TOL-13831	$7.95
1/Raspberry Pi	Raspberry Pi™ - 16GB MicroSD NOOBS Card	Sparkfun	COM-13945	$24.95
1/Raspberry Pi	Raspberry Pi LCD - 7" Touchscreen	Sparkfun	LCD-13733	$64.95
1/Bioreactor	Power Supply 12V, 5A	Amazon	B06Y64QLBM	$8.99
1/8 Bioreactors	4-way DC Jack Splitter	Amazon	B00MHUGL7W	$8.29
1/Bioreactor	5 PCS L298N Motor Drive Controller Board	Amazon	B06X9D1PR9	$15.99 (Pack of 5)
1/Bioreactor	100ft 4 Pin RGB Extension Cable Wire	Amazon	B074H7DM4B	$16.99
1/Motor	2-pin JST SM Male & Female Plug Housing	Amazon	B0188DMF3A	$14.99
1/L298N Bridge	In-line Power Toggle (*Optional)*	Amazon	B0782JXQNP	$5.85
1/LCD Screen	SmartPi Touch Case *(Optional)*	Amazon	B01HV97F64	$27.99
1/LCD Screen	Wireless Bluetooth Keyboard	Amazon	B00BX0YKX4	$24.99

Table 5. Key Resource Table (Chapter 3)

REAGENT or RESOURCE	SOURCE	IDENTIFIER
ANTIBODIES		
Primary Antibodies (Immunocytochemistry)		
Mouse anti-MAP2	Thermo Fisher Scientific	Cat # 131500, AB_2533001
Rabbit anti-GFAP	Agilent Technologies	Cat # Z0334, AB_10013382
Rabbit anti-HOPX	Sigma-Aldrich	Cat # HPA030180, AB_10603770
Mouse anti-mitochondria	Abcam	Cat # ab92824, AB_10562769
Rabbit anti-SOX2	Cell Signaling Technology	Cat # 5049S, AB_10828386
Rabbit anti-PAX6	Cell Signaling Technology	Cat # 60433, AB_2797599
Rabbit anti-SOX17	Cell Signaling Technology	Cat # 81778S, AB_2650582
Rabbit anti-BRACHYURY	Cell Signaling Technology	Cat # 81694S, AB_2799983
Mouse anti-CD184 (CXCR4)	STEMCELL Technologies	Cat # 60089
Mouse anti-β3 TUBULIN	Cell Signaling Technology	Cat # 4466, AB_10270973
Rabbit anti-S100	Abcam	Cat # ab868, AB_306716
Mouse anti-Olig2	Millipore Sigma	Cat # MABN50, AB_10807410
Rat anti-α TUBULIN	Thermo Fisher Scientific	Cat # MA180017, AB_2210201
Mouse anti-ZO-1	Thermo Fisher Scientific	Cat # 339100, AB_2533147
Rabbit anti-CDK5RAP2	Bethyl Laboratories	Cat # IHC00063, AB_2076863
Mouse anti-NESTIN	STEMCELL Technologies	Cat # 60091, AB_2650581
Chicken anti-TBR2	Millipore Sigma	Cat # AB15894, AB_10615604
Mouse anti-REELIN	Millipore Sigma	Cat # MAB5366, AB_2285132
Rat anti-CTIP2	Abcam	Cat # ab18465, AB_2064130

Rabbit anti-TBR1	Abcam	Cat # ab31940, AB_2200219
Rabbit anti-TOM20	Cell Signaling Technology	Cat # 42406, AB_2687663
Mouse anti-SATB2	Abcam	Cat # ab51502, AB_882455
Mouse anti-BRN2 (POU3F2)	Millipore Sigma	Cat # MABD51, AB_11204531
Mouse anti-CASP (CUX1)	Abcam	Cat # ab54583, AB_941209
Rabbit anti-ALDH1L1	Cell Signaling Technology	Cat # 85828S

Secondary Antibodies (Immunocytochemistry)		
Goat anti Chicken Alexa Fluor 647	Thermo Fisher Scientific	Cat # A-21449, AB_2535866
Goat anti Rat Alexa Fluor 647	Thermo Fisher Scientific	Cat # A-21247, AB_2535864
Donkey anti Rabbit Alexa Fluor 647	Thermo Fisher Scientific	Cat # A-31573, AB_2536183
Donkey anti Mouse Alexa Fluor 647	Thermo Fisher Scientific	Cat # A-31571, AB_162542
Donkey anti Rabbit Alexa Fluor 546	Thermo Fisher Scientific	Cat # A-10040, AB_2534016
Donkey anti Mouse Alexa Fluor 546	Thermo Fisher Scientific	Cat # A-10036, AB_2534012
Donkey anti Rabbit Alexa Fluor 488	Thermo Fisher Scientific	Cat # A-21206, AB_2535792
Donkey anti Mouse Alexa Fluor 488	Thermo Fisher Scientific	Cat # A-21202, AB_141607
Primary Antibodies (Western Blotting)		
Rabbit anti-PAX6	Cell Signaling Technology	Cat # 60433, AB_2797599
Mouse anti-NESTIN	STEMCELL Technologies	Cat # 60091, AB_2650581
Rabbit anti-Sox2	Cell Signaling Technology	Cat # 3579, AB_2195767

Mouse anti- α TUBULIN	Sigma-Aldrich	Cat # T9026, AB_477593
Secondary Antibodies -HRP conjugated (Western Blotting)		
Peroxidase AffiniPure Donkey Anti-Rabbit IgG (H+L)	Jackson ImmunoResearch Inc	Cat # 711-035-152, AB_10015282
Peroxidase AffiniPure Donkey Anti-Mouse IgG (H+L)	Jackson ImmunoResearch Inc	Cat # 715-035-151, AB_2340771
Chemicals, Peptide, and Recombinant Proteins		
Y-27632 Rho/Rock pathway inhibitor	STEMCELL Technologies	Cat # 72307
Dorsomorphin	Millipore Sigma	Cat # P5499
SB431542	REPROCELL	Cat # 04-0010-10
Etoposide	Millipore Sigma	Cat # E1383
Carbonyl cyanide 3-chlorophenylhydrazone (CCCP)	Sigma Aldrich	Cat # C2759
Nocodazole	Sigma Aldrich	Cat # M1404
Neocarzinostatin	Sigma Aldrich	Cat # 9162

Critical Commercial Assays and Kits		
PluriTest Assay	Thermo Fisher Scientific	Cat# A38154
KaryoStat Assay	Thermo Fisher Scientific	Cat# A38153
Mitochondrial DNA sequencing	Girihlet	
Whole Exome sequencing	Genewiz LLC	
CytoTune iPS 2.0 Sendai Reprogramming Kit	Thermo Fisher Scientific	Cat # A16517
STEMdiff Trilineage Differentiation Kit	STEMCELL Technologies	Cat# 05230

STEMdiff™ SMADi Neural Induction medium	STEMCELL Technologies	Cat# 08581
NeuroCult™ media	STEMCELL Technologies	Cat # 05752
Astrocyte medium	ScienCell	Cat # 1801
STEMdiff™ Cerebral Organoid Kit	STEMCELL Technologies	Cat # 08570
STEMdiff™ Cerebral Organoid Maturation Kit	STEMCELL Technologies	Cat # 08571
Seahorse Cell Mito Stress Test	Agilent	Cat # 103015-100
Seahorse XF DMEM medium pH 7.4	Agilent	Cat#103575-100
Seahorse XF 1.0 M glucose solution	Agilent	Cat#103577-100
Seahorse XF 100mM pyruvate solution	Agilent	Cat#103578-100
Seahorse XF 200 mM glutamine solution	Agilent	Cat#103579-100
Seahorse XF calibrant	Agilent	Cat#100840-000
Seahorse XF96 V3 PS cell culture microplates	Agilent	Cat#101085-004
CellTiter Blue Viability Assay	Promega	Cat # G8081
Deposited Data		
Raw and analyzed sequencing data	Done by Creative Solutions (J.P.C, Vanderbilt University	https://www.ncbi.nlm.nih.gov/sra/PRJNA626388 https://vandydata.github.io/Romero-Morales-Gama-Leigh-Syndrome-WES/

Experimental Models: Cell Lines		
AG16409 control fibroblasts – analyzed for contamination	Coriell Institute	https://www.coriell.org/0/Sections/Search/Sample_Detail.aspx?Ref=AG16409&Product=CC

GM13411 (MT-ATP6/PDH) fibroblasts – analyzed for contamination	Coriell Institute	https://www.coriell.org/0/Sections/Search/Sample_Detail.aspx?Ref=GM13411&Product=CC
GM03672 (PDH Mutant) fibroblasts – analyzed for contamination	Coriell Institute	https://www.coriell.org/0/Sections/Search/Sample_Detail.aspx?Ref=GM03672&Product=CC
GM01503 (DLD Mutant) fibroblasts – analyzed for contamination	Coriell Institute	https://www.coriell.org/0/Sections/Search/Sample_Detail.aspx?Ref=GM01503&Product=CC
Sequence-Based Reagents		
Primers for Trilineage assay		
POU5F1	Integrated DNA Technologies	Forward GGGCTCTCCCATGCATTCAAAC Reverse CACCTTCCCTCCAACCAGTTGC
Nanog	Integrated DNA Technologies	Forward TGGGATTTACAGGCGTGAGCCAC Reverse AAGCAAAGCCTCCCAATCCCAAAC
GAPDH	Integrated DNA Technologies	Harvard Primer Bank, ID: 378404907c2 Forward ACAACTTTGGTATCGTGGAAGG Reverse GCCATCACGCCACAGTTTC
GPI	Integrated DNA Technologies	Forward GTGTACCTTCTAGTCCCGCC Reverse GGTCAAGCTGAAGTGGTTGAAGC
Gata3	Integrated DNA Technologies	Forward TGGAGGAGGAATGCCAATGGG Reverse GCCGGGTTAAACGAGCTGTTCTTG
Nestin	Integrated DNA Technologies	Harvard Primer Bank, ID: 38176299c1 Forward CTGCTACCCTTGAGACACCTG Reverse GGGCTCTGATCTCTGCATCTAC
Pax6	Integrated DNA Technologies	Harvard Primer Bank, ID: 189083679c1 Forward TGGGCAGGTATTACGAGACTG Reverse ACTCCCGCTTATACTGGGCTA
CDX2	Integrated DNA Technologies	Forward CTGGAGCTGGAGAAGGAGTTTCAC Reverse GACACTTCTCAGAGGACCTGGCTG
SOX17	Integrated DNA Technologies	Harvard Primer Bank, ID:145275218c1 Forward GTGGACCGCACGGAATTTG Reverse GGAGATTCACACCGGAGTCA

TBXT	Integrated DNA Technologies	Forward ACAATGCCAGCCCACCTACCAG Reverse CGTACTGGCTGTCCACGATGTCTG
NCAM	Integrated DNA Technologies	Harvard Primer Bank, ID:316659209c1 Forward GGGGTTGCTTGTCAGTAGC Reverse TTCAGGTTCACCAATCGCTGT
Primers for Multipotency		
S100B	Integrated DNA Technologies	Harvard Primer Bank, ID: 114520588c1 Forward TGGCCCTCATCGACGTTTTC Reverse ATGTTCAAAGAACTCGTGGCA
GFAP	Integrated DNA Technologies	Reference: (Marton et al., 2019) Forward GGCAAAAGCACCAAAGACGG Reverse GGCGGCGTTCCATTTACAAT
O4 (FOXO4)	Integrated DNA Technologies	Harvard Primer Bank, ID: 283436081c1 Forward GGCTGCCGCGATCATAGAC Reverse GGCTGGTTAGCGATCTCTGG
OLIG2	Integrated DNA Technologies	Reference: (Marton et al., 2019) Forward AAGGCAGTTGCTGTGGAAAC Reverse GCAAACAGCTTAGCATTGCG
TUBB3	Integrated DNA Technologies	Harvard Primer Bank, ID: 308235961c1 Forward GGCCAAGGGTCACTACACG Reverse GCAGTCGCAGTTTTCACACTC
MAP2	Integrated DNA Technologies	Harvard Primer Bank, ID: 87578393c1 Forward CTCAGCACCGCTAACAGAGG Reverse CATTGGCGCTTCGGACAAG
Primers for Brain Organoids		
Reelin	Integrated DNA Technologies	Harvard Primer Bank, ID: 223718142c2 Forward ACATCTACAAGTGTTCAGGCATC Reverse TGGTTACCAAACTGGTGGTCA
HOPX	Integrated DNA Technologies	Harvard Primer Bank, ID: 21311737a1 Forward GAGACCCAGGGTAGTGATTTGA Reverse AAAAGTAATCGAAAGCCAAGCAC
CTIP2 (BCL11B)	Integrated DNA Technologies	Harvard Primer Bank, ID: 12597634c2 Forward TCCAGCTACATTTGCACAACA Reverse GCTCCAGGTAGATGCGGAAG

TBR2 (EOMES)	Integrated DNA Technologies	Harvard Primer Bank, ID: 22538469c2 Forward GTGCCCACGTCTACCTGTG Reverse CCTGCCCTGTTTCGTAATGAT
TBR1	Integrated DNA Technologies	Harvard Primer Bank, ID: 22547231c1 Forward GCAGCAGCTACCCACATTCA Reverse AGGTTGTCAGTGGTCGAGATA
SOX2	Integrated DNA Technologies	Forward CCATGCAGGTTGACACCGTTG Reverse TCGGCAGACTGATTCAAATAATACAG
SATB2	Integrated DNA Technologies	Harvard Primer Bank, ID: 289547595c2 Forward GACAGTGGCCGACATGCTAC Reverse AGGCAAGTCTTCCAACTTTGAA
BRN2 (POU3F2)	Integrated DNA Technologies	Harvard Primer Bank, ID: 380254475c1 Forward CGGCGGATCAAACTGGGATTT Reverse TTGCGCTGCGATCTTGTCTAT
CUX1	Integrated DNA Technologies	Harvard Primer Bank, ID: 321400113c1 Forward GAAGAACCAAGCCGAAACCAT Reverse AGGCTCTGAACCTTATGCTCA
Vimentin	Integrated DNA Technologies	Harvard Primer Bank, ID: 240849334c2 Forward AGTCCACTGAGTACCGGAGAC Reverse CATTTCACGCATCTGGCGTTC
SOX9	Integrated DNA Technologies	Harvard Primer Bank, ID: 182765453c1 Forward AGCGAACGCACATCAAGAC Reverse CTGTAGGCGATCTGTTGGGG
ALDH1L1	Integrated DNA Technologies	Harvard Primer Bank, ID: 21614512c3 Forward TCCAGACCTTCCGCTACTTTG Reverse CAGGGGATAGTTCCAGGGGAT

Housekeeping primers		
GAPDH	Integrated DNA Technologies	Harvard Primer Bank, ID: 378404907c2 Forward ACAACTTTGGTATCGTGGAAGG Reverse GCCATCACGCCACAGTTTC
GPI (F1/R1)	Integrated DNA Technologies	Forward GTGTACCTTCTAGTCCCGCC Reverse GGTCAAGCTGAAGTGGTTGAAGC
Software and Algorithms		

Image Studio™ Lite	LI-COR	https://www.licor.com/bio/image-studio-lite/download
Fiji	Schindelin et al., 2012	https://imagej.net/Fiji
GraphPad Prism v8.1.2	GraphPad	https://www.graphpad.com/scientific-software/prism/
NIS-Elements	Nikon Instruments	https://www.microscope.healthcare.nikon.com/products/software/nis-elements
MetaboAnalyst 5.0	(Chong and Xia, 2018; Chong et al., 2018, 2019; Xia and Wishart, 2010, 2011a, 2011b; Xia et al., 2009)	https://www.metaboanalyst.ca/home.xhtml
SnpSift	(Cingolani et al., 2012)	http://snpeff.sourceforge.net/SnpSift.html
R 3.5.3	R Foundation	https://www.r-project.org/
BioCircos	(Cui et al., 2016)	https://cran.r-project.org/web/packages/BioCircos/index.html
Seahorse Wave	Agilent	https://www.agilent.com/en/product/cell-analysis/real-time-cell-metabolic-analysis/xf-software/seahorse-wave-desktop-software-740897
Other		
Mitotracker Red CMXRos	Fisher Scientific	Cat # M7512
Matrigel™	Corning	Cat # 354277
Gentle dissociation solution	STEMCELL Technologies	Cat # 07174
Seahorse XFe96 Analyzer	Agilent	N/A
Aggrewell™ 800 24-well plate	STEMCELL Technologies	Cat # 34815
AggreWell™ Rinsing Solution	STEMCELL Technologies	Cat # 07010

References

Aaku-Saraste, E., Hellwig, A., and Huttner, W.B. (1996). Loss of occludin and functional tight junctions, but not ZO-1, during neural tube closure - Remodeling of the neuroepithelium prior to neurogenesis. Dev. Biol. *180*, 664–679.

Aaku-Saraste, E., Oback, B., Hellwig, A., and Huttner, W.B. (1997). Neuroepithelial cells downregulate their plasma membrane polarity prior to neural tube closure and neurogenesis. Mech. Dev. *69*, 71–81.

Acín-Pérez, R., Fernández-Silva, P., Peleato, M.L., Pérez-Martos, A., and Enriquez, J.A. (2008). Respiratory Active Mitochondrial Supercomplexes. Mol. Cell *32*, 529–539.

Agana, M., Frueh, J., Kamboj, M., Patel, D.R., and Kanungo, S. (2018). Common metabolic disorder (inborn errors of metabolism) concerns in primary care practice. Ann. Transl. Med. *6*, 469–469.

Agathocleous, M., Love, N.K., Randlett, O., Harris, J.J., Liu, J., Murray, A.J., and Harris, W.A. (2012). Metabolic differentiation in the embryonic retina. Nat. Cell Biol. *14*, 859–864.

Agius, E., Soukkarieh, C., Danesin, C., Kan, P., Takebayashi, H., Soula, C., and Cochard, P. (2004). Converse control of oligodendrocyte and astrocyte lineage development by Sonic hedgehog in the chick spinal cord. Dev. Biol. *270*, 308–321.

Akhtar, R.S., Ness, J.M., and Roth, K.A. (2004). Bcl-2 family regulation of neuronal development and neurodegeneration. Biochim. Biophys. Acta - Mol. Cell Res. *1644*, 189–203.

Albrecht, J., and Schousboe, A. (2005). Taurine Interaction with Neurotransmitter Receptors in the CNS: An Update. Neurochem. Res. *30*, 1615–1621.

Albright, C.D., Friedrich, C.B., Brown, E.C., Mar, M.H., and Zeisel, S.H. (1999a). Maternal dietary choline availability alters mitosis, apoptosis and the localization of TOAD-64 protein in the developing fetal rat septum. Dev. Brain Res. *115*, 123–129.

Albright, C.D., Tsai, A.Y., Friedrich, C.B., Mar, M.-H., and Zeisel, S.H. (1999b). Choline availability alters embryonic development of the hippocampus and septum in the rat. Dev. Brain Res. *113*, 13–20.

Alcamo, E.A., Chirivella, L., Dautzenberg, M., Dobreva, G., Fariñas, I., Grosschedl, R., and McConnell, S.K. (2008). Satb2 Regulates Callosal Projection Neuron Identity in the Developing Cerebral Cortex. Neuron *57*, 364–377.

Alvarez-Buylla, A., García-Verdugo, J.M., and Tramontin, A.D. (2001). A unified hypothesis on the lineage of neural stem cells. Nat. Rev. Neurosci. *2*, 287–293.

Alves, C.A.P.F., Teixeira, S.R., Martin-Saavedra, J.S., Guimarães Gonçalves, F., Lo Russo, F., Muraresku, C., McCormick, E.M., Falk, M.J., Zolkipli-Cunningham, Z., Ganetzky, R., et al. (2020). Pediatric Leigh Syndrome: Neuroimaging Features and Genetic Correlations. Ann. Neurol. *88*, 218–232.

Ambasudhan, R., Talantova, M., Coleman, R., Yuan, X., Zhu, S., Lipton, S.A., and Ding, S. (2011). Direct reprogramming of adult human fibroblasts to functional neurons under defined conditions. Cell Stem Cell *9*, 113–118.

Anlar, B., Atilla, P., Cakar, N., Tombakoglu, M., and Bulun, A. (2003). Apoptosis in the developing human brain: A preliminary study of the frontal region. Early Hum. Dev. *71*, 53–60.

Anthony, T.E., Klein, C., Fishell, G., and Heintz, N. (2004). Radial glia serve as neuronal progenitors in all regions of the central nervous system. Neuron *41*, 881–890.

Anzil, A.P., Weindl, A., and Struppler, A. (1981). Ultrastructure of a cerebral white matter lesion in a 41-year-old man with Leigh's encephalomyelopathy (LEM). Acta Neuropathol. Suppl. *7*, 233–238.

Arbour, N., Vanderluit, J.L., Le Grand, J.N., Jahani-Asl, A., Ruzhynsky, V.A., Cheung, E.C.C., Kelly, M.A., MacKenzie, A.E., Park, D.S., Opferman, J.T., et al. (2008). Mcl-1 Is a Key Regulator of Apoptosis during CNS Development and after DNA Damage. J. Neurosci. *28*, 6068–6078.

Arlotta, P., and Paşca, S.P. (2019). Cell diversity in the human cerebral cortex: from the embryo to brain organoids. Curr. Opin. Neurobiol. *56*, 194–198.

Arlotta, P., Molyneaux, B.J., Chen, J., Inoue, J., Kominami, R., and MacKlis, J.D. (2005). Neuronal subtype-specific genes that control corticospinal motor neuron development in vivo. Neuron *45*, 207–221.

Arnò, B., Grassivaro, F., Rossi, C., Bergamaschi, A., Castiglioni, V., Furlan, R., Greter, M., Favaro, R., Comi, G., Becher, B., et al. (2014). Neural progenitor cells orchestrate microglia migration and positioning into the developing cortex. Nat. Commun. *5*, 1–13.

Arnold, S.J., Huang, G.-J., Cheung, A.F.P., Era, T., Nishikawa, S.-I., Bikoff, E.K., Molnár, Z., Robertson, E.J., and Groszer, M. (2008). The T-box transcription factor Eomes/Tbr2 regulates neurogenesis in the cortical subventricular zone. Genes Dev. *22*, 2479–2484.

Arnoult, D., Grodet, A., Lee, Y.J., Estaquier, J., and Blackstone, C. (2005). Release of OPA1 during apoptosis participates in the rapid and complete release of cytochrome c and subsequent mitochondrial fragmentation. J. Biol. Chem. *280*, 35742–35750.

Azizi, A., Herrmann, A., Wan, Y., Buse, S.J.R.P., Keller, P.J., Goldstein, R.E., and Harris, W.A. (2020). Nuclear crowding and nonlinear diffusion during interkinetic nuclear migration in the zebrafish retina. Elife *9*, 1–31.

Baala, L., Briault, S., Etchevers, H.C., Laumonnier, F., Natiq, A., Amiel, J., Boddaert, N., Picard, C., Sbiti, A., Asermouh, A., et al. (2007). Homozygous silencing of T-box transcription factor EOMES leads to microcephaly with polymicrogyria and corpus callosum agenesis. Nat. Genet. *39*, 454–456.

Baburamani, A.A., Hurling, C., Stolp, H., Sobotka, K., Gressens, P., Hagberg, H., and Thornton, C. (2015). Mitochondrial Optic Atrophy (OPA) 1 processing is altered in response to neonatal hypoxic-ischemic brain injury. Int. J. Mol. Sci. *16*, 22509–22526.

Baertling, F., Rodenburg, R.J., Schaper, J., Smeitink, J.A., Koopman, W.J.H., Mayatepek, E., Morava, E., and Distelmaier, F. (2014). A guide to diagnosis and treatment of Leigh syndrome. J. Neurol. Neurosurg. Psychiatry *85*, 257–265.

Baertling, F., Klee, D., Haack, T.B., Prokisch, H., Meitinger, T., Mayatepek, E., Schaper, J., and Distelmaier, F. (2016). The many faces of paediatric mitochondrial disease on neuroimaging. Child's Nerv. Syst. *32*, 2077–2083.

Bagley, J.A., Reumann, D., Bian, S., Lévi-Strauss, J., and Knoblich, J.A. (2017). Fused cerebral organoids model interactions between brain regions. Nat. Methods *14*, 743–751.

Bain, G., Kitchens, D., Yao, M., Huettner, J.E., and Gottlieb, D.I. (1995). Embryonic stem cells express neuronal properties in vitro. Dev. Biol. *168*, 342–357.

Bang, A.G., Papalopulu, N., Kintner, C., and Goulding, M.D. (1997). Expression of Pax-3 is initiated in the early neural plate by posteriorizing signals produced by the organizer and by posterior non-axial mesoderm. Development *124*, 2075–2085.

Baranov, S. V., Baranova, O. V., Yablonska, S., Suofu, Y., Vazquez, A.L., Kozai, T.D.Y., Tracy Cui, X., Ferrando, L.M., Larkin, T.M., Tyurina, Y.Y., et al. (2019). Mitochondria modulate programmed neuritic retraction. Proc. Natl. Acad. Sci. U. S. A. *116*, 650–659.

Barshop, B.A. (2004). Metabolomic approaches to mitochondrial disease: Correlation of urine organic acids. Mitochondrion *4*, 521–527.

Barth, K.A., Kishimoto, Y., Rohr, K.B., Seydler, C., Schulte-Merker, S., and Wilson, S.W. (1999). Bmp activity establishes a gradient of positional information throughout the entire neural plate. Development *126*, 4977–4987.

Battiste, J., Helms, A.W., Kim, E.J., Savage, T.K., Lagace, D.C., Mandyam, C.D., Eisch, A.J., Miyoshi, G., and Johnson, J.E. (2007). Ascl 1 defines sequentially generated lineage-resricted neuronal and oligodendrocyte precursor cells in the spinal cord. Development *134*, 285–293.

Bayer, S.A., and Altman, J. (2007). The Human Brain During the Early First Trimester (CRC Press).

Bedogni, F., Hodge, R.D., Elsen, G.E., Nelson, B.R., Daza, R.A.M., Beyer, R.P., Bammler, T.K., Rubenstein, J.L.R., and Hevner, R.F. (2010). Tbr1 regulates regional and laminar identity of postmitotic neurons in developing neocortex. Proc. Natl. Acad. Sci. U. S. A. *107*, 13129–13134.

Behar, S., Brunner, D., Kaplinsky, E., Mandelzweig, L., and Benderly, M. (2000). Secondary prevention by raising HDL cholesterol and reducing triglycerides in patients with coronary artery disease: The bezafibrate infarction prevention (BIP) study. Circulation *102*, 21–27.

Bélanger, M., Allaman, I., and Magistretti, P.J. (2011). Brain Energy Metabolism: Focus on Astrocyte-Neuron Metabolic Cooperation. Cell Metab. *14*, 724–738.

Ben-Reuven, L., and Reiner, O. (2020). Toward spatial identities in human brain organoids-on-chip induced by morphogen-soaked beads. Bioengineering *7*, 1–17.

Del Bene, F., Wehman, A.M., Link, B.A., and Baier, H. (2008). Regulation of Neurogenesis by Interkinetic Nuclear Migration through an Apical-Basal Notch Gradient. Cell *134*, 1055–1065.

Bentivoglio, M., and Mazzarello, P. (1999). The history of radial glia. Brain Res. Bull. *49*, 305–315.

Berg, S., Kutra, D., Kroeger, T., Straehle, C.N., Kausler, B.X., Haubold, C., Schiegg, M., Ales, J., Beier, T., Rudy, M., et al. (2019). ilastik: interactive machine learning for (bio)image analysis. Nat. Methods *16*, 1226–1232.

Bertrand, N., Medevielle, F., and Pituello, F. (2000). FGF signalling controls the timing of Pax6 activation in the neural tube. Development *127*, 4837–4843.

Bhaduri, A., Andrews, M.G., Mancia Leon, W., Jung, D.D., Shin, D., Allen, D., Jung, D.D., Schmunk, G., Haeussler, M., Salma, J., et al. (2020). Cell stress in cortical organoids impairs molecular subtype specification. Nature *578*, 142–148.

Birey, F., Andersen, J., Makinson, C.D., Islam, S., Wei, W., Huber, N., Fan, H.C., Metzler, K.R.C.C., Panagiotakos, G., Thom, N., et al. (2017). Assembly of functionally integrated human forebrain spheroids. Nature *545*, 54–59.

Boisvert, E.M., Means, R.E., Michaud, M., Madri, J.A., and Katz, S.G. (2019). Minocycline mitigates the effect of neonatal hypoxic insult on human brain organoids. Cell Death Dis. *10*, 325.

Bredenoord, A.L., Clevers, H., and Knoblich, J.A. (2017). Human tissues in a dish: The research and ethical implications of organoid technology. Science (80-.). *355*.

Brekke, E., Berger, H.R., Widerøe, M., Sonnewald, U., and Morken, T.S. (2017). Glucose and Intermediary Metabolism and Astrocyte–Neuron Interactions Following Neonatal Hypoxia–Ischemia in Rat. Neurochem. Res. *42*, 115–132.

Brennand, K., Savas, J.N., Kim, Y., Tran, N., Simone, A., Hashimoto-Torii, K., Beaumont, K.G., Kim, H.J., Topol, A., Ladran, I., et al. (2015). Phenotypic differences in hiPSC NPCs derived from patients with schizophrenia. Mol. Psychiatry *20*, 361–368.

Bridi, R., Latini, A., Braum, C.A., Zorzi, G.K., Wajner, M., Lissi, E., and Dutra-Filho, C.S. (2005). Evaluation of the mechanisms involved in leucine-induced oxidative damage in cerebral cortex of young rats. Free Radic. Res. *39*, 71–79.

Britanova, O., de Juan Romero, C., Cheung, A., Kwan, K.Y., Schwark, M., Gyorgy, A., Vogel, T., Akopov, S., Mitkovski, M., Agoston, D., et al. (2008). Satb2 Is a Postmitotic Determinant for Upper-Layer Neuron Specification in the Neocortex. Neuron *57*, 378–392.

Brockman, A.A., Mobley, B.C., and Ihrie, R.A. (2021). Histological Studies of the Ventricular–Subventricular Zone as Neural Stem Cell and Glioma Stem Cell Niche. J. Histochem. Cytochem. 002215542110320.

Brüstle, O., Spiro, A.C., Karram, K., Choudhary, K., Okabe, S., and Mckay, R.D.G. (1997). In vitro-generated neural precursors participate in mammalian brain development. Proc. Natl. Acad. Sci. U. S. A. *94*, 14809–14814.

Bubici, C., and Papa, S. (2019). Editorial: The Warburg Effect Regulation Under Siege: the Intertwined Pathways in Health and Disease. Front. Cell Dev. Biol. *7*, 80.

Bultje, R.S., Castaneda-Castellanos, D.R., Jan, L.Y., Jan, Y.N., Kriegstein, A.R., and Shi, S.H. (2009). Mammalian Par3 Regulates Progenitor Cell Asymmetric Division via Notch Signaling in the Developing Neocortex. Neuron *63*, 189–202.

Buniello, A., MacArthur, J.A.L., Cerezo, M., Harris, L.W., Hayhurst, J., Malangone, C., McMahon, A., Morales, J., Mountjoy, E., Sollis, E., et al. (2019). The NHGRI-EBI GWAS Catalog of published genome-wide association studies, targeted arrays and summary statistics 2019. Nucleic Acids Res. *47*, D1005–D1012.

Buzkova, J., Nikkanen, J., Ahola, S., Hakonen, A.H., Sevastianova, K., Hovinen, T., Yki-Järvinen, H., Pietiläinen, K.H., Lönnqvist, T., Velagapudi, V., et al. (2018). Metabolomes of mitochondrial diseases and inclusion body myositis patients: treatment targets and biomarkers. EMBO Mol. Med. *10*.

Bystron, I., Blakemore, C., and Rakic, P. (2008). Development of the human cerebral cortex: Boulder Committee revisited. Nat. Rev. Neurosci. *9*, 110–122.

Caiazzo, M., Dell'Anno, M.T., Dvoretskova, E., Lazarevic, D., Taverna, S., Leo, D., Sotnikova, T.D., Menegon, A., Roncaglia, P., Colciago, G., et al. (2011). Direct generation of functional dopaminergic neurons from mouse and human fibroblasts. Nature *476*, 224–227.

Calegari, F., Haubensak, W., Haffher, C., and Huttner, W.B. (2005). Selective lengthening of the cell cycle in the neurogenic subpopulation of neural progenitor cells during mouse brain development. J. Neurosci. *25*, 6533–6538.

Callaerts, P., Halder, G., and Gehring, W.J. (1997). PAX-6 in development and evolution. Annu. Rev. Neurosci. *20*, 483–532.

Cameron, R.S., and Rakic, P. (1991). Glial cell lineage in the cerebral cortex: A review and synthesis. Glia *4*, 124–137.

Camp, J.G., Badsha, F., Florio, M., Kanton, S., Gerber, T., Wilsch-Bräuninger, M., Lewitus, E., Sykes, A., Hevers, W., Lancaster, M., et al. (2015). Human cerebral organoids recapitulate gene expression programs of fetal neocortex development. Proc. Natl. Acad. Sci. *112*, 201520760.

Campbell, K., and Götz, M. (2002). Radial glia: Multi-purpose cells for vertebrate brain development. Trends Neurosci. *25*, 235–238.

Cansev, M. (2006). Uridine and cytidine in the brain: Their transport and utilization. Brain Res. Rev. *52*, 389–397.

Cartier, L., Laforge, T., Feki, A., Arnaudeau, S., Dubois-Dauphin, M., and Krause, K.H. (2006). Pax6-induced alteration of cell fate: Shape changes, expression of neuronal α tubulin, postmitotic phenotype, and cell migration. J. Neurobiol. *66*, 421–436.

Casano, A.M., Albert, M., and Peri, F. (2016). Developmental Apoptosis Mediates Entry and Positioning of Microglia in the Zebrafish Brain. Cell Rep. *16*, 897–906.

Cavanagh, J.B. (1994). Is Purkinje cell loss in Leigh's disease an excitotoxic event secondary to damage to inferior olivary nuclei? Neuropathol. Appl. Neurobiol. *20*, 599–603.

Cederquist, G.Y., Asciolla, J.J., Tchieu, J., Walsh, R.M., Cornacchia, D., Resh, M.D., and Studer, L. (2019). Specification of positional identity in forebrain organoids. Nat. Biotechnol. *37*, 436–444.

Cella Zanacchi, F., Lavagnino, Z., Perrone Donnorso, M., Del Bue, A., Furia, L., Faretta, M., and Diaspro, A. (2011). Live-cell 3D super-resolution imaging in thick biological samples. Nat. Methods *8*, 1047–1050.

Cerutti, R., Pirinen, E., Lamperti, C., Marchet, S., Sauve, A.A., Li, W., Leoni, V., Schon, E.A., Dantzer, F., Auwerx, J., et al. (2014). NAD+-dependent activation of Sirt1 corrects the phenotype in a mouse model of mitochondrial disease. Cell Metab. *19*, 1042–1049.

Chakrabarty, R.P., and Chandel, N.S. (2021). Mitochondria as Signaling Organelles Control Mammalian Stem Cell Fate. Cell Stem Cell *28*, 394–408.

Chambers, S.M., Fasano, C.A., Papapetrou, E.P., Tomishima, M., Sadelain, M., and Studer, L. (2009). Highly efficient neural conversion of human ES and iPS cells by dual inhibition of SMAD signaling. Nat. Biotechnol. *27*, 275–280.

Chan, D.C. (2012). Fusion and Fission: Interlinked Processes Critical for Mitochondrial Health. Annu. Rev. Genet. *46*, 265–287.

Chanas-Sacre, G., Rogister, B., Moonen, G., and Leprince, P. (2000). Radial glia phenotype: Origin, regulation, and transdifferentiation. J. Neurosci. Res. *61*, 357–363.

Chandel, N.S., Jasper, H., Ho, T.T., and Passegué, E. (2016). Metabolic regulation of stem cell function in tissue homeostasis and organismal ageing. Nat. Cell Biol. *18*, 823–832.

Chandrasekaran, A., Avci, H.X., Ochalek, A., Rösingh, L.N., Molnár, K., László, L., Bellák, T., Téglási, A., Pesti, K., Mike, A., et al. (2017). Comparison of 2D and 3D neural induction methods for the generation of neural progenitor cells from human induced pluripotent stem cells. Stem Cell Res. *25*, 139–151.

Chaudhry, A., Shi, R., and Luciani, D.S. (2020). A pipeline for multidimensional confocal analysis of mitochondrial morphology, function, and dynamics in pancreatic β-cells. Am. J. Physiol. Metab. *318*, E87–E101.

Chen, H., and Chan, D.C. (2004). Mitochondrial Dynamics in Mammals. Curr. Top. Dev. Biol. *59*, 119–144.

Chen, H., and Chan, D.C. (2017). Mitochondrial Dynamics in Regulating the Unique Phenotypes of Cancer and Stem Cells. Cell Metab. *26*, 39–48.

Chen, B., Schaevitz, L.R., and McConnell, S.K. (2005). Fezl regulates the differentiation and axon targeting of layer 5 subcortical projection neurons in cerebral cortex. Proc. Natl. Acad. Sci. U. S.

A. *102*, 17184–17189.

Chen, B., Wang, S.S., Hattox, A.M., Rayburn, H., Nelson, S.B., and McConnell, S.K. (2008). The Fezf2-Ctip2 genetic pathway regulates the fate choice of subcortical projection neurons in the developing cerebral cortex. Proc. Natl. Acad. Sci. U. S. A. *105*, 11382–11387.

Chenn, A., and McConnell, S.K. (1995). Cleavage orientation and the asymmetric inheritance of notchl immunoreactivity in mammalian neurogenesis. Cell *82*, 631–641.

Chenn, A., Zhang, Y.A., Chang, B.T., and McConnell, S.K. (1998). Intrinsic Polarity of Mammalian Neuroepithelial Cells. Mol. Cell. Neurosci. *11*, 183–193.

Cho, Y.M., Kwon, S., Pak, Y.K., Seol, H.W., Choi, Y.M., Park, D.J., Park, K.S., and Lee, H.K. (2006). Dynamic changes in mitochondrial biogenesis and antioxidant enzymes during the spontaneous differentiation of human embryonic stem cells. Biochem. Biophys. Res. Commun. *348*, 1472–1478.

Choi, B.H. (1981). Radial glia of developing human fetal spinal cord: Golgi, immunohistochemical and electron microscopic study. Dev. Brain Res. *1*, 249–267.

Chong, J., and Xia, J. (2018). MetaboAnalystR: an R package for flexible and reproducible analysis of metabolomics data. Bioinformatics *34*, 4313–4314.

Chong, J., Soufan, O., Li, C., Caraus, I., Li, S., Bourque, G., Wishart, D.S., and Xia, J. (2018). MetaboAnalyst 4.0: towards more transparent and integrative metabolomics analysis. Nucleic Acids Res. *46*, W486–W494.

Chong, J., Wishart, D.S., and Xia, J. (2019). Using MetaboAnalyst 4.0 for Comprehensive and Integrative Metabolomics Data Analysis. Curr. Protoc. Bioinforma. *68*.

Chung, S., Arrell, D.K., Faustino, R.S., Terzic, A., and Dzeja, P.P. (2010). Glycolytic network restructuring integral to the energetics of embryonic stem cell cardiac differentiation. J. Mol. Cell. Cardiol. *48*, 725–734.

Cingolani, P., Patel, V.M., Coon, M., Nguyen, T., Land, S.J., Ruden, D.M., and Lu, X. (2012). Using Drosophila melanogaster as a model for genotoxic chemical mutational studies with a new program, SnpSift. Front. Genet. *3*, 35.

Cipriani, S., Journiac, N., Nardelli, J., Verney, C., Delezoide, A.-L., Guimiot, F., Gressens, P., and Adle-Biassette, H. (2015). Dynamic Expression Patterns of Progenitor and Neuron Layer Markers in the Developing Human Dentate Gyrus and Fimbria. Cereb. Cortex *27*, bhv223.

Clancy, B., Darlington, R.B., and Finlay, B.L. (2001). Translating developmental time across mammalian species. Neuroscience *105*, 7–17.

Clarke, L.E., Liddelow, S.A., Chakraborty, C., Münch, A.E., Heiman, M., and Barres, B.A. (2018). Normal aging induces A1-like astrocyte reactivity. Proc. Natl. Acad. Sci. *115*, E1896–E1905.

Cogliati, S., Enriquez, J.A., and Scorrano, L. (2016). Mitochondrial Cristae: Where Beauty Meets Functionality. Trends Biochem. Sci. *41*, 261–273.

Colas, J.F., and Schoenwolf, G.C. (2001). Towards a cellular and molecular understanding of neurulation. Dev. Dyn. *221*, 117–145.

Cook, G.M.W., Lewis, K.E., and Keynes, R.J. (2017). Neural Patterning: Spinal Cord Segmentation and Somite Patterning☆. In Reference Module in Neuroscience and Biobehavioral Psychology, (Elsevier), pp. 537–544.

Craigen, W.J. (1996). Leigh disease with deficiency of lipoamide dehydrogenase: Treatment failure with dichloroacetate. Pediatr. Neurol. *14*, 69–71.

Cui, Y., Chen, X., Luo, H., Fan, Z., Luo, J., He, S., Yue, H., Zhang, P., and Chen, R. (2016). BioCircos.js: An interactive Circos JavaScript library for biological data visualization on web applications. Bioinformatics *32*, 1740–1742.

D'Arcangelo, G., Miao, G.G., Chen, S.C., Scares, H.D., Morgan, J.I., and Curran, T. (1995). A protein related to extracellular matrix proteins deleted in the mouse mutant reeler. Nature *374*, 719–723.

Das, A.M., Steuerwald, U., and Illsinger, S. (2010). Inborn errors of energy metabolism associated with myopathies. J. Biomed. Biotechnol. *2010*.

Daviaud, N., Chevalier, C., Friedel, R.H., and Zou, H. (2019). Distinct Vulnerability and Resilience of Human Neuroprogenitor Subtypes in Cerebral Organoid Model of Prenatal Hypoxic Injury.

Front. Cell. Neurosci. *13*, 336.

Davies, K.M., Strauss, M., Daum, B., Kief, J.H., Osiewacz, H.D., Rycovska, A., Zickermann, V., and Kühlbrandt, W. (2011). Macromolecular organization of ATP synthase and complex I in whole mitochondria. Proc. Natl. Acad. Sci. U. S. A. *108*, 14121–14126.

DeBerardinis, R.J., and Chandel, N.S. (2020). We need to talk about the Warburg effect. Nat. Metab. *2*, 127–129.

Dehay, C., and Kennedy, H. (2020). Evolution of the human brain. Science (80-.). *369*, 506–507.

Delgado, R.N., Allen, D.E., Keefe, M.G., Mancia Leon, W.R., Ziffra, R.S., Crouch, E.E., Alvarez-Buylla, A., and Nowakowski, T.J. (2022). Individual human cortical progenitors can produce excitatory and inhibitory neurons. Nature *601*, 397–403.

Delivani, P., and Martin, S.J. (2006). Mitochondrial membrane remodeling in apoptosis: an inside story. Cell Death Differ. *13*, 2007–2010.

Delivani, P., Adrain, C., Taylor, R.C., Duriez, P.J., and Martin, S.J. (2006). Role for CED-9 and Egl-1 as regulators of mitochondrial fission and fusion dynamics. Mol. Cell *21*, 761–773.

Demarest, T.G., Waite, E.L., Kristian, T., Puche, A.C., Waddell, J., McKenna, M.C., and Fiskum, G. (2016). Sex-dependent mitophagy and neuronal death following rat neonatal hypoxia–ischemia. Neuroscience *335*, 103–113.

Deneen, B., Ho, R., Lukaszewicz, A., Hochstim, C.J., Gronostajski, R.M., and Anderson, D.J. (2006). The Transcription Factor NFIA Controls the Onset of Gliogenesis in the Developing Spinal Cord. Neuron *52*, 953–968.

Desai, A.R., and McConnell, S.K. (2000). Progressive restriction in fate potential by neural progenitors during cerebral cortical development. Development *127*, 2863–2872.

Dhara, S.K., and Stice, S.L. (2008). Neural differentiation of human embryonic stem cells. J. Cell. Biochem. *105*, 633–640.

Diez del Corral, R., and Storey, K.G. (2004). Opposing FGF and retinoid pathways: a signalling switch that controls differentiation and patterning onset in the extending vertebrate body axis.

Bioessays *26*, 857–869.

Diez del Corral, R., Breitkreuz, D.N., and Storey, K.G. (2002). Onset of neuronal differentiation is regulated by paraxial mesoderm and requires attenuation of FGF signalling. Development *129*, 1681–1691.

Dimou, L., Simon, C., Kirchhoff, F., Takebayashi, H., and Götz, M. (2008). Progeny of Olig2-expressing progenitors in the gray and white matter of the adult mouse cerebral cortex. J. Neurosci. *28*, 10434–10442.

Dolmetsch, R., and Geschwind, D.H. (2011). The human brain in a dish: The promise of iPSC-derived neurons. Cell *145*, 831–834.

Dominguez, M.H., Ayoub, A.E., and Rakic, P. (2013). POU-III transcription factors (Brn1, Brn2, and Oct6) influence neurogenesis, molecular identity, and migratory destination of upper-layer cells of the cerebral cortex. Cereb. Cortex *23*, 2632–2643.

Douvaras, P., and Fossati, V. (2015). Generation and isolation of oligodendrocyte progenitor cells from human pluripotent stem cells. Nat. Protoc. *10*, 1143–1154.

Douvaras, P., Wang, J., Zimmer, M., Hanchuk, S., O'Bara, M.A., Sadiq, S., Sim, F.J., Goldman, J., and Fossati, V. (2014). Efficient generation of myelinating oligodendrocytes from primary progressive multiple sclerosis patients by induced pluripotent stem cells. Stem Cell Reports *3*, 250–259.

Dudkina, N. V., Eubel, H., Keegstra, W., Boekema, E.J., and Braun, H.P. (2005). Structure of a mitochondrial supercomplex formed by respiratory-chain complexes I and III. Proc. Natl. Acad. Sci. U. S. A. *102*, 3225–3229.

Dulabon, L., Olson, E.C., Taglienti, M.G., Eisenhuth, S., McGrath, B., Walsh, C.A., Kreidberg, J.A., and Anton, E.S. (2000). Reelin binds α3β1 integrin and inhibits neuronal migration. Neuron *27*, 33–44.

Edlow, A.G. (2021). Maternal Metabolic Disease and Offspring Neurodevelopment—An Evolving Public Health Crisis. JAMA Netw. Open *4*, e2129674.

Ehses, S., Raschke, I., Mancuso, G., Bernacchia, A., Geimer, S., Tondera, D., Martinou, J.C.,

Westermann, B., Rugarli, E.I., and Langer, T. (2009). Regulation of OPA1 processing and mitochondrial fusion by m-AAA protease isoenzymes and OMA1. J. Cell Biol. *187*, 1023–1036.

Eiraku, M., Watanabe, K., Matsuo-Takasaki, M., Kawada, M., Yonemura, S., Matsumura, M., Wataya, T., Nishiyama, A., Muguruma, K., and Sasai, Y. (2008). Self-Organized Formation of Polarized Cortical Tissues from ESCs and Its Active Manipulation by Extrinsic Signals. Cell Stem Cell *3*, 519–532.

Elkabetz, Y., Panagiotakos, G., Al Shamy, G., Socci, N.D., Tabar, V., and Studer, L. (2008). Human ES cell-derived neural rosettes reveal a functionally distinct early neural stem cell stage. Genes Dev. *22*, 152–165.

Empie, K., Rangarajan, V., and Juul, S.E. (2015). Is the ferret a suitable species for studying perinatal brain injury? Int. J. Dev. Neurosci. *45*, 2–10.

Englund, C. (2005). Pax6, Tbr2, and Tbr1 Are Expressed Sequentially by Radial Glia, Intermediate Progenitor Cells, and Postmitotic Neurons in Developing Neocortex. J. Neurosci. *25*, 247–251.

Escartin, C., Galea, E., Lakatos, A., O'Callaghan, J.P., Petzold, G.C., Serrano-Pozo, A., Steinhäuser, C., Volterra, A., Carmignoto, G., Agarwal, A., et al. (2021). Reactive astrocyte nomenclature, definitions, and future directions. Nat. Neurosci. *24*, 312–325.

Espuny-Camacho, I., Michelsen, K.A., Gall, D., Linaro, D., Hasche, A., Bonnefont, J., Bali, C., Orduz, D., Bilheu, A., Herpoel, A., et al. (2013). Pyramidal Neurons Derived from Human Pluripotent Stem Cells Integrate Efficiently into Mouse Brain Circuits In Vivo. Neuron *77*, 440–456.

Esterhuizen, K., van der Westhuizen, F.H., and Louw, R. (2017). Metabolomics of mitochondrial disease. Mitochondrion *35*, 97–110.

Evans, M.J., and Kaufman, M.H. (1981). Establishment in culture of pluripotential cells from mouse embryos. Nature *292*, 154–156.

Fadero, T.C., Gerbich, T.M., Rana, K., Suzuki, A., DiSalvo, M., Schaefer, K.N., Heppert, J.K., Boothby, T.C., Goldstein, B., Peifer, M., et al. (2018). LITE microscopy: Tilted light-sheet excitation of model organisms offers high resolution and low photobleaching. J. Cell Biol. *217*, 1869–1882.

Faitg, J., Lacefield, C., Davey, T., White, K., Laws, R., Kosmidis, S., Reeve, A.K., Kandel, E.R.,

Vincent, A.E., and Picard, M. (2021). 3D neuronal mitochondrial morphology in axons, dendrites, and somata of the aging mouse hippocampus. Cell Rep. *36*, 2021.02.26.433056.

Fan, X., Fu, Y., Zhou, X., Sun, L., Yang, M., Wang, M., Chen, R., Wu, Q., Yong, J., Dong, J., et al. (2020). Single-cell transcriptome analysis reveals cell lineage specification in temporal-spatial patterns in human cortical development. Sci. Adv. *6*.

Fang, Q., Zhang, Y., Chen, X., Li, H., Cheng, L., Zhu, W., Zhang, Z., Tang, M., Liu, W., Wang, H., et al. (2020). Three-Dimensional Graphene Enhances Neural Stem Cell Proliferation Through Metabolic Regulation. Front. Bioeng. Biotechnol. *7*, 436.

Farahany, N.A., Greely, H.T., Hyman, S., Koch, C., Grady, C., Pasca, S.P., Sestan, N., Arlotta, P., Bernat, J.L., Ting, J., et al. (2018). The ethics of experimenting with human brain tissue comment. Nature *556*, 429–432.

Fedorova, V., Vanova, T., Elrefae, L., Pospisil, J., Petrasova, M., Kolajova, V., Hudacova, Z., Baniariova, J., Barak, M., Peskova, L., et al. (2019). Differentiation of neural rosettes from human pluripotent stem cells in vitro is sequentially regulated on a molecular level and accomplished by the mechanism reminiscent of secondary neurulation. Stem Cell Res. *40*, 101563.

Ferrari, M., Jain, I.H., Goldberger, O., Rezoagli, E., Thoonen, R., Chen, K.-H., Sosnovik, D.E., Scherrer-Crosbie, M., Mootha, V.K., and Zapol, W.M. (2017). Hypoxia treatment reverses neurodegenerative disease in a mouse model of Leigh syndrome. Proc. Natl. Acad. Sci. *114*, E4241–E4250.

Fietz, S.A., Kelava, I., Vogt, J., Wilsch-Bräuninger, M., Stenzel, D., Fish, J.L., Corbeil, D., Riehn, A., Distler, W., Nitsch, R., et al. (2010). OSVZ progenitors of human and ferret neocortex are epithelial-like and expand by integrin signaling. Nat. Neurosci. *13*, 690–699.

Finsterer, J. (2008). Leigh and Leigh-Like Syndrome in Children and Adults. Pediatr. Neurol. *39*, 223–235.

Fishell, G., and Kriegstein, A.R. (2003). Neurons from radial glia: The consequences of asymmetric inheritance. Curr. Opin. Neurobiol. *13*, 34–41.

Florio, M., and Huttner, W.B. (2014). Neural progenitors, neurogenesis and the evolution of the

neocortex. Development *141*, 2182–2194.

Fogo, G.M., Anzell, A.R., Maheras, K.J., Raghunayakula, S., Wider, J.M., Emaus, K.J., Bryson, T.D., Bukowski, M.J., Neumar, R.W., Przyklenk, K., et al. (2021). Machine learning-based classification of mitochondrial morphology in primary neurons and brain. Sci. Rep. *11*, 1–12.

Folmes, C.D.L., Nelson, T.J., Martinez-Fernandez, A., Arrell, D.K., Lindor, J.Z., Dzeja, P.P., Ikeda, Y., Perez-Terzic, C., and Terzic, A. (2011). Somatic oxidative bioenergetics transitions into pluripotency-dependent glycolysis to facilitate nuclear reprogramming. Cell Metab. *14*, 264–271.

Forbes, C.E., and Grafman, J. (2010). The role of the human prefrontal cortex in social cognition and moral judgment. Annu. Rev. Neurosci. *33*, 299–324.

Fort, L., Gama, V., and Macara, I.G. (2021). Apoptotic Find-me Signals are an Essential Driver of Stem Cell Conversion To The Cardiac Lineage. BioRxiv 2021.06.21.449262.

Frade, J.M. (2002). Interkinetic nuclear movement in the vertebrate neuroepithelium: Encounters with an old acquaintance. In Progress in Brain Research, pp. 67–71.

Francklyn, C.S., and Mullen, P. (2019). Progress and challenges in aminoacyl-tRNA synthetase-based therapeutics. J. Biol. Chem. *294*, 5365–5385.

Franco, P.G., Paganelli, A.R., Löpez, S.L., and Carrasco, A.E. (1999). Functional association of retinoic acid and hedgehog signaling in Xenopus primary neurogenesis. Development *126*, 4257–4265.

Franco, S.J., Gil-Sanz, C., Martinez-Garay, I., Espinosa, A., Harkins-Perry, S.R., Ramos, C., and Müller, U. (2012). Fate-restricted neural progenitors in the mammalian cerebral cortex. Science (80-.). *337*, 746–749.

Frank, S., Gaume, B., Bergmann-Leitner, E.S., Leitner, W.W., Robert, E.G., Catez, F., Smith, C.L., and Youle, R.J. (2001). The Role of Dynamin-Related Protein 1, a Mediator of Mitochondrial Fission, in Apoptosis. Dev. Cell *1*, 515–525.

Frantz, G.D., and McConnell, S.K. (1996). Restriction of late cerebral cortical progenitors to an upper-layer fate. Neuron *17*, 55–61.

Frantz, G.D., Weimann, J.M., Levin, M.E., and McConnell, S.K. (1994). Otx1 and Otx2 define layers and regions in developing cerebral cortex and cerebellum. J. Neurosci. *14*, 5725–5740.

Frotscher, M. (1998). Cajal-Retzius cells, Reelin, and the formation of layers. Curr. Opin. Neurobiol. *8*, 570–575.

Fumagalli, M., Lecca, D., Abbracchio, M.P., and Ceruti, S. (2017). Pathophysiological Role of Purines and Pyrimidines in Neurodevelopment: Unveiling New Pharmacological Approaches to Congenital Brain Diseases. Front. Pharmacol. *8*, 941.

Fuster, J.M. (2002). Frontal lobe and cognitive development. J. Neurocytol. *31*, 373–385.

Galera-Monge, T., Zurita-Díaz, F., González-Páramos, C., Moreno-Izquierdo, A., Fraga, M.F., Fernández, A.F., Garesse, R., and Gallardo, M.E. (2016). Generation of a human iPSC line from a patient with Leigh syndrome caused by a mutation in the MT-ATP6 gene. Stem Cell Res. *16*, 766–769.

García-Cazorla, A., Oyarzabal, A., Fort, J., Robles, C., Castejón, E., Ruiz-Sala, P., Bodoy, S., Merinero, B., Lopez-Sala, A., Dopazo, J., et al. (2014). Two Novel Mutations in the BCKDK (Branched-Chain Keto-Acid Dehydrogenase Kinase) Gene Are Responsible for a Neurobehavioral Deficit in Two Pediatric Unrelated Patients. Hum. Mutat. *35*, 470–477.

García-Marqués, J., and López-Mascaraque, L. (2013). Clonal identity determines astrocyte cortical heterogeneity. Cereb. Cortex *23*, 1463–1472.

Garnett, A.T., Square, T.A., and Medeiros, D.M. (2012). BMP, WNT and FGF signals are integrated through evolutionarily conserved enhancers to achieve robust expression of Pax3 and Zic genes at the zebrafish neural plate border. Development *139*, 4220–4231.

Gaspard, N., Bouschet, T., Hourez, R., Dimidschstein, J., Naeije, G., Van Den Ameele, J., Espuny-Camacho, I., Herpoel, A., Passante, L., Schiffmann, S.N., et al. (2008). An intrinsic mechanism of corticogenesis from embryonic stem cells. Nature *455*, 351–357.

Ge, W.P., Miyawaki, A., Gage, F.H., Jan, Y.N., and Jan, L.Y. (2012). Local generation of glia is a major astrocyte source in postnatal cortex. Nature *484*, 376–380.

Geng, X., Shen, J., Li, F., Yip, J., Guan, L., Rajah, G., Peng, C., DeGracia, D., and Ding, Y. (2021).

Phosphoenolpyruvate Carboxykinase (PCK) in the Brain Gluconeogenic Pathway Contributes to Oxidative and Lactic Injury After Stroke. Mol. Neurobiol. 1–13.

Gerards, M., Sallevelt, S.C.E.H., and Smeets, H.J.M. (2016). Leigh syndrome: Resolving the clinical and genetic heterogeneity paves the way for treatment options. Mol. Genet. Metab. *117*, 300–312.

Gerrard, L., Rodgers, L., and Cui, W. (2005). Differentiation of Human Embryonic Stem Cells to Neural Lineages in Adherent Culture by Blocking Bone Morphogenetic Protein Signaling. Stem Cells *23*, 1234–1241.

Giandomenico, S.L., Mierau, S.B., Gibbons, G.M., Wenger, L.M.D., Masullo, L., Sit, T., Sutcliffe, M., Boulanger, J., Tripodi, M., Derivery, E., et al. (2019). Cerebral organoids at the air–liquid interface generate diverse nerve tracts with functional output. Nat. Neurosci. *22*, 669–679.

Goda, N., and Kanai, M. (2012). Hypoxia-inducible factors and their roles in energy metabolism. Int. J. Hematol. *95*, 457–463.

Gogos, J.A., Santha, M., Takacs, Z., Beck, K.D., Luine, V., Lucas, L.R., Nadler, J.V., and Karayiorgou, M. (1999). The gene encoding proline dehydrogenase modulates sensorimotor gating in mice. Nat. Genet. *21*, 434–439.

Gonzalez, F.F., and Miller, S.P. (2006). Does perinatal asphyxia impair cognitive function without cerebral palsy? Arch. Dis. Child. Fetal Neonatal Ed. *91*, F454–F459.

Gordon, A., Yoon, S.-J., Tran, S.S., Makinson, C.D., Park, J.Y., Andersen, J., Valencia, A.M., Horvath, S., Xiao, X., Huguenard, J.R., et al. (2021). Long-term maturation of human cortical organoids matches key early postnatal transitions. Nat. Neurosci. *24*, 331–342.

Gorman, G.S., Chinnery, P.F., DiMauro, S., Hirano, M., Koga, Y., McFarland, R., Suomalainen, A., Thorburn, D.R., Zeviani, M., and Turnbull, D.M. (2016). Mitochondrial diseases. Nat. Rev. Dis. Prim. *2*, 1–22.

Götz, M., and Barde, Y.A. (2005). Radial glial cells: Defined and major intermediates between embryonicstem cells and CNS neurons. Neuron *46*, 369–372.

Götz, M., and Huttner, W.B. (2005). The cell biology of neurogenesis. Nat. Rev. Mol. Cell Biol. *6*,

777–788.

Götz, M., Stoykova, A., and Gruss, P. (1998). Pax6 controls radial glia differentiation in the cerebral cortex. Neuron *21*, 1031–1044.

Grabiec, M., Hříbková, H., Vařecha, M., Střítecká, D., Hampl, A., Dvořák, P., and Sun, Y.M. (2016). Stage-specific roles of FGF2 signaling in human neural development. Stem Cell Res. *17*, 330–341.

Grace, H.E., Galdun, P., Lesnefsky, E.J., West, F.D., and Iyer, S. (2019). mRNA Reprogramming of T8993G Leigh's Syndrome Fibroblast Cells to Create Induced Pluripotent Stem Cell Models for Mitochondrial Disorders. Stem Cells Dev. *28*, 846–859.

Greely, H.T., Ramos, K.M., and Grady, C. (2016). Neuroethics in the Age of Brain Projects. Neuron *92*, 637–641.

Green, D.R. (2000). Apoptotic pathways: Paper wraps stone blunts scissors. Cell *102*, 1–4.

Di Gregorio, A. (2020). The notochord gene regulatory network in chordate evolution: Conservation and divergence from Ciona to vertebrates. In Current Topics in Developmental Biology, (Academic Press Inc.), pp. 325–374.

Greig, L.C., Woodworth, M.B., Galazo, M.J., Padmanabhan, H., and Macklis, J.D. (2013). Molecular logic of neocortical projection neuron specification, development and diversity. Nat. Rev. Neurosci. *14*, 755–769.

Grier, J., Hirano, M., Karaa, A., Shepard, E., and Thompson, J.L.P. (2018). Diagnostic odyssey of patients with mitochondrial disease. Neurol. Genet. *4*, e230.

Grivennikova, V.G., Kareyeva, A. V., and Vinogradov, A.D. (2010). What are the sources of hydrogen peroxide production by heart mitochondria? Biochim. Biophys. Acta - Bioenerg. *1797*, 939–944.

Grohm, J., Kim, S.W., Mamrak, U., Tobaben, S., Cassidy-Stone, A., Nunnari, J., Plesnila, N., and Culmsee, C. (2012). Inhibition of Drp1 provides neuroprotection in vitro and in vivo. Cell Death Differ. *19*, 1446–1458.

Grow, W.A. (2018). Development of the Nervous System. In Fundamental Neuroscience for Basic

and Clinical Applications: Fifth Edition, (Elsevier Inc.), pp. 72-90.e1.

Hakim, A.M., Moss, G., and Scuderi, D. (1980). The Pentose Phosphate Pathway in Brain during Development. Neonatology *37*, 15–21.

Halfter, W., Dong, S., Yip, Y.P., Willem, M., and Mayer, U. (2002). A critical function of the pial basement membrane in cortical histogenesis. J. Neurosci. *22*, 6029–6040.

Halim, N.D., Mcfate, T., Mohyeldin, A., Okagaki, P., Korotchkina, L.G., Patel, M.S., Jeoung, N.H., Harris, R.A., Schell, M.J., and Verma, A. (2010). Phosphorylation status of pyruvate dehydrogenase distinguishes metabolic phenotypes of cultured rat brain astrocytes and neurons. Glia *58*, 1168–1176.

Hallin, U., Kondo, E., Ozaki, Y., Hagberg, H., Shibasaki, F., and Blomgren, K. (2006). Bcl-2 phosphorylation in the BH4 domain precedes caspase-3 activation and cell death after neonatal cerebral hypoxic-ischemic injury. Neurobiol. Dis. *21*, 478–486.

Hamanaka, R.B., and Chandel, N.S. (2010). Mitochondrial reactive oxygen species regulate cellular signaling and dictate biological outcomes. Trends Biochem. Sci. *35*, 505–513.

Han, W., Kwan, K.Y., Shim, S., Lam, M.M.S., Shin, Y., Xu, M., Zhu, Y., Li, M., and Šestan, N. (2011). TBR1 directly represses Fezf2 to control the laminar origin and development of the corticospinal tract. Proc. Natl. Acad. Sci. U. S. A. *108*, 3041–3046.

Hanashima, C., Li, S.C., Shen, L., Lai, E., and Fishell, G. (2004). Foxg1 Suppresses Early Cortical Cell Fate. Science (80-.). *303*, 56–59.

Handel, A.E., Chintawar, S., Lalic, T., Whiteley, E., Vowles, J., Giustacchini, A., Argoud, K., Sopp, P., Nakanishi, M., Bowden, R., et al. (2016). Assessing similarity to primary tissue and cortical layer identity in induced pluripotent stem cell-derived cortical neurons through single-cell transcriptomics. Hum. Mol. Genet. *25*, 989–1000.

Hansen, D. V., Lui, J.H., Parker, P.R.L., and Kriegstein, A.R. (2010). Neurogenic radial glia in the outer subventricular zone of human neocortex. Nature *464*, 554–561.

Hara, Y., Yuk, F., Puri, R., Janssen, W.G.M.M., Rapp, P.R., and Morrison, J.H. (2014). Presynaptic mitochondrial morphology in monkey prefrontal cortex correlates with working memory and is

improved with estrogen treatment. Proc. Natl. Acad. Sci. *111*, 486–491.

Haremaki, T., Metzger, J.J., Rito, T., Ozair, M.Z., Etoc, F., and Brivanlou, A.H. (2019). Self-organizing neuruloids model developmental aspects of Huntington's disease in the ectodermal compartment. Nat. Biotechnol. *37*, 1198–1208.

Hartfuss, E., Galli, R., Heins, N., and Götz, M. (2001). Characterization of CNS precursor subtypes and radial glia. Dev. Biol. *229*, 15–30.

Hattori, T., Hamazaki, T., Kudo, S., and Shintaku, H. (2016). Metabolic Signature of MELAS/Leigh Overlap Syndrome in Patient-specific Induced Pluripotent Stem Cells Model. Osaka City Med. J. *62*, 69–76.

Haubensak, W., Attardo, A., Denk, W., and Huttner, W.B. (2004). Neurons arise in the basal neuroepithelium of the early mammalian telencephalon: A major site of neurogenesis. Proc. Natl. Acad. Sci. U. S. A. *101*, 3196–3201.

Hay, E.D. (2005). The mesenchymal cell, its role in the embryo, and the remarkable signaling mechanisms that create it. Dev. Dyn. *233*, 706–720.

Head, B., Griparic, L., Amiri, M., Gandre-Babbe, S., and Van Der Bliek, A.M. (2009). Inducible proteolytic inactivation of OPA1 mediated by the OMA1 protease in mammalian cells. J. Cell Biol. *187*, 959–966.

Heide, M., Haffner, C., Murayama, A., Kurotaki, Y., Shinohara, H., Okano, H., Sasaki, E., and Huttner, W.B. (2020). Human-specific ARHGAP11B increases size and folding of primate neocortex in the fetal marmoset. Science (80-.). *369*, 546–550.

Vander Heiden, M.G., Chandel, N.S., Williamson, E.K., Schumacker, P.T., and Thompson, C.B. (1997). Bcl-x(L) regulates the membrane potential and volume homeostasis of mitochondria. Cell *91*, 627–637.

Heins, N., Malatesta, P., Cecconi, F., Nakafuku, M., Tucker, K.L., Hack, M.A., Chapouton, P., Barde, Y.A., and Goötz, M. (2002). Glial cells generate neurons: The role of the transcription factor Pax6. Nat. Neurosci. *5*, 308–315.

Herculano-Houzel, S., Catania, K., Manger, P.R., and Kaas, J.H. (2015). Mammalian Brains Are

Made of These: A Dataset of the Numbers and Densities of Neuronal and Nonneuronal Cells in the Brain of Glires, Primates, Scandentia, Eulipotyphlans, Afrotherians and Artiodactyls, and Their Relationship with Body Mass. Brain. Behav. Evol. *86*, 145–163.

Herculano-Houzel, S., Kaas, J.H., and de Oliveira-Souza, R. (2016). Corticalization of motor control in humans is a consequence of brain scaling in primate evolution. J. Comp. Neurol. *524*, 448–455.

Herst, P.M., and Berridge, M. V. (2007). Cell surface oxygen consumption: A major contributor to cellular oxygen consumption in glycolytic cancer cell lines. Biochim. Biophys. Acta - Bioenerg. *1767*, 170–177.

Hevner, R.F., Shi, L., Justice, N., Hsueh, Y.P., Sheng, M., Smiga, S., Bulfone, A., Goffinet, A.M., Campagnoni, A.T., and Rubenstein, J.L.R. (2001). Tbr1 regulates differentiation of the preplate and layer 6. Neuron *29*, 353–366.

Hiesberger, T., Trommsdorff, M., Howell, B.W., Goffinet, A., Mumby, M.C., Cooper, J.A., and Herz, J. (1999). Direct binding of Reelin to VLDL receptor and ApoE receptor 2 induces tyrosine phosphorylation of Disabled-1 and modulates tau phosphorylation. Neuron *24*, 481–489.

Hinman, L.M., Sheu, K.-F.R., Baker, A.C., Kim, Y.T., and Blass, J.P. (1989). Deficiency of pyruvate dehydrogenase complex (PDHC) in Leigh's disease fibroblasts: An abnormality in lipoamide dehydrogenase affecting PDHC activation. Neurology *39*, 70–70.

Hippocrates HIPPOCRATES OF COS, Decorum | Loeb Classical Library.

His, W. (1889). Die Neuroblasten und deren Entstehung im embryonal Marke. Abh.Math.Phys.Cl.Kgl.Sach.Ges.Wiss. *15*, 313–372.

Hoerder-Suabedissen, A., and Molnár, Z. (2015). Development, evolution and pathology of neocortical subplate neurons. Nat. Rev. Neurosci. *16*, 133–146.

Hoffman, G.E., Hartley, B.J., Flaherty, E., Ladran, I., Gochman, P., Ruderfer, D.M., Stahl, E.A., Rapoport, J., Sklar, P., and Brennand, K.J. (2017). Transcriptional signatures of schizophrenia in hiPSC-derived NPCs and neurons are concordant with post-mortem adult brains. Nat. Commun. *8*, 1–15.

Hoffman, G.E., Schrode, N., Flaherty, E., and Brennand, K.J. (2019). New considerations for hiPSC-

based models of neuropsychiatric disorders. Mol. Psychiatry *24*, 49–66.

Homem, C.C.F., Repic, M., and Knoblich, J.A. (2015). Proliferation control in neural stem and progenitor cells. Nat. Rev. Neurosci. *16*, 647–659.

Hoppins, S., Lackner, L., and Nunnari, J. (2007). The machines that divide and fuse mitochondria. Annu. Rev. Biochem. *76*, 751–780.

Hříbková, H., Grabiec, M., Klemová, D., Slaninová, I., and Sun, Y.-M. (2018). Calcium signaling mediates five types of cell morphological changes to form neural rosettes. J. Cell Sci. *131*, jcs206896.

Hsu, S.Y., Kaipia, A., McGee, E., Lomeli, M., and Hsueh, A.J.W. (1997). Bok is a pro-apoptotic Bcl-2 protein with restricted expression in reproductive tissues and heterodimerizes with selective anti-apoptotic Bcl-2 family members. Proc. Natl. Acad. Sci. U. S. A. *94*, 12401–12406.

Huang, W., Bhaduri, A., Velmeshev, D., Wang, S., Wang, L., Rottkamp, C.A., Alvarez-Buylla, A., Rowitch, D.H., and Kriegstein, A.R. (2020). Origins and Proliferative States of Human Oligodendrocyte Precursor Cells. Cell *182*, 594-608.e11.

Huh, T.L., Casazza, J.P., Huh, J.W., Chi, Y.T., and Song, B.J. (1990). Characterization of two cDNA clones for pyruvate dehydrogenase E1β subunit and its regulation in tricarboxylic acid cycle-deficient fibroblast. J. Biol. Chem. *265*, 13320–13326.

Huisken, J., Swoger, J., Del Bene, F., Wittbrodt, J., and Stelzer, E.H.K. (2004). Optical sectioning deep inside live embryos by selective plane illumination microscopy. Science (80-.). *305*, 1007–1009.

Hutsler, J.J., Lee, D.G., and Porter, K.K. (2005). Comparative analysis of cortical layering and supragranular layer enlargement in rodent carnivore and primate species. Brain Res. *1052*, 71–81.

Huttenlocher, P.R. (1979). Synaptic density in human frontal cortex - developmental changes and effects of aging. Brain Res. *163*, 195–205.

Huttner, W.B., and Brand, M. (1997). Asymmetric division and polarity of neuroepithelial cells. Curr. Opin. Neurobiol. *7*, 29–39.

Hutton, S.R., and Pevny, L.H. (2011). SOX2 expression levels distinguish between neural progenitor populations of the developing dorsal telencephalon. Dev. Biol. *352*, 40–47.

Inak, G., Lorenz, C., Lisowski, P., Zink, A., Mlody, B., and Prigione, A. (2017). Concise Review: Induced Pluripotent Stem Cell-Based Drug Discovery for Mitochondrial Disease. Stem Cells *35*, 1655–1662.

Inak, G., Rybak-Wolf, A., Lisowski, P., Pentimalli, T.M., Jüttner, R., Glažar, P., Uppal, K., Bottani, E., Brunetti, D., Secker, C., et al. (2021). Defective metabolic programming impairs early neuronal morphogenesis in neural cultures and an organoid model of Leigh syndrome. Nat. Commun. *12*, 1–22.

Inohara, N., Ekhterae, D., Garcia, I., Carrio, R., Merino, J., Merry, A., Chen, S., and Núñez, G. (1998). Mtd, a novel Bcl-2 family member activates apoptosis in the absence of heterodimerization with Bcl-2 and Bcl-X(L). J. Biol. Chem. *273*, 8705–8710.

Inoue, K., Terashima, T., Nishikawa, T., and Takumi, T. (2004). Fez1 is layer-specifically expressed in the adult mouse neocortex. Eur. J. Neurosci. *20*, 2909–2916.

Ioannou, M.S., Jackson, J., Sheu, S.H., Chang, C.L., Weigel, A. V., Liu, H., Pasolli, H.A., Xu, C.S., Pang, S., Matthies, D., et al. (2019). Neuron-Astrocyte Metabolic Coupling Protects against Activity-Induced Fatty Acid Toxicity. Cell *177*, 1522-1535.e14.

Itoh, Y., Esaki, T., Shimoji, K., Cook, M., Law, M.J., Kaufman, E., and Sokoloff, L. (2003). Dichloroacetate effects on glucose and lactate oxidation by neurons and astroglia in vitro and on glucose utilization by brain in vivo. Proc. Natl. Acad. Sci. *100*, 4879–4884.

Iwata, R., Casimir, P., and Vanderhaeghen, P. (2020). Mitochondrial dynamics in postmitotic cells regulate neurogenesis. Science (80-.). *369*, 858–862.

Iyer, S., Bergquist, K., Young, K., Gnaiger, E., Rao, R.R., and Bennett, J.P. (2012). Mitochondrial Gene Therapy Improves Respiration, Biogenesis, and Transcription in G11778A Leber's Hereditary Optic Neuropathy and T8993G Leigh's Syndrome Cells. Hum. Gene Ther. *23*, 647–657.

Jain, I.H., Zazzeron, L., Goli, R., Alexa, K., Schatzman-Bone, S., Dhillon, H., Goldberger, O., Peng, J., Shalem, O., Sanjana, N.E., et al. (2016). Hypoxia as a therapy for mitochondrial disease. Science

(80-.). *352*, 54–61.

Jain, I.H., Zazzeron, L., Goldberger, O., Marutani, E., Wojtkiewicz, G.R., Ast, T., Wang, H., Schleifer, G., Stepanova, A., Brepoels, K., et al. (2019). Leigh Syndrome Mouse Model Can Be Rescued by Interventions that Normalize Brain Hyperoxia, but Not HIF Activation. Cell Metab. *0*, 824-832.e3.

Jakobs, S. (2006). High resolution imaging of live mitochondria. Biochim. Biophys. Acta - Mol. Cell Res. *1763*, 561–575.

Jessell, T.M., and Dodd, J. (1990). Floor plate-derived signals and the control of neural cell pattern in vertebrates. Harvey Lect. *86*, 87–128.

Jiang, W., Tian, X., Yang, P., Li, J., Xiao, L., Liu, J., Liu, C., Tan, W., and Tu, H. (2019). Enolase1 Alleviates Cerebral Ischemia-Induced Neuronal Injury via Its Enzymatic Product Phosphoenolpyruvate. ACS Chem. Neurosci. *10*, 2877–2889.

Johnson, S.C., Martinez, F., Bitto, A., Gonzalez, B., Tazaerslan, C., Cohen, C., Delaval, L., Timsit, J., Knebelmann, B., Terzi, F., et al. (2019). mTOR inhibitors may benefit kidney transplant recipients with mitochondrial diseases. Kidney Int. *95*, 455–466.

Jones-Villeneuve, E.M., Rudnicki, M.A., Harris, J.F., and McBurney, M.W. (1983). Retinoic acid-induced neural differentiation of embryonal carcinoma cells. Mol. Cell. Biol. *3*, 2271–2279.

Joshi, P., Bodnya, C., Rasmussen, M.L., Romero-Morales, A.I., Bright, A., and Gama, V. (2020). Modeling the function of BAX and BAK in early human brain development using iPSC-derived systems. Cell Death Dis. *11*, 808.

Juchniewicz, P., Piotrowska, E., Kloska, A., Podlacha, M., Mantej, J., Węgrzyn, G., Tukaj, S., and Jakóbkiewicz-banecka, J. (2021). Dosage compensation in females with X-linked metabolic disorders. Int. J. Mol. Sci. *22*, 4514.

Jürgensmeier, J.M., Xie, Z., Deveraux, Q., Ellerby, L., Bredesen, D., and Reed, J.C. (1998). Bax directly induces release of cytochrome c from isolated mitochondria. Proc. Natl. Acad. Sci. U. S. A. *95*, 4997–5002.

Kaas, J.H. (2008). The evolution of the complex sensory and motor systems of the human brain. Brain Res. Bull. *75*, 384–390.

Kadoshima, T., Sakaguchi, H., Nakano, T., Soen, M., Ando, S., Eiraku, M., and Sasai, Y. (2013). Self-organization of axial polarity, inside-out layer pattern, and species-specific progenitor dynamics in human ES cell-derived neocortex. Proc. Natl. Acad. Sci. *110*, 20284–20289.

Kalebic, N., and Huttner, W.B. (2020). Basal Progenitor Morphology and Neocortex Evolution. Trends Neurosci. *43*, 843–853.

Kan, A. (2017). Machine learning applications in cell image analysis. Immunol. Cell Biol. *95*, 525–530.

Kang, P., Lee, H.K., Glasgow, S.M., Finley, M., Donti, T., Gaber, Z.B., Graham, B.H., Foster, A.E., Novitch, B.G., Gronostajski, R.M., et al. (2012). Sox9 and NFIA Coordinate a Transcriptional Regulatory Cascade during the Initiation of Gliogenesis. Neuron *74*, 79–94.

Kanton, S., Boyle, M.J., He, Z., Santel, M., Weigert, A., Sanchís-Calleja, F., Guijarro, P., Sidow, L., Fleck, J.S., Han, D., et al. (2019). Organoid single-cell genomic atlas uncovers human-specific features of brain development. Nature *574*, 418–422.

Karbowski, M., Lee, Y.J., Gaume, B., Jeong, S.Y., Frank, S., Nechushtan, A., Santel, A., Fuller, M., Smith, C.L., and Youle, R.J. (2002). Spatial and temporal association of Bax with mitochondrial fission sites, Drp1, and Mfn2 during apoptosis. J. Cell Biol. *159*, 931–938.

Karbowski, M., Norris, K.L., Cleland, M.M., Jeong, S.Y., and Youle, R.J. (2006). Role of Bax and Bak in mitochondrial morphogenesis. Nature *443*, 658–662.

Ke, F.F.S., Vanyai, H.K., Cowan, A.D., Delbridge, A.R.D., Whitehead, L., Grabow, S., Czabotar, P.E., Voss, A.K., and Strasser, A. (2018). Embryogenesis and Adult Life in the Absence of Intrinsic Apoptosis Effectors BAX, BAK, and BOK. Cell *173*, 1217-1230.e17.

Kelava, I., and Lancaster, M.A. (2016). Stem Cell Models of Human Brain Development. Cell Stem Cell *18*, 736–748.

Khacho, M., and Slack, R.S. (2018). Mitochondrial dynamics in the regulation of neurogenesis: From development to the adult brain. Dev. Dyn. *247*, 47–53.

Khacho, M., Clark, A., Svoboda, D.S., Azzi, J., MacLaurin, J.G., Meghaizel, C., Sesaki, H., Lagace, D.C., Germain, M., Harper, M.E., et al. (2016). Mitochondrial Dynamics Impacts Stem Cell Identity

and Fate Decisions by Regulating a Nuclear Transcriptional Program. Cell Stem Cell.

Khacho, M., Harris, R., and Slack, R.S. (2019). Mitochondria as central regulators of neural stem cell fate and cognitive function. Nat. Rev. Neurosci. *20*, 34–48.

Kiecker, C., and Niehrs, C. (2001). A morphogen gradient of Wnt/β-catenin signalling regulates anteroposterior neural patterning in Xenopus. Development *128*, 4189–4201.

Kim, H.M., Qu, T., Kriho, V., Lacor, P., Smalheiser, N., Pappas, G.D., Guidotti, A., Costa, E., and Sugaya, K. (2002). Reelin function in neural stem cell biology. Proc. Natl. Acad. Sci. U. S. A. *99*, 4020–4025.

Kitahara, T., Sakaguchi, H., Morizane, A., Kikuchi, T., Miyamoto, S., and Takahashi, J. (2020). Axonal Extensions along Corticospinal Tracts from Transplanted Human Cerebral Organoids. Stem Cell Reports *15*, 467–481.

Kluck, R.M., Bossy-Wetzel, E., Green, D.R., and Newmeyer, D.D. (1997). The release of cytochrome c from mitochondria: A primary site for Bcl- 2 regulation of apoptosis. Science (80-.). *275*, 1132–1136.

Kluck, R.M., Degli Esposti, M., Perkins, G., Renken, C., Kuwana, T., Bossy-Wetzel, E., Goldberg, M., Allen, T., Barber, M.J., Green, D.R., et al. (1999). The pro-apoptotic proteins, Bid and Bax, cause a limited permeabilization of the mitochondrial outer membrane that is enhanced by cytosol. J. Cell Biol. *147*, 809–822.

Knight, G.T., Lundin, B.F., Iyer, N., Ashton, L.M.T., Sethares, W.A., Willett, R.M., and Ashton, R.S. (2018). Engineering induction of singular neural rosette emergence within hPSC-derived tissues. Elife *7*.

Knudson, C.M., Tung, K.S.K., Tourtellotte, W.G., Brown, G.A.J., and Korsmeyer, S.J. (1995). Bax-deficient mice with lymphoid hyperplasia and male germ cell death. Science (80-.). *270*, 96–99.

Koch, P., Opitz, T., Steinbeck, J.A., Ladewig, J., and Brüstle, O. (2009). A rosette-type, self-renewing human ES cell-derived neural stem cell with potential for in vitro instruction and synaptic integration. Proc. Natl. Acad. Sci. U. S. A. *106*, 3225–3230.

Koelliker, A. (1896). Handbuch der Gewebelehre des Menschen. J. Anat. Physiol. *31*, 1–896.

Kondoh, H., Lleonart, M.E., Nakashima, Y., Yokode, M., Tanaka, M., Bernard, D., Gil, J., and Beach, D. (2007). A high glycolytic flux supports the proliferative potential of murine embryonic stem cells. Antioxidants Redox Signal. *9*, 293–299.

Kornack, D.R., and Rakic, P. (1995). Radial and horizontal deployment of clonally related cells in the primate neocortex: Relationship to distinct mitotic lineages. Neuron *15*, 311–321.

Kostovic, I., and Rakic, P. (1990). Developmental history of the transient subplate zone in the visual and somatosensory cortex of the macaque monkey and human brain. J. Comp. Neurol. *297*, 441–470.

Kowalczyk, T., Pontious, A., Englund, C., Daza, R.A.M., Bedogni, F., Hodge, R., Attardo, A., Bell, C., Huttner, W.B., and Hevner, R.F. (2009). Intermediate neuronal progenitors (basal progenitors) produce pyramidal-projection neurons for all layers of cerebral cortex. Cereb. Cortex *19*, 2439–2450.

Koyanagi-Aoi, M., Ohnuki, M., Takahashi, K., Okita, K., Noma, H., Sawamura, Y., Teramoto, I., Narita, M., Sato, Y., Ichisaka, T., et al. (2013). Differentiation-defective phenotypes revealed by large-scale analyses of human pluripotent stem cells. Proc. Natl. Acad. Sci. U. S. A. *110*, 20569–20574.

Kriegstein, A., and Alvarez-Buylla, A. (2009). The glial nature of embryonic and adult neural stem cells. Annu. Rev. Neurosci. *32*, 149–184.

Krisher, R.L., and Prather, R.S. (2012). A role for the Warburg effect in preimplantation embryo development: Metabolic modification to support rapid cell proliferation. Mol. Reprod. Dev. *79*, 311–320.

Kuan, C.-Y.Y., Roth, K.A., Flavell, R.A., and Rakic, P. (2000). Mechanisms of programmed cell death in the developing brain. Trends Neurosci. *23*, 291–297.

Kuang, Y.-L., Munoz, A., Nalula, G., Santostefano, K.E., Sanghez, V., Sanchez, G., Terada, N., Mattis, A.N., Iacovino, M., Iribarren, C., et al. (2019). Evaluation of commonly used ectoderm markers in iPSC trilineage differentiation. Stem Cell Res. *37*, 101434.

Kudin, A.P., Bimpong-Buta, N.Y.B., Vielhaber, S., Elger, C.E., and Kunz, W.S. (2004).

Characterization of Superoxide-producing Sites in Isolated Brain Mitochondria. J. Biol. Chem. *279*, 4127–4135.

Kühlbrandt, W., and Davies, K.M. (2016). Rotary ATPases: A New Twist to an Ancient Machine. Trends Biochem. Sci. *41*, 106–116.

Kumar, R., Bukowski, M.J., Wider, J.M., Reynolds, C.A., Calo, L., Lepore, B., Tousignant, R., Jones, M., Przyklenk, K., and Sanderson, T.H. (2016). Mitochondrial dynamics following global cerebral ischemia. Mol. Cell. Neurosci. *76*, 68–75.

Kumps, A., Duez, P., and Mardens, Y. (2002). Metabolic, nutritional, iatrogenic, and artifactual sources of urinary organic acids: A comprehensive table. Clin. Chem.

Kwan, K.Y., Lam, M.M.S., Krsnik, Ž., Kawasawa, Y.I., Lefebvre, V., and Šestan, N. (2008). SOX5 postmitotically regulates migration, postmigratory differentiation, and projections of subplate and deep-layer neocortical neurons. Proc. Natl. Acad. Sci. U. S. A. *105*, 16021–16026.

Lages, Y.M., Nascimento, J.M., Lemos, G.A., Galina, A., Castilho, L.R., and Rehen, S.K. (2015). Low oxygen alters mitochondrial function and response to oxidative stress in human neural progenitor cells. PeerJ *2015*, e1486.

Lai, T., Jabaudon, D., Molyneaux, B.J., Azim, E., Arlotta, P., Menezes, J.R.L., and Macklis, J.D. (2008). SOX5 Controls the Sequential Generation of Distinct Corticofugal Neuron Subtypes. Neuron *57*, 232–247.

Lake, N.J., Bird, M.J., Isohanni, P., and Paetau, A. (2015). Leigh syndrome: neuropathology and pathogenesis. J. Neuropathol. Exp. Neurol. *74*, 482–492.

Lake, N.J., Compton, A.G., Rahman, S., and Thorburn, D.R. (2016). Leigh syndrome: One disorder, more than 75 monogenic causes. Ann. Neurol. *79*, 190–203.

Lancaster, M.A., and Knoblich, J.A. (2014). Generation of cerebral organoids from human pluripotent stem cells. Nat. Protoc. *9*, 2329–2340.

Lancaster, M.A., Renner, M., Martin, C.A., Wenzel, D., Bicknell, L.S., Hurles, M.E., Homfray, T., Penninger, J.M., Jackson, A.P., and Knoblich, J.A. (2013). Cerebral organoids model human brain development and microcephaly. Nature *501*, 373–379.

Lancaster, M.A., Corsini, N.S., Wolfinger, S., Gustafson, E.H., Phillips, A.W., Burkard, T.R., Otani, T., Livesey, F.J., and Knoblich, J.A. (2017). Guided self-organization and cortical plate formation in human brain organoids. Nat. Biotechnol. *35*, 659–666.

Laughton, J.D., Bittar, P., Charnay, Y., Pellerin, L., Kovari, E., Magistretti, P.J., and Bouras, C. (2007). Metabolic compartmentalization in the human cortex and hippocampus: evidence for a cell- and region-specific localization of lactate dehydrogenase 5 and pyruvate dehydrogenase. BMC Neurosci. *8*, 35.

Lee, K.J., and Jessell, T.M. (1999). The specification of dorsal cell fates in the vertebrate central nervous system. Annu. Rev. Neurosci. *22*, 261–294.

Lee, H., Shamy, G. Al, Elkabetz, Y., Schofield, C.M., Harrsion, N.L., Panagiotakos, G., Socci, N.D., Tabar, V., and Studer, L. (2007). Directed Differentiation and Transplantation of Human Embryonic Stem Cell-Derived Motoneurons. Stem Cells *25*, 1931–1939.

Lee, K.J., Mendelsohn, M., and Jessell, T.M. (1998). Neuronal patterning by BMPs: a requirement for GDF7 in the generation of a discrete class of commissural interneurons in the mouse spinal cord. Genes Dev. *12*, 3394–3407.

Leelatian, N., Doxie, D.B., Greenplate, A.R., Mobley, B.C., Lehman, J.M., Sinnaeve, J., Kauffmann, R.M., Werkhaven, J.A., Mistry, A.M., Weaver, K.D., et al. (2017). Single cell analysis of human tissues and solid tumors with mass cytometry. Cytom. Part B Clin. Cytom. *92*, 68–78.

Leigh, D. (1951). Subacute necrotizing encephalomyelopathy in an infant. J. Neurol. Neurosurg. Psychiatry *14*, 216–221.

Leingärtner, A., Richards, L.J., Dyck, R.H., Akazawa, C., and O'Leary, D.D.M. (2003). Cloning and cortical expression of rat Emx2 and adenovirus-mediated overexpression to assess its regulation of area-specific targeting of thalamocortical axons. Cereb. Cortex *13*, 648–660.

Leonard, A.P., Cameron, R.B., Speiser, J.L., Wolf, B.J., Peterson, Y.K., Schnellmann, R.G., Beeson, C.C., and Rohrer, B. (2015). Quantitative analysis of mitochondrial morphology and membrane potential in living cells using high-content imaging, machine learning, and morphological binning. Biochim. Biophys. Acta - Mol. Cell Res. *1853*, 348–360.

Leone, D.P., Srinivasan, K., Chen, B., Alcamo, E., and McConnell, S.K. (2008). The determination of projection neuron identity in the developing cerebral cortex. Curr. Opin. Neurobiol. *18*, 28–35.

Letts, J.A., and Sazanov, L.A. (2017). Clarifying the supercomplex: The higher-order organization of the mitochondrial electron transport chain. Nat. Struct. Mol. Biol. *24*, 800–808.

Levitt, P., and Rakic, P. (1980). Immunoperoxidase localization of glial fibrillary acidic protein in radial glial cells and astrocytes of the developing rhesus monkey brain. J. Comp. Neurol. *193*, 815–840.

Li, H., Chen, Y., Jones, A.F., Sanger, R.H., Collis, L.P., Flannery, R., McNay, E.C., Yu, T., Schwarzenbacher, R., Bossy, B., et al. (2008). Bcl-xL induces Drp1-dependent synapse formation in cultured hippocampal neurons. Proc. Natl. Acad. Sci. U. S. A. *105*, 2169–2174.

Li, H., Alavian, K.N., Lazrove, E., Mehta, N., Jones, A., Zhang, P., Licznerski, P., Graham, M., Uo, T., Guo, J., et al. (2013). A Bcl-x L -Drp1 complex regulates synaptic vesicle membrane dynamics during endocytosis. Nat. Cell Biol. *15*, 773–785.

Li, X.J., Du, Z.W., Zarnowska, E.D., Pankratz, M., Hansen, L.O., Pearce, R.A., and Zhang, S.C. (2005). Specification of motoneurons from human embryonic stem cells. Nat. Biotechnol. *23*, 215–221.

Li, X.J., Zhang, X., Johnson, M.A., Wang, Z.B., LaVaute, T., and Zhang, S.C. (2009). Coordination of sonic hedgehog and Wnt signaling determines ventral and dorsal telencephalic neuron types from human embryonic stem cells. Development *136*, 4055–4063.

Liddelow, S.A., and Barres, B.A. (2017). Reactive Astrocytes: Production, Function, and Therapeutic Potential. Immunity *46*, 957–967.

Liddelow, S.A., Guttenplan, K.A., Clarke, L.E., Bennett, F.C., Bohlen, C.J., Schirmer, L., Bennett, M.L., Münch, A.E., Chung, W.-S.S., Peterson, T.C., et al. (2017). Neurotoxic reactive astrocytes are induced by activated microglia. Nature *541*, 481–487.

Lieberman, O.J., McGuirt, A.F., Tang, G., and Sulzer, D. (2019). Roles for neuronal and glial autophagy in synaptic pruning during development. Neurobiol. Dis. *122*, 49–63.

Liem, J., Jessell, T.M., and Briscoe, J. (2000). Regulation of the neural patterning activity of sonic hedgehog by secreted BMP inhibitors expressed by notochord and somites. Development *127*,

4855–4866.

Liesa, M., and Shirihai, O.S. (2013). Mitochondrial dynamics in the regulation of nutrient utilization and energy expenditure. Cell Metab. *17*, 491–506.

Lima, J.P.M., Rayêe, D., Silva-Rodrigues, T., Pereira, P.R.P., Mendonca, A.P.M., Rodrigues-Ferreira, C., Szczupak, D., Fonseca, A., Oliveira, M.F., Lima, F.R.S., et al. (2018). Perinatal Asphyxia and Brain Development: Mitochondrial Damage Without Anatomical or Cellular Losses. Mol. Neurobiol. *55*, 8668–8679.

Lissens, W., De Meirleir, L., Seneca, S., Liebaers, I., Brown, G.K., Brown, R.M., Ito, M., Naito, E., Kuroda, Y., Kerr, D.S., et al. (2000). Mutations in the X-linked pyruvate dehydrogenase (E1) α subunit gene (PDHA1) in patients with a pyruvate dehydrogenase complex deficiency. Hum. Mutat. *15*, 209–219.

Liu, Y., Liu, H., Sauvey, C., Yao, L., Zarnowska, E.D., and Zhang, S.C. (2013). Directed differentiation of forebrain GABA interneurons from human pluripotent stem cells. Nat. Protoc. *8*, 1670–1679.

Lodato, S., Molyneaux, B.J., Zuccaro, E., Goff, L.A., Chen, H.H., Yuan, W., Meleski, A., Takahashi, E., Mahony, S., Rinn, J.L., et al. (2014). Gene co-regulation by Fezf2 selects neurotransmitter identity and connectivity of corticospinal neurons. Nat. Neurosci. *17*, 1046–1054.

Lorenz, C., Lesimple, P., Bukowiecki, R., Zink, A., Inak, G., Mlody, B., Singh, M., Semtner, M., Mah, N., Auré, K., et al. (2017). Human iPSC-Derived Neural Progenitors Are an Effective Drug Discovery Model for Neurological mtDNA Disorders. Cell Stem Cell *20*, 659-674.e9.

Lui, J.H., Hansen, D. V., and Kriegstein, A.R. (2011). Development and evolution of the human neocortex. Cell *146*, 18–36.

Di Lullo, E., and Kriegstein, A.R. (2017). The use of brain organoids to investigate neural development and disease. Nat. Rev. Neurosci. *18*, 573–584.

Lv, X., Ren, S.-Q., Zhang, X.-J., Shen, Z., Ghosh, T., Xianyu, A., Gao, P., Li, Z., Lin, S., Yu, Y., et al. (2019). TBR2 coordinates neurogenesis expansion and precise microcircuit organization via Protocadherin 19 in the mammalian cortex. Nat. Commun. *10*, 3946.

Ma, H., Folmes, C.D.L., Wu, J., Morey, R., Mora-Castilla, S., Ocampo, A., Ma, L., Poulton, J., Wang,

X., Ahmed, R., et al. (2015). Metabolic rescue in pluripotent cells from patients with mtDNA disease. Nature *524*, 234–238.

Magini, G. (1888). Nouvelles recherches histologiques sur le cerveau du foetus. Arch. Ital. Biol. *10*, 384–387.

Malatesta, P., Hartfuss, E., and Götz, M. (2000). Isolation of radial glial cells by fluorescent-activated cell sorting reveals a neural lineage. Development *127*, 5253–5263.

Malatesta, P., Hack, M.A., Hartfuss, E., Kettenmann, H., Klinkert, W., Kirchhoff, F., and Götz, M. (2003). Neuronal or glial progeny: Regional differences in radial glia fate. Neuron *37*, 751–764.

Manabe, N., Hirai, S.I., Imai, F., Nakanishi, H., Takai, Y., and Ohno, S. (2002). Association of ASIP/mPAR-3 with adherens junctions of mouse neuroepithelial cells. Dev. Dyn. *225*, 61–69.

Mandal, S., Lindgren, A.G., Srivastava, A.S., Clark, A.T., and Banerjee, U. (2011). Mitochondrial Function Controls Proliferation and Early Differentiation Potential of Embryonic Stem Cells. Stem Cells *29*, 486–495.

Manes, C., and Lai, N.C. (1995). Nonmitochondrial oxygen utilization by rabbit blastocytes and surface production of superoxide radicals. J. Reprod. Fertil. *104*, 69–75.

Manoli, I., and Venditti, C.P. (2016). Disorders of branched chain amino acid metabolism. Transl. Sci. Rare Dis. *1*, 91–110.

Mariani, J., Simonini, M.V., Palejev, D., Tomasini, L., Coppola, G., Szekely, A.M., Horvath, T.L., and Vaccarino, F.M. (2012). Modeling human cortical development in vitro using induced pluripotent stem cells. Proc. Natl. Acad. Sci. *109*, 12770–12775.

Marin-Padilla, M. (1978). Dual origin of the mammalian neocortex and evolution of the cortical plate. Anat. Embryol. (Berl). *152*, 109–126.

Marín-Padilla, M. (2014). The mammalian neocortex new pyramidal neuron: A new conception. Front. Neuroanat. *7*, 51.

Maroof, A.M., Keros, S., Tyson, J.A., Ying, S.W., Ganat, Y.M., Merkle, F.T., Liu, B., Goulburn, A., Stanley, E.G., Elefanty, A.G., et al. (2013). Directed differentiation and functional maturation of

cortical interneurons from human embryonic stem cells. Cell Stem Cell *12*, 559–572.

Martínez-Cerdeño, V., Noctor, S.C., and Kriegstein, A.R. (2006). The role of intermediate progenitor cells in the evolutionary expansion of the cerebral cortex. Cereb. Cortex *16*.

Martínez-Reyes, I., and Chandel, N.S. (2020). Mitochondrial TCA cycle metabolites control physiology and disease. Nat. Commun. *11*.

Marton, R.M., Miura, Y., Sloan, S.A., Li, Q., Revah, O., Levy, R.J., Huguenard, J.R., and Pașca, S.P. (2019). Differentiation and maturation of oligodendrocytes in human three-dimensional neural cultures. Nat. Neurosci. *22*, 484–491.

McEvilly, R.J., Ortiz de Diaz, M., Schonemann, M.D., Hooshmand, F., and Rosenfeld, M.G. (2002). Transcriptional regulation of cortical neuron migration by POU domain factors. Science (80-.). *295*, 1528–1532.

McGrew, L.L., Lai, C.J., and Moon, R.T. (1995). Specification of the Anteroposterior Neural Axis through Synergistic Interaction of the Wnt Signaling Cascade withnogginandfollistatin. Dev. Biol. *172*, 337–342.

McKenna, W.L., Betancourt, J., Larkin, K.A., Abrams, B., Guo, C., Rubenstein, J.L.R., and Chen, B. (2011). Tbr1 and Fezf2 regulate alternate corticofugal neuronal identities during neocortical development. J. Neurosci. *31*, 549–564.

McTague, A., Rossignoli, G., Ferrini, A., Barral, S., and Kurian, M.A. (2021). Genome Editing in iPSC-Based Neural Systems: From Disease Models to Future Therapeutic Strategies. Front. Genome Ed. *3*, 8.

Medelnik, J.-P., Roensch, K., Okawa, S., del Sol, A., Chara, O., Mchedlishvili, L., and Tanaka, E.M. (2018). Signaling-Dependent Control of Apical Membrane Size and Self-Renewal in Rosette-Stage Human Neuroepithelial Stem Cells. Stem Cell Reports *10*, 1751–1765.

Meijer, M., Rehbach, K., Brunner, J.W., Classen, J.A., Lammertse, H.C.A., van Linge, L.A., Schut, D., Krutenko, T., Hebisch, M., Cornelisse, L.N., et al. (2019). A Single-Cell Model for Synaptic Transmission and Plasticity in Human iPSC-Derived Neurons. Cell Rep. *27*, 2199-2211.e6.

Mekki-Dauriac, S., Agius, E., Kan, P., and Cochard, P. (2002). Bone morphogenetic proteins

negatively control oligodendrocyte precursor specification in the chick spinal cord. Development *129*, 5117–5130.

Di Meo, I., Marchet, S., Lamperti, C., Zeviani, M., and Viscomi, C. (2017). AAV9-based gene therapy partially ameliorates the clinical phenotype of a mouse model of Leigh syndrome. Gene Ther. *24*, 661–667.

Mertens, J., Reid, D., Lau, S., Kim, Y., and Gage, F.H. (2018). Aging in a dish: IPSC-derived and directly induced neurons for studying brain aging and age-related neurodegenerative diseases. Annu. Rev. Genet. *52*, 271–293.

Meshrkey, F., Cabrera Ayuso, A., Rao, R.R., and Iyer, S. (2021). Quantitative analysis of mitochondrial morphologies in human induced pluripotent stem cells for Leigh syndrome. Stem Cell Res. *57*, 102572.

Migeon, B.R. (2020). X-linked diseases: susceptible females. Genet. Med. *22*, 1156–1174.

Miller, D.J., Bhaduri, A., Sestan, N., and Kriegstein, A. (2019). Shared and derived features of cellular diversity in the human cerebral cortex. Curr. Opin. Neurobiol. *56*, 117–124.

Mione, M.C., Cavanagh, J.F.R., Harris, B., and Parnavelas, J.G. (1997). Cell fate specification and symmetrical/asymmetrical divisions in the developing cerebral cortex. J. Neurosci. *17*, 2018–2929.

Miura, Y., Li, M.Y., Birey, F., Ikeda, K., Revah, O., Thete, M.V., Park, J.Y., Puno, A., Lee, S.H., Porteus, M.H., et al. (2020). Generation of human striatal organoids and cortico-striatal assembloids from human pluripotent stem cells. Nat. Biotechnol. *38*, 1421–1430.

Miyata, T., Kawaguchi, A., Okano, H., and Ogawa, M. (2001). Asymmetric inheritance of radial glial fibers by cortical neurons. Neuron *31*, 727–741.

Molnár, Z., and Pollen, A. (2014). How unique is the human neocortex? Development *141*, 11–16.

Molnár, Z., Clowry, G.J., Šestan, N., Alzu'bi, A., Bakken, T., Hevner, R.F., Hüppi, P.S., Kostović, I., Rakic, P., Anton, E.S., et al. (2019). New insights into the development of the human cerebral cortex. J. Anat. *235*, 432–451.

Molyneaux, B.J., Arlotta, P., Menezes, J.R.L., and Macklis, J.D. (2007). Neuronal subtype specification in the cerebral cortex. Nat. Rev. Neurosci. *8*, 427–437.

Molyneaux, B.J., Arlotta, P., Fame, R.M., MacDonald, J.L., MacQuarrie, K.L., and Macklis, J.D. (2009). Novel subtype-specific genes identify distinct subpopulations of callosal projection neurons. J. Neurosci. *29*, 12343–12354.

Monsoro-Burq, A.H., Wang, E., and Harland, R. (2005). Msx1 and Pax3 cooperate to mediate FGF8 and WNT signals during Xenopus neural crest induction. Dev. Cell *8*, 167–178.

Mujtaba, T., Piper, D.R., Kalyani, A., Groves, A.K., Lucero, M.T., and Rao, M.S. (1999). Lineage-restricted neural precursors can be isolated from both the mouse neural tube and cultured ES cells. Dev. Biol. *214*, 113–127.

Muller, B., Lewis, N., Adeniyi, T., Leese, H.J., Brison, D.R., and Sturmey, R.G. (2019). Application of extracellular flux analysis for determining mitochondrial function in mammalian oocytes and early embryos. Sci. Rep. *9*, 1–14.

Müller, F.J., Schuldt, B.M., Williams, R., Mason, D., Altun, G., Papapetrou, E.P., Danner, S., Goldmann, J.E., Herbst, A., Schmidt, N.O., et al. (2011). A bioinformatic assay for pluripotency in human cells. Nat. Methods *8*, 315–317.

Muñoz-Sanjuán, I., and Brivanlou, A.H. (2002). Neural induction, the default model and embryonic stem cells. Nat. Rev. Neurosci. *3*, 271–280.

Muratore, C.R., Srikanth, P., Callahan, D.G., and Young-Pearse, T.L. (2014). Comparison and optimization of hiPSC forebrain cortical differentiation protocols. PLoS One *9*, e105807.

Murciano, A., Zamora, J., López-Sánchez, J., and Frade, J.M. (2002). Interkinetic nuclear movement may provide spatial clues to the regulation of neurogenesis. Mol. Cell. Neurosci. *21*, 285–300.

Namihira, M., Kohyama, J., Semi, K., Sanosaka, T., Deneen, B., Taga, T., and Nakashima, K. (2009). Committed Neuronal Precursors Confer Astrocytic Potential on Residual Neural Precursor Cells. Dev. Cell *16*, 245–255.

Nat, R., Nilbratt, M., Narkilahti, S., Winblad, B., Hovatta, O., and Nordberg, A. (2007). Neurogenic

neuroepithelial and radial glial cells generated from six human embryonic stem cell lines in serum-free suspension and adherent cultures. Glia *55*, 385–399.

National Academies of Sciences, Engineering, and M. (2021). The Emerging Field of Human Neural Organoids, Transplants, and Chimeras (Washington, D.C.: National Academies Press).

Nguyen, V.H., Trout, J., Connors, S.A., Andermann, P., Weinberg, E., and Mullins, M.C. (2000). Dorsal and intermediate neuronal cell types of the spinal cord are established by a BMP signaling pathway. Development *127*, 1209–1220.

Niatsetskaya, Z. V., Sosunov, S.A., Matsiukevich, D., Utkina-Sosunova, I. V., Ratner, V.I., Starkov, A.A., and Ten, V.S. (2012). The Oxygen Free Radicals Originating from Mitochondrial Complex I Contribute to Oxidative Brain Injury Following Hypoxia-Ischemia in Neonatal Mice. J. Neurosci. *32*, 3235–3244.

Nicholas, C.R., Chen, J., Tang, Y., Southwell, D.G., Chalmers, N., Vogt, D., Arnold, C.M., Chen, Y.J.J., Stanley, E.G., Elefanty, A.G., et al. (2013). Functional maturation of hPSC-derived forebrain interneurons requires an extended timeline and mimics human neural development. Cell Stem Cell *12*, 573–586.

Nieto, M., Monuki, E.S., Tang, H., Imitola, J., Haubst, N., Khoury, S.J., Cunningham, J., Gotz, M., and Walsh, C.A. (2004). Expression of Cux-1 and Cux-2 in the subventricular zone and upper layers II-IV of the cerebral cortex. J. Comp. Neurol. *479*, 168–180.

Noctor, S.C., Flint, A.C., Weissman, T.A., Dammerman, R.S., and Kriegstein, A.R. (2001). Neurons derived from radial glial cells establish radial units in neocortex. Nature *409*, 714–720.

Noctor, S.C., Martínez-Cerdeño, V., and Kriegstein, A.R. (2008). Distinct behaviors of neural stem and progenitor cells underlie cortical neurogenesis. J. Comp. Neurol. *508*, 28–44.

Noguchi, M., and Kasahara, A. (2017). Mitochondrial dynamics coordinate cell differentiation. Biochem. Biophys. Res. Commun.

Nonomura, K., Yamaguchi, Y., Hamachi, M., Koike, M., Uchiyama, Y., Nakazato, K., Mochizuki, A., Sakaue-Sawano, A., Miyawaki, A., Yoshida, H., et al. (2013). Local apoptosis modulates early mammalian brain development through the elimination of morphogen-producing cells. Dev. Cell

27, 621–634.

Northington, F.J., Flock, D.L., Martin, L.J., and Ferriero, D.M. (2001). Delayed neurodegeneration in neonatal rat thalamus after hypoxia-ischemia is apoptosis. J. Neurosci. *21*, 1931–1938.

Nowakowski, T.J., Bhaduri, A., Pollen, A.A., Alvarado, B., Mostajo-Radji, M.A., Di Lullo, E., Haeussler, M., Sandoval-Espinosa, C., Liu, S.J., Velmeshev, D., et al. (2017). Spatiotemporal gene expression trajectories reveal developmental hierarchies of the human cortex. Science (80-.). *358*, 1318–1323.

O'Rahilly, R., and Müller, F. (2005). The Embryonic Human Brain: An Atlas of Developmental Stages, Third Edition (Hoboken, NJ, USA: John Wiley & Sons, Inc.).

O'Rahilly, R., and Müller, F. (2008). Significant features in the early prenatal development of the human brain. Ann. Anat. *190*, 105–118.

O'Rahilly, R., and Müller, F. (2010). Developmental stages in human embryos: Revised and new measurements. Cells Tissues Organs *192*, 73–84.

Ognjenović, J., and Simonović, M. (2018). Human aminoacyl-tRNA synthetases in diseases of the nervous system. RNA Biol. *15*, 623–634.

Okabe, S., Forsberg-Nilsson, K., Spiro, A.C., Segal, M., and McKay, R.D.G. (1996). Development of neuronal precursor cells and functional postmitotic neurons from embryonic stem cells in vitro. Mech. Dev. *59*, 89–102.

Orentas, D.M., Hayes, J.E., Dyer, K.L., and Miller, R.H. (1999). Sonic hedgehog signaling is required during the appearance of spinal cord oligodendrocyte precursors. Development *126*, 2419–2429.

Oshida, K., Shimizu, T., Takase, M., Tamura, Y., Shimizu, T., and Yamashiro, Y. (2003). Effects of dietary sphingomyelin on central nervous system myelination in developing rats. Pediatr. Res. *53*, 589–593.

Pampaloni, F., Reynaud, E.G., and Stelzer, E.H.K. (2007). The third dimension bridges the gap between cell culture and live tissue. Nat. Rev. Mol. Cell Biol. *8*, 839–845.

Pang, Z.P., Yang, N., Vierbuchen, T., Ostermeier, A., Fuentes, D.R., Yang, T.Q., Citri, A., Sebastiano,

V., Marro, S., Südhof, T.C., et al. (2011). Induction of human neuronal cells by defined transcription factors. Nature *476*, 220–223.

Pankratz, M.T., Li, X.-J., LaVaute, T.M., Lyons, E.A., Chen, X., and Zhang, S.-C. (2007). Directed Neural Differentiation of Human Embryonic Stem Cells via an Obligated Primitive Anterior Stage. Stem Cells *25*, 1511–1520.

Parikh, S., Goldstein, A., Karaa, A., Koenig, M.K., Anselm, I., Brunel-Guitton, C., Christodoulou, J., Cohen, B.H., Dimmock, D., Enns, G.M., et al. (2017). Patient care standards for primary mitochondrial disease: A consensus statement from the mitochondrial medicine society. Genet. Med. *19*, 1–18.

Paşca, A.M., Sloan, S.A., Clarke, L.E., Tian, Y., Makinson, C.D., Huber, N., Kim, C.H., Park, J.-Y., O'Rourke, N.A., Nguyen, K.D., et al. (2015). Functional cortical neurons and astrocytes from human pluripotent stem cells in 3D culture. Nat. Methods *12*, 671–678.

Pașca, S.P. (2018). The rise of three-dimensional human brain cultures. Nature *553*, 437–445.

Pașca, A.M., Park, J.Y., Shin, H.W., Qi, Q., Revah, O., Krasnoff, R., O'Hara, R., Willsey, A.J., Palmer, T.D., and Pașca, S.P. (2019). Human 3D cellular model of hypoxic brain injury of prematurity. Nat. Med. 1.

Pastores, G.M., Santorelli, F.M., Shanske, S., Gelb, B.D., Fyfe, B., Wolfe, D., and Willner, J.P. (1994). Leigh syndrome and hypertrophic cardiomyopathy in an infant with a mitochondrial DNA point mutation (T8993G). Am. J. Med. Genet. *50*, 265–271.

Perrier, A.L., Tabar, V., Barberi, T., Rubio, M.E., Bruses, J., Topf, N., Harrison, N.L., and Studer, L. (2004). Derivation of midbrain dopamine neurons from human embryonic stem cells. Proc. Natl. Acad. Sci. U. S. A. *101*, 12543–12548.

Petanjek, Z., Judaš, M., Kostović, I., and Uylings, H.B.M. (2008). Lifespan alterations of basal dendritic trees of pyramidal neurons in the human prefrontal cortex: A layer-specific pattern. Cereb. Cortex *18*, 915–929.

Petanjek, Z., Judaš, M., Šimić, G., Rašin, M.R., Uylings, H.B.M., Rakic, P., and Kostović, I. (2011). Extraordinary neoteny of synaptic spines in the human prefrontal cortex. Proc. Natl. Acad. Sci. U.

S. A. *108*, 13281–13286.

Petryniak, M.A., Potter, G.B., Rowitch, D.H., and Rubenstein, J.L.R. (2007). Dlx1 and Dlx2 Control Neuronal versus Oligodendroglial Cell Fate Acquisition in the Developing Forebrain. Neuron *55*, 417–433.

Pfisterer, U., Wood, J., Nihlberg, K., Hallgren, O., Bjermer, L., Westergren-Thorsson, G., Lindvall, O., and Parmar, M. (2011a). Efficient induction of functional neurons from adult human fibroblasts. Cell Cycle *10*, 3311–3316.

Pfisterer, U., Kirkeby, A., Torper, O., Wood, J., Nelander, J., Dufour, A., Björklund, A., Lindvall, O., Jakobsson, J., and Parmar, M. (2011b). Direct conversion of human fibroblasts to dopaminergic neurons. Proc. Natl. Acad. Sci. U. S. A. *108*, 10343–10348.

Picard, M., and McEwen, B.S. (2014). Mitochondria impact brain function and cognition. Proc. Natl. Acad. Sci. *111*, 7–8.

Di Pietro, N.C., Whiteley, L., and Illes, J. (2012). Treatments and services for neurodevelopmental disorders on advocacy websites: Information or evaluation? Neuroethics *5*, 197–209.

Pilaz, L.J., Patti, D., Marcy, G., Ollier, E., Pfister, S., Douglas, R.J., Betizeau, M., Gautier, E., Cortay, V., Doerflinger, N., et al. (2009). Forced G1-phase reduction alters mode of division, neuron number, and laminar phenotype in the cerebral cortex. Proc. Natl. Acad. Sci. U. S. A. *106*, 21924–21929.

Pixley, S.K.R., and de Vellis, J. (1984). Transition between immature radial glia and mature astrocytes studied with a monoclonal antibody to vimentin. Dev. Brain Res. *15*, 201–209.

Pliss, L., Pentney, R.J., Johnson, M.T., and Patel, M.S. (2004). Biochemical and structural brain alterations in female mice with cerebral pyruvate dehydrogenase deficiency. J. Neurochem. *91*, 1082–1091.

Pollen, A.A., Nowakowski, T.J., Chen, J., Retallack, H., Sandoval-Espinosa, C., Nicholas, C.R., Shuga, J., Liu, S.J., Oldham, M.C., Diaz, A., et al. (2015). Molecular Identity of Human Outer Radial Glia during Cortical Development. Cell *163*, 55–67.

Power, R.M., and Huisken, J. (2017). A guide to light-sheet fluorescence microscopy for multiscale

imaging. Nat. Methods *14*, 360–373.

Praefcke, G.J.K., and McMahon, H.T. (2004). The dynamin superfamily: Universal membrane tubulation and fission molecules? Nat. Rev. Mol. Cell Biol. *5*, 133–147.

Presidential Commission for the Study of Bioethical (2015). Gray Matters: Integrative Approaches for Neuroscience, Ethics, and Society. *19*, 305–326.

Pressler, R., and Auvin, S. (2013). Comparison of brain maturation among species: An example in translational research suggesting the possible use of bumetanide in newborn. Front. Neurol. *4 APR*, 1.

Prieto, J., León, M., Ponsoda, X., Sendra, R., Bort, R., Ferrer-Lorente, R., Raya, A., López-Garciá, C., Torres, J., López-García, C., et al. (2016). Early ERK1/2 activation promotes DRP1-dependent mitochondrial fission necessary for cell reprogramming. Nat. Commun. *7*, 1–13.

Prigione, A., Fauler, B., Lurz, R., Lehrach, H., and Adjaye, J. (2010). The Senescence-Related Mitochondrial/Oxidative Stress Pathway is Repressed in Human Induced Pluripotent Stem Cells. Stem Cells *28*, 721–733.

Puka-Sundvall, M., Gajkowska, B., Cholewinski, M., Blomgren, K., Lazarewicz, J.W., and Hagberg, H. (2000). Subcellular distribution of calcium and ultrastructural changes after cerebral hypoxia-ischemia in immature rats. Dev. Brain Res. *125*, 31–41.

Qi, Y., Zhang, X.-J., Renier, N., Wu, Z., Atkin, T., Sun, Z., Ozair, M.Z., Tchieu, J., Zimmer, B., Fattahi, F., et al. (2017). Combined small-molecule inhibition accelerates the derivation of functional cortical neurons from human pluripotent stem cells. Nat. Biotechnol. *35*, 154–163.

Qian, L., and TCW, J. (2021). Human iPSC-Based Modeling of Central Nerve System Disorders for Drug Discovery. Int. J. Mol. Sci. *22*, 1–36.

Qian, X., Goderie, S.K., Shen, Q., Stern, J.H., and Temple, S. (1998). Intrinsic programs of patterned cell lineages in isolated vertebrate CNS ventricular zone cells. Development *125*, 3143–3152.

Qian, X., Nguyen, H.N., Song, M.M., Hadiono, C., Ogden, S.C., Hammack, C., Yao, B., Hamersky, G.R., Jacob, F., Zhong, C., et al. (2016). Brain-Region-Specific Organoids Using Mini-bioreactors for Modeling ZIKV Exposure. Cell *165*, 1238–1254.

Qian, X., Jacob, F., Song, M.M., Nguyen, H.N., Song, H., and Ming, G.L. (2018). Generation of human brain region–specific organoids using a miniaturized spinning bioreactor. Nat. Protoc. *13*, 565–580.

Qian, X., Song, H., and Ming, G.L. (2019). Brain organoids: Advances, applications and challenges. Development *146*.

Quadrato, G., Brown, J., and Arlotta, P. (2016). The promises and challenges of human brain organoids as models of neuropsychiatric disease. Nat. Med. *22*, 1220–1228.

Quadrato, G., Nguyen, T., Macosko, E.Z., Sherwood, J.L., Yang, S.M., Berger, D.R., Maria, N., Scholvin, J., Goldman, M., Kinney, J.P., et al. (2017). Cell diversity and network dynamics in photosensitive human brain organoids. Nature *545*, 48–53.

Quintana, A., Kruse, S.E., Kapur, R.P., Sanz, E., and Palmiter, R.D. (2010). Complex I deficiency due to loss of Ndufs4 in the brain results in progressive encephalopathy resembling Leigh syndrome. Proc. Natl. Acad. Sci. U. S. A. *107*, 10996–11001.

Raedler, E., and Raedler, A. (1978). Autoradiographic study of early neurogenesis in rat neocortex. Anat. Embryol. (Berl). *154*, 267–284.

Rafelski, S.M. (2013). Mitochondrial network morphology: Building an integrative, geometrical view. BMC Biol. *11*, 71.

Rahman, J., and Rahman, S. (2018). Mitochondrial medicine in the omics era. Lancet *391*, 2560–2574.

Raichle, M.E., and Gusnard, D.A. (2002). Appraising the brain's energy budget. Proc. Natl. Acad. Sci. *99*, 10237–10239.

Rakic, P. (1972). Mode of cell migration to the superficial layers of fetal monkey neocortex. J. Comp. Neurol. *145*, 61–83.

Rakic, P. (1978). Neuronal migration and contact guidance in the primate telencephalon. Postgrad. Med. J. *54 Suppl 1*, 25–40.

Ramonet, D., Perier, C., Recasens, A., Dehay, B., Bové, J., Costa, V., Scorrano, L., and Vila, M.

(2013). Optic atrophy 1 mediates mitochondria remodeling and dopaminergic neurodegeneration linked to complex i deficiency. Cell Death Differ. *20*, 77–85.

Rash, B.G., Duque, A., Morozov, Y.M., Arellano, J.I., Micali, N., and Rakic, P. (2019). Gliogenesis in the outer subventricular zone promotes enlargement and gyrification of the primate cerebrum. Proc. Natl. Acad. Sci. U. S. A. *116*, 7089–7094.

Rasmussen, M.L., Kline, L.A., Park, K.P., Ortolano, N.A., Romero-Morales, A.I., Anthony, C.C., Beckermann, K.E., and Gama, V. (2018). A Non-apoptotic Function of MCL-1 in Promoting Pluripotency and Modulating Mitochondrial Dynamics in Stem Cells. Stem Cell Reports *10*, 684–692.

Rasmussen, M.L., Taneja, N., Neininger, A.C., Wang, L., Robertson, G.L., Riffle, S.N., Shi, L., Knollmann, B.C., Burnette, D.T., and Gama, V. (2020). MCL-1 Inhibition by Selective BH3 Mimetics Disrupts Mitochondrial Dynamics Causing Loss of Viability and Functionality of Human Cardiomyocytes. IScience *23*, 101015.

Rastogi, A., Joshi, P., Contreras, E., and Gama, V. (2019). Remodeling of mitochondrial morphology and function: an emerging hallmark of cellular reprogramming. Cell Stress *3*, 181–194.

Reid, C.B., Tavazoie, S.F., and Walsh, C.A. (1997). Clonal dispersion and evidence for asymmetric cell division in ferret cortex. Development *124*, 2441–2450.

Rema, V., Bali, K.K., Ramachandra, R., Chugh, M., Darokhan, Z., and Chaudhary, R. (2008). Cytidine-5-diphosphocholine supplement in early life induces stable increase in dendritic complexity of neurons in the somatosensory cortex of adult rats. Neuroscience *155*, 556–564.

Renner, M., Lancaster, M.A., Bian, S., Choi, H., Ku, T., Peer, A., Chung, K., and Knoblich, J.A. (2017). Self-organized developmental patterning and differentiation in cerebral organoids. EMBO J.

Reubinoff, B.E., Itsykson, P., Turetsky, T., Pera, M.F., Reinhartz, E., Itzik, A., and Ben-Hur, T. (2001). Neural progenitors from human embryonic stem cells. Nat. Biotechnol. *19*, 1134–1140.

Rhee, H.J., Shaib, A.H., Rehbach, K., Lee, C.K., Seif, P., Thomas, C., Gideons, E., Guenther, A., Krutenko, T., Hebisch, M., et al. (2019). An Autaptic Culture System for Standardized Analyses of

iPSC-Derived Human Neurons. Cell Rep. *27*, 2212-2228.e7.

Ribes, V., and Briscoe, J. (2009). Establishing and interpreting graded Sonic Hedgehog signaling during vertebrate neural tube patterning: the role of negative feedback. Cold Spring Harb. Perspect. Biol. *1*, a002014.

Rice, D.S., and Curran, T. (2001). Role of the Reelin signaling pathway in central nervous system development. Annu. Rev. Neurosci. *24*, 1005–1039.

Richardson, W.D., Kessaris, N., and Pringle, N. (2006). Oligodendrocyte wars. Nat. Rev. Neurosci. *7*, 11–18.

Rieger, B., Junge, W., and Busch, K.B. (2014). Lateral pH gradient between OXPHOS complex IV and F(0)F(1) ATP-synthase in folded mitochondrial membranes. Nat. Commun. *5*, 3103.

Ring, K.L., Tong, L.M., Balestra, M.E., Javier, R., Andrews-Zwilling, Y., Li, G., Walker, D., Zhang, W.R., Kreitzer, A.C., and Huang, Y. (2012). Direct reprogramming of mouse and human fibroblasts into multipotent neural stem cells with a single factor. Cell Stem Cell *11*, 100–109.

Robel, S., Mori, T., Zoubaa, S., Schlegel, J., Sirko, S., Faissner, A., Goebbels, S., Dimou, L., and Götz, M. (2009). Conditional deletion of β1-integrin in astroglia causes partial reactive gliosis. Glia *57*, 1630–1647.

Robel, S., Berninger, B., and Götz, M. (2011). The stem cell potential of glia: Lessons from reactive gliosis. Nat. Rev. Neurosci. *12*, 88–104.

Roberts, B., Hendershott, M.C., Arakaki, J., Gerbin, K.A., Malik, H., Nelson, A., Gehring, J., Hookway, C., Ludmann, S.A., Yang, R., et al. (2019). Fluorescent Gene Tagging of Transcriptionally Silent Genes in hiPSCs. Stem Cell Reports *12*, 1145–1158.

Rodrigues, R.S., Lourenço, D.M., Paulo, S.L., Mateus, J.M., Ferreira, M.F., Mouro, F.M., Moreira, J.B., Ribeiro, F.F., Sebastião, A.M., and Xapelli, S. (2019). Cannabinoid actions on neural stem cells: Implications for pathophysiology. Molecules *24*, 1350.

Romero-Morales, A., Rastogi, A., Temuri, H., Rasmussen, M., McElroy, G.S., Hsu, L., Almonacid, P., Millis, B., Chandel, N., Cartailler, J.-P., et al. (2020). Human iPSC-derived cerebral organoids model features of Leigh Syndrome and reveal abnormal corticogenesis. BioRxiv

2020.04.21.054361.

Romero-Morales, A.I., O'Grady, B.J., Balotin, K.M., Bellan, L.M., Lippmann, E.S., and Gama, V. (2019). Spin∞ an improved miniaturized spinning bioreactor for the generation of human cerebral organoids from pluripotent stem cells. BioRxiv 687095.

Saha, K., and Jaenisch, R. (2009). Technical Challenges in Using Human Induced Pluripotent Stem Cells to Model Disease. Cell Stem Cell *5*, 584–595.

Saito, T., Hanai, S., Takashima, S., Nakagawa, E., Okazaki, S., Inoue, T., Miyata, R., Hoshino, K., Akashi, T., Sasaki, M., et al. (2011). Neocortical Layer Formation of Human Developing Brains and Lissencephalies: Consideration of Layer-Specific Marker Expression. Cereb. Cortex *21*, 588–596.

Salisbury-Ruf, C.T., Bertram, C.C., Vergeade, A., Lark, D.S., Shi, Q., Heberling, M.L., Fortune, N.L., Okoye, G.D., Jerome, W.G., Wells, Q.S., et al. (2018). Bid maintains mitochondrial cristae structure and function and protects against cardiac disease in an integrative genomics study. Elife *7*.

Samanta, J., and Kessler, J.A. (2004). Interactions between ID and OLIG proteins mediate the inhibitory effects of BMP4 on oligodendroglial differentiation. Development *131*, 4131–4142.

Sanderson, T.H., Raghunayakula, S., and Kumar, R. (2015). Neuronal hypoxia disrupts mitochondrial fusion. Neuroscience *301*, 71–78.

Sansom, S.N., Griffiths, D.S., Faedo, A., Kleinjan, D.-J., Ruan, Y., Smith, J., van Heyningen, V., Rubenstein, J.L., and Livesey, F.J. (2009). The Level of the Transcription Factor Pax6 Is Essential for Controlling the Balance between Neural Stem Cell Self-Renewal and Neurogenesis. PLoS Genet. *5*, e1000511.

Santore, M.T., McClintock, D.S., Lee, V.Y., Budinger, G.R.S., and Chandel, N.S. (2002). Anoxia-induced apoptosis occurs through a mitochondria-dependent pathway in lung epithelial cells. Am. J. Physiol. - Lung Cell. Mol. Physiol. *282*.

Sauer, F.C. (1935). Mitosis in the neural tube. J. Comp. Neurol. *62*, 377–405.

Sauerland, C., Menzies, B.R., Glatzle, M., Seeger, J., Renfree, M.B., and Fietz, S.A. (2018). The basal radial glia occurs in marsupials and underlies the evolution of an expanded neocortex in

therian mammals. Cereb. Cortex *28*, 145–157.

Schaefer, A., Lim, A., and Gorman, G. (2019). Epidemiology of Mitochondrial Disease. In Diagnosis and Management of Mitochondrial Disorders, (Cham: Springer International Publishing), pp. 63–79.

Schägger, H., and Pfeiffer, K. (2001). The Ratio of Oxidative Phosphorylation Complexes I-V in Bovine Heart Mitochondria and the Composition of Respiratory Chain Supercomplexes. J. Biol. Chem. *276*, 37861–37867.

Schaper, A. (1897). Die frühesten Differenzirungsvorgänge im Centralnervensystem. Arch. Für Entwickelungsmechanik Der Org. *5*, 81–132.

Schier, A.F. (2003). Nodal Signaling in Vertebrate Development. In Annual Review of Cell and Developmental Biology, (Annual Reviews 4139 El Camino Way, P.O. Box 10139, Palo Alto, CA 94303-0139, USA), pp. 589–621.

Schubert, M.B., and Vilarinho, L. (2020). Molecular basis of Leigh syndrome: A current look. Orphanet J. Rare Dis. *15*, 1–14.

Schwarz, T.L. (2013). Mitochondrial trafficking in neurons. Cold Spring Harb. Perspect. Med. *3*.

Seal, S., and Monsoro-Burq, A.H. (2020). Insights Into the Early Gene Regulatory Network Controlling Neural Crest and Placode Fate Choices at the Neural Border. Front. Physiol. *11*, 1528.

Sessa, A., Mao, C. an, Hadjantonakis, A.K., Klein, W.H., and Broccoli, V. (2008). Tbr2 Directs Conversion of Radial Glia into Basal Precursors and Guides Neuronal Amplification by Indirect Neurogenesis in the Developing Neocortex. Neuron *60*, 56–69.

Sessa, A., Mao, C.-A., Colasante, G., Nini, A., Klein, W.H., and Broccoli, V. (2010). Tbr2-positive intermediate (basal) neuronal progenitors safeguard cerebral cortex expansion by controlling amplification of pallial glutamatergic neurons and attraction of subpallial GABAergic interneurons. Genes Dev. *24*, 1816–1826.

Seth, E.A., Lee, H.-C., Yusof, H.H. bin M., Nordin, N., Cheah, Y.K., Ho, E.T.W., Ling, K.-H., and Cheah, P.-S. (2020). Phenotype microarrays reveal metabolic dysregulations of neurospheres derived from embryonic Ts1Cje mouse model of Down syndrome. PLoS One *15*, e0236826.

Shafit-Zagardo, B., and Kalcheva, N. (1998). Making sense of the multiple MAP-2 transcripts and their role in the neuron. Mol. Neurobiol. *16*, 149–162.

Shen, Q., Wang, Y., Dimos, J.T., Fasano, C.A., Phoenix, T.N., Lemischka, I.R., Ivanova, N.B., Stifani, S., Morrisey, E.E., and Temple, S. (2006). The timing of cortical neurogenesis is encoded within lineages of individual progenitor cells. Nat. Neurosci. *9*, 743–751.

Shi, Y., Kirwan, P., Smith, J., Robinson, H.P.C.C., and Livesey, F.J. (2012). Human cerebral cortex development from pluripotent stem cells to functional excitatory synapses. Nat. Neurosci. *15*, 477–486.

Shibata, M., Gulden, F.O., and Sestan, N. (2015). From trans to cis: Transcriptional regulatory networks in neocortical development. Trends Genet. *31*, 77–87.

Shim, S., Kwan, K.Y., Li, M., Lefebvre, V., and Šestan, N. (2012). Cis-regulatory control of corticospinal system development and evolution. Nature *486*, 74–79.

Shimizu, T., Kagawa, T., Wada, T., Muroyama, Y., Takada, S., and Ikenaka, K. (2005). Wnt signaling controls the timing of oligodendrocyte development in the spinal cord. Dev. Biol. *282*, 397–410.

Shook, L.L., Kislal, S., and Edlow, A.G. (2020). Fetal brain and placental programming in maternal obesity: A review of human and animal model studies. Prenat. Diagn. *40*, 1126–1137.

Shtilbans, A., Shanske, S., Goodman, S., Sue, C.M., Bruno, C., Johnson, T.L., Lava, N.S., Waheed, N., and DiMauro, S. (2000). G8363A mutation in the mitochondrial DNA transfer ribonucleic acidLys gene: Another cause of Leigh syndrome. J. Child Neurol. *15*, 759–761.

Silbereis, J.C., Nobuta, H., Tsai, H.H., Heine, V.M., McKinsey, G.L., Meijer, D.H., Howard, M.A., Petryniak, M.A., Potter, G.B., Alberta, J.A., et al. (2014). Olig1 Function Is Required to Repress Dlx1/2 and Interneuron Production in Mammalian Brain. Neuron *81*, 574–587.

Sloan, S.A., Darmanis, S., Huber, N., Khan, T.A., Birey, F., Caneda, C., Reimer, R., Quake, S.R., Barres, B.A., and Paşca, S.P. (2017). Human Astrocyte Maturation Captured in 3D Cerebral Cortical Spheroids Derived from Pluripotent Stem Cells. Neuron *95*, 779-790.e6.

Sloan, S.A., Andersen, J., Paşca, A.M., Birey, F., and Pașca, S.P. (2018). Generation and assembly of human brain region–specific three-dimensional cultures. Nat. Protoc. *13*, 2062–2085.

Smart, I.H.M., Dehay, C., Giroud, P., Berland, M., and Kennedy, H. (2002). Unique morphological features of the proliferative zones and postmitotic compartments of the neural epithelium giving rise to striate and extrastriate cortex in the monkey. Cereb. Cortex *12*, 37–53.

Smith, W.C., and Harland, R.M. (1992). Expression cloning of noggin, a new dorsalizing factor localized to the Spemann organizer in Xenopus embryos. Cell *70*, 829–840.

Smith, J.R., Vallier, L., Lupo, G., Alexander, M., Harris, W.A., and Pedersen, R.A. (2008). Inhibition of Activin/Nodal signaling promotes specification of human embryonic stem cells into neuroectoderm. Dev. Biol. *313*, 107–117.

Sofou, K., De Coo, I.F.M., Isohanni, P., Ostergaard, E., Naess, K., De Meirleir, L., Tzoulis, C., Uusimaa, J., De Angst, I.B., Lonnqvist, T., et al. (2014). A multicenter study on Leigh syndrome: disease course and predictors of survival. Orphanet J. Rare Dis. *9*, 52.

Sofou, K., De Coo, I.F.M., Ostergaard, E., Isohanni, P., Naess, K., De Meirleir, L., Tzoulis, C., Uusimaa, J., Lönnqvist, T., Bindoff, L.A., et al. (2018). Phenotype-genotype correlations in leigh syndrome: New insights from a multicentre study of 96 patients. J. Med. Genet. *55*, 21–27.

Son, E.Y., Ichida, J.K., Wainger, B.J., Toma, J.S., Rafuse, V.F., Woolf, C.J., and Eggan, K. (2011). Conversion of mouse and human fibroblasts into functional spinal motor neurons. Cell Stem Cell *9*, 205–218.

Sorbi, S., and Blass, J.P. (1982). Abnormal activation of private dehydrogenase in Leigh disease fibroblasts. Neurology *32*, 555–555.

Soula, C., Danesin, C., Kan, P., Grob, M., Poncet, C., and Cochard, P. (2001). Distinct sites of origin of oligodendrocytes and somatic motoneurons in the chick spinal cord: Oligodendrocytes arise from Nkx2.2-expressing progenitors by a Shh-dependent mechanism. Development *128*, 1369–1379.

Sousa, A.M.M., Meyer, K.A., Santpere, G., Gulden, F.O., and Sestan, N. (2017). Evolution of the Human Nervous System Function, Structure, and Development. Cell *170*, 226–247.

Spear, P.C., and Erickson, C.A. (2012). Interkinetic nuclear migration: A mysterious process in search of a function. Dev. Growth Differ. *54*, 306–316.

Spemann, H., and Mangold, H. (1924). über Induktion von Embryonalanlagen durch Implantation artfremder Organisatoren. Arch. Für Mikroskopische Anat. Und Entwicklungsmechanik *100*, 599–638.

Spemann, H., and Mangold, H. (2001). Induction of embryonic primordia by implantation of organizers from a different species. Int. J. Dev. Biol. *45*, 13–38.

Srinivasan, K., Leone, D.P., Bateson, R.K., Dobreva, G., Kohwi, Y., Kohwi-Shigematsu, T., Grosschedl, R., and McConnell, S.K. (2012). A network of genetic repression and derepression specifies projection fates in the developing neocortex. Proc. Natl. Acad. Sci. U. S. A. *109*, 19071–19078.

Starkov, A.A. (2008). The role of mitochondria in reactive oxygen species metabolism and signaling. In Annals of the New York Academy of Sciences, (John Wiley & Sons, Ltd), pp. 37–52.

Steinman, K.J., Gorno-Tempini, M.L., Glidden, D. V, Kramer, J.H., Miller, S.P., Barkovich, A.J., and Ferriero, D.M. (2009). Neonatal Watershed Brain Injury on Magnetic Resonance Imaging Correlates With Verbal IQ at 4 Years. Pediatrics *123*, 1025–1030.

Stern, H.J. (1994). Lactic acidosis in paediatrics: Clinical and laboratory evaluation. Ann. Clin. Biochem. *31*, 410–419.

Stolt, C.C., Rehberg, S., Ader, M., Lommes, P., Riethmacher, D., Schachner, M., Bartsch, U., and Wegner, M. (2002). Terminal differentiation of myelin-forming oligodendrocytes depends on the transcription factor Sox10. Genes Dev. *16*, 165–170.

Stolt, C.C., Schlierf, A., Lommes, P., Hillgärtner, S., Werner, T., Kosian, T., Sock, E., Kessaris, N., Richardson, W.D., Lefebvre, V., et al. (2006). SoxD Proteins Influence Multiple Stages of Oligodendrocyte Development and Modulate SoxE Protein Function. Dev. Cell *11*, 697–709.

Strauss, M., Hofhaus, G., Schröder, R.R., and Kühlbrandt, W. (2008). Dimer ribbons of ATP synthase shape the inner mitochondrial membrane. EMBO J. *27*, 1154–1160.

Sturman, J.A. (1993). Taurine in development. Physiol. Rev. *73*, 119–148.

Subramanian, L., Bershteyn, M., Paredes, M.F., and Kriegstein, A.R. (2017). Dynamic behaviour of human neuroepithelial cells in the developing forebrain. Nat. Commun. *8*, 14167.

Sugimori, M., Nagao, M., Parras, C.M., Nakatani, H., Lebel, M., Guillemot, F., and Nakafuku, M. (2008). Ascl1 is required for oligodendrocyte development in the spinal cord. Development *135*, 1271–1281.

Sugitani, Y., Nakai, S., Minowa, O., Nishi, M., Jishage, K., Kawano, H., Mori, K., Ogawa, M., and Noda, T. (2002). Brn-1 and Brn-2 share crucial roles in the production and positioning of mouse neocortical neurons. Genes Dev. *16*, 1760–1765.

Suhr, S.T., Chang, E.A., Tjong, J., Alcasid, N., Perkins, G.A., Goissis, M.D., Ellisman, M.H., Perez, G.I., and Cibelli, J.B. (2010). Mitochondrial Rejuvenation After Induced Pluripotency. PLoS One *5*, e14095.

Sun, W., Cornwell, A., Li, J., Peng, S., Joana Osorio, M., Aalling, N., Wang, S., Benraiss, A., Lou, N., Goldman, S.A., et al. (2017). SOX9 is an astrocyte-specific nuclear marker in the adult brain outside the neurogenic regions. J. Neurosci. *37*, 4493–4507.

Sun, Y., Nadal-Vicens, M., Misono, S., Lin, M.Z., Zubiaga, A., Hua, X., Fan, G., and Greenberg, M.E. (2001). Neurogenin promotes neurogenesis and inhibits glial differentiation by independent mechanisms. Cell *104*, 365–376.

Sutcliffe, M., and Lancaster, M.A. (2017). A Simple Method of Generating 3D Brain Organoids Using Standard Laboratory Equipment. In Organoids. Methods in Molecular Biology, (Humana Press), pp. 1–12.

Suter, D.M., Tirefort, D., Julien, S., and Krause, K.-H. (2009). A Sox1 to Pax6 Switch Drives Neuroectoderm to Radial Glia Progression During Differentiation of Mouse Embryonic Stem Cells. Stem Cells *27*, 49–58.

Takahashi, K., and Yamanaka, S. (2006). Induction of Pluripotent Stem Cells from Mouse Embryonic and Adult Fibroblast Cultures by Defined Factors. Cell *126*, 663–676.

Takahashi, K., Tanabe, K., Ohnuki, M., Narita, M., Ichisaka, T., Tomoda, K., and Yamanaka, S. (2007). Induction of Pluripotent Stem Cells from Adult Human Fibroblasts by Defined Factors. Cell *131*, 861–872.

Takizawa, T., Nakashima, K., Namihira, M., Ochiai, W., Uemura, A., Yanagisawa, M., Fujita, N.,

Nakao, M., and Taga, T. (2001). DNA Methylation Is a Critical Cell-Intrinsic Determinant of Astrocyte Differentiation in the Fetal Brain. Dev. Cell *1*, 749–758.

Tan, C.P., and Craighead, H.G. (2010). Surface engineering and patterning using parylene for biological applications. Materials (Basel). *3*, 1803–1832.

Tanaka, A., and Youle, R.J. (2008). A Chemical Inhibitor of DRP1 Uncouples Mitochondrial Fission and Apoptosis. Mol. Cell *29*, 409–410.

Tao, W., and Lai, E. (1992). Telencephalon-restricted expression of BF-1, a new member of the HNF-3/fork head gene family, in the developing rat brain. Neuron *8*, 957–966.

Tao, Y., and Zhang, S.C. (2016). Neural Subtype Specification from Human Pluripotent Stem Cells. Cell Stem Cell *19*, 573–586.

Tarabykin, V., Stoykova, A., Usman, N., and Gruss, P. (2001). Cortical upper layer neurons derive from the subventricular zone as indicated by Svet1 gene expression. Development *128*, 1983–1993.

Taverna, E., Götz, M., and Huttner, W.B. (2014). The cell biology of neurogenesis: toward an understanding of the development and evolution of the neocortex. Annu. Rev. Cell Dev. Biol. *30*, 465–502.

TCW, J., Wang, M., Pimenova, A.A., Bowles, K.R., Hartley, B.J., Lacin, E., Machlovi, S.I., Abdelaal, R., Karch, C.M., Phatnani, H., et al. (2017). An Efficient Platform for Astrocyte Differentiation from Human Induced Pluripotent Stem Cells. Stem Cell Reports *9*, 600–614.

Ten, V.S., and Starkov, A. (2012). Hypoxic-Ischemic Injury in the Developing Brain: The Role of Reactive Oxygen Species Originating in Mitochondria. Neurol. Res. Int. *2012*, 1–10.

Thakurela, S., Tiwari, N., Schick, S., Garding, A., Ivanek, R., Berninger, B., and Tiwari, V.K. (2016). Mapping gene regulatory circuitry of Pax6 during neurogenesis. Cell Discov. *2*, 1–22.

Thomson, J.A., and Marshall, V.S. (1998). Primate embryonic stem cells. Curr. Top. Dev. Biol. *38*, 133–165.

Thomson, J.A., Kalishman, J., Golos, T.G., Durning, M., Harris, C.P., Becker, R.A., and Hearn, J.P.

(1995). Isolation of a primate embryonic stem cell line. Proc. Natl. Acad. Sci. U. S. A. *92*, 7844–7848.

Thomson, J.A., Itskovitz-Eldor, J., Shapiro, S.S., Waknitz, M.A., Swiergiel, J.J., Marshall, V.S., and Jones, J.M. (1998). Embryonic stem cell lines derived from human blastocysts. Science (80-.). *282*, 1145–1147.

Tibbitt, M.W., and Anseth, K.S. (2012). Dynamic microenvironments: The fourth dimension. Sci. Transl. Med. *4*, 160ps24-160ps24.

Tissir, F., and Goffinet, A.M. (2003). Reelin and brain development. Nat. Rev. Neurosci. *4*, 496–505.

Toma, K., Kumamoto, T., Hanashima, C., Toma, K., and Hanashima, C. (2014). The timing of upper-layer neurogenesis is conferred by sequential derepression and negative feedback from deep-layer neurons. J. Neurosci. *34*, 13259–13276.

Toresson, H., De Urquiza, A.M., Fagerström, C., Perlmann, T., and Campbell, K. (1999). Retinoids are produced by glia in the lateral ganglionic eminence and regulate striatal neuron differentiation. Development *126*, 1317–1326.

Trommsdorff, M., Gotthardt, M., Hiesberger, T., Shelton, J., Stockinger, W., Nimpf, J., Hammer, R.E., Richardson, J.A., and Herz, J. (1999). Reeler/disabled-like disruption of neuronal migration in knockout mice lacking the VLDL receptor and ApoE receptor 2. Cell *97*, 689–701.

Uittenbogaard, M., Brantner, C.A., Fang, Z.S., Wong, L.J.C., Gropman, A., and Chiaramello, A. (2018). Novel insights into the functional metabolic impact of an apparent de novo m.8993T>G variant in the MT-ATP6 gene associated with maternally inherited form of Leigh Syndrome. Mol. Genet. Metab. *124*, 71–81.

Valenzuela, D.M., Economides, A.N., Rojas, E., Lamb, T.M., Nuñez, L., Jones, P., Ip, N.Y., Espinosa, R., Brannan, C.I., Gilbert, D.J., et al. (1995). Identification of mammalian noggin and its expression in the adult nervous system. J. Neurosci. *15*, 6077–6084.

Vasistha, N.A., García-Moreno, F., Arora, S., Cheung, A.F.P., Arnold, S.J., Robertson, E.J., and Molnár, Z. (2015). Cortical and clonal contribution of Tbr2 expressing progenitors in the

developing mouse brain. Cereb. Cortex *25*, 3290–3302.

Velasco, S., Kedaigle, A.J., Simmons, S.K., Nash, A., Rocha, M., Quadrato, G., Paulsen, B., Nguyen, L., Adiconis, X., Regev, A., et al. (2019). Individual brain organoids reproducibly form cell diversity of the human cerebral cortex. Nature *570*, 523–527.

Vierbuchen, T., Ostermeier, A., Pang, Z.P., Kokubu, Y., Südhof, T.C., and Wernig, M. (2010). Direct conversion of fibroblasts to functional neurons by defined factors. Nature *463*, 1035–1041.

Villalón-García, I., Álvarez-Córdoba, M., Suárez-Rivero, J.M., Povea-Cabello, S., Talaverón-Rey, M., Suárez-Carrillo, A., Munuera-Cabeza, M., and Sánchez-Alcázar, J.A. (2020). Precision Medicine in Rare Diseases. Diseases *8*, 42.

Villanueva-Paz, M., Povea-Cabello, S., Villalón-García, I., Suárez-Rivero, J.M., Álvarez-Córdoba, M., de la Mata, M., Talaverón-Rey, M., Jackson, S., and Sánchez-Alcázar, J.A. (2019). Pathophysiological characterization of MERRF patient-specific induced neurons generated by direct reprogramming. Biochim. Biophys. Acta - Mol. Cell Res. *1866*, 861–881.

Visch, H.J., Koopman, W.J.H., Leusink, A., Van Emst-De Vries, S.E., Van Den Heuvel, L.W.P.J., Willems, P.H.G.M., and Smeitink, J.A.M. (2006). Decreased agonist-stimulated mitochondrial ATP production caused by a pathological reduction in endoplasmic reticulum calcium content in human complex I deficiency. Biochim. Biophys. Acta - Mol. Basis Dis. *1762*, 115–123.

Vo, T.D., Paul Lee, W.N., and Palsson, B.O. (2007). Systems analysis of energy metabolism elucidates the affected respiratory chain complex in Leigh's syndrome. Mol. Genet. Metab. *91*, 15–22.

Volpato, V., and Webber, C. (2020). Addressing variability in iPSC-derived models of human disease: Guidelines to promote reproducibility. Dis. Model. Mech. *13*.

Volpe, J.J. (2012). Neonatal encephalopathy: An inadequate term for hypoxic-ischemic encephalopathy. Ann. Neurol. *72*, 156–166.

Vorstman, J.A.S., Turetsky, B.I., Sijmens-Morcus, M.E.J., De Sain, M.G., Dorland, B., Sprong, M., Rappaport, E.F., Beemer, F.A., Emanuel, B.S., Kahn, R.S., et al. (2009). Proline affects brain function in 22q11DS children with the low activity COMT158 allele. Neuropsychopharmacology

34, 739–746.

Walsh, C., and Cepko, C.L. (1993). Clonal dispersion in proliferative layers of developing cerebral cortex. Nature *362*, 632–635.

Wang, L., Bluske, K.K., Dickel, L.K., and Nakagawa, Y. (2011a). Basal progenitor cells in the embryonic mouse thalamus - their molecular characterization and the role of neurogenins and Pax6. Neural Dev. *6*, 1–19.

Wang, X., Tsai, J.W., Lamonica, B., and Kriegstein, A.R. (2011b). A new subtype of progenitor cell in the mouse embryonic neocortex. Nat. Neurosci. *14*, 555–562.

Watanabe, K., Kamiya, D., Nishiyama, A., Katayama, T., Nozaki, S., Kawasaki, H., Watanabe, Y., Mizuseki, K., and Sasai, Y. (2005). Directed differentiation of telencephalic precursors from embryonic stem cells. Nat. Neurosci. *8*, 288–296.

Watanabe, K., Ueno, M., Kamiya, D., Nishiyama, A., Matsumura, M., Wataya, T., Takahashi, J.B., Nishikawa, S., Nishikawa, S.I., Muguruma, K., et al. (2007). A ROCK inhibitor permits survival of dissociated human embryonic stem cells. Nat. Biotechnol. *25*, 681–686.

Wei, M.C., Lindsten, T., Mootha, V.K., Weiler, S., Gross, A., Ashiya, M., Thompson, C.B., and Korsmeyer, S.J. (2000). tBID, a membrane-targeted death ligand, oligomerizes BAK to release cytochrome c. Genes Dev. *14*, 2060–2071.

Weidemann, A., and Johnson, R.S. (2008). Biology of HIF-1α. Cell Death Differ. *15*, 621–627.

Weimann, J.M., Zhang, Y.A., Levin, M.E., Devine, W.P., Brûlet, P., and McConnell, S.K. (1999). Cortical neurons require Otx1 for the refinement of exuberant axonal projections to subcortical targets. Neuron *24*, 819–831.

White, L.D., and Barone, S. (2001). Qualitative and quantitative estimates of apoptosis from birth to senescence in the rat brain. Cell Death Differ. *8*, 345–356.

Wilkens, V., Kohl, W., and Busch, K. (2013). Restricted diffusion of OXPHOS complexes in dynamic mitochondria delays their exchange between cristae and engenders a transitory mosaic distribution. J. Cell Sci. *126*, 103–116.

Wilson, P.G., and Stice, S.S. (2006). Development and differentiation of neural rosettes derived from human embryonic stem cells. Stem Cell Rev. *2*, 67–77.

Wodarz, A., and Huttner, W.B. (2003). Asymmetric cell division during neurogenesis in Drosophila and vertebrates. Mech. Dev. *120*, 1297–1309.

Wu, J., Ocampo, A., and Belmonte, J.C.I. (2016). Cellular Metabolism and Induced Pluripotency. Cell *166*, 1371–1385.

Wu, S.X., Goebbels, S., Nakamura, K., Nakamura, K., Kometani, K., Minato, N., Kaneko, T., Nave, K.A., and Tamamaki, N. (2005). Pyramidal neurons of upper cortical layers generated by NEX-positive progenitor cells in the subventricular zone. Proc. Natl. Acad. Sci. U. S. A. *102*, 17172–17177.

Xia, J., and Wishart, D.S. (2010). MetPA: a web-based metabolomics tool for pathway analysis and visualization. Bioinformatics *26*, 2342–2344.

Xia, J., and Wishart, D.S. (2011a). Metabolomic data processing, analysis, and interpretation using MetaboAnalyst. Curr. Protoc. Bioinforma. *34*, 1–48.

Xia, J., and Wishart, D.S. (2011b). Web-based inference of biological patterns, functions and pathways from metabolomic data using MetaboAnalyst. Nat. Protoc. *6*, 743–760.

Xia, J., Psychogios, N., Young, N., and Wishart, D.S. (2009). MetaboAnalyst: a web server for metabolomic data analysis and interpretation. Nucleic Acids Res. *37*, W652–W660.

Xiang, Y., Tanaka, Y., Patterson, B., Kang, Y.J., Govindaiah, G., Roselaar, N., Cakir, B., Kim, K.Y., Lombroso, A.P., Hwang, S.M., et al. (2017). Fusion of Regionally Specified hPSC-Derived Organoids Models Human Brain Development and Interneuron Migration. Cell Stem Cell *21*, 383-398.e7.

Xiang, Y., Tanaka, Y., Cakir, B., Patterson, B., Kim, K.-Y., Sun, P., Kang, Y.-J., Zhong, M., Liu, X., Patra, P., et al. (2019). hESC-Derived Thalamic Organoids Form Reciprocal Projections When Fused with Cortical Organoids. Cell Stem Cell *24*, 487-497.e7.

Xie, Y.W., and Wolin, M.S. (1996). Role of nitric oxide and its interaction with superoxide in the suppression of cardiac muscle mitochondrial respiration: Involvement in response to

hypoxia/reoxygenation. Circulation *94*, 2580–2586.

Yamaguchi, T.P. (2001). Heads or tails: Wnts and anterior-posterior patterning. Curr. Biol. *11*, R713–R724.

Yamaguchi, Y., and Miura, M. (2015). Programmed cell death in neurodevelopment. Dev. Cell *32*, 478–490.

Yamanaka, S. (2020). Pluripotent Stem Cell-Based Cell Therapy—Promise and Challenges. Cell Stem Cell *27*, 523–531.

Yanes, O., Clark, J., Wong, D.M., Patti, G.J., Sánchez-Ruiz, A., Benton, H.P., Trauger, S.A., Desponts, C., Ding, S., and Siuzdak, G. (2010). Metabolic oxidation regulates embryonic stem cell differentiation. Nat. Chem. Biol. *6*, 411–417.

Ybot-Gonzalez, P., Gaston-Massuet, C., Girdler, G., Klingensmith, J., Arkell, R., Greene, N.D.E., and Copp, A.J. (2007). Neural plate morphogenesis during mouse neurulation is regulated by antagonism of Bmp signalling. Development *134*, 3203–3211.

Yoo, A.S., Sun, A.X., Li, L., Shcheglovitov, A., Portmann, T., Li, Y., Lee-Messer, C., Dolmetsch, R.E., Tsien, R.W., and Crabtree, G.R. (2011). MicroRNA-mediated conversion of human fibroblasts to neurons (Nature Publishing Group).

Yoon, S.J., Elahi, L.S., Pașca, A.M., Marton, R.M., Gordon, A., Revah, O., Miura, Y., Walczak, E.M., Holdgate, G.M., Fan, H.C., et al. (2019). Reliability of human cortical organoid generation. Nat. Methods *16*, 75–78.

Youle, R.J., and Karbowski, M. (2005). Mitochondrial fission in apoptosis. Nat. Rev. Mol. Cell Biol. *6*, 657–663.

Zahedi, A., On, V., Phandthong, R., Chaili, A., Remark, G., Bhanu, B., and Talbot, P. (2018). Deep Analysis of Mitochondria and Cell Health Using Machine Learning. Sci. Rep. *8*, 16354.

Zamanian, J.L., Xu, L., Foo, L.C., Nouri, N., Zhou, L., Giffard, R.G., and Barres, B.A. (2012). Genomic analysis of reactive astrogliosis. J. Neurosci. *32*, 6391–6410.

Zanotelli, M.R., Goldblatt, Z.E., Miller, J.P., Bordeleau, F., Li, J., VanderBurgh, J.A., Lampi, M.C.,

King, M.R., and Reinhart-King, C.A. (2018). Regulation of ATP utilization during metastatic cell migration by collagen architecture. Mol. Biol. Cell *29*, 1–9.

Zanotelli, M.R., Rahman-Zaman, A., VanderBurgh, J.A., Taufalele, P. V., Jain, A., Erickson, D., Bordeleau, F., and Reinhart-King, C.A. (2019). Energetic costs regulated by cell mechanics and confinement are predictive of migration path during decision-making. Nat. Commun. *10*, 1–12.

Zecevic, N., Chen, Y., and Filipovic, R. (2005). Contributions of cortical subventricular zone to the development of the human cerebral cortex. J. Comp. Neurol. *491*, 109–122.

Zeisel, S.H. (2006). The fetal origins of memory: The role of dietary choline in optimal brain development. J. Pediatr. *149*, S131–S136.

Zeisel, S.H., and Niculescu, M.D. (2006). Perinatal Choline Influences Brain Structure and Function. Nutr. Rev. *64*, 197–203.

Zeng, H., Guo, M., Martins-Taylor, K., Wang, X., Zhang, Z., Park, J.W., Zhan, S., Kronenberg, M.S., Lichtler, A., Liu, H.-X., et al. (2010). Specification of Region-Specific Neurons Including Forebrain Glutamatergic Neurons from Human Induced Pluripotent Stem Cells. PLoS One *5*, e11853.

Zhadanov, A.B., Provance, D.W., Speer, C.A., Coffin, J.D., Goss, D., Blixt, J.A., Reichert, C.M., and Mercer, J.A. (1999). Absence of the tight junctional protein AF-6 disrupts epithelial cell-cell junctions and cell polarity during mouse development. Curr. Biol. *9*, 880–888.

Zhang, J., Khvorostov, I., Hong, J.S., Oktay, Y., Vergnes, L., Nuebel, E., Wahjudi, P.N., Setoguchi, K., Wang, G., Do, A., et al. (2011). UCP2 regulates energy metabolism and differentiation potential of human pluripotent stem cells. EMBO J. *30*, 4860–4873.

Zhang, M., Ngo, J., Pirozzi, F., Sun, Y.-P., and Wynshaw-Boris, A. (2018). Highly efficient methods to obtain homogeneous dorsal neural progenitor cells from human and mouse embryonic stem cells and induced pluripotent stem cells. Stem Cell Res. Ther. *9*, 67.

Zhang, S.-C., Wernig, M., Duncan, I.D., Brüstle, O., and Thomson, J.A. (2001). In vitro differentiation of transplantable neural precursors from human embryonic stem cells. Nat. Biotechnol. *19*, 1129–1133.

Zhang, Y., Pak, C.H., Han, Y., Ahlenius, H., Zhang, Z., Chanda, S., Marro, S., Patzke, C., Acuna, C.,

Covy, J., et al. (2013). Rapid single-step induction of functional neurons from human pluripotent stem cells. Neuron *78*, 785–798.

Zheng, X., Boyer, L., Jin, M., Kim, Y., Fan, W., Bardy, C., Berggren, T., Evans, R.M., Gage, F.H., and Hunter, T. (2016a). Alleviation of neuronal energy deficiency by mtor inhibition as a treatment for mitochondria-related neurodegeneration. Elife *5*.

Zheng, X., Boyer, L., Jin, M., Mertens, J., Kim, Y., Ma, L., Ma, L., Hamm, M., Gage, F.H., and Hunter, T. (2016b). Metabolic reprogramming during neuronal differentiation from aerobic glycolysis to neuronal oxidative phosphorylation. Elife *5*.

Zimmer, C., Tiveron, M.C., Bodmer, R., and Cremer, H. (2004). Dynamics of Cux2 expression suggests that an early pool of SVZ precursors is fated to become upper cortical layer neurons. Cereb. Cortex *14*, 1408–1420.

Zurita-Díaz, F., Galera-Monge, T., Moreno-Izquierdo, A., Fraga, M.F., Ayuso, C., Fernández, A.F., Garesse, R., and Gallardo, M.E. (2016). Generation of a human iPSC line from a patient with a mitochondrial encephalopathy due to mutations in the GFM1 gene. Stem Cell Res. *16*, 124–127.

Zweifel, S., Marcy, G., Lo Guidice, Q., Li, D., Heinrich, C., Azim, K., and Raineteau, O. (2018). HOPX Defines Heterogeneity of Postnatal Subventricular Zone Neural Stem Cells. Stem Cell Reports *11*, 770–783.